Distribution and Activity of Anammox and Sulfide-Oxidizing Nitrate-Reducing Bacteria in Oxygen Minimum Zones

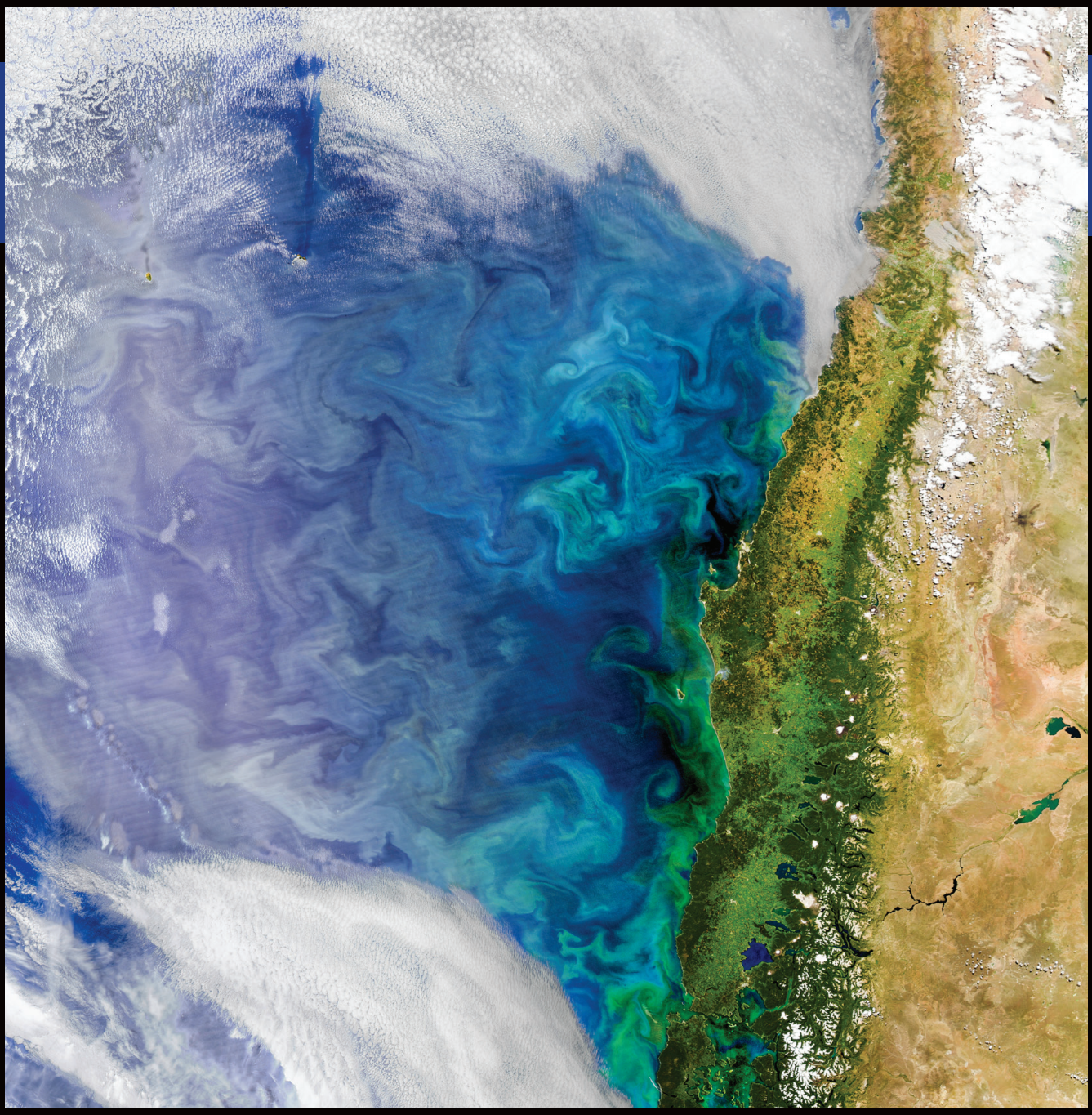

Cameron M. Callbeck

Distribution and Activity of Anammox and Sulfide-Oxidizing Nitrate-Reducing Bacteria in Oxygen Minimum Zones

Diese Arbeit wurde in der Zeit vom August 2012 bis Juni 2017 im Rahmen des Programms "The International Max Planck Research School of Marine Microbiology" (MarMic) angefertigt. Die Ergebnisse Arbeit wurden am Max Planck Institut für Marine Mikrobiologie (Biogeochemie) erarbeitet

Datum Promotionskolloquiums: 18.9.2017

Autor: **Cameron M. Callbeck**

Universität Bremen

Max Planck Institut für Marine Mikrobiologie

Gutachter: **Prof. Dr. Marcel M. M. Kuypers**

Universität Bremen

Max Planck Institut für Marine Mikrobiologie

Zweitgutachter: **Prof. Dr. Alexander Loy**

Division of Microbial Ecology

Universität Wien

Front cover: Extensive heterogeneity in the waters off the coast of Chile and Peru. Image is courtesy of NASA Ocean Color taken November 29, 2016 (aquired by Aqua/MODIS/Suomi-NPP/VIIRS data).

Summary

Zusammenfassung

Highly productive marine upwelling regions that are located along continental boundaries play a critical role in the global ocean nitrogen budget. These eutrophic and oxygen depleted waters, referred to as oxygen minimum zones (OMZs) account for 30-50% of global ocean fixed nitrogen loss. Anammox has been shown to be the main contributor to this nitrogen loss. Further OMZ nitrogen loss can be supported by an active, but overlooked, microbial sulfur cycle mediated by activities of sulfide-oxidizing nitrate-reducing bacteria. Sulfide-driven denitrification is most prevalent in highly sulfidic shelf waters. New evidence has emerged that such a coupled nitrogen-sulfur cycle also contributes to offshore denitrification in waters detached from benthic processes. Moreover, rates of anammox and denitrification activity exhibit a high degree of spatial and temporal variability, particularly in the open ocean OMZ (***Chapter 1***). The physical and microbiological controls on this variability in nitrogen loss processes have remained poorly constrained. This thesis work aims to elucidate the dynamics that govern the activity and distribution of anammox and sulfide-oxidizing denitrifying bacteria in OMZs using a comprehensive range, genomic, cultivation, biogeochemical and single-cell methods studied within the framework of OMZ hydrodynamics. We specifically explored nitrogen loss regulation in the Eastern Tropical South Pacific (ETSP) and the Bay of Bengal (BoB) OMZs; areas that are bellwethers of global climate change and anthropogenic induced eutrophication.

The monsoonal driven upwelling in the BoB maintains moderate to high levels of primary production in surface waters resulting in low oxygen concentrations in the subeuphotic zone. Despite these low oxygen concentrations (< 2 μM), the BoB, exhibits no clear evidence of nitrogen loss. For the first time, we investigated nitrogen loss processes and the factors regulating anammox activity in these waters using a combination of molecular methods, ^{15}N-labelled stable isotope incubation experiments and geochemical tools (***Chapter 2***). Using a highly sensitive STOX sensor, we find that the BoB contained submicromolar oxygen concentrations, and indeed, supported low but consistent rates of anammox activity. Moreover, oxygen manipulation experiments revealed that anammox and nitrite oxidation activities could co-exist at low-levels of oxygen. This overlap of aerobic and anaerobic processes combined with the lack of nitrite accumulation in the BoB, suggested that oxygen concentrations supported nitrite oxidization that restricted the amount of nitrite available for anammox. Thus, oxygen, was indirectly limiting fixed nitrogen loss in the BoB. However, a slight increase in organic matter induced by anthropogenic eutrophication, could remove these last traces of oxygen causing the BoB to become a major sink of inorganic nitrogen, analogous to other OMZs.

The highly productive ETSP region, in contrast, maintains substantial organic matter rain rates. Therefore, broad areas of the water column are "functionally anoxic", i.e. oxygen concentrations fall below 10 nM. The functionally anoxic water column in combination with enhanced organic matter export and reminerlization sustain elevated rates of nitrogen loss by anammox as well a widespread community of sulfide-oxidizing denitrifying bacteria. However, these processes display a high degree of heterogeneity suggestive that complex regional oceanography underlines ETSP nitrogen loss.

Mesoscale eddies, found ubiquitously in OMZs, have the potential to be important features shaping the distribution and activity of nitrogen loss processes. Eddies have been suggested to enhance vertical nutrient transport stimulating primary productivity and thereby organic matter export. In ***Chapter 3*** we investigated the impact of mesoscale eddies on anammox and denitrification activity in the offshore ETSP region using ^{15}N-labelled incubation experiments. We find that anammox dominated nitrogen loss within the eddies, but varied across these features. Rates of anammox were highest along the eddy periphery coinciding with where the highest depth-integrated chlorophyll concentrations were observed, suggesting that the high organic matter export along the periphery likely sustained enhanced nitrogen loss. The enhanced primary productivity and nitrogen loss along the eddy periphery was driven by eddy-induced submesoscale vertical transport processes.

The ubiquity of eddies, in addition to the heterogeneity of anammox rates, indicated that such features regulate regional offshore primary production and thereby nitrogen loss.

Mesoscale eddies, not only drive the vertical transport of nutrients, but the strong eddy-induced annular velocities, mediate lateral advection. In ***Chapter 5*** we demonstrated using oceanographic and molecular techniques that eddy formations in near-shore waters co-transports elemental sulfur and sulfide-oxidizing denitrifying bacteria from the coast into open ocean waters. In accordance, offshore waters influenced by cross-shelf transport sustained enhanced denitrification rates. Sulfidic OMZ shelf waters, which supported abundant populations of gamma- and epsilon-proteobacteria including SUP05 and *Arcobacter*, represented large inventories of elemental sulfur and active sulfide-oxidizing nitrate-reducing bacteria.

Although SUP05 and *Arcobacter* co-occurred in sulfidic shelf waters, their distribution, activity, and ecophysiology in offshore ETSP waters varied, and were the subject of further investigation in ***Chapters 5 and 6***. Employing cultivation, genomic, biogeochemical and single-cell techniques, we find that both SUP05 and *Arcobacter* have the capacity to oxidize sulfide and to reduce nitrate to N_2. For growth, SUP05 performed autotrophic CO_2 fixation, while *Arcobacter* was solely reliant on organic matter growing best in the presence of sulfide and nitrate. These findings reveal that both chemolithoautotrophy and chemolithoheterotrophy may play an important role in near-shore eutrophic, sulfide-rich upwelling environments promoting the detoxification of sulfidic shelf waters and the removal of fixed nitrogen. However, *Arcobacter*'s requirement for labile organic matter restricted it to the highly sulfidic and eutrophic Peruvian shelf waters, whereas SUP05 bacteria were also abundant and active in offshore waters advected from the coast by the mesoscale eddy. SUP05's ability to survive in offshore waters void of sulfide was enabled by its capacity to use co-transported elemental sulfur. Eddy-driven cross-shelf transport combined with SUP05's capacity to use elemental sulfur and denitrify, feasibly underpin reports of offshore OMZ sulfur cycling and nitrogen loss driven by denitrification.

Employing an interdisciplinary approach, this thesis work demonstrates that regional mesoscale dynamics are important in shaping the distribution and activity of key organisms involved in OMZ anammox and denitrification. Work here also highlights the importance of oxygen dynamics as an indirect regulator of nitrogen loss in OMZs and the susceptibility of areas such as the Bay of Bengal, to global change and anthropogenic induced eutrophication.

Regionen mit Auftrieb von nährstoffreichem Tiefenwasser entlang der kontinentalen Küstenlinien sind hoch produktiv und spielen eine zentrale Rolle im globalen Stickstoffhaushalt des Ozeans. Diese nährstoffreichen, aber sauerstoffarmen Gewässer werden auch als Sauerstoffminimumzonen (OMZs-von (engl.) Oxygen Minimum Zones) bezeichnet und tragen 30-50% zum globalen Stickstoffverlust der Wassersäule bei. Es stellte sich heraus, dass hauptsächlich die anaerobe Oxidation von Ammonium (Anammox) für diesen Stickstoffverlust verantwortlich ist. Ausserdem wird der Stickstoffverlust in OMZ Gewässern durch einen aktiven, jedoch oft vernachlässigten, mikrobiellen Schwefelkreislauf begünstigt, der die Aktivität von Sulfid-oxidierenden, Nitrat-reduzierenden Bakterien begünstigt. Die durch Sulfid angetriebene Denitrifizierung ist in stark sulfidischen Schelfgewässern sehr verbreitet und neuen Erkenntnissen nach könnte solch ein gekoppelter Stickstoff-Schwefel Kreislauf die küstennahe Denitrifizierung in den von benthischen Prozessen getrennten Wassermassen antreiben. Gemeinsam mit Anammox kann der gekoppelte N-S Kreislauf zum Verlust von gebundenem Stickstoff in OMZs beitragen. Dennoch weisen die Anammox- und Denitrifizierungsraten starke räumliche sowie zeitliche Variabilität auf, besonders in den OMZs auf offener See; der grössten Senke von gebundenem Stickstoff (***Kapitel 1***). Aufgrund der Komplexität der regionalen Ozeanographie sind bisher die Faktoren, die die Aktivität und Verteilung von Stickstoffverlustprozessen regulieren, in OMZ

Gewässern weiterhin schlecht verstanden.

Das Ziel dieser Arbeit ist es, die Prozesse zu verstehen, die die Verteilung von Anammox und Sulfid-oxidierenden, Nitrat-reduzierenden Bakterien in OMZs beherrschen. Zu diesem Zweck wurden ozeanographische, gnomische, kultivierungs und biogeochemische Methoden sowie Einzelzell-Techniken angewandt. Insbesondere wurde Stickstoffverlust Regulierung im südöstlichen tropischen Pazifik (ETSP-von (engl.) Eastern Tropical South Pacific) und im Golf von Bengalen (BoB-von (engl.) Bay of Bengal) analysiert; Regionen die besonders vom globalen Klimawandel und anthropogener Eutrophierung betroffen sind.

Die Zirkulation im BoB wird durch Monsungetriebenen Auftrieb bestimmt. Die Primärproduktion ist dadurch in den Oberflächenwassern sehr hoch. Dies senkt die Sauerstoffkonzentrationen unter der euphotischen Zone erheblich. Trotz dieser niedrigen Sauerstoffkonzentrationen (< 2 μM) gibt es im BoB keine Anzeichen auf Stickstoffverluste. In dieser Arbeit werden zum ersten Mal Stickstoffverlustprozesse sowie die Faktoren, die die Anammox Aktivität in diesen Gewässern bestimmen mit einer Kombination aus molekularen Methoden, Inkubationsexperimenten mit dem stabilen Isotop von N (^{15}N) und geochemischen Methoden erforscht (***Kapitel 2***). Mithilfe eines hochsensitiven STOX Sensors konnten wir herausfinden, dass der BoB submikromolare Sauerstoffkonzentrationen sowie niedrige, aber beständige Raten an Anammox Aktivität aufweist. Zudem konnten wir in Sauerstoffmanipulations-Experimenten zeigen, dass Anammox und Nitrit-Oxidation Aktivitäten unter den niedrigen Sauerstoffkonzentrationen koexistieren können. Die Überschneidung von aeroben und anaeroben Prozessen sowie ein Mangel an Nitrit Akkumulation im BoB lassen darauf schliessen, dass die Sauerstoffkonzentrationen Nitrit Oxidation indirekt begünstigen und somit die für Anammox verfügbare Menge an Nitrit verkleinern. Sogar ein kleiner Anstieg an organischem Material (zum Beispiel durch anthropogenen Eutrophierung) könnte die letzten Spuren von Sauerstoff beseitigen und der BoB könnte somit, analog zu anderen OMZs, eine bedeutende Senke für anorganischen Stickstoff werden.

Im Gegensatz dazu werden in der hoch produktiven ETSP Region hohe Niederschlagsraten an organischem Material beobachtet, was weite «funktional anoxische» Bereiche in der Wassersäule hervorruft, in denen Sauerstoff unter 10 nM fällt. Diese funktional anoxische Wassersäule, in Kombination mit erhöhtem Transport von organischem Material und Remineralisierung, erhalten erhöhte Raten an Stickstoffverlust durch Anammox sowie eine weite Ausbreitung von vermeintlich Sulfid-oxidierenden, denitrifizierenden Bakterien aufrecht. Neben großskaligen Zirkulationsmustern können mesoskalige Wirbel (welche allgegenwertig in OMZs sind) die Verteilung sowie die Aktivität von Stickstoffverlustprozessen regulieren. Es wird vermutet, dass diese Wirbel den vertikalen Transport von Nährstoffen verstärken und somit die Primärproduktion und den folgenden Transport von organischem Material anregen können.

In ***Kapitel 3*** haben wir den Einfluss von mesoskaligen Wirbeln auf die Verteilung und Aktivität von Anammox und die Denitrifizierungs Aktivität in der küstenfernen ETSP Region mithilfe von ^{15}N Inkubationsexperimenten untersucht. Wir legen dar, dass Anammox den Stickstoffverlust in den Wirbeln dominiert, jedoch räumlich variiert. Anammoxraten waren entlang der Aussengrenze des Wirbels am höchsten. Diese Beobachtung geht mit den höchsten tiefenintegrierten Chlorophyll Konzentrationen einher, was vermuten lässt, dass der hohe Transport von organischem Material entlang der Aussengrenze der Wirbel den verstärkten Stickstoffverlust aufrechterhält. Diese Ergebnisse sind insgesamt konsistent mit einem durch Wirbel induzierten, sub-mesoskaligen, vertikalen Transport-Mechanismus, der an den Kanten der Wirbel tätig ist. Die Allgegenwärtigkeit von Wirbeln zusätzlich zu der Heterogenität von Anammox zeigte, dass solche Wirbel den regionalen küstenfernen Stickstoffverlust regulieren.

Mesoskalige Wirbel bestimmen nicht nur den vertikalen Transport von Nährstoffen. Wenn sie entlang der Küste entstehen führen sie zu einer lateralen Advektion von Chlorophyll und Nährstoffen seewärts. In ***Kapitel 5*** zeigten wir durch ozeanographische und molekulare Methoden, dass durch die in

Wirbeln hervorgerufene Advektion von elementarem Schwefel und Sulfid-oxidierenden, denitrifizierende Bakterien von der Küste in den Ozean transportiert werden. Sulfidische OMZ-Schelfwasser, die eine große und aktive Population von Gamma- und Epsilon-Proteobakterien wie SUP05 und *Arcobacter* unterstützen, repräsentierten große Bestände von elementarem Schwefel und Sulfid-oxidierenden, Nitrat-reduzierenden Bakterien.

Obwohl *Arcobacter* und SUP05 in sulfidischen Schelfgewässern gleichzeitig auftraten, variierte ihre Verteilung, Aktivität und Ökophysiologie in küstenfernen ETSP Gewässern, was in den ***Kapiteln 5 und 6*** näher beleuchtet wird. Durch die Anwendung von kultivierungs, gnomischen, biogeochemischen und Einzelzell-Techniken konnten wir herausfinden, dass sowohl SUP05 als auch *Arcobacter* die Fähigkeit besitzen, Sulfid zu oxidieren und Nitrat zu N_2 zu reduzieren. Für ihr Wachstum führt SUP05 autotrophe CO_2 Bindung durch, während *Arcobacter* einzig von organischem Material abhängig ist und am Besten im Beisein von Sulfid und Nitrat wächst. Diese Befunde zeigen, dass Litho- Heterotrophie eine wichtige Rolle in küstennahen, eutrophen, sulfidreichen Auftriebsregionen spielt, was die Entgiftung in sulfidischen Schelfwassern und den Verlust von gebundenem Stickstoff durch einen Zusammenschluss von chemolithoautotrophoben und chemolithoheterotrophoben Bakterien fördert. *Arcobacters* Bedarf an labilem organischen Material beschränkt es jedoch auf die stark sulfidischen und eutrophen Peruanischen Schelfwasser, während SUP05 Bakterien ebenfalls in küstenfernen Wassermassen aktiv sind, die von der Küste durch mesoskalige Wirbel advehiert wurden. Die Fähigkeit von SUP05 in küstenfernen und schwefelarmen Gewässern zu überleben wurde durch seine Fähigkeit, den mittransportierten elementaren Schwefel zu benutzen ermöglicht, was wahrscheinlich die gemessenen Raten an küstenferner Denitrifizierung unterstützt. Der durch Wirbel betriebene Schelftransport in Kombination mit der Fähigkeit von SUP05, den elementaren Schwefel zu benutzen und zu denitrifizieren, untermauert Berichte über einen küstenfernen Schwefelkreislauf und Stickstoffverlust welche durch Denitrifizierung in OMZs angetrieben wird.

Mit einem interdisziplinären Ansatz zeigt diese Arbeit, dass mesoskalige und sub-mesoskalige Dynamik die Verteilung und Aktivität von Anammox die Denitrifizierung in OMZ Gewässern beeinflusst. Diese Arbeit hebt ausserdem die Bedeutung der Sauerstoffdynamik als einen indirekten Regulator von Stickstoffverlust in OMZs, sowie die Anfälligkeit von Regionen wie dem BoB auf den Klimawandel und anthropogene Eutrophierung hervor.

Acknowledgements

Undoubtedly, this work would not have been possible without the unwavering support and advice of so many of my friends and colleagues. I would like to first thank Marcel Kuypers for the professional support over the years and the research opportunity that afforded me a chance to not only travel the world, but to carry out cutting edge research. I am also incredibly grateful to Gaute Lavik, Laura Bristow, Tim Ferdelman, Casey Hubert, Sten Littmann and Bernhard Fuchs who offered valuable guidance with respect to drafting manuscripts, as well as the technical expertise and knowhow to carry out experiments.

I owe a wholehearted thanks to all past and present members of the Biogeochemistry group as friends and as colleagues you have supported me along the way, and perhaps most importantly -- provided a life outside of the lab. I would especially like to thank Niels Schoffelen, Clara Martínez Pérez, Jon Graf, Jasmine Berg, Soeren Ahmerkamp, Nadine Lehnen, Caroline Buckner, Philipp Hach, Katharina Kitzinger, Dima Meier, Adrien Assie and Mario Schimak. I can recall many fond memories and no doubt we shared a steady stream of laughs over the years.

This work was enabled by the financial support of the Max Planck Gesellschaft, the Sonderforschungsbereich (SFB754) GEOMAR and by a scholarship from the Natural Sciences and Engineering Research Council of Canada (NSERC). I thank the captain, crew and fellow scientists of the *RV Meteor* (M90 and M93 research campaigns off the coast of Peru) and the *RV Sagar Kanya* (SK308 expedition off the coast of India), who provided the technical assistance needed for sampling the ocean.

I am especially fortunate to have such a supportive and loving family back home in Canada; my parents Marg and Dave Callbeck, my brother and sister James and Christyne Callbeck. Of course, it can be challenging integrating into another country for that I would like to express a warm thanks to Hannes Eirund, Helmut Eirund and Gerlinde Schreiber who have been patient with my German and who have welcomed me with open arms into their family. Finally, I would like to thank Gesa Eirund who has been there for me no matter what, through the ups, and through the arduous times at the lab that happen on occasion.

Content

INTRODUCTION

Distribution of anammox and denitrification activity in oxygen minimum zones

In the modern ocean, the conveyor-belt circulation controlled by a combination of wind-driven and thermohaline currents maintains an oxygenated ocean, with the exception of eutrophic regions called oxygen minimum zones (OMZs). OMZs, at an O_2 cutoff of < 20 µmol kg^{-1}, make up less than 1% of the global ocean volume (1) (Fig. 1). Water column oxygen dynamics are controlled by the physical processes that ventilate OMZ waters and by the biological processes that both produce and consume dissolved oxygen (2). Nutrient upwelling along continental margins drives high primary productivity in surface waters of OMZs. Consequently, the enhanced downward flux of organic matter and its remineralization due to respiratory processes draws down water column oxygen concentrations, yielding deficits in dissolved oxygen relative to productive, often oversaturated surface waters. Such subeuphotic zone oxygen deficits are seen in many of the world's productive oceans (2, 3). In OMZs, however, such as in the Eastern Tropical South Pacific (ETSP), the Eastern Tropical Northern Pacific (ETNP), the Eastern Tropical South Atlantic (ETSA), the Arabian Sea and the Bay of Bengal (Fig. 1), high rates of organic matter export combined with poor regional ventilation exacerbates this deficit (4). Consequently, oxygen concentrations within OMZs often fall below the detection limit (<1-10 nM O_2) of even the most sensitive oxygen sensors (5, 6). These zones are defined as 'functionally anaerobic/anoxic' (7). Though, notably, vertical mixing processes, can periodically introduce oxygen into the OMZ (6-9).

The high productivity of surface waters associated with OMZs supports some 17% of global fish catches (10). The deeper waters within OMZs, in contrast, generally preclude Eukaryotic life, except for such organisms that carry special low-oxygen adaptions (11). Nevertheless a diverse assemblage of microorganisms thrives in the absence of dissolved oxygen. These microorganisms may use the alternative terminal electron acceptor nitrate, leading to the microbial conversion of fixed inorganic nitrogen to its more inert form, N_2 gas (denitrification). If nitrate becomes depleted, microbial sulfate reduction becomes favorable (12). OMZ shelf sediments, which experience high rates of organic matter deposition, are dominated by sulfate reduction (13-17). The end-product of sulfate reduction – hydrogen sulfide – may be released into the overlying anoxic water column,

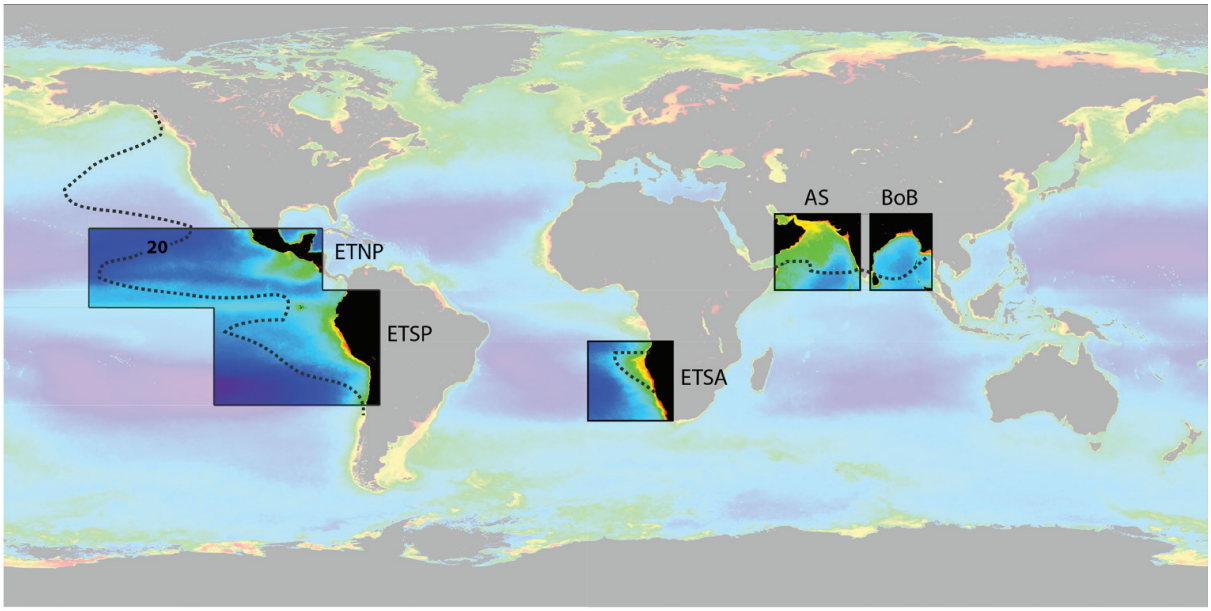

Fig. 1. Distribution of chlorophyll and major oxygen minimum zones. A ten-year surface chlorophyll composite; the image is courtesy of NASA ocean color. Abbreviated OMZ names are as follows: ETNP; Eastern Tropical North Pacific, ETSP; Eastern Tropical South Pacific, ETSA; Eastern Tropical South Atlantic, AS; Arabian Sea, and BoB; the Bay of Bengal. The minimum O_2 value of 20 µmol kg^{-1} (dotted line) is used to delineate the boundary of the OMZs, as defined by Lam and Kuypers (74).

where it accumulates in bottom waters. Such "sulfidic events" are not only toxic to eukaryotic life, but may accelerate water column fixed nitrogen loss due to denitrification (18-20).

Canonical denitrification, either chemolithoautotrophic or heterotrophic, was for many years considered to be the main nitrogen loss process contributing to the fixed nitrogen deficit relative to the expected Redfield N:P stoichiometry in OMZs (21, 22). Not until the emergence of a modified ^{15}N-stable isotope technique in the early 2000's (23) was the alternative nitrogen loss pathway, anammox (Anaerobic Oxidation of Ammonium with Nitrite), discovered in marine sediments and water columns (23-25). Later, anammox was shown to dominate in OMZs (26-35) – fulfilling a key missing link in the N-cycle. OMZs, together account for some 30-50% of global oceanic nitrogen loss, despite comprising only a minor fraction of the ocean volume (21, 36).

OMZs have been expanding over the past 50-years as indicated by time series measurements of dissolved oxygen (37), with many models projecting that this trend continues into the Anthropocene epoch in response to increasing human activity (38, 39). Global warming will lower the solubility of oxygen in water (37, 40). Furthermore, increased anthropogenic nutrient inputs (introduced by fluvial or by atmospheric deposition), stimulates primary productivity and organic matter respiration in the water column (41-43). Both vehicles could accelerate trends toward lowered oxygen concentrations, turning OMZs into even larger sinks of fixed nitrogen (44, 45). How these systems respond to climate change will, however, vary depending on the OMZ.

OMZ hydrodynamics and nitrogen loss

Eastern boundary upwelling OMZs, such as the ETNP, ETSP, and ETSA (Fig. 1), are maintained by regional trade winds that drive Ekman transport along the continental margin (4). In the ETSP region, for example, the perennial coastal upwelling of cold nutrient loaded waters, driven by the Peru-Chile undercurrent, sustains some of the highest rates of primary production in the ocean (10) (Fig. 2a, b). The organic matter export combined with the long residence time (1-10 years (31, 46)) maintains a ~700 m thick OMZ (47), with a core reporting oxygen concentrations of <1-10 nM (6, 7). The functionally anoxic ETSP waters in combination with the high organic matter export supports 25% of global water column nitrogen loss (46, 48), making it a significant player in the marine nitrogen budget.

Located in the north Indian Ocean is the Bay of Bengal and Arabian Sea OMZs (Fig. 1). The upwelling in these regions is driven by the southwesterly summer monsoon winds that promote moderate to high chlorophyll *a* concentrations in surface waters (Fig. 1), and subside during intermonsoon periods (49, 50). Like the ETSP region, the Arabian Sea sustains broad functionally anoxic zones (30), and significant nitrogen loss (albeit roughly half of the nitrogen loss as compared to the ETSP region) (46). In contrast, the weaker winds in the Bay of Bengal appear to curtail vertical upwelling, and thus, reduce primary productivity and subsequent oxygen consumption (51). The Bay of Bengal, therefore, reports low but persistent oxygen concentrations (< 2 μM O_2) that are, at or just above, the detection limit of conventional oxygen sensors (52). Geochemical estimates of nitrogen loss are scarce in the Bay of Bengal, but the few measurements that exist indicate no clear evidence of nitrogen loss (3, 53, 54), possibly because the geochemical indicators of nitrogen loss are diluted by the large fluvial input into the Bay (i.e. from the Ganges river). Thus, it is remains unclear whether the Bay of Bengal supports active nitrogen loss. Nevertheless, the Bay of Bengal, like the Arabian Sea, are enclosed by highly populated and agriculturally intensive regions, and are arguably the most susceptible of the major OMZs to anthropogenic induced eutrophication (43).

Apart from large-scale upwelling that drives coastal primary productivity along the continental margin (Fig. 1 and 2a, b), a cursory inspection of remote sensing imagery also shows that chlorophyll is variable at small spatial (<100 km) and temporal (days-weeks) scales in OMZ waters (55, 56), as exemplified in Fig. 2b. These heterogeneous chlorophyll patterns hint at the presence of much finer regional hydrodynamics, including submesoscale fronts (<10

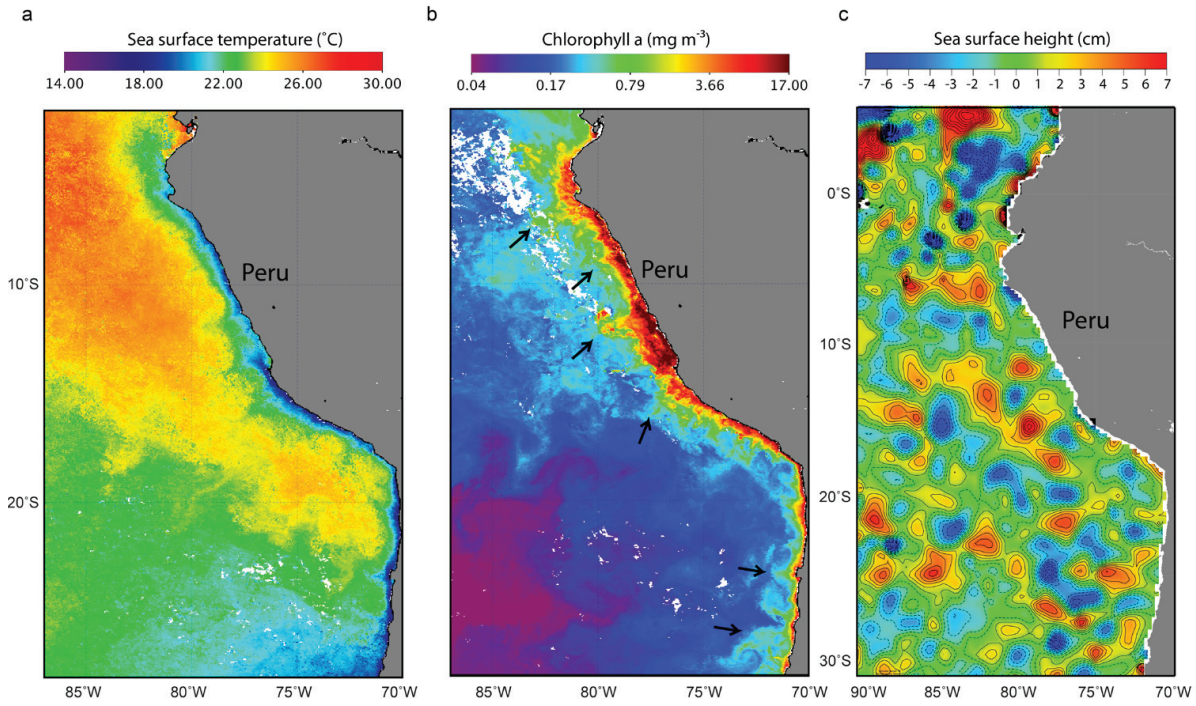

Fig. 2. Coastal upwelling and the distribution of chlorophyll and mesoscale eddies in the ETSP region. (a, b) Monthly composites of sea surface temperature and chlorophyll from MODIS data on February, 2007. Note that the low sea surface temperature along the continental margin is diagnostic of regional coastal upwelling. (c) Sea surface height altimetry, taken on February 22, 2007, indicates the presence of mesoscale eddies; negative and positive anomalies indicate cyclonic and anticyclonic eddies, respectively.

km) and mesoscale eddies (~50-200 km), which are ubiquitous features in the ocean (57-60). In the ocean, eddies drive significant vertical transport that deliver nutrients from deeper waters to the photic zone, stimulating primary production. In the North Atlantic, mesoscale eddies cause the formation of large phytoplankton blooms (58, 61, 62). Two-way eddy-driven vertical transport also acts to subduct significant amounts of particulate organic matter and oxygen below the ocean mixed layer (60, 63). Moreover, the large eddy-driven annular velocities contribute to the lateral transport and redistribution of nutrients, including the long distance dispersal of organisms (61, 64, 65). Thus, in the ocean, eddy-driven horizontal and vertical transport processes introduce a high degree of spatial-temporal variance that plays an important role regulating ocean primary production (58, 66, 67).

Mesoscale eddies are also widespread and persistent features of OMZs (68). In the ETSP region, mesoscale eddies comprise 50% of surface waters as seen from remote sensing altimetry (e.g. Fig. 2c) (69). In OMZ waters, eddy-induced vertical transport mechanisms (***Chapter 3***) have been suggested to enhance primary productivity by replenishing nutrients to surface waters (70, 71). In addition, the eddy-induced horizontal advection facilitates the cross-shelf transport of nutrients into the offshore OMZ (55, 72). Thus, mesoscale eddy activity (through both vertical and horizontal transport) potentially underpins OMZ primary production and organic matter export. It is organic matter export that drives oxygen dynamics and nitrogen loss in OMZs, a topic that I will briefly review below.

Nitrogen loss pathways and the N-cycle

Fluxes of organic matter are central to nitrogen loss in OMZs. They sustain low-oxygen concentrations, and hence, the use of alternative electron acceptors, such as nitrate (Fig. 3a). Anaerobic ammonium oxidation (anammox)

$$NH_4^+ + NO_2^- \rightarrow N_2 + 2H_2O \quad [Eq.\ 1]$$

and denitrification

$$8NO_3^- + 5C_2H_3O_2^- + 3H^+ \rightarrow 4N_2 + HCO_3^+ + 4H_2O \quad [Eq.\ 2]$$

mediate the removal of fixed nitrogen substrates ammonium, nitrite and nitrate (Fig. 3b). Organic matter provides the reduced matter needed to drive nitrate reduction by heterotrophic denitrifying bacteria (Eq. 2). In turn, the remineralization of organic matter produces ammonium – a key substrate for anammox (31, 73, 74). While the broad anoxic zones of the OMZ support extensive anammox and denitrification activity, the upper oxycline and the periodic oxygen intrusions introduced by mixing processes, also enable the overlap of aerobic and anaerobic processes illustrated in Fig. 3a (6, 7, 9, 75, 76). Here, the oxidative branch of the microbial nitrogen cycle including aerobic ammonium

$$NH_3 + 1.5O_2 \rightarrow HNO_2 + H_2O \quad [Eq.\ 3]$$

and nitrite oxidation

$$NO_2^- + 0.5O_2 \rightarrow NO_3^- \quad [Eq.\ 4]$$

processes play a role in controlling the availability of nitrate and nitrite for anammox and denitrification (Fig. 3b).

Denitrification occurs in both *Bacteria* and *Archaea* across a wide variety of lineages, consisting of mostly facultative microbes that utilize nitrate as an alternative to aerobic or fermentative growth (77). The activities of heterotrophic bacteria are fueled by the availability of organic matter and its quality. Preferred organic substrates generally include labile organic matter such as volatile fatty acids (78-80). Heterotrophic denitrification of nitrate to N_2 is carried out in a stepwise fashion through a number of intermediate oxidation state oxy-nitrogen species ($NO_3^- \rightarrow NO_2^- \rightarrow NO \rightarrow N_2O \rightarrow N_2$). This set of stepwise reductions can be carried out by a single microbe or involve a bacterial consortium (77). In dissimilatory nitrate reduction, once nitrate is transported into the cell, it is reduced with two electrons to form nitrite by either a membrane-bound (Nar) or periplasmic (Nap) NO_3^- reductase complex, although some microbes may have both (74, 81, 82). Produced nitrite is then reduced by the NO_2^- reductase (Nir) to form NO, which is further reduced to N_2O with the membrane-bound NO reductase complex (Nor). Each step requires one electron (77). Lastly, N_2O is reduced with one electron to generate N_2 catalyzed by the N_2O reductase (Nos) (77). Many microbes are capable of nitrate reduction to N_2, whereas others may lack the complete pathway (e.g. (83)), producing nitrite via the following stoichiometry:

$$4NO_3^- + C_2H_3O_2^- \rightarrow 4NO_2^- + 2HCO_3^- + H^+ \quad [Eq.\ 5]$$

Indeed, nitrate reduction to nitrite is considered an independent process in OMZs (73). Other denitrifying bacteria may produce N_2O – a potent greenhouse gas – as the terminal end product of nitrate reduction. Both nitrite and N_2O have been observed to accumulate in OMZ waters (3, 7, 31, 75, 84, 85).

Denitrification coupled to sulfide oxidation

$$2NO_3^- + 5HS^- + 7H^+ \rightarrow N_2 + 5S^0 + 6H_2O \quad [Eq.\ 6]$$

is also prevalent in OMZs (18). Sulfide-oxidizing nitrate-reducing bacteria grow by assimilating either inorganic or organic carbon for growth as chemolithoautotrophs or chemolithoheterotrophs, respectively. Chemolithoautotrophic bacteria are considered to dominate the oxidation of sulfide containing shelf waters, because sulfidic waters are often associated with elevated rates of carbon fixation (18-20). Key sulfide-oxidizing denitrifying bacteria associated with sulfidic OMZ waters include the gammaproteobacteria SUP05 clade and the genus *Arcobacter* in the epsilonproteobacteria (18, 19, 86). Sulfur cycling and associated microbes in OMZs are further reviewed in ***Chapter 4***.

Nitrate can also be reduced to produce ammonium a process known as dissimilatory nitrate reduction to ammonium (DNRA) (Fig. 3). Like denitrification,

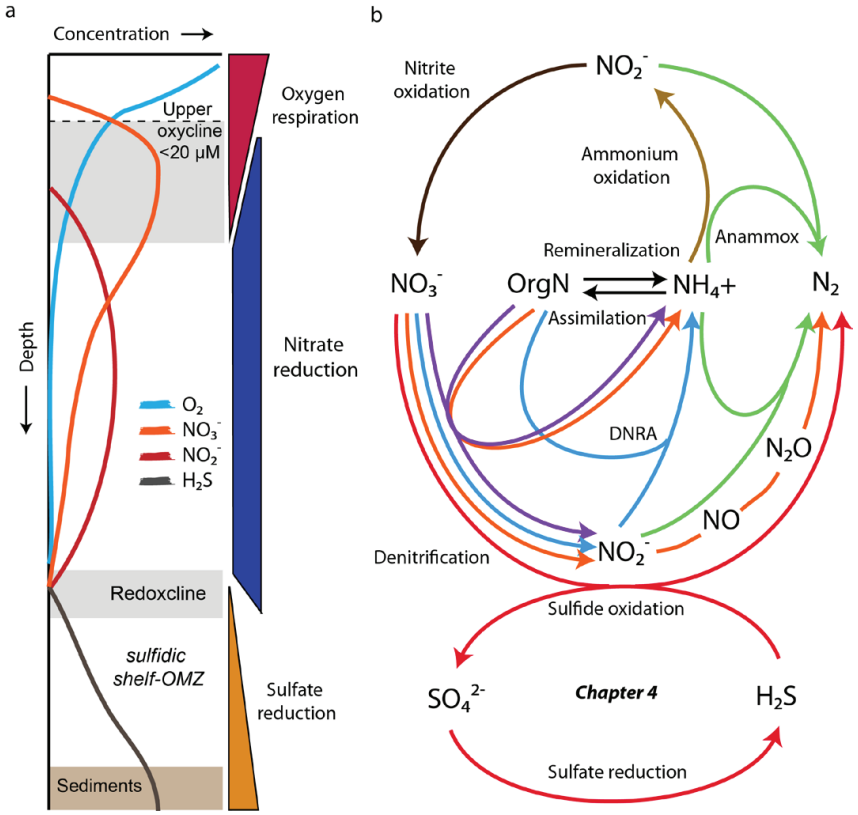

Fig. 3. Chemical zonation and nitrogen cycling pathways associated with shelf waters of oxygen minimum zones. (a) Characteristic biogeochemical profile of an OMZ. Concentrations of oxygen, nutrients, and sulfide are shown as a function of depth. The upper grey box indicates the region where aerobic (nitrification) and anaerobic (anammox, denitrification, DNRA, nitrate reduction to nitrite) N-cycling processes might overlap (0-20 µmol L^{-1}). (b) Anammox (green) and denitrification (orange/red) pathways both contribute to N_2 production. Denitrification and DNRA (blue) are the stepwise reduction of nitrate to N_2 and ammonium, respectively. Nitrate reduction to nitrite (purple) is considered a standalone process. Nitrate reduction is either coupled to organic matter (heterotrophy; orange) or sulfide oxidation (chemolithoheterotrophy; red). In panel (a), the lower grey box represents the sulfide-nitrate redoxcline where sulfide-oxidizing denitrifying bacteria dominate. Sulfur cycling associated with the OMZs is further reviewed in ***Chapter 4***. Ammonium (light brown) and nitrite oxidation (dark brown) form the oxidative pathways of the nitrogen cycle. This image is adapted from references (1, 3).

DNRA can be coupled to either sulfide or organic matter oxidation.

$$NO_3^- + C_2H_3O_2^- + H^+ + H_2O \rightarrow NH_4^+ + 2HCO_3^- \quad \text{[Eq. 7]}$$

In DNRA, nitrate is reduced to form nitrite by nitrate reductase, analogous to the first step of denitrification, however, in DNRA, nitrite is reduced via the cytochrome C nitrite reductase (NrfA) to ammonium (87). Thus, DNRA does not directly contribute to fixed nitrogen loss. Both DNRA and nitrate reduction to nitrite, however, effect the availability of nitrite and ammonium for anammox (30, 31, 73).

The anammox (Eq. 1) reaction generates a moderate energy yield of $\Delta G° = -357$ kJ reaction^{-1} (88). Its autotrophic metabolism (assimilation of CO_2 into biomass) is, however, energy demanding and therefore anammox bacteria grow slowly with a doubling rate of ~11 days under laboratory conditions (89, 90). The anammox reaction takes place in intracellular anammoxosomes that are used for energy conservation (91). Once nitrite is transported into the anammoxosome it is reduced to form NO via nitrite reductase (Nir). Produced NO is then condensed with ammonium to form hydrazine (N_2H_2), catalyzed by hydrazine synthase (Hzs). Finally, hydrazine is oxidized to generate N_2 using hydrazine oxidoreductase (Hdh) (92, 93). This molecular pathway has been elucidated for *Kuenenia stuttgartiensis*, a commonly occurring genus in a subgroup composed of species mostly enriched from wastewater treatment facilities (94). The more commonly identified subgroup in marine environments is *Candidatus scalindua* (3, 24, 95-97). In OMZ waters, abundances of "*Ca.* Scalindua" bacteria generally do not exceed 4% of the microbial community,

nevertheless they contribute significantly to the removal of inorganic nitrogen from the ocean (26, 28, 74). Based on ^{15}N-labelled incubation experiments, anammox has been shown to dominate nitrogen loss processes in the ETSP (Fig. 4a), ETNP, ETSA, and the Arabian Sea OMZs (26-35).

Nitrogen loss regulation and heterogeneity

A large fraction of the requisite nitrite needed to fuel anammox activity is supplied via nitrate reduction to nitrite (31, 73). Nitrite production rates from nitrate reduction generally exceed consumption rates by anammox in OMZs, this results in the accumulation of significant nitrite concentrations (up to 9 μM) under low-oxygen conditions, referred to as "secondary nitrite maximum" (3, 31, 34, 75, 98) (Fig. 3a). Ammonium concentrations, however, are several fold lower, and most likely limit anammox activity in OMZ waters (31, 73, 74). DNRA activity can supply some of the anammox ammonium demand (30, 31, 73, 75), however, a more significant source of ammonium derives from the remineralization of sinking organic matter catalyzed by microaerobic bacteria (8, 31) (Fig. 3b).

In addition, aerobic processes nitrite and ammonium oxidation, represent important constraints on the ammonium and nitrite supplies (Fig. 3b) (9, 75). Recently it was shown that aerobic nitrification can occur at remarkably low oxygen concentrations of only a few nanomolars (9), while anammox has been found to tolerate O_2 concentrations from submicromolar to micromolar levels (76, 99), suggesting that both processes have the potential to overlap in OMZs. The formation of such overlapping niches is likely to occur in oxycline waters where anammox and nitrification activity are prominent (e.g. Fig. 3a) (9, 31, 75), and where oxygen is periodically introduced into the OMZ via vertical transport processes (6-9). Thus, the role that oxygen plays in structuring OMZ community dynamics and nitrogen loss is complex. Unknown is to what degree aerobic nitrification processes restrict nitrogen loss in OMZs? In this respect, the Bay of Bengal, which contains low but persistent oxygen in the water column yet no evidence of nitrogen loss (3, 52-54), would provide an interesting test case to evaluate the effects of low oxygen on anammox.

Anammox rates are tightly constrained by organic matter export production rates (31), and therefore decrease as a function of distance from the coastal upwelling in OMZs (Fig. 2a, b and 4a). However, anammox activity, experiences a high degree of variability in OMZ waters (26-28, 31-34, 73, 100, 101). For example, a compilation of anammox rate process measurements in the ETSP region reveal that rates vary in coastal (8-250 nmol N L^{-1} d^{-1}) and offshore (0-9 nmol N L^{-1} d^{-1}; >600 m water depth) OMZ waters by orders of magnitude (27, 28, 31, 34, 73, 100). Interestingly, this variability occurs over relatively short spatial (<100 km) and temporal (few days) timescales, indicative that processes other than coastal upwelling, such as mesoscale eddies, may also contribute to regulating anammox activity.

Denitrification in OMZs exhibits similar, if not stronger spatial-temporal heterogeneity compared to anammox (27, 32, 34, 102). In the ETSP region, rates of denitrification are often below the limit of detection at most measured stations (27, 28, 31, 73), whereas at others, maximum rates can exceed anammox activity by several fold (27, 34, 100) (Fig. 4b). Dalsgaard et al., (34) find that the highest rates are often associated with elevated chlorophyll concentrations in surface waters, suggestive that episodic inputs of organic matter drive the measured rates of heterotrophic denitrification. Notably, however, ^{15}N-labelled stable isotope experiments used in these studies are unable to distinguish between heterotrophic or chemolithoautotrophic denitrification activity. Recent research highlights the potential for a cryptic sulfur cycle to be involved in offshore OMZ nitrogen loss (100). In sulfide-free offshore OMZ waters, Canfield et al., (100) measured rates of sulfate reduction along with rates of potential sulfide oxidation coupled to denitrification. In further support, a community of chemolithoautotrophic sulfide-oxidizing nitrate-reducing bacteria is consistently reported in sulfide-free offshore OMZ waters (100, 103-106), suggestive that an offshore sulfur cycle is widespread and possibly responsible

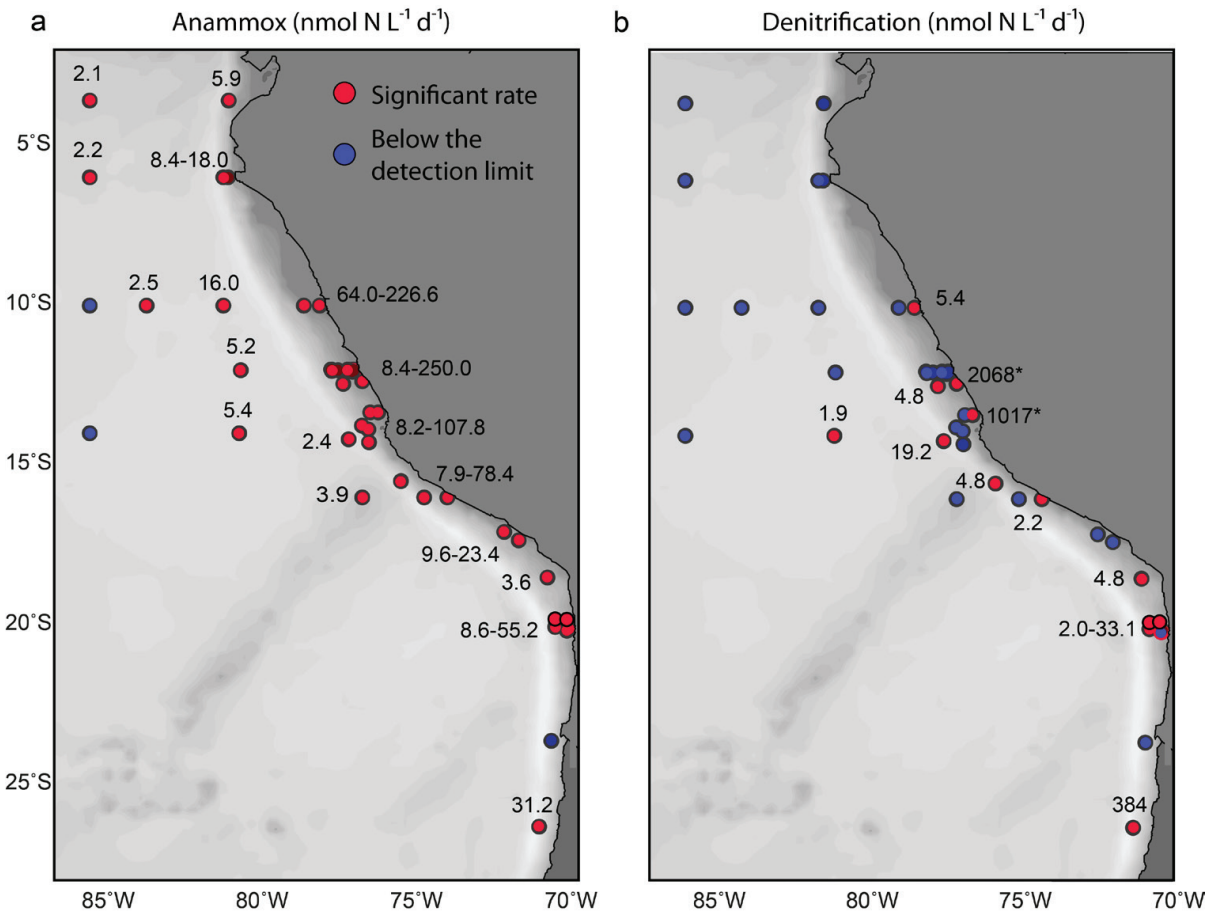

Fig. 4. Distribution and activity of water column (a) anammox and (b) denitrification rate processes from a compilation of ETSP studies: (27, 28, 31, 34, 73, 100). Maximum process rates of anammox and denitrification from ^{15}N-labelled incubation experiments are shown at each sampled station. Denitrification values indicated with an asterisk were measured in the presence of dissolved water column sulfide.

for measured rates of denitrification (100).

However, the provenance of such an offshore sulfur cycle is still contested. Stevens et al., (103) originally posited that the widespread distribution of sulfate-reducing and sulfide-oxidizing bacteria in offshore waters reflects cross-shelf transport of sulfidic shelf waters offshore. Indeed, the microbial community involved in the cryptic sulfur cycle is strikingly similar to sulfidic shelf waters (i.e. SUP05 bacteria dominated) (19, 100). Moreover, shelf waters exhibit enhanced rates of denitrification in the presence of sulfide (Fig. 4b) (19, 20). Eddy-driven cross-shelf transport processes commonly occur in ETSP waters (55, 56, 72) (e.g. Fig. 2b, black arrows). Offshore denitrification activity, often observed within 150 km from the coast, falls well within the range of many coastal protruding filaments (Fig. 4b). Whether eddy-driven cross-shelf transport enables the long distance dispersal of sulfide-oxidizing denitrifying bacteria and associated activity into the open ocean remains unknown.

Approaches to studying OMZ biogeochemistry and hydrodynamics

Mesoscale eddies, persistent and widespread features in ETSP waters have great potential to mediate the various facets of regional biogeochemistry including the distribution and activity of anammox and denitrification processes in these waters. Thus, addressing questions concerning regional distribution and activity of anammox and sulfide-oxidizing, denitrifying

bacteria calls for a multidisciplinary approach grounded on an understanding of regional hydrodynamics. Traditionally oceanographic research is conducted from research vessels where temperature, salinity and in some cases current speeds, in addition, to oxygen and nutrient concentrations are measured. Owing to advances in ocean monitoring tools, autonomous gliders and moorings that enable high-resolution profiling and improved spatial-temporal coverage can be deployed alongside research vessels. Data can also be collected remotely. Measurements of chlorophyll concentrations and sea surface height altimetry are gathered by satellite remote sensing technologies (e.g. Fig. 2). Together these approaches provide a synoptic view of OMZ hydrodynamics that includes the detection of surface and subsurface mesoscale eddies and cross-shelf advected filaments. Such real-time data helps guide station selection for more in-depth ecological and biogeochemical analyses.

Once seawater is collected, the activity and abundances of anammox and sulfide-oxidizing nitrate-reducing bacteria can be examined using various approaches. In the past decade, ^{15}N-labelled stable isotope incubation experiments have become a pivotal tool in quantifying rate processes of anammox and denitrification, as well as other N-cycling processes in OMZs (23, 25, 26, 31, 75, 107, 108). Experiments can be conducted using various ^{15}N-labelled substrates (NO_3^-, NO_2^- and NH_4^+), which can be used according to the principles of nitrogen isotope pairing (109-111), to distinguish N_2 production isotope ratios of anammox and denitrification processes. The caveat is that, care must be taken in the assignment of rates to particular processes. For example, DNRA activity coupled to anammox can mistakenly yield denitrification like N_2 production signals. These processes can only be deconvoluted if multiple substrate additions are performed in parallel (30, 109, 112). In addition, over the course of the incubation period (<48 hours) 'bottle effects' may alter the community composition. For instance denitrification activity often experiences a lag followed by a sudden increase in activity over time, hence linear rates are considered only (26, 27). With careful attention to detail, however, such incubation experiments can effectively resolve N-cycling processes in the environment where applied. In addition, ^{15}N-labelled incubation experiments can also be amended with ^{13}C-bicarbonate in order to quantify bulk rates of autotrophic carbon assimilation with the added advantage that such experiments can be later used to determine single-cell rates of uptake (113).

While, rate process measurements provide data over short time periods other avenues exist to measure cumulative nitrogen loss over larger timescales. These include geochemical tools, such as the nitrogen deficit calculated according to Redfield stoichiometry ($N_{def} = (NO_3^- + NO_2^-) - 16PO_4^{3-}$ (originally defined by (21), later modified by (70, 71)), and the dissolved N_2/Ar ratios which calculate excess N_2 production based on background levels (46, 114). These tools, unlike rate process measurements, quantify net nitrogen loss independent of the pathway, and are typically employed to estimate the role of OMZs in global N loss (21, 36, 46, 48, 114). N-cycling processes also imprint the distribution of natural abundance ^{15}N and ^{18}O isotopes of nitrate and nitrite, providing another means of distinguishing anaerobic and aerobic processes and their coupling (71, 115-117).

Information regarding the microbial community diversity and its metabolic capacity can be accessed through a number of methods. Microbial biodiversity is "quantified" using the phylogenetic 16S rRNA gene marker, which is found in all microbes. 16S rRNA genes contains slow- and fast- evolving regions, and thus affords phylum to genus level resolution (118). Recovering environmental 16S rRNA genes can involve different molecular tools, however, for highest taxonomic resolution full length sequences are recommended (119). In this respect, clone library preparations have the benefit of providing near-full length 16S rRNA gene sequences, and thus have remained a staple of microbial ecology. Next generation sequencers, such as Illumina and PacBio chemistry, have expanded the phylotype detection limits beyond what was originally possible. Currently, thousands of 16S rRNA reads can be generated from these massive parallel sequencing platforms (120). The principal drawback is that only partial 16S rRNA fragments are recovered. In combination with downstream sequencing analysis pipelines and binning methods,

it is still possible to generate draft genomes and reconstruct full length 16S rRNA gene sequences from environmental genomic DNA (121, 122). Metabolic pathways can be identified from this "metagenome", using readily available annotation tools (123-125). Metagenomic sequencing can also complement culture-dependent approaches. Cultivation, which still stands as one of the most effective techniques at understanding a microbe's physiology can be used to further disentangle a microbe's metabolic capacity and versatility under laboratory conditions (126).

Tag sequencing of 16S rRNA genes provides only a semi-quantitative analysis of species abundance. For absolute abundances one can estimate these for a target genus or group of microorganisms using either quantitative PCR (qPCR) or by florescent in situ hybridization (FISH) (127-129). While these quantification tools differ in terms of methodology, in principle, both rely on using predesigned oligonucleotide primers/probes that can be searched for in curated databases (130, 131). Or new probes can be designed *in silico* towards conserved or variable 16S rRNA gene regions targeting large microbial clusters or specific microbial genera (132). qPCR lends itself to high-throughput analysis (133). The drawback is that some microbes may contain multiple 16S rRNA gene copies in their genomes, so absolute cell densities are difficult to estimate (132). In addition, PCR based methods as well as the techniques used to extract DNA for qPCR analysis have inherent biases that can skew the microbial community profile. These biases can be minimized if multiple primers are employed. FISH enables single-cell identification via microscopy and gives direct cell counts (134). In addition, FISH can be paired with stable-isotope experiments and nanoscale secondary ion mass spectrometry (nanoSIMS) to ascertain the single-cell activity of targeted organisms (113). In this arrangement (FISH-SIMS), stable isotope incubation experiments provide a tracer of activity (e.g. ^{13}C-bicarbonate), FISH provides identification, while nanoSIMS enables nanoscale mass spectral resolution of single-cells. The isotopic cell enrichment measured by nanoSIMS can be used to determine single-cell growth rates of a target organism, revealing if a cell is active in the uptake of amended carbon and nitrogen substrates.

In summary, stable isotope incubations, FISH and FISH-SIMS provide quantitative information related to a microbe's distribution and activity, while cultivation and metagenomic techniques enable insights into an organism's metabolic potential. Information gleaned from these methods can be integrated into the framework of regional hydrodynamics.

Aims and scope

The overarching aim of this thesis is to better constrain the oceanographic and biological dynamics that shape the distribution and activity of anammox and sulfide-oxidizing nitrate-reducing bacteria in OMZ waters.

We carried out research in the ETSP and the Bay of Bengal OMZs. The Bay of Bengal is arguably one of the most heavily impacted OMZs of anthropogenic riverine and atmospheric nutrient input (42, 43). However, at present, the Bay of Bengal seems to support low, but persistent oxygen concentrations (<2 μM) at the detection of conventional methods (e.g. Winkler titration). Despite the low oxygen, the Bay of Bengal has no clear evidence of anaerobic nitrogen loss based on geochemical tools (3, 52-54), in part, because geochemical nitrogen loss signatures may be diluted by massive riverine input (e.g. from the Ganges). Thus, whether nitrogen loss is occurring in these waters remains an open question. And if these waters do support nitrogen loss, what factors constrain this system from being a major fixed N sink, like other OMZ regions. ***Chapter 2*** explores, for the first time, oxygen concentrations using the highly sensitive STOX sensor, as well as nitrogen cycling processes in the Bay of Bengal using molecular, ^{15}N-labelled stable isotope incubation experiments in combination with geochemical tools. Moreover we performed oxygen regulation experiments designed to test the sensitivity of aerobic and anaerobic N-cycling processes to varying oxygen concentrations.

In contrast the perennial upwelling in the ETSP region sustains some of the highest rates of primary production in the ocean (10), driving enhanced organic matter rain rates that maintain large functionally anaerobic zones (6, 7). In these waters a strong

correlation between anammox rates and the export of organic matter has been observed (31). However, ETSP waters exhibit extensive heterogeneity not only in nutrients such as nitrite, ammonium and nitrate, but also anammox and denitrification processes (28, 31, 34, 70, 71). In addition, in offshore ETSP waters less influenced by upwelling processes, the vertical nutrient transport mechanisms fueling primary productivity and thereby nitrogen loss remain unknown. Mesoscale eddies, ubiquitous in ETSP waters (68, 69, 135), are compelling features that potentially regulate the vertical transport of nutrients. ***Chapter 3*** investigates eddy-driven vertical-transport mechanisms and their ability to regulate regional nitrogen loss and primary production in ETSP waters. In this work, we report the first in situ rate process measurements of anammox and denitrification activity across mesoscale eddies using ^{15}N-labelled incubation experiments, moreover we analyze the distribution of chlorophyll content across such features.

Cross-shelf transport, induced by eddies developing in close proximity to the coast, may also be an important process contributing to the widespread distribution of sulfide-oxidizing denitrifying bacteria in sulfide-free offshore OMZs (100, 103, 105, 106). The presence of a widespread community of sulfide-oxidizing denitrifying bacteria in offshore ETSP waters has remained puzzling. Canfield et al., (100) have proposed that such bacteria thrive in a so-called cryptic sulfur cycle, while Stevens et al., (103) have posited that cross-shelf transport of sulfide-oxidizing denitrifying bacteria from sulfidic shelf waters may account for their widespread distribution in the sulfide-free open ocean. ***Chapters 5 and 6*** investigate the factors that govern the distribution and activity of key sulfide-oxidizing denitrifying bacteria in ETSP waters. The most commonly identified sulfide-oxidizing denitrifying bacteria in OMZs include SUP05 and *Arcobacter,* within the gamma- and epsilonproteobacteria. (A more thorough review of sulfide-oxidizing denitrifying bacteria and OMZ sulfur cycling can be found in ***Chapter 4***). To investigate their metabolic potential, activity and distribution in ETSP waters we employ cultivation, metagenomics, stable isotope incubation experiments, and single-cell analyses. Oceanographic data (e.g. current velocities and satellite sea surface height altimetry provided by autonomous glider deployments and remote sensing analysis) were used to better constrain the regional mesocale hydrodynamics and their impact on the distribution and activity of sulfide-oxidizing, denitrifying bacteria.

Finally, ***Chapter 7***, the last chapter of this thesis, provides a synopsis of the factors regulating the distribution and activity of anammox and sulfide-oxidizing denitrifying bacteria in OMZs. The outlook section of this chapter discusses the potential for mesoscale dynamics to regulate sulfidic event development and termination, as well as the potential impact of eddy-driven cross-shelf transport on anammox in OMZs. I finish this section, with suggestions on how to improve future sampling strategies in OMZs, based on findings presented in this thesis.

References

1. *Lam P & Kuypers MMM (2011) Microbial Nitrogen Cycling Processes in Oxygen Minimum Zones. Annual Review of Marine Science 3(1):317-345.*
2. *Wyrtki K (1962) The oxygen minima in relation to ocean circulation. Deep Sea Research and Oceanographic Abstracts 9(1):11-23.*
3. *Ulloa O, Canfield DE, DeLong EF, Letelier RM, & Stewart FJ (2012) Microbial oceanography of anoxic oxygen minimum zones. Proceedings of the National Academy of Sciences of the United States of America 109(40):15996-16003.*
4. *Karstensen J, Stramma L, & Visbeck M (2008) Oxygen minimum zones in the eastern tropical Atlantic and Pacific oceans. Progress in Oceanography 77(4):331-350.*
5. *Revsbech NP, et al. (2009) Determination of ultra-low oxygen concentrations in oxygen minimum zones by the STOX sensor. Limnology and Oceanography: Methods 7(5):371-381.*
6. *Tiano L, et al. (2014) Oxygen distribution and aerobic respiration in the north and south eastern tropical Pacific oxygen minimum zones. Deep Sea Research Part I: Oceanographic Research Papers 94:173-183.*
7. *Thamdrup B, Dalsgaard T, & Revsbech NP (2012) Widespread functional anoxia in the oxygen minimum zone of the Eastern South Pacific. Deep Sea Research*

Part I: Oceanographic Research Papers 65:36-45.

8. *Kalvelage T, et al. (2015) Aerobic Microbial Respiration In Oceanic Oxygen Minimum Zones. PloS one 10(7):e0133526.*

9. *Bristow LA, et al. (2016) Ammonium and nitrite oxidation at nanomolar oxygen concentrations in oxygen minimum zone waters. Proceedings of the National Academy of Sciences 113(38):10601-10606.*

10. *Carr M-E (2001) Estimation of potential productivity in Eastern Boundary Currents using remote sensing. Deep Sea Research Part II: Topical Studies in Oceanography 49(1–3):59-80.*

11. *Childress JJ & Seibel BA (1998) Life at stable low oxygen levels: adaptations of animals to oceanic oxygen minimum layers. Journal of Experimental Biology 201(8):1223-1232.*

12. *Jorgensen BB (2005) Bacteria and marine biogeochemistry. Marine geochemistry, eds Schulz HD & Zabel M (Springer, Heidelberg, Germany), Vol 2, pp 169-201.*

13. *Ferdelman TG, Fossing H, Neumann K, & Schulz HD (1999) Sulfate reduction in surface sediments of the southeast Atlantic continental margin between 15°38'S and 27°57'S (Angola and Namibia). Limnology and Oceanography 44(3):650-661.*

14. *Ferdelman TG, et al. (1997) Sulfate reduction and methanogenesis in a Thioploca-dominated sediment off the coast of Chile. Geochimica et Cosmochimica Acta 61(15):3065-3079.*

15. *Fossing H (1990) Sulfate reduction in shelf sediments in the upwelling region off Central Peru. Continental Shelf Research 10(4):355-367.*

16. *Fossing H, et al. (1995) Concentration and transport of nitrate by the mat-forming sulphur bacterium Thioploca. Nature 374(6524):713-715.*

17. *Brüchert V, et al. (2003) Regulation of bacterial sulfate reduction and hydrogen sulfide fluxes in the central namibian coastal upwelling zone. Geochimica et Cosmochimica Acta 67(23):4505-4518.*

18. *Lavik G, et al. (2009) Detoxification of sulphidic African shelf waters by blooming chemolithotrophs. Nature 457(7229):581-584.*

19. *Schunck H, et al. (2013) Giant hydrogen sulfide plume in the oxygen minimum zone off Peru supports chemolithoautotrophy. PloS one 8(8):e68661.*

20. *Galán A, Faúndez J, Thamdrup B, Santibáñez JF, & Farías L (2014) Temporal dynamics of nitrogen loss in the coastal upwelling ecosystem off central Chile: Evidence of autotrophic denitrification through sulfide oxidation. Limnology and Oceanography 59(6):1865-1878.*

21. *Gruber N & Sarmiento JL (1997) Global patterns of marine nitrogen fixation and denitrification. Global Biogeochemical Cycles 11(2):235-266.*

22. *Tyrrell T (1999) The relative influences of nitrogen and phosphorus on oceanic primary production. Nature 400(6744):525-531.*

23. *Thamdrup B & Dalsgaard T (2002) Production of N2 through anaerobic ammonium oxidation coupled to nitrate reduction in marine sediments. Applied and environmental microbiology 68(3):1312-1318.*

24. *Kuypers MMM, et al. (2003) Anaerobic ammonium oxidation by anammox bacteria in the Black Sea. Nature 422(6932):608-611.*

25. *Dalsgaard T, Canfield DE, Petersen J, Thamdrup B, & Acuna-Gonzalez J (2003) N2 production by the anammox reaction in the anoxic water column of Golfo Dulce, Costa Rica. Nature 422(6932):606-608.*

26. *Kuypers MM, et al. (2005) Massive nitrogen loss from the Benguela upwelling system through anaerobic ammonium oxidation. Proceedings of the National Academy of Sciences of the United States of America 102(18):6478-6483.*

27. *Thamdrup B, et al. (2006) Anaerobic ammonium oxidation in the oxygen-deficient waters off northern Chile. Limnology and Oceanography 51(5):2145-2156.*

28. *Hamersley MR, et al. (2007) Anaerobic ammonium oxidation in the Peruvian oxygen minimum zone. Limnology and Oceanography 52(3):923-933.*

29. *Galán A, et al. (2009) Anammox bacteria and the anaerobic oxidation of ammonium in the oxygen minimum zone off northern Chile. Deep Sea Research Part II: Topical Studies in Oceanography 56(16):1021-1031.*

30. *Jensen MM, et al. (2011) Intensive nitrogen loss over the Omani Shelf due to anammox coupled with dissimilatory nitrite reduction to ammonium. The ISME journal 5(10):1660-1670.*

31. *Kalvelage T, et al. (2013) Nitrogen cycling driven by organic matter export in the South Pacific oxygen minimum zone. Nature Geosci 6(3):228-234.*

32. *Ward BB, et al. (2009) Denitrification as the domi-*

nant nitrogen loss process in the Arabian Sea. Nature 461(7260):78-81.

33. *Bulow SE, Rich JJ, Naik HS, Pratihary AK, & Ward BB (2010) Denitrification exceeds anammox as a nitrogen loss pathway in the Arabian Sea oxygen minimum zone. Deep Sea Research Part I: Oceanographic Research Papers 57(3):384-393.*

34. *Dalsgaard T, Thamdrup B, Farías L, & Revsbech NP (2012) Anammox and denitrification in the oxygen minimum zone of the eastern South Pacific. Limnology and Oceanography 57(5):1331-1346.*

35. *Babbin AR, Keil RG, Devol AH, & Ward BB (2014) Organic Matter Stoichiometry, Flux, and Oxygen Control Nitrogen Loss in the Ocean. Science 344(6182):406-408.*

36. *Codispoti LA, et al. (2001) The oceanic fixed nitrogen and nitrous oxide budgets: Moving targets as we enter the anthropocene? Scientia Marina 65(2):85-105.*

37. *Stramma L, Johnson GC, Sprintall J, & Mohrholz V (2008) Expanding oxygen-minimum zones in the tropical oceans. Science 320(5876):655-658.*

38. *Bopp L, Le Quéré C, Heimann M, Manning AC, & Monfray P (2002) Climate-induced oceanic oxygen fluxes: Implications for the contemporary carbon budget. Global Biogeochemical Cycles 16(2):6-1-6-13.*

39. *Matear RJ & Hirst AC (2003) Long-term changes in dissolved oxygen concentrations in the ocean caused by protracted global warming. Global Biogeochemical Cycles 17(4):n/a-n/a.*

40. *Keeling RF, Körtzinger A, & Gruber N (2010) Ocean Deoxygenation in a Warming World. Annual Review of Marine Science 2(1):199-229.*

41. *Diaz RJ & Rosenberg R (2008) Spreading dead zones and consequences for marine ecosystems. Science 321(5891):926-929.*

42. Duce RA, et al. (2008) Impacts of Atmospheric Anthropogenic Nitrogen on the Open Ocean. Science 320(5878):893-897.

43. *Jickells TD, et al. (2017) A reevaluation of the magnitude and impacts of anthropogenic atmospheric nitrogen inputs on the ocean. Global Biogeochemical Cycles 31(2):2016GB005586.*

44. *Canfield DE (2006) Models of oxic respiration, denitrification and sulfate reduction in zones of coastal upwelling. Geochimica et Cosmochimica Acta 70(23):5753-5765.*

45. *Schmittner A, Oschlies A, Matthews HD, & Galbraith ED (2008) Future changes in climate, ocean circulation, ecosystems, and biogeochemical cycling simulated for a business-as-usual CO2 emission scenario until year 4000 AD. Global Biogeochemical Cycles 22(1).*

46. *DeVries T, Deutsch C, Primeau F, Chang B, & Devol A (2012) Global rates of water-column denitrification derived from nitrogen gas measurements. Nature Geosci 5(8):547-550.*

47. *Fuenzalida R, Schneider W, Garcés-Vargas J, Bravo L, & Lange C (2009) Vertical and horizontal extension of the oxygen minimum zone in the eastern South Pacific Ocean. Deep Sea Research Part II: Topical Studies in Oceanography 56(16):992-1003.*

48. *Codispoti LA (2007) An oceanic fixed nitrogen sink exceeding 400 Tg N a-1 vs the concept of homeostasis in the fixed-nitrogen inventory. Biogeosciences 4(2):233-253.*

49. *Sardessai S, Ramaiah N, Prasanna Kumar S, & de Sousa SN (2007) Influence of environmental forcings on the seasonality of dissolved oxygen and nutrients in the Bay of Bengal. Journal of Marine Research 65(2):301-316.*

50. *Wiggert JD, Hood RR, Banse K, & Kindle JC (2005) Monsoon-driven biogeochemical processes in the Arabian Sea. Progress in Oceanography 65(2–4):176-213.*

51. *Prasanna Kumar S, et al. (2002) Why is the Bay of Bengal less productive during summer monsoon compared to the Arabian Sea? Geophysical Research Letters 29(24):88-81-88-84.*

52. *Naqvi SAW, Narvekar PV, & Desai E (2005) Coastal biogeochemical processes in the North Indian Ocean (14, S-W). The Sea, eds Robinson AR & Brink KH (Harvard University Press, Cambridge, MA), Vol 14B.*

53. *Howell EA, Doney SC, Fine RA, & Olson DB (1997) Geochemical estimates of denitrification in the Arabian Sea and the Bay of Bengal during WOCE. Geophysical Research Letters 24(21):2549-2552.*

54. *Rao CK, et al. (1994) Hydrochemistry of the Bay of Bengal: possible reasons for a different water-column cycling of carbon and nitrogen from the Arabian Sea. Marine Chemistry 47(3):279-290.*

55. *Gruber N, et al. (2011) Eddy-induced reduction of biological production in eastern boundary upwelling*

systems. Nature Geosci 4(11):787-792.

56. *Nagai T, et al. (2015) Dominant role of eddies and filaments in the offshore transport of carbon and nutrients in the California Current System. Journal of Geophysical Research: Oceans 120(8):5318-5341.*

57. *Chelton DB, Schlax MG, Samelson RM, & de Szoeke RA (2007) Global observations of large oceanic eddies. Geophysical Research Letters 34(15).*

58. *Mahadevan A (2016) The Impact of Submesoscale Physics on Primary Productivity of Plankton. Annual Review of Marine Science 8(1):161-184.*

59. *McGillicuddy DJ, Anderson LA, Doney SC, & Maltrud ME (2003) Eddy-driven sources and sinks of nutrients in the upper ocean: Results from a 0.1° resolution model of the North Atlantic. Global Biogeochemical Cycles 17(2):n/a-n/a.*

60. *Levy M, Klein P, & Treguier A-M (2001) Impact of sub-mesoscale physics on production and subduction of phytoplankton in an oligotrophic regime. Journal of Marine Research 59(4):535-565.*

61. *McGuillicuddy. DJM (2016) Mechanisms of Physical-Biological-Biogeochemical Interaction at the Oceanic Mesoscale. Annual Review of Marine Science 8(1):125-159.*

62. *McGillicuddy DJ, et al. (1998) Influence of mesoscale eddies on new production in the Sargasso Sea. Nature 394(6690):263-266.*

63. *Omand MM, et al. (2015) Eddy-driven subduction exports particulate organic carbon from the spring bloom. Science 348(6231):222-225.*

64. *Mitarai S, Siegel DA, Watson JR, Dong C, & McWilliams JC (2009) Quantifying connectivity in the coastal ocean with application to the Southern California Bight. Journal of Geophysical Research: Oceans 114(C10).*

65. *Adams DK, et al. (2011) Surface-Generated Mesoscale Eddies Transport Deep-Sea Products from Hydrothermal Vents. Science 332(6029):580-583.*

66. *Lévy M & Klein P (2004) Does the low frequency variability of mesoscale dynamics explain a part of the phytoplankton and zooplankton spectral variability? Proceedings of the Royal Society of London A: Mathematical, Physical and Engineering Sciences 460(2046):1673-1687.*

67. *Klein P & Lapeyre G (2009) The Oceanic Vertical Pump Induced by Mesoscale and Submesoscale Turbulence. Annual Review of Marine Science 1(1):351-375.*

68. *Chaigneau A, Eldin G, & Dewitte B (2009) Eddy activity in the four major upwelling systems from satellite altimetry (1992–2007). Progress in Oceanography 83(1–4):117-123.*

69. *Chaigneau A, Gizolme A, & Grados C (2008) Mesoscale eddies off Peru in altimeter records: Identification algorithms and eddy spatio-temporal patterns. Progress in Oceanography 79(2–4):106-119.*

70. *Stramma L, Bange HW, Czeschel R, Lorenzo A, & Frank M (2013) On the role of mesoscale eddies for the biological productivity and biogeochemistry in the eastern tropical Pacific Ocean off Peru. Biogeosciences 10(11):7293-7306.*

71. *Altabet MA, et al. (2012) An eddy-stimulated hotspot for fixed nitrogen-loss from the Peru oxygen minimum zone. Biogeosciences 9(12):4897-4908.*

72. *Thomsen S, et al. (2016) The formation of a subsurface anticyclonic eddy in the Peru-Chile Undercurrent and its impact on the near-coastal salinity, oxygen, and nutrient distributions. Journal of Geophysical Research: Oceans.*

73. *Lam P, et al. (2009) Revising the nitrogen cycle in the Peruvian oxygen minimum zone. Proceedings of the National Academy of Sciences of the United States of America 106(12):4752-4757.*

74. *Lam P & Kuypers MMM (2011) Microbial nitrogen cycling processes in oxygen minimum zones. Ann Rev Mar Sci 3:317-345.*

75. *Fussel J, et al. (2012) Nitrite oxidation in the Namibian oxygen minimum zone. The ISME journal 6(6):1200-1209.*

76. *Kalvelage T, et al. (2011) Oxygen Sensitivity of Anammox and Coupled N-Cycle Processes in Oxygen Minimum Zones. PloS one 6(12):e29299.*

77. *Zumft WG (1997) Cell biology and molecular basis of denitrification. Microbiology and Molecular Biology Reviews 61(4):533-616.*

78. *Grigoryan AA, et al. (2008) Competitive Oxidation of Volatile Fatty Acids by Sulfate- and Nitrate-Reducing Bacteria from an Oil Field in Argentina. Applied and environmental microbiology 74(14):4324-4335.*

79. *Hubert C & Voordouw G (2007) Oil Field Souring Control by Nitrate-Reducing Sulfurospirillum spp. That Outcompete Sulfate-Reducing Bacteria for Organic*

Electron Donors. Applied and environmental microbiology 73(8):2644-2652.

80. *Canfield DE, Erik K, & Bo T (2005) The Nitrogen Cycle. Advances in Marine Biology, eds Donald E. Canfield EK & Bo T (Academic Press), Vol Volume 48, pp 205-267.*

81. *Jormakka M, Byrne B, & Iwata S (2003) Protonmotive force generation by a redox loop mechanism. FEBS Letters 545(1):25-30.*

82. *Richardson DJ (2000) Bacterial respiration: a flexible process for a changing environment. Microbiology 146(3):551-571.*

83. *Gevertz D, Telang AJ, Voordouw G, & Jenneman GE (2000) Isolation and characterization of ctrains CVO and FWKO B, two novel nitrate-reducing, sulfide-oxidizing bacteria isolated from oil field brine. Applied and environmental microbiology 66(6):2491-2501.*

84. *Arevalo-Martinez DL, Kock A, Loscher CR, Schmitz RA, & Bange HW (2015) Massive nitrous oxide emissions from the tropical South Pacific Ocean. Nature Geosci 8(7):530-533.*

85. *Naqvi SWA, et al. (2000) Increased marine production of N2O due to intensifying anoxia on the Indian continental shelf. Nature 408(6810):346-349.*

86. *Walsh DA, et al. (2009) Metagenome of a versatile chemolithoautotroph from expanding oceanic dead zones. Science 326(5952):578-582.*

87. *Einsle O, et al. (1999) Structure of cytochrome c nitrite reductase. Nature 400(6743):476-480.*

88. *van de Graaf AA, de Bruijn P, Robertson LA, Jetten MSM, & Kuenen JG (1996) Autotrophic growth of anaerobic ammonium-oxidizing micro-organisms in a fluidized bed reactor. Microbiology 142(8):2187-2196.*

89. *Strous M, Heijnen JJ, Kuenen JG, & Jetten MSM (1998) The sequencing batch reactor as a powerful tool for the study of slowly growing anaerobic ammonium-oxidizing microorganisms. Applied microbiology and biotechnology 50(5):589-596.*

90. *van Teeseling MCF, Neumann S, & van Niftrik L (2013) The Anammoxosome Organelle Is Crucial for the Energy Metabolism of Anaerobic Ammonium Oxidizing Bacteria. Journal of Molecular Microbiology and Biotechnology 23(1-2):104-117.*

91. *Lindsay MR, et al. (2001) Cell compartmentalisation in planctomycetes: novel types of structural organisation for the bacterial cell. Archives of Microbiology 175(6):413-429.*

92. *Kartal B, et al. (2011) Molecular mechanism of anaerobic ammonium oxidation. Nature 479(7371):127-130.*

93. *Kartal B, et al. (2013) How to make a living from anaerobic ammonium oxidation. FEMS Microbiology Reviews 37(3):428-461.*

94. *Schmid M, et al. (2000) Molecular Evidence for Genus Level Diversity of Bacteria Capable of Catalyzing Anaerobic Ammonium Oxidation. Systematic and Applied Microbiology 23(1):93-106.*

95. *Woebken D, et al. (2008) A microdiversity study of anammox bacteria reveals a novel Candidatus Scalindua phylotype in marine oxygen minimum zones. Environmental microbiology 10(11):3106-3119.*

96. *Schmid MC, et al. (2007) Anaerobic ammonium-oxidizing bacteria in marine environments: widespread occurrence but low diversity. Environmental microbiology 9(6):1476-1484.*

97. *Ganesh S, et al. (2015) Size-fraction partitioning of community gene transcription and nitrogen metabolism in a marine oxygen minimum zone. The ISME journal 9(12):2682-2696.*

98. *Lam P, et al. (2011) Origin and fate of the secondary nitrite maximum in the Arabian Sea. Biogeosciences 8(6):1565-1577.*

99. *Dalsgaard T, et al. (2014) Oxygen at Nanomolar Levels Reversibly Suppresses Process Rates and Gene Expression in Anammox and Denitrification in the Oxygen Minimum Zone off Northern Chile. mBio 5(6).*

100. *Canfield DE, et al. (2010) A cryptic sulfur cycle in oxygen-minimum-zone waters off the Chilean coast. Science 330(6009):1375-1378.*

101. *Beman JM, Leilei Shih J, & Popp BN (2013) Nitrite oxidation in the upper water column and oxygen minimum zone of the eastern tropical North Pacific Ocean. The ISME journal 7(11):2192-2205.*

102. *Ward BB, et al. (2008) Organic carbon, and not copper, controls denitrification in oxygen minimum zones of the ocean. Deep Sea Research Part I: Oceanographic Research Papers 55(12):1672-1683.*

103. *Stevens H & Ulloa O (2008) Bacterial diversity in the oxygen minimum zone of the eastern tropical South Pacific. Environmental microbiology 10(5):1244-1259.*

104. *Stewart FJ, Ulloa O, & DeLong EF (2012) Microbial*

metatranscriptomics in a permanent marine oxygen minimum zone. Environmental microbiology 14(1):23-40.

105. *Fuchs BM, Woebken D, Zubkov MV, Burkill P, & Amann R (2005) Molecular identification of picoplankton populationsin contrasting waters of the Arabian Sea. Aquatic Microbial Ecology 39(2):145-157.*

106. *Carolan M & Beman JM (2015) Transcriptomic evidence for microbial sulfur cycling in the eastern tropical North Pacific oxygen minimum zone. Frontiers in microbiology 6.*

107. *Trimmer M, Nicholls JC, & Deflandre B (2003) Anaerobic Ammonium Oxidation Measured in Sediments along the Thames Estuary, United Kingdom. Applied and environmental microbiology 69(11):6447-6454.*

108. *Jensen MM, et al. (2011) Intensive nitrogen loss over the Omani Shelf due to anammox coupled with dissimilatory nitrite reduction to ammonium. The ISME journal 5(10):1660-1670.*

109. *Holtappels M, Lavik G, Jensen MM, & Kuypers MMM (2011) 15N-labeling experiments to dissect the contributions of heterotrophic denitrification and anammox to nitrogen removal in the OMZ waters of the ocean. Methods in Enzymology, ed Martin GK (Academic Press), Vol Volume 486, pp 223-251.*

110. *Risgaard-Petersen N, Nielsen LP, Rysgaard S, Dalsgaard T, & Meyer RL (2003) Application of the isotope pairing technique in sediments where anammox and denitrification coexist. Limnology and Oceanography: Methods 1(1):63-73.*

111. *Nielsen LP (1992) Denitrification in sediment determined from nitrogen isotope pairing. FEMS microbiology ecology 9(4):357-361.*

112. *Kartal B, et al. (2007) Anammox bacteria disguised as denitrifiers: nitrate reduction to dinitrogen gas via nitrite and ammonium. Environmental microbiology 9(3):635-642.*

113. *Musat N, Foster R, Vagner T, Adam B, & Kuypers MMM (2012) Detecting metabolic activities in single cells, with emphasis on nanoSIMS. FEMS Microbiology Reviews 36(2):486-511.*

114. *Devol AH, et al. (2006) Denitrification rates and excess nitrogen gas concentrations in the Arabian Sea oxygen deficient zone. Deep Sea Research Part I: Oceanographic Research Papers 53(9):1533-1547.*

115. *Brunner B, et al. (2013) Nitrogen isotope effects induced by anammox bacteria. Proceedings of the National Academy of Sciences 110(47):18994-18999.*

116. *Casciotti KL, Buchwald C, & McIlvin M (2013) Implications of nitrate and nitrite isotopic measurements for the mechanisms of nitrogen cycling in the Peru oxygen deficient zone. Deep Sea Research Part I: Oceanographic Research Papers 80:78-93.*

117. *Bourbonnais A, et al. (2015) N-loss isotope effects in the Peru oxygen minimum zone studied using a mesoscale eddy as a natural tracer experiment. Global Biogeochemical Cycles 29(6):793-811.*

118. *Reeder J & Knight R (2009) The 'rare biosphere': a reality check. Nat Meth 6(9):636-637.*

119. *Yarza P, et al. (2014) Uniting the classification of cultured and uncultured bacteria and archaea using 16S rRNA gene sequences. Nat Rev Micro 12(9):635-645.*

120. *Degnan PH & Ochman H (2012) Illumina-based analysis of microbial community diversity. The ISME journal 6(1):183-194.*

121. *Strous M, Kraft B, Bisdorf R, & Tegetmeyer HE (2012) The binning of metagenomic contigs for microbial physiology of mixed cultures. Frontiers in microbiology 3:410.*

122. *Wick RR, Schultz MB, Zobel J, & Holt KE (2015) Bandage: interactive visualization of de novo genome assemblies. Bioinformatics 31(20):3350-3352.*

123. *Seemann T (2014) Prokka: rapid prokaryotic genome annotation. Bioinformatics 30(14):2068-2069.*

124. *Caspi R, et al. (2012) The MetaCyc database of metabolic pathways and enzymes and the BioCyc collection of pathway/genome databases. Nucleic Acids Research 40(D1):D742-D753.*

125. *Aziz RK, et al. (2008) The RAST Server: Rapid Annotations using Subsystems Technology. BMC Genomics 9(1):75.*

126. *Joint I, Muhling M, & Querellou J (2010) Culturing marine bacteria - an essential prerequisite for biodiscovery. Microbial biotechnology 3(5):564-575.*

127. *Zhang T & Fang HHP (2006) Applications of real-time polymerase chain reaction for quantification of microorganisms in environmental samples. Applied microbiology and biotechnology 70(3):281-289.*

128. *Callbeck CM, et al. (2013) Improving PCR efficiency for accurate quantification of 16S rRNA genes. Journal*

of microbiological methods 93(2):148-152.

129. *Pernthaler A, Pernthaler J, & Amann R (2002) Fluorescence in situ hybridization and catalyzed reporter deposition for the identification of marine bacteria. Applied and environmental microbiology 68(6):3094-3101.*

130. *Loy A, Horn M, & Wagner M (2003) probeBase: an online resource for rRNA-targeted oligonucleotide probes. Nucleic Acids Research 31(1):514-516.*

131. *Greuter D, Loy A, Horn M, & Rattei T (2016) probeBase—an online resource for rRNA-targeted oligonucleotide probes and primers: new features 2016. Nucleic Acids Research 44(D1):D586-D589.*

132. *Bustin SA & Nolan T (2004) Pitfalls of Quantitative Real-Time Reverse-Transcription Polymerase Chain Reaction. Journal of Biomolecular Techniques : JBT 15(3):155-166.*

133. *Smith CJ & Osborn AM (2009) Advantages and limitations of quantitative PCR (Q-PCR)-based approaches in microbial ecology. FEMS microbiology ecology 67(1):6-20.*

134. *Amann R & Fuchs BM (2008) Single-cell identification in microbial communities by improved fluorescence in situ hybridization techniques. Nat Rev Micro 6(5):339-348.*

135. *Chaigneau A, et al. (2013) Near-coastal circulation in the Northern Humboldt Current System from shipboard ADCP data. Journal of Geophysical Research: Oceans 118(10):5251-5266.*

CHAPTER 2

N_2 production rates limited by nitrite availability in the Bay of Bengal oxygen minimum zone

Laura A. Bristow*, Cameron M. Callbeck*, Morten Larsen*, Mark A. Altabet, Julien Dekaezemacker, Michael Forth, Mangesh Gauns, Ronnie N. Glud, Marcel M. M. Kuypers, Gaute Lavik, Jana Milucka, Syed Wajih Ahmad Naqvi, Anil Pratihary, Niels P. Revsbech, Bo Thamdrup, Alexander H. Treusch, Donald E. Canfield. (2017) N_2 production rates limited by nitrite availability in the Bay of Bengal oxygen minimum zone. *Nature Geoscience.* 10: 24-29. doi:10.1038/ngeo2847

***These authors contributed equally to the work.**

Abstract

A third or more of the fixed nitrogen lost from the oceans as N_2 is removed by anaerobic microbial processes in open ocean oxygen minimum zones. These zones have expanded over the past decades, and further anthropogenically-induced expansion could accelerate nitrogen loss. However, in the Bay of Bengal there has been no indication of nitrogen loss, although oxygen levels are below the detection level of conventional methods (1 to 2 μM). Here we quantify the abundance of microbial genes associated with N_2 production, measure nitrogen transformations in incubations of sampled seawater with isotopically labeled nitrogen compounds, and analyse geochemical signatures of these processes in the water column. We find that the Bay of Bengal supports denitrifier and anammox microbial populations, mediating low, but significant N loss. Yet, unlike other oxygen minimum zones, our measurements using a highly sensitive oxygen sensor demonstrate that the Bay of Bengal has persistent concentrations of oxygen in the 10 to 200 nM range. We propose that this oxygen supports nitrite oxidation, thereby restricting the nitrite available for anammox or denitrification. If these traces of oxygen were removed, nitrogen loss in the Bay of Bengal oxygen minimum zone waters could accelerate to global significance.

Oxygen deficient regions of the open ocean account for 20 to 40% of fixed nitrogen loss, while making up only approximately 1% (O_2 < 20 μM) of global ocean volume (1). Regions of nitrogen loss associated with oxygen depletion are presently recognized in the Eastern Tropical Pacific Ocean, off the coast of Namibia, and in the Arabian Sea (1, 2, 3). In this regard the Bay of Bengal (BoB) has proven an enigma, with no clear evidence for nitrogen loss despite oxygen depletion (< 2 μM O_2; (4)), although only geochemical indicators of nitrogen loss have been investigated to date in this region (4, 5, 6).

We sampled the BoB in January 2014 during the winter monsoon (Fig. 1; S1). At five stations we measured oxygen in situ with a highly sensitive STOX sensor (switchable trace oxygen) (7, 8), with a limit of detection (LOD) of 7 to 12 nM. We used Niskin bottles to collect samples for nutrients, dissolved gases, nitrate isotopic analyses, molecular characterization of microbial populations and for experiments exploring aerobic and anaerobic microbial nitrogen metabolism.

Oxygen levels and microbial populations in Bay of Bengal

STOX oxygen data revealed sub-micromolar oxygen concentrations over a depth interval of about 200 meters throughout the study area (Fig. 1). Only six single measurements were below the LOD, and these were confined to thin layers in the depth range between 280 and 360 m at Station 7 (Table S1). There was no evidence for distinct broad anoxic zones as seen in the other OMZs at any station, even at Station 1, where a secondary nitrite maximum of up to 180 nM was observed in the depth range 115 m to 150 m (Fig. 1a; nitrite was at or below the LOD of 10 nM at all other stations analyzed). At this station, the lowest oxygen concentration was 36 nM at ~150 m (Fig. 1; Table S1). Persistent oxygen and low nitrite in the BoB contrasts with other major OMZs, which have anoxic cores (oxygen below STOX sensor detection) with > 500 nM nitrite (9), 10. When calibrated to the STOX data (Fig. S2), a Seabird oxygen sensor revealed tremendous vertical structure in the oxygen profiles (Fig.1), indicating oxygen input by lateral intrusions.

Despite the lack of evidence for anoxia in BoB OMZ waters, the vertical zonation of microorganisms with nitrogen-metabolizing capabilities resembled typical OMZs supporting active N_2 production as indicated by 16S rRNA and functional gene abundances (Fig. 2). Anammox bacteria, as quantified through their nitrite reductase gene (*Scalindua* nirS, or *Sc nirS*), were present within the OMZ waters, peaking at the depth of 150 m with about 1300 copies mL^{-1}, some 40 to 60% of the maximal abundance found in other OMZs with active N_2 production (11, 12). Nitrite reductase genes attributed to denitrifiers (Denitrifier *nirS*) were found at similar distribution

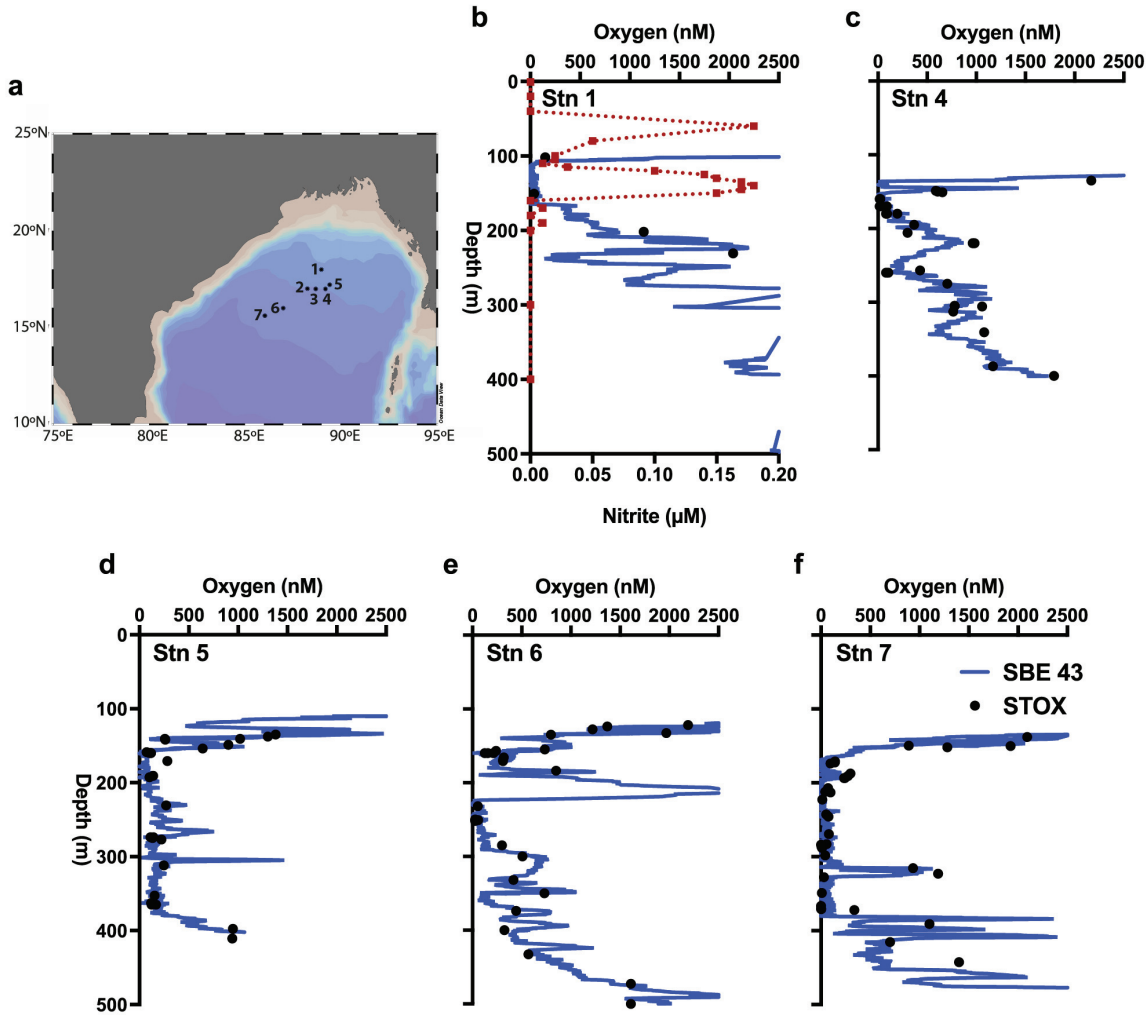

Fig. 1. Station locations and oxygen data for the Bay of Bengal. Oxygen concentration profiles focus on the upper 500 m of the water column containing the oxygen minimum zone (OMZ). Black dots represent STOX oxygen data, while the blue line represents Seabird oxygen data, calibrated with the STOX data at the low oxygen levels. At Station 1 (a), nitrite concentrations are indicated by the red line (a distinct primary nitrite maximum in the oxic upper 100m, and a secondary nitrite maximum under nanomolar oxygen concentrations). Nitrite was not detected at any of the other stations.

and abundance to the *Sc nirS*, and were even more abundant than in the Eastern Tropical South Pacific (ETSP) OMZ (11, 13). In addition, the distribution of functional genes of aerobic ammonium and nitrite oxidizers, thaumarchaeotal *amoA* (Th *amoA*) and *Nitrospira/Nitrospina nxrB* (*nxrB*) respectively, resembled the distributions in other OMZ waters (11, 13, 14, 15), where Th amoA abundance peaks in the upper oxycline, here at about 80 m, and *nxrB* abundance peaks lower in the water column where *Sc nirS* is also most abundant. The similarity with other OMZs was further supported by the presence of the SUP05 clade, gammaproteobacterial sulfur oxidizers (GSO), and abundant adenylylsulfate (APS) reductase genes (*aprA*), suggesting a role for sulfur cycling in the BoB OMZ waters (16) (Fig. S3).

Activity of microbial nitrogen transformations

Thus, microbial populations in BoB OMZ waters are capable of both anaerobic and aerobic nitrogen (and maybe sulfur) cycling as in other OMZs supporting N_2 production, despite a lack of any prior evidence

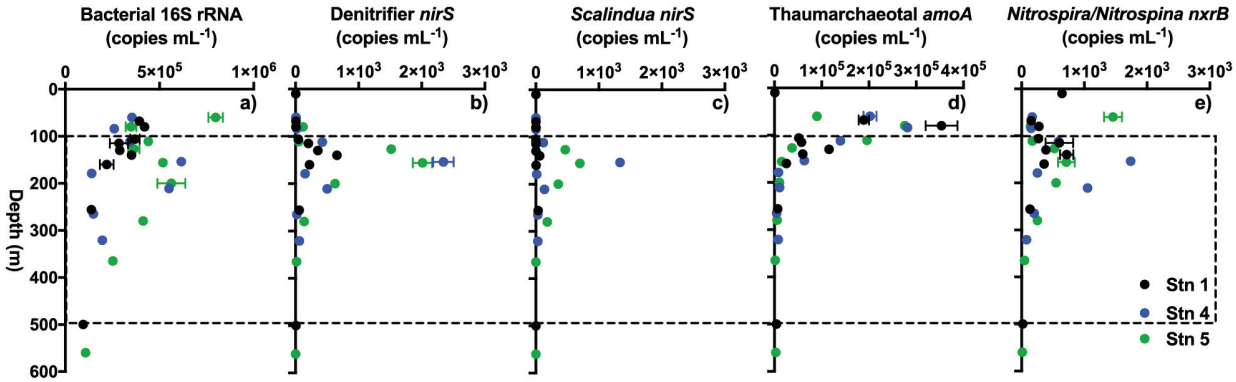

Fig. 2. Abundance of bacterial 16S rRNA and selected functional genes in the Bay of Bengal. Copy numbers were obtained with qPCR using primer sets as shown in Table S3. Shown are total copies of bacterial 16S rRNA (a), nitrite reductase genes attributed to denitrifiers (Denitrifier *nirS*; b) and to anammox bacteria (*Scalindua, Sc nirS*; c), thaumarchaeotal ammonia monooxygenase (Th *amoA*; d) and *Nitrospira/Nitrospina* nitrite oxidoreductase (*nxrB*; e). The dashed rectangle outlines the approximate depth interval where oxygen concentrations drop below 2.5 µM. Error bars represent the standard deviation. Note variability in x axes scales.

for N_2 production. We performed parallel experiments with ^{15}N-labeling to survey rates of microbial nitrate reduction and N_2 production in BoB OMZ waters (process rate experiments). With additions of $^{15}NH_4^+$ alone, anammox ($NH_4^+ + NO_2^- \rightarrow N_2 + 2H_2O$) rates were below detection (LOD 1.3 nM N d^{-1}) at all stations. Anammox rates of up to 6.2 nM N d^{-1}, however, were observed when NH_4^+ and NO_2^- were added together, with labeling of either of the substrates (Fig. 3a; S4). These potential rates are comparable to off-shore locations in the OMZs of the ETSP (13) and Eastern Tropical North Pacific (ETNP)(17).

Anammox was also detected at rates of up to 5.5 nM N d^{-1} in separate experiments designed to explore the oxygen regulation of nitrite transformations (oxygen regulation experiments) where $^{15}NO_2^-$ was added alone (Fig. 3b). Anammox activity decreased with increasing oxygen concentrations in three of the four experiments, but activity was observed up to our maximum concentration of 9.5 µM, in line with a number of previous observations (18). Indeed, anammox rates remained high across the oxygen concentrations of the BoB OMZ. Summarizing our results, anammox was not measurable when ammonium was added alone, but was only detected with added nitrite. Thus, there is a large potential for N-loss via anammox in the BoB, but in situ anammox bacteria are likely nitrite-limited rather than being limited by ammonium or inhibited by oxygen. Denitrification was below the LOD (2.7 nM N d^{-1}) in BoB OMZ waters in our process rate experiments (Fig. 3A). We did, however, detect denitrification (up to 0.9 nM N d^{-1}) with $^{15}NO_2^-$ at Station 5 (but not Stations 1 or 4) in our oxygen regulation experiments with a lower median detection limit of 0.4 nM N d^{-1} (Fig. 3b), suggesting a patchy distribution of denitrification in BoB OMZ waters. When present, denitrification exhibited higher oxygen sensitivity than anammox (Fig. 3b), with complete inhibition at O_2 concentrations above 4-5 µM (with a single point deviating from this trend), consistent with observations from the ETSP OMZ (19).

Despite the low rates of anammox and denitrification, and the general absence of nitrite in BoB OMZ waters, we measured nitrite production rates from nitrate ($^{15}NO_3^-$) of up to 12.1 nM N d^{-1} at Stations 4 and 5 (Fig. 3a). We also measured potential nitrite oxidation rates of up to 52 nM N d^{-1} in our oxygen regulation experiments (Fig. 3b; Table S2). The presence of nitrite-oxidizing bacteria was confirmed by the detection of *Nitrospira/Nitrospina*-related *nxrB* sequences (Fig. 2). The rates of nitrite oxidation exceeded those of nitrite production even at low oxygen concentrations, reaching maximum values at ~1 µM O_2, suggesting nitrite oxidizing bacteria have a high affinity for oxygen (Fig. 3a) in agreement with

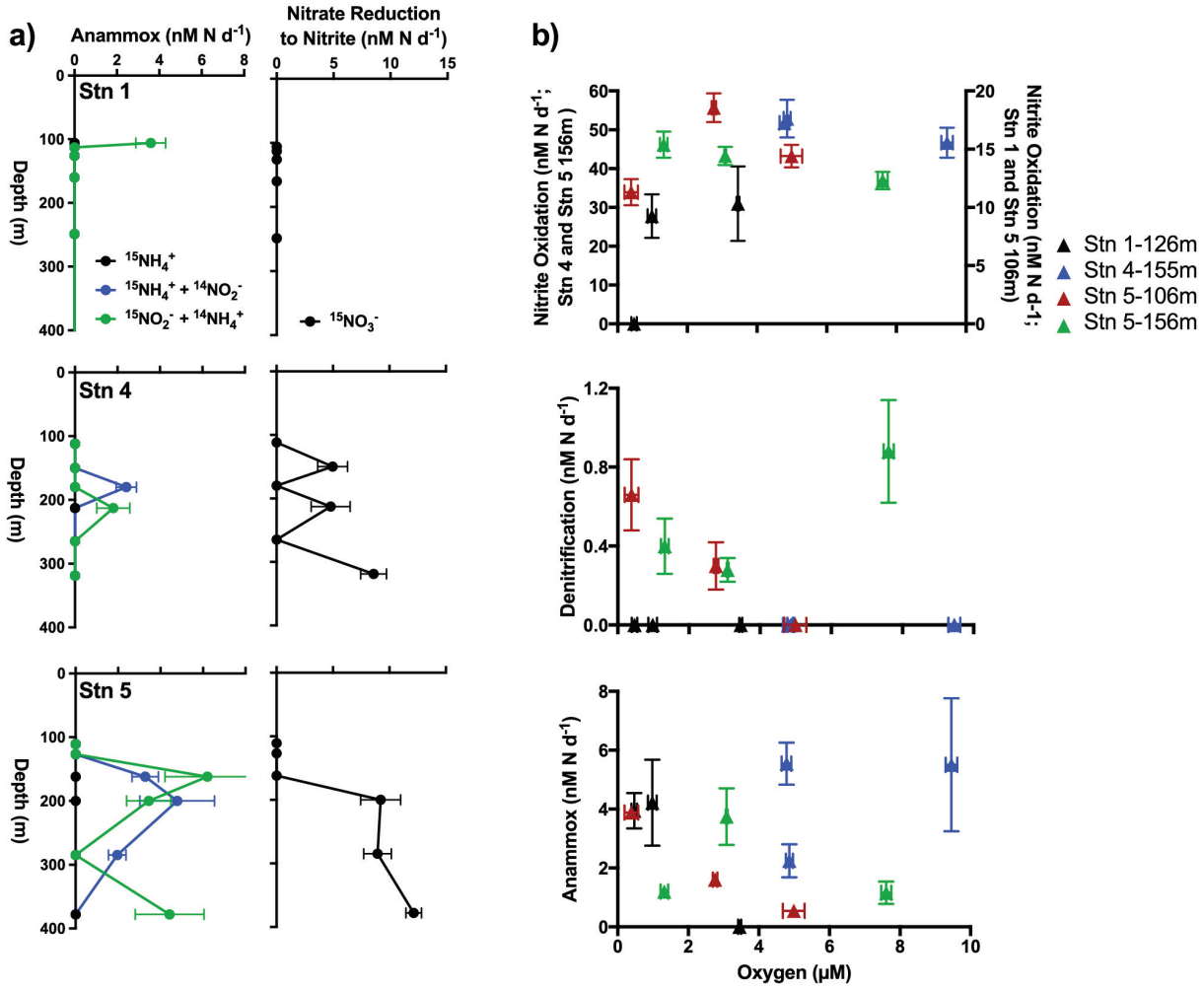

Fig. 3. Depth profiles and regulation experiments of N transformations in the Bay of Bengal a) Process rate experiments showing rates of anammox and nitrate reduction to nitrite using ^{15}N labeling experiments. Denitrification was below detection in these experiments: b) Experiments using ^{15}N-labeled nitrite to explore the oxygen regulation of nitrogen transformations. The top panel shows the oxygen regulation of nitrite oxidation (note the use of both y axes), the middle panel shows the oxygen regulation of denitrification, while the bottom panel shows the oxygen regulation of anammox. Error bars represent the standard error.

recent observations (20). Our combined data indicate an active, coupled, anaerobic/aerobic nitrogen cycle where nitrate is reduced to nitrite and rapidly oxidized again to nitrate in the OMZ waters. A close coupling between nitrate reduction to nitrite and subsequent nitrite oxidation has also been described in the oxyclines of other OMZs, where nitrite also fails to accumulate despite active nitrate reduction to nitrite (18, 21).

Thus, based on our experimental data, we conclude that the BoB OMZ oxygen concentrations (10 to 200 nM) limit N_2 production through anammox indirectly, by enabling aerobic nitrite oxidizing bacteria to outcompete anammox bacteria for the available nitrite. Denitrification was also not inhibited by the oxygen levels of BoB OMZ waters, but was generally low and only detected at two stations. Such patchiness may be related to the presence or absence of organic-matter rich aggregates in the incubations (17).

Geochemical evidence of nitrogen cycling

Our molecular results and process rate measurements are supported by geochemical data that indicate a slow, but functioning, anaerobic nitrogen cycle in BoB OMZ waters. A small, albeit noisy, nitrogen deficit

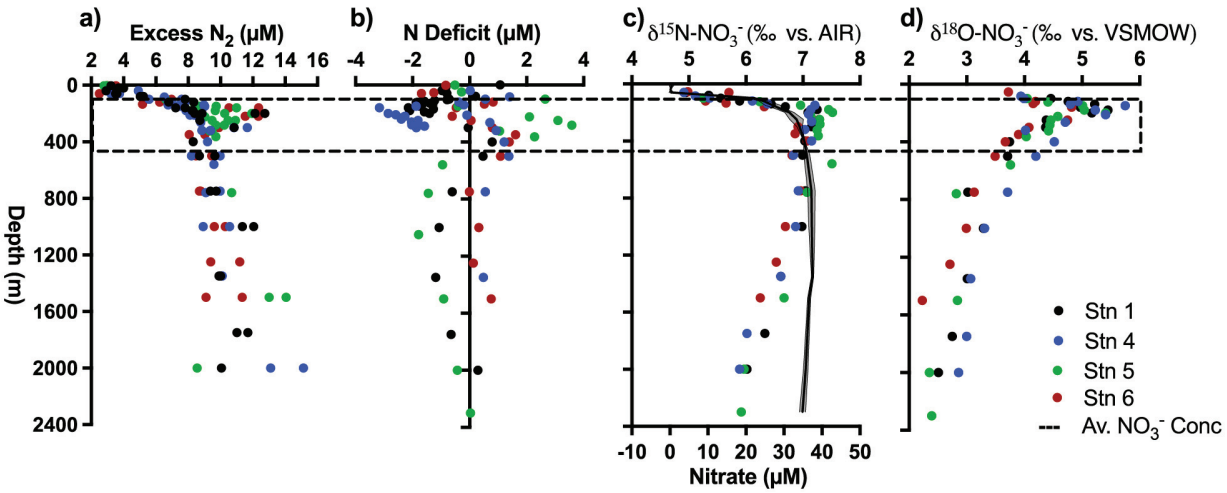

Fig. 4. Geochemical indicators of nitrogen cycling in the Bay of Bengal OMZ waters. Depth profiles of excess N_2 (calculated from N_2/Ar ratios; a), and the N deficit (b; calculated as $[NO_3^- + NO_2^-] - (N/Pbw * [PO_4^{3-}])$, with N/Pbw being the average $NO_3^- + NO_2^-$, PO_4^{3-} ratio seen in bottom waters during this cruise, which was assigned a value of 14). The $\delta^{15}N$ of nitrate, along with a depth profile of average nitrate concentrations (solid black line; grey shading shows upper and lower bounds) from all stations (c), and the $\delta^{18}O$ of nitrate (d). The dashed rectangle outlines the approximate depth interval where oxygen concentrations drop below 2.5 µM.

of 2 to 3 µM, indicative of net N loss, was calculated from our nutrient data (Fig. 4; Table S4). We also observed a maximum N_2 excess (calculated from N_2/Ar ratios) on the order of 2 to 3 µM N_2 in the OMZ waters (equivalent to 4 to 6 µM N). Throughout the sub-surface ocean, N_2 excess increases monotonically with depth due to abiotic factors (22) but a local maximum within OMZs is strongly indicative of biogenic N_2 production (23). The $\delta^{15}N$ of NO_3^- from the BoB OMZ showed small enrichments of up to 1.5‰ relative to deep-water values consistent with net nitrate reduction. The larger ^{18}O enrichment in NO_3^- of 3‰ is consistent with the coupled anaerobic/aerobic nitrogen cycle explored above, with nitrate reduction to nitrite followed by reoxidation back to nitrate (24) (see SI). These three geochemical indicators integrate over larger water volumes and over longer timescales than our rate measurements, and, therefore, imply that nitrogen cycling and N_2 production are persistent phenomena in the BoB, although these signals are smaller in magnitude than in other major OMZs (23, 24).

Taken together, our nitrogen deficit and N_2 excess measurements point to ~2 µM of biologically produced N_2 (4 µM N_2-N) in BoB OMZ waters. Previous studies have estimated annual water exchange of 18 x 10^{12} m^3 y^{-1} in the depth interval from 150 to 250 meters, and 31 x 10^{12} $m^3 y^{-1}$ in the interval from 250 to 500 m (25). We take 40% of the latter (12 x 10^{12} m^3 y^{-1}) to estimate the exchange from 250 to 350 m, obtaining a total annual water exchange of 30 x 10^{12} m^3 y^{-1} from 150 to 350 meters depth, and a turnover time of 12 years for the 372 x 10^{12} m^3 volume of this interval (25). This exchange rate, combined with a biogenic N_2 excess of 2 µM, yields an annual production rate of ~1.7 Tg N y^{-1}. This N_2 production is about 12% of the production rate in the Arabian Sea, and some 2.5% of the global water-column production in OMZ settings (66±6 Tg N y^{-1})(26).

This annual rate of N_2 production amounts to an average N_2 production rate of 0.88 nM-N d^{-1} for the volume between 150 to 350 m. As we were unable to measure N_2 production by anammox without added nitrite, and as denitrification rates were low when detected at all (Fig. 3), there must be either seasonal or spatial variability in N_2 production that we have not captured in our process rate experiments. Still, our process rate and oxygen regulation experiments (Fig. 3) suggest a potential for N_2 production of about 3 nM-N d^{-1} under nitrite replete conditions, some 3.5

times greater than the average rate calculated from the N_2 excess. Therefore, there is considerable potential for additional N_2 production in the BoB OMZ above that indicated from the geochemical indicators. As N_2 production, particularly through anammox, is nitrite limited, the rates should increase if oxygen is depleted further, suppressing nitrite oxidation and allowing nitrite to accumulate (9) in BoB OMZ waters. An accumulation of nitrite in the sub-micromolar range may be sufficient to stimulate anammox substantially, judging from the independence of anammox rates on nitrite concentrations across OMZs (27). If N_2 production increased to an average of 3 nM-N d^{-1} (as our experiments suggest), then N_2 production rates would increase to about 6 Tg N y^{-1} or about 40% of Arabian Sea rates and 9% of global water-column rates (26). Such an increase would make the BoB an important player in the global nitrogen cycle.

The Bay of Bengal at a tipping point

The stable accumulation of nitrite in BoB OMZ waters would require the removal of the last traces of oxygen. The oxygen concentration reflects the dynamic balance between the processes mixing oxygen into the OMZ and the processes consuming it. An increase in the flux of organic matter to the OMZ waters would be one way to increase oxygen consumption, and an increase in primary production could accomplish this. Possible vehicles for increased primary production include the accelerated input of anthropogenic nitrogen into the BoB, as projected for the coming decades (28) and changing intensity of the summer monsoon. In particular, the high southwesterly summer monsoon winds generate coastal upwelling, producing high concentrations of chlorophyll a (29) and enhanced oxygen depletion in coastal waters (30). Therefore, accelerated summer monsoon intensity could potentially increase the flux of organic matter to OMZ waters, drawing down oxygen and accelerating N_2 production.

However, an enhanced summer monsoon would also increase river runoff and the flux of particulates to the BoB. Riverine particulates ballast sinking organic material resulting in rapid sedimentation of labile organics through the OMZ, reducing their decomposition in OMZ waters (6). Thus, the main climate driver in the BoB, the summer monsoon, generates what appear to be opposing influences on the development of anoxia in the BoB OMZ waters. A test of summer monsoon intensity on N_2 loss in the BoB could come from current climate change as some climate models suggest future increases in the intensity of the Asian summer monsoon (31).

Historical evidence indeed suggests a potential relationship between climate change and an active anaerobic nitrogen cycle in the BoB (32). Elevated sediment nitrogen isotope values are correlated with elevated concentrations of organic matter and organic nitrogen about 42,000 years ago. These results suggest that higher rates of organic matter productivity at that time enabled a nitrogen cycle with higher N loss rates, although the driver of this relationship is unclear.

Overall, we demonstrate that the BoB is like the other well known OMZs with microbial populations supporting N_2 production, although at low rates. The BoB OMZ also maintains widespread nanomolar oxygen concentrations that inhibit the stable accumulation of nitrite, a key substrate for N-loss. If these last traces of oxygen were removed, allowing nitrite to accumulate, rates of N_2 production would increase considerably. Thus, the BoB OMZ sits at a geochemical "tipping point" where any process removing the last of the oxygen, such as anthropogenic nutrient input or climate change, would make the BoB a major player in the marine nitrogen cycle.

Methods

Samples were collected at seven stations (Table S4) in the Bay of Bengal between the 24th of January and 3rd of February 2014 onboard the ORV Sagar Kanya. Seawater samples were collected using Niskin bottles (4 x 30 L and 8 x 5 L) on a rosette containing a Conductivity Temperature Depth (CTD) profiler (SBE 9/11 – SeaBird Electronics). The CTD was furthermore equipped with a SBE 43 oxygen sensor (see below) and WET Labs ECO-AFL/FL chlorophyll sensor. A complete array of samples, hydrographic, molecular, nutrients, geochemical and rate measurements

were undertaken at stations 1, 4, and 5. At station 6, hydrographic, nutrient, geochemical and a reduced number of rate measurements were sampled for. Only hydrographic and a reduced number of rate measurements were undertaken at station 7 and, at stations 2 and 3 hydrographic profiles only.

In situ O_2 measurements

Concentrations of oxygen were measured in situ with two methods. In order to assess the possibility of true anoxia in BoB waters we used STOX (Switchable Trace amount OXygen) amperometric oxygen (7) sensors mounted to a CTD frame. The signal from the STOX sensor was recorded on a custom-made Trace oxygen profiler (TOP) (8), consisting of a 16-bit A/D converter (DT9818, Data translation) controlled by a single board computer (fit-PC2i, CompuLab) housed in a titanium cylinder. The amplification of the STOX sensor signal was performed by a custom-made amplifier and the operation of the sensor switching was controlled by a cyclic switch operating with a 40 s on/off cycle. Data was sampled at 60 s^{-1}, filtered using 1.5 s^{-1} low-pass filter, smoothed using a 5 s moving average and finally down-sampled to 1 s^{-1}. The detection limit of the STOX sensors in the given configuration was estimated to be 7-12 nM based on three times the standard deviations of the noise recorded in the zero signal. Calibration and calculations were performed as described previously (7,9).

STOX measurements were performed at Stations 1,4,5,6 and 7. At Station 1, STOX measurements were only preformed to a depth of 270 m, due to a software error. The STOX data were recorded during the up-cast (except at Station 1) and the majority of the data were recorded while the instrument was moving. Additionally, several recordings were performed while the instrument was kept at a given depth for 3-5 min. These data are not distinguishable from data recorded as the CTD moved. All STOX oxygen data are presented in Table S1.

We also measured oxygen with the SBE 43 polarographic oxygen sensor mounted on the CTD. The data from the CTD was sampled at 24 s^{-1}, low-pass filtered at 0.15 s^{-1} and down sampled to 1 s^{-1}. Only data from the up-cast was used, as typical for oxygen measurements in OMZs (e.g. ref 9), and casts were performed with a CTD speed of approximately 1 m s^{-1} below 100 m and 0.5 m s^{-1} above 100 m. The data from the SBE 43 and STOX were aligned using the pressure data recorded by both instruments.

When compared, the data from the SeaBird and STOX sensors showed excellent linearity (Fig. S2), but with a positive offset on the order of 400 to 500 nM in the SeaBird oxygen reading. In principle we could have used this offset to calibrate the Seabird data to the STOX data, but when doing so, we found that the SeaBird sensor produced a large number of negative readings at the lowest oxygen levels. Since the STOX sensor clearly showed the persistence of oxygen in the OMZ, we elected instead to align the lowest readings on the SeaBird sensor with the readings from the same depth from the STOX sensor. This ensured that the Seabird readings were always positive values, and the offset ranged from 380 nM to 450 nM at the different sites.

DNA sampling and methods

Samples for molecular biological work were collected at Stations 1, 4, and 5 at water depths ranging from 10 m to 2300 m. Between 5 and 27 L of water per depth was filtered through a 3 µm pre-filter prior to a 0.22 µm Supor® PES membrane disc filter (PALL) on which we collected material for DNA analysis. Each membrane was stored in 2.7 mL sucrose lysis buffer (SLB) at -20°C until DNA extraction.

DNA extraction

DNA was extracted after a modified version of the phenol:chloroform extraction (33). Membranes in 2.7 mL SLB were allowed to thaw at room temperature. After addition of 150 µL of lysozyme (20 mg/ml) tubes were incubated at 37 °C for 30 min under constant rotation. After this, 150 µL 20% (w/v) sodium dodecyl sulfate and 150 µL of proteinase K (20 mg/ml) were added and tubes were incubated at 55 °C for 120 min under continuous mixing. Nucleic acids were extracted with 1 volume phenol:chloroform:isoam

ylalcohol (IAA) (25:24:1) followed by centrifugation at 2,500 relative centrifugal force (rcf) for 10 min. The remaining phenol was extracted by 1 volume chloroform:IAA (24:1) followed by a centrifugation at 2,500 rcf for 5 min. Genomic DNA was precipitated with 0.1 volume of 3 M sodium acetate and 2-3 volumes of 96% ethanol, incubation at -20 °C for 8 hr. DNA was pelleted at 14,000 rcf for 45 min at 4 °C and washed with 70% ice-cold ethanol and centrifuged at 14,000 rcf for 30 min at 4 °C. The DNA was air dried at RT and resuspended in 100 µL preheated TE buffer (60 °C; pH 7.5). DNA concentrations, quality, and purity were checked spectrophotometrically (NanoDrop) and by the Quant-iT™ PicoGreen® dsDNA kit (Invitrogen).

qPCR

Copy numbers of 16S rRNA genes and functional genes were determined by qPCR using primer sets, concentrations, and specific conditions listed in Table S3. Each 20 µL reaction contained 10 µL SsoAdvanced™ SYPER® Green Supermix (Bio-Rad), 1-8 ng of template DNA and was adjusted to 20 µL final volume with nuclease-free water. Reactions were carried out in clear 96 Multiply® PCR plates (Sarstedt) and performed on a CFX Connect Real-Time System (Bio-Rad) running CFX Manager™ Software V3.0. General conditions were as follows: 98 °C for 2 min followed by 40 cycles of 98 °C for 5 s, listed annealing temperature for 15 s, 72 °C for 15 s and a plate read. Finally, a melt curve from 65 °C to 95 °C held at each 0.5 °C for 5 sec was performed to check the specificity of the reaction.

All reactions were run alongside standard curves of the corresponding gene ranging from 101 to 107 copies per µL. Mean PCR efficiencies for the standard curves are listed in Table S3 (R^2 values were all >0.99). Standards for each target gene were derived from clone libraries prepared from environmental samples with the same primers that were used for the qPCR.

Nutrients

Nitrate, nitrite and phosphate concentrations were determined following methods outlined in ref (34). The nitrogen deficit was calculated as $[NO_3^- + NO_2^-] - (N/Pbw * [PO_4^{3-}])$, with N/Pbw being the average $NO_3^- + NO_2^-$, PO_4^{3-} ratio seen in bottom waters during this cruise, which was 14. Nutrient data is presented in Table S4. It is important to note here the weakness in using the N deficit in these waters. The various source waters, water masses, riverine input, and monsoonal rains are poorly constrained, and likely have varying N/P ratios, which could impact the N deficit calculation.

Excess N_2: Sampling and Analysis

Samples for high precision N_2/Ar measurements for the determination of biogenic N_2 were collected and analyzed following the protocol outlined in ref (35). Samples were collected bubble-free in 60mL serum bottles, preserved with 100 µL of saturated $HgCl_2$ and stored at ambient temperature until analysis. Analyses were carried out on a custom-made on-line gas extraction system coupled to a multicollector IRMS (GV Isoprime). Oxygen was removed during gas purification by a hot copper furnace to avoid artifacts associated with varying N_2/O_2. Calibration was achieved through reference gas injections (N_2+Ar) and air equilibrated water standards of known temperature and salinity (35). To assess the contribution from biogenically produced N_2 an additional background correction was applied. This was done by subtracting values from waters uninfluenced by N loss processes (23,36). In our study, no stations outside of the low-oxygen region were sampled, so background data was taken from the WOCE 107N line (23,36).

Samples collected at depth (temperature 3 to 10 oC) showed unusually high excess N_2. Increases with depth may be expected due to bubble injection during water mass formation (22), but should have been accounted for within the background correction. Samples were analyzed within 4 months of collection, at which time the integrity of the excess N_2 measurements should not have been compromised based on sample longevity tests (35). However the longevity tests were conducted with storage at room temperature and not elevated and fluctuating temperatures as our

samples likely experienced during transport. Storage effects will be highly dependent on the temperature difference between that observed in situ and that experienced during storage. As temperature in the open ocean has a clear monotonic distribution, we therefore also expect the residual excess N_2 as a result of storage to follow a similar distribution whereas a peak of excess N_2 in the shallower, warmer, low oxygen waters would suggest a biogenic signature from processes occurring in situ. Results are presented in Table S4.

Nitrate Isotopes

Samples for $\delta^{15}NNO_3$ ($\delta^{15}N$ (‰ vs. atmospheric N_2) = [($^{15}N/^{14}N$)NO_3/($^{15}N/^{14}N$)N_2-1] x 1000) and $\delta^{18}ONO_3$ ($\delta^{18}O$ (‰ vs. VSMOW) = [($^{18}O/^{16}O$)NO_3/($^{18}O/^{16}O$) VSMOW-1] x 1000) were collected in 60 mL acid-washed HDPE bottles and stored frozen until analysis. Samples were analyzed by cadmium reduction to NO_2^- followed by reduction to N_2O with azide (37, 38). Pre-existing NO_2^- was removed by adding sulfamic acid (39) prior to cadmium reduction. International standards IAEA-N3, USGS-34 and USGS-3540 were used for calibration. Reproducibility was 0.3 and 0.5 ‰ for $\delta^{15}NNO_3$ and $\delta^{18}ONO_3$ respectively. Results are presented in Table S4.

Process rate experiments

Rates of microbial nitrogen turnover were determined using ^{15}N labeled substrates. Experiments were carried out at six depths at stations 1, 4 and 5 and at three depths at stations 6 and 7, following the methods outlined in refs. (21, 41). For each incubation, a 250 mL serum bottle was filled directly from the Niskin bottle and overflowed for at least three volume changes, then immediately capped with a butyl rubber stopper and crimped with an aluminum cap. Bottles were stored in the dark at in situ temperature until all depths were collected. After this, bottles were purged with helium for 15 min and amended with ^{15}N-labeled substrates during the purging. Four amendments were made: 1) 5μM $^{15}NH_4^+$, 2) 5μM $^{15}NO_2^-$ + 5μM $^{14}NH_4^+$, 3) 5μM $^{14}NO_2^-$ + 5μM $^{15}NH_4^+$ and 4) 25μM $^{15}NO_3^-$ (only amendments 2 and 3 were carried out at stations 6 and 7). ^{15}N-amended samples were transferred into 12 mL exetainers (LabCo, UK), and capped with helium degassed caps to avoid oxygen contamination (42). Exetainers were incubated in the dark at in situ temperature. At each time point (approximately 0, 3, 6, 12 and 24 hr), microbial activity was terminated in a single exetainer by the addition of 100 μL of saturated mercuric chloride solution. It is worthwhile to note that although the incubation approach used here was originally intended to yield anoxic conditions, the introduction of highly sensitive oxygen sensors have revealed that slight oxygen contamination is essentially unavoidable (17, 43).

The production of $^{14}N^{15}N$ and $^{15}N^{15}N$ was determined on a gas-chromatography isotope ratio mass spectrometer (GC-IRMS; VG Optima, Manchester, UK). The production of nitrite was determined from samples amended with $^{15}NO_3^-$ according to ref (21) with conversion to N_2 and determination of $^{14}N^{15}N$ by GC-IRMS (customized TraceGas coupled to a multicollector IsoPrime100, Manchester, UK). Rates for all processes were evaluated from the slope of the linear regression of $^{14}N^{15}N$ and/or $^{15}N/^{15}N$ with time, correcting for the ^{15}N labeling percentages of the initial substrate pool. Rates of N_2 production by anammox and denitrification were calculated according to the equations in ref (44). T-tests were applied in all cases to determine whether rates were significantly different from zero ($p < 0.05$). Detection limits varied from experiment to experiment and were estimated from the median of the standard error of the slope, multiplied by the t value for $p = 0.05$. Thus, the median detection limits for anammox were 1.3 and 2.2 nM N d^{-1} for $^{15}NH_4^+$ and $^{15}NO_2^-$ incubations, 2.7 nM N d^{-1} for denitrification ($^{15}NO_2^-$ incubation) and 3.0 nM N d^{-1} for nitrate reduction ($^{15}NO_3^-$ incubation; anammox and denitrification rates were all non-significant with $^{15}NO_3^-$ amendments).

Oxygen Regulation Experiments

Water for oxygen regulation experiments was sampled immediately after the Niskin bottles arrived on deck and transferred to a 20 L glass bottle. The bottle was overflowed (at least two volume equivalents) and

sealed without bubbles using deoxygenated butyl rubber stoppers (42), then stored in the dark at in situ temperature until the experiment began. The bottle was spiked with $^{15}NO_2^-$ to a final concentration of 5 μM and then degassed with helium (~ 1 hr). At this point, the water was dispensed into custom-modified Schott Duran glass bottles (1160 mL) as described in ref (45). An additional modification was the placement of a third glass port on the bottle, which held a 100 mL glass reservoir filled with sample water, that was continually degassed with helium for the duration of the experiment. During the incubations the bottles were continuously stirred (45), kept in the dark, and submersed in a water bath to maintain in situ temperature. Oxygen additions were made by injecting known volumes of air-saturated seawater. In this setup, oxygen was monitored throughout the incubations using a highly sensitive optical trace oxygen optode and readout device (43), mounted on the side of the bottle. Sensors were individually calibrated after each experiment, with zero point calibrations using a 0.1% w/v sodium-dithionite solution.

Time-series sampling was undertaken at 0, 4, 8, 12 and 16 hr, by inserting a long needle down the pressure compensation tube, opening the reservoir and withdrawing 10mL of sample. Sample was injected into 6 mL exetainers (LabCo, UK), pre-spiked with 50 μL 50% w/v $ZnCl_2$. Analysis of $^{14}N^{15}N$ and $^{15}N^{15}N$ for N_2 production rates were performed on a gas chromatography isotope ratio mass spectrometer as in ref. (46). Anammox and denitrification rates were determined using the equations presented in ref. (44).

Nitrite oxidation was determined from the production of $^{15}NO_3^-$. After the removal of residual $^{15}NO_2^-$ with sulfamic acid, $^{15}NO_3^-$ was converted to $^{15}NO_2^-$ by cadmium reduction and then to N_2 with sulfamic acid (21,37). Process rates were calculated from the linear regression of $^{14}N^{15}N$ and/or $^{15}N^{15}N$ as a function of time. T-tests were applied in all cases to determine whether rates were significantly different from zero ($p < 0.05$). Detection limits for the oxygen regulation experiments were estimated from the median of the standard error of the slope, multiplied by the t value for $p = 0.05$. Detection limits vary from experiment to experiment, but median detection limits were 0.9 nM N d^{-1} for anammox in $^{15}NO_2^-$ incubations, 0.4 nM N d^{-1} for denitrification and 6.3 nM N d^{-1} for nitrite oxidation. Data from these experiments are shown in Table S2.

Data Availability

The authors declare that data supporting the findings of this study are available within this article and its supplementary information, and all additional data are available from the corresponding author upon request.

Competing Financial Interests

The authors declare no competing financial interests in association with this study.

Author Contributions

L.A.B., M.L., M.G., R.N.G., M.M.M.K., G.L., S.W.A.N., N.P.R., B.T. and D.E.C. designed the study; L.A.B., C.M.C., M.L., J.D., M.F., G.L., J. M., D.E.C. performed experiments; L.A.B., C.M.C., M.L., M.A.A., M.F., G.L., B.T., A.H.T. and D.E.C. analyzed data; A.P. provided nutrient data; L.A.B., C.M.C., M.L., R.N.G., G.L., B.T. and D.E.C. wrote the manuscript with input from all co-authors.

Acknowledgments

We thank the captain and crew of the *RV Sagar Kanya* for their support during sampling. We are grateful to A. Glud, G. Klockgether, J. Larkum, L. Piepgras, P. Sørensen for technical and analytical assistance. This study was supported by the Danish National Research Foundation (DNRF53), European Research Council 'Oxygen' grant (267233), and the Max Planck Society. We gratefully acknowledge the Ministry of Earth Sciences (MoES), INDIA for funding the research through the SIBER (INDIA) project GAP2425 and for making RV Sagar Kanya available for this work. J.D. was supported by the Sonderforschungsbereiche (SFB754) GEOMAR, Kiel and C.M.C by a scholarship from the Natural Sciences and Engineering Research Council of Canada (NSERC).

References

1. Codispoti, L. A. et al. The oceanic fixed nitrogen and nitrous oxide budgets: Moving targets as we enter the anthropocene? Sci. Mar. 65, 85-105 (2001).

2. Kuypers, M. M. M. et al. Massive nitrogen loss from the Benguela upwelling system through anaerobic ammonium oxidation. Proc. Natl. Acad. Sci. USA 102(18), 6478-6483 (2005).

3. Ulloa, O., Canfield, D. E., DeLong, E. F., Letelier, R. M. & Stewart, F. J. Microbial oceanography of anoxic oxygen minimum zones. Proc. Natl. Acad. Sci. USA 109(40), 15996-16003 (2012).

4. Naqvi, W. S. A., Narvekar, P. V. & Desa, E. Coastal biogeochemical processes in the North Indian Ocean. In: Robinson, A. R. & Brink, K. H. (eds). The Sea, vol. 14, 723-781 (2005).

5. Sarma, V. et al. Intensified oxygen minimum zone on the western shelf of Bay of Bengal during summer monsoon: influence of river discharge. J. Oceanogr. 69(1), 45-55 (2013).

6. Rao, C. K. et al. Hydrochemistry of the Bay of Bengal: possible reasons for a different water-column cycling of carbon and nitrigen from the Arabian Sea. Mar. Chem. 47(3-4), 279-290 (1994).

7. Revsbech, N. P. et al. Determination of ultra-low oxygen concentrations in oxygen minimum zones by the STOX sensor. Limnol. Oceanogr: Methods 7, 371-381 (2009).

8. Larsen, M. et al. In situ quantification of ultra-low O2 concentrations in oxygen minimum zones: Application of novel optodes. Limnol. Oceanogr: Methods doi: 10.1002/lom3.10126 (2016).

9. Thamdrup, B., Dalsgaard, T. & Revsbech, N. P. Widespread functional anoxia in the oxygen minimum zone of the Eastern South Pacific. Deep-Sea Res. I 65, 36-45 (2012).

10. Tiano, L. et al. Oxygen distribution and aerobic respiration in the north and south eastern tropical Pacific oxygen minimum zones. Deep-Sea Res. I 94, 173-183 (2014).

11. Lam, P. et al. Revising the nitrogen cycle in the Peruvian oxygen minimum zone. Proc. Natl. Acad. Sci. USA 106(12), 4752-4757 (2009).

12. Jensen, M. M. et al. Intensive nitrogen loss over the Omani Shelf due to anammox coupled with dissimilatory nitrite reduction to ammonium. ISME J 5(10), 1660-1670 (2011).

13. Kalvelage, T. et al. Nitrogen cycling driven by organic matter export in the South Pacific oxygen minimum zone. Nat. Geosci. 6(3), 228-234 (2013).

14. Beman, J. M., Shih, J. L. & Popp, B. N. Nitrite oxidation in the upper water column and oxygen minimum zone of the eastern tropical North Pacific Ocean. ISME J 7(11), 2192-2205 (2013).

15. Beman, J. M., Popp, B. N. & Alford, S. E. Quantification of ammonia oxidation rates and ammonia-oxidizing archaea and bacteria at high resolution in the Gulf of California and eastern tropical North Pacific Ocean. Limnol. Oceanogr. 57(3), 711-726 (2012).

16. Canfield, D. E. et al. A cryptic sulfur cycle in oxygen-minimum-zone waters off the Chilean Coast. Science 330, 1375-1378 (2010).

17. Ganesh, S. et al. Size-fraction partitioning of community gene transcription and nitrogen metabolism in a marine oxygen minimum zone. ISME J 9(12), 2682-2696 (2015).

18. Kalvelage, T. et al. Oxygen Sensitivity of Anammox and Coupled N-Cycle Processes in Oxygen Minimum Zones. PloS ONE 6(12), e29299 (2011).

19. Dalsgaard, T. et al. Oxygen at Nanomolar Levels Reversibly Suppresses Process Rates and Gene Expression in Anammox and Denitrification in the Oxygen Minimum Zone off Northern Chile. mBio 5(6), e01966-14 (2014).

20. Bristow, L. A. et al. Ammonium and nitrite oxidation at nanomolar oxygen concentrations in oxygen minimum zone waters. Proc. Natl. Acad. Sci. USA 113(38), 10601-10606 (2016).

21. Füssel, J. et al. Nitrite oxidation in the Namibian oxygen minimum zone. ISME J 6(6), 1200-1209 (2012).

22. Hamme, R. C. & Emerson, S. R. Mechanisms controlling the global oceanic distribution of the inert gases argon, nitrogen and neon. Geophy. Res. Lett. 29(23), 2120 (2009).

23. Chang, B. X., Devol, A. H. & Emerson, S. R. Fixed

nitrogen loss from the eastern tropical North Pacific and Arabian Sea oxygen deficient zones determined from measurements of N2:Ar. Glob. Biogeochem. Cycles 26(3), GB3030 (2012).

24. *Casciotti, K. L., Buchwald, C. & McIlvin, M. Implications of nitrate and nitrite isotope measurements for the mechanisms of nitrogen cycling in the Peru oxygen deficient zone. Deep-Sea Res. I 80, 78-93 (2013).*

25. *Sarma, V. V. S. S. An evaluation of physical and biogeochemical processes regulating perennial suboxic conditions in the water column of the Arabian Sea. Glob. Biogeochem. Cycles 16(4), 1082 (2002).*

26. *DeVries, T., Deutsch, C., Primeau, F., Chang, B. X. & Devol, A. Global rates of water-column denitrification derived from nitrogen gas measurements. Nat. Geosci. 5(8), 547-550 (2012).*

27. *Lam, P. & Kuypers, M. M. M. Microbial Nitrogen Cycling Processes in Oxygen Minimum Zones. Annu. Rev. Mar. Sci. 3(1), 317-345 (2011).*

28. *Duce, R.A. et al. Impacts of atmospheric anthropogenic nitrogen on the open ocean. Science 320(5878), 893-897 (2008).*

29. *Gomes, H.R., Goes, J. I. & Saino, T. Influence of physical processes and freshwater discharge on the seasonality of phytoplankton regime in the Bay of Bengal. Cont. Shelf Res. 20(3), 313-330 (2000).*

30. *Sardessai, S., Ramaiah, N., Kumar, S. P. & de Sousa, S. N. Influence of environmental forcings on the seasonality of dissolved oxygen and nutrients in the Bay of Bengal. J. Mar. Res. 65(2), 301-316 (2007).*

31. *Turner, A. G. & Annamalai, H. Climate change and the South Asian summer monsoon. Nat. Clim. Change 2(8), 587-595 (2012).*

32. *Pattan, J. N. et al. Coupling between suboxic condition in sediments of the western Bay of Bengal and southwest monsoon intensification: A geochemical study. Chem. Geol. 343, 55-66 (2013)*

Supporting information

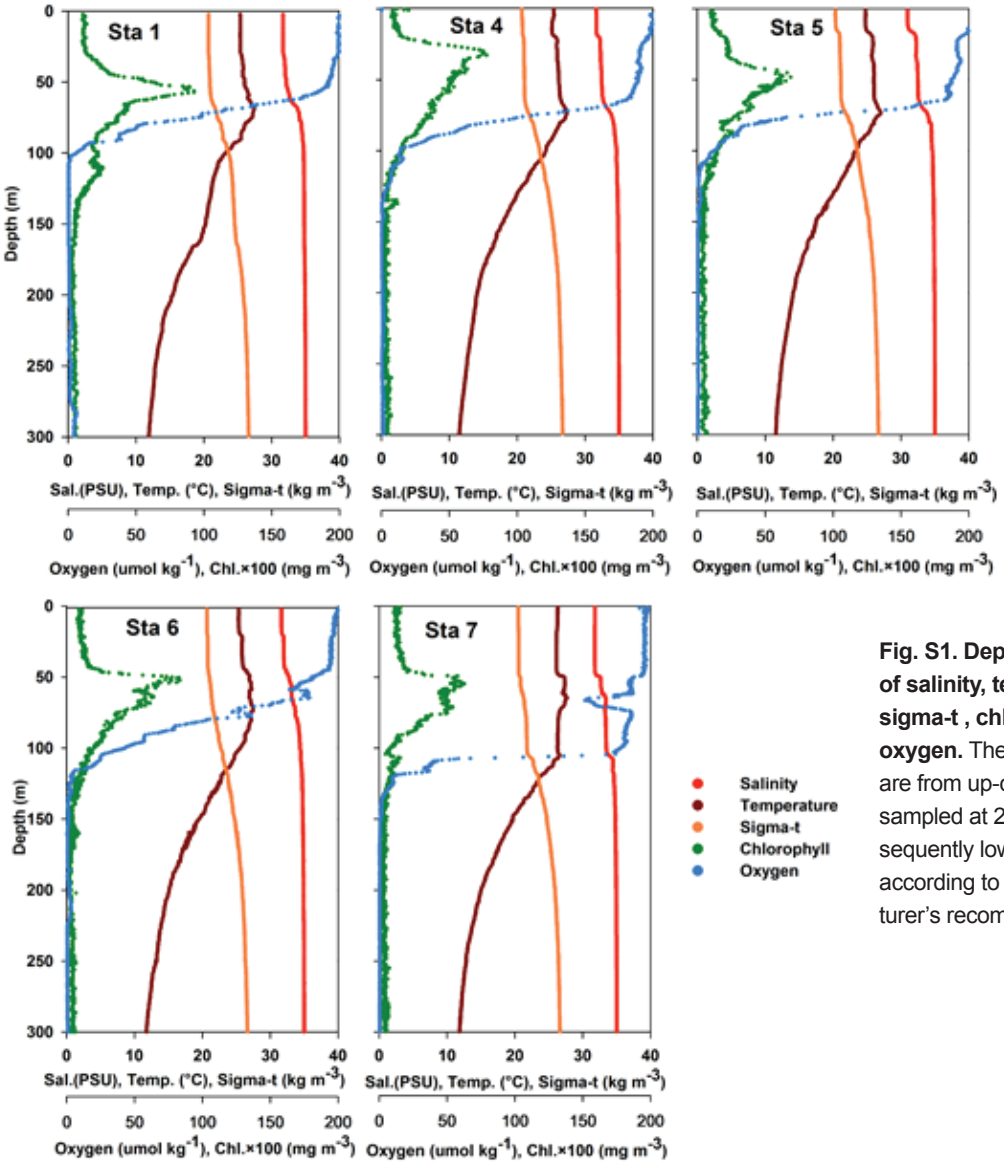

Fig. S1. Depth profiles of salinity, temperature, sigma-t , chlorophyll and oxygen. The data presented are from up-casts only, sampled at 24 s-1, and subsequently low-pass filtered according to the manufacturer's recommendations.

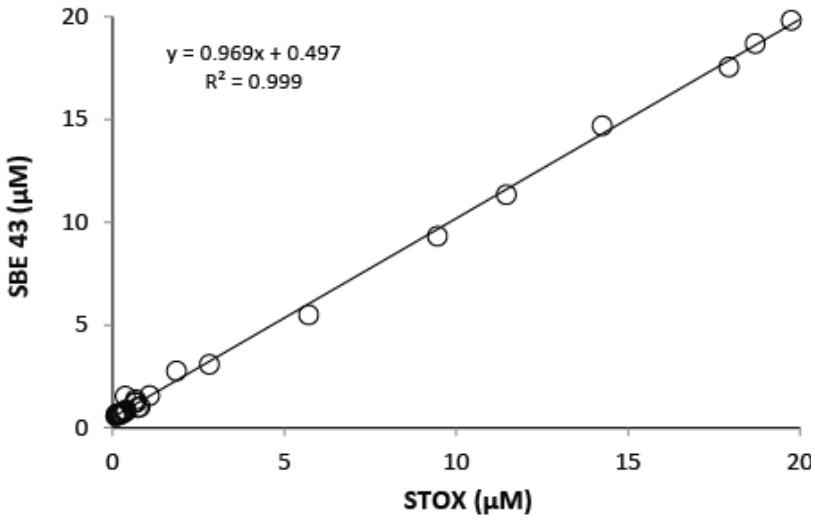

Fig. S2. Comparison of in situ oxygen recordings. Measurements with the SBE 43 polarographic oxygen sensor compared to the STOX sensor, at station 6.

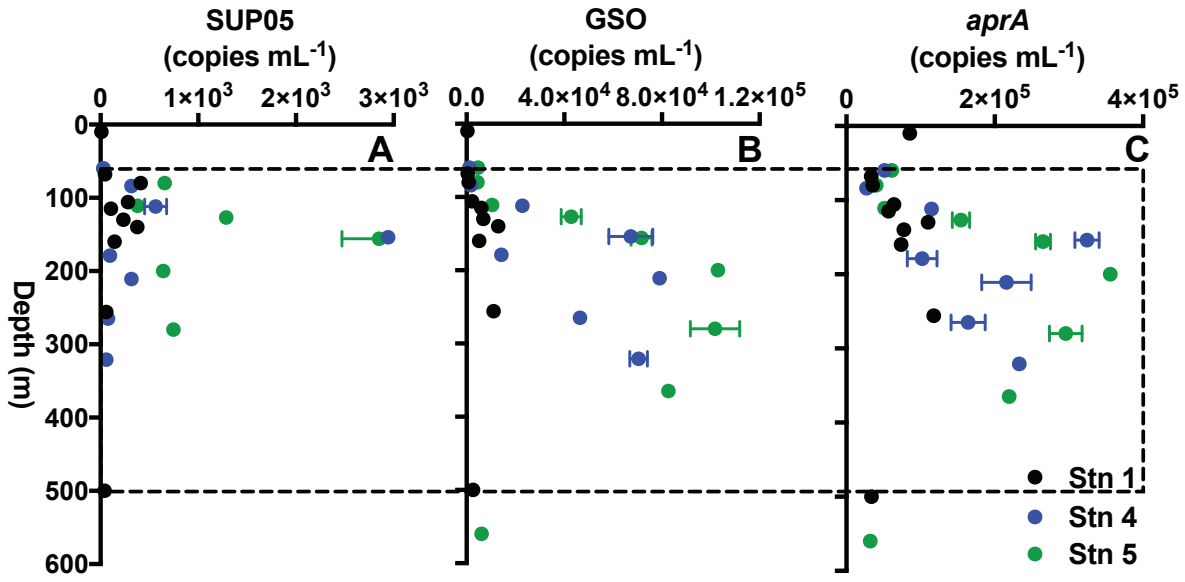

Fig. S3. Abundance of 16S rRNA genes for the SUP05 group and Gammaproteobacterial sulfur-oxidizing group (GSO) as well as the abundance of the functional gene APS reductase (aprA). The dashed box outlines the approximate depth interval of the OMZ. Note variability in x axes scales.

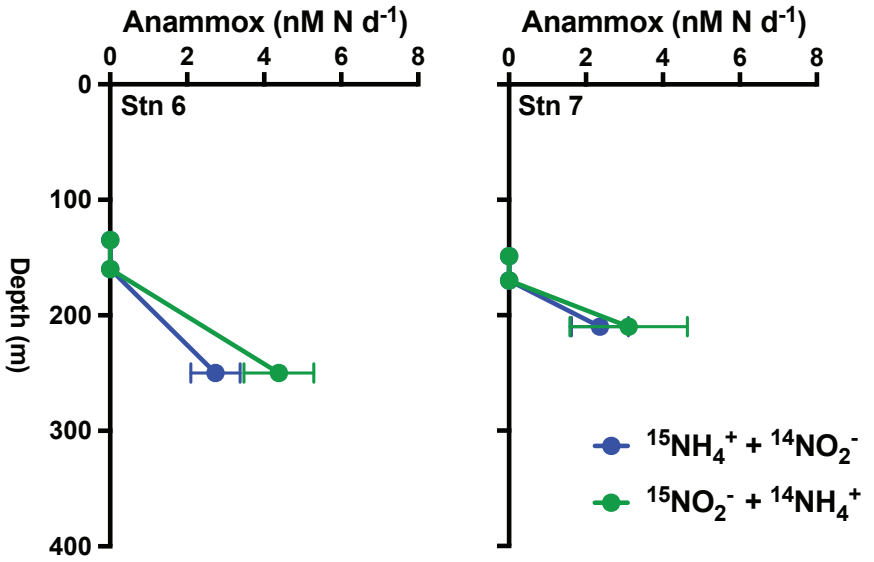

Fig. S4: Depth profiles of anammox rates at stations 6 and 7. Error bars represent the standard error.

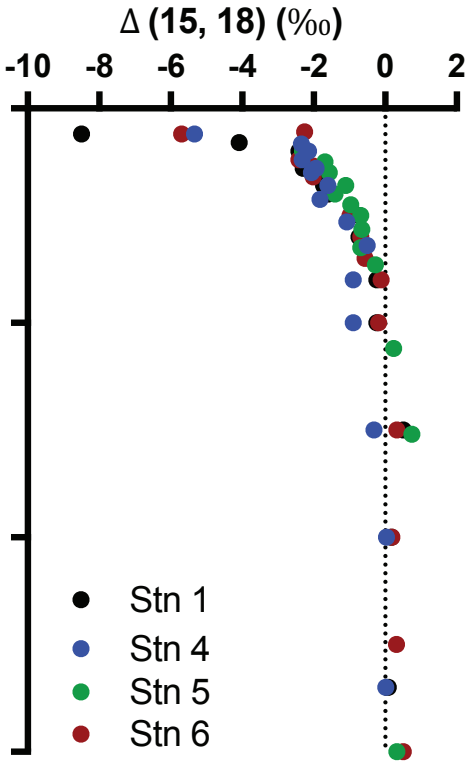

Fig. S5: Depth profiles of the nitrate isotope anomaly; Δ(15, 18) (‰).

BoB OMZ sulfur cycle

Gene abundance results suggest an active sulfur cycle as found in other OMZs supporting N_2 production. Thus, the abundance of 16S rRNA genes affiliated to the sulfide-oxidizing SUP05 group peaked in the low-oxygen waters of the BoB, similar to the OMZs in the ETSP and ETNP (1,2). We also found high copy numbers of 16S rRNA genes related to the Gammaproteobacterial Sulfur Oxidizers (GSO) (3,4). The GSO group includes SUP05, but the much higher numbers for the GSO suggest the presence of additional taxa. We also found high numbers of the functional gene APS reductase of subunit A (*aprA*) (Fig. S3) used in sulfide oxidation, with similar distribution and numbers to the GSO group, suggesting that the GSO may house the *aprA*.

A role for nitrite reoxidation

Field and laboratory studies have highlighted that during dissimilatory nitrate reduction to nitrite, the ratio of kinetic isotope effects (15ε:18ε) is approximately 1:15. Deviations from this expected 1:1 relationship in low oxygen systems, can be used to identify processes acting concurrently to nitrate reduction, this is described by the nitrate isotope anomaly, Δ(15, 18) (6). This anomaly is expressed as $\Delta(15,18) = (\delta^{15}NO_3^- - \delta^{15}NO_3^-\text{deep}) - 15\varepsilon/18\varepsilon \times (\delta^{18}NO_3^- - \delta^{18}NO_3^-\text{deep})$, where $\delta 15NO_3^-$ and $\delta^{18}NO_3^-$ are the values measured, $\delta 15NO_3^-$ deep and $\delta^{18}NO_3^-$ deep are the average values in the regional deep water (with values of 6.1 and 2.6 ‰ used for $\delta^{15}NO_3^-$ and $\delta^{18}NO_3^-$ respectively in the BoB) and 15ε /18ε is the ratio of the N to O isotope effects of dissimilatory nitrate reduction. If nitrate reduction is the only process influencing the nitrate pool Δ(15, 18) values should be close to zero. Negative Δ(15, 18) values have been observed in low-oxygen waters and attributed to the remineralisation of newly fixed N or the reoxidation of nitrite (6-9). The cycling of N between nitrate reduction and nitrite oxidation would have little net effect on the isotopic signature of $\delta 15NO_3^-$, but would cause $\delta^{18}NO_3^-$ values to increase as the nitrate reduced is initially lower in $\delta^{18}O$ than the reoxidised nitrite, resulting in the negative anomaly. In the low-oxygen waters of the BoB (100 to 350 m), persistent negative Δ(15, 18) values (Fig. S5) indicate a coupled anaerobic /aerobic N cycle, likely regulating N loss in this system.

Supporting information references

1. *Canfield, D. E. et al. A cryptic sulfur cycle in oxygen-minimum-zone waters off the Chilean Coast. Science 330, 1375-1378 (2010).*
2. *Carolan, M. T. & Beman, J. M. Transcriptomic evidence for microbial sulfur cycling in the eastern tropical North Pacific oxygen minimum zone. Front. Microbiol. 6, doi:10.3389/fmicb.2015.00334 (2015).*
3. *Glaubitz, S., Kiesslich, K., Meeske, C., Labrenz, M. & Jurgens, K. SUP05 Dominates the Gammaproteobacterial Sulfur Oxidizer Assemblages in Pelagic Redoxclines of the Central Baltic and Black Seas. Applied and environmental microbiology 79, 2767-2776, doi:10.1128/aem.03777-12 (2013).*
4. *Stewart, F. J., Ulloa, O. & DeLong, E. F. Microbial metatranscriptomics in a permanent marine oxygen mini-*

mum zone Environ Microbiol 14, 23-40 (2012).

5. *Granger, J., Sigman, D. M., Lehmann, M. F. & Tortell, P. D. Nitrogen and oxygen isotope fractionation during dissimilatory nitrate reduction by denitrifying bacteria. Limnol. Oceanogr. 53, 2533-2545, doi:10.4319/lo.2008.53.6.2533 (2008).*

6. *Sigman, D. M. et al. Coupled nitrogen and oxygen isotope measurements of nitrate along the eastern North Pacific margin. Glob. Biogeochem. Cycle 19, doi:10.1029/2005gb002458 (2005).*

7. *Casciotti, K. L., Buchwald, C. & McIlvin, M. Implications of nitrate and nitrite isotope measurements for the mechanisms of nitrogen cycling in the Peru oxygen deficient zone. Deep-C Research I 80, 78-93 (2013).*

8. *Casciotti, K. L., Bohlke, J. K., McIlvin, M. R., Mroczkowski, S. J. & Hannon, J. E. Oxygen isotopes in nitrite: Analysis, calibration, and equilibration. Anal. Chem. 79, 2427-2436, doi:10.1021/ac061598h (2007).*

9. *Gaye, B., Nagel, B., Dahnke, K., Rixen, T. & Emeis, K. C. Evidence of parallel denitrification and nitrite oxidation in the ODZ of the Arabian Sea from paired stable isotopes of nitrate and nitrite. Glob. Biogeochem. Cycle 27, 1059-1071, doi:10.1002/2011gb004115 (2013).*

10. *Mason, O. U. et al. Prokaryotic diversity, distribution, and insights into their role in biogeochemical cycling in marine basalts. The ISME journal 3, 231-242, doi:10.1038/ismej.2008.92 (2009).*

11. *Ovreas, L., Forney, L., Daae, F. L. & Torsvik, V. Distribution of bacterioplankton in meromictic Lake Saelenvannet, as determined by denaturing gradient gel electrophoresis of PCR-amplified gene fragments coding for 16S rRNA. Applied and environmental microbiology 63, 3367-3373 (1997).*

12. *Zaikova, E. et al. Microbial community dynamics in a seasonally anoxic fjord: Saanich Inlet, British Columbia. Environ Microbiol 12, 172-191 (2010).*

13. *Lavik, G. et al. Detoxification of sulphidic African shelf waters by blooming chemolithotrophs. Nature 457, 581-584, doi:10.1038/nature07588 (2009).*

14. *Wuchter, C. et al. Archaeal nitrification in the ocean. Proc. Natl. Acad. Sci. U. S. A. 103, 12317-12322 (2006).*

15. *Throback, I. N., Enwall, K., Jarvis, A. & Hallin, S. Reassessing PCR primers targeting nirS, nirK and nosZ genes for community surveys of denitrifying bacteria with DGGE. FEMS microbiology ecology 49, 401-417, doi:10.1016/j.femsec.2004.04.011 (2004).*

16. *Lam, P. et al. Revising the nitrogen cycle in the Peruvian oxygen minimum zone. Proc. Natl. Acad. Sci. U. S. A. 106, 4752-4757, doi:10.1073/pnas.0812444106 (2009).*

17. *Pester, M. et al. NxrB encoding the beta subunit of nitrite oxidoreductase as functional and phylogenetic marker for nitrite-oxidizing Nitrospira. Environ Microbiol 16, 3055-3071, doi:10.1111/1462-2920.12300 (2014).*

18. *Blazejak, A., Kuever, J., Erseus, C., Amann, R. & Dubilier, N. Phylogeny of 16S rRNA, ribulose 1,5-bisphosphate carboxylase/oxygenase, and adenosine 5 '-phosphosulfate reductase genes from gamma- and alphaproteobacterial symbionts in gutless marine worms (Oligochaeta) from Bermuda and the Bahamas. Applied and environmental microbiology 72, 5527-5536 (2006)*

.

Table S1. STOX measurements. Values below the LOD of the sensor are indicated in red and by *. Only concentrations below 2x10^4 nM are shown. At Stn 5 and 6, STOX measurements were performed in two consecutive CTD casts.

Stn 1		Stn 4		Stn 5#1		Stn 5#2		Stn 6#1		Stn 6#2		Stn 7	
Depth (m)	O_2 (nM)	Depth (m)	O_2 (nM)	Depth (m)	O_2 (nM)	Depth (m)	O_2 (nM)	Depth (m)	O_2 (nM)	Depth (m)	O_2 (nM)	Depth (m)	O_2 (nM)
102	149	400	1.79E+03	412	941	400	1.24E+03	754	1.98.E+04	600	6.58E+03	500	8.83E+03
151	36.2	387	1.17E+03	411	947	399	1.29E+03	748	1.94.E+04	584	4.15E+03	474	5.98E+03
202	1.14E+03	341	1.08E+03	398	153	378	349	705	1.58.E+04	552	2.74E+03	443	1.40E+03
231	2.04E+03	313	765	353	167	344	127	662	1.32.E+04	519	1.78E+03	416	700
		305	781	365	121	330	164	619	1.04.E+04	497	1.25E+03	391	1.10.E+03
		305	781	365	118	331	208	575	6.89E+03	466	445	372	339
		306	1.06E+03	363	247	331	157	532	3.53E+03	450	483	367	0.900*
		275	707	312	222	313	296	500	1.61E+03	421	45	371	1.80*
		260	106	277	111	276	524	473	1.61E+03	400	194	371	3.10*
		260	82.3	274	140	249	198	433	567			349	8.90*
		257	428	274	132	251	231	400	324			328	30.7
		220	983	275	270	252	256	374	443			323	1.19E+03
		220	963	231	138	229	423	350	730			316	934
		206	300	191	101	191	229	332	416			299	41.8
		195	367	193	282	153	153	300	507			287	5.80*
		180	93.3	171	71.9	151	112	285	298			283	56.5
		180	97.5	159	101	152	117	250	25.1			289	12.4
		180	81.8	160	116	147	1.26E+03	251	56.9			284	1.30*
		170	20.1	160	116	110	1.38E+03	252	29.8			270	79.6
		170	17.8	161	640	108	4.10E+03	252	25.5			246	75.6
		170	90.1	154	902	106	5.99E+03	232	52.5			243	53.3
		160	23.3	149	1.30E+03	106	5.42E+03	184	850			223	13.3
		160	17.8	138	1.02E+03	97	1.26E+04	166	318			213	42.2
		151	655	141	262			160	211			213	96.9
		150	607	142	257			155	735			207	71.1
		149	589	141	1.38E+03			171	309			191	273
				135	2.87E+03			169	310			194	244
				110	2.83E+03			160	123			194	234
				110	3.41E+03			160	156			188	298
								157	239			171	142
								124	1.37E+03			174	96.0
								128	1.22E+03			173	140
								133	1.97E+03			150	892
								135	797			152	1.28E+03
								122	2.19E+03			138	2.09E+03

Table S2. Results from the oxygen regulation experiments.

Site	Depth	Manipulated Oxygen Conc		Anammox		Denitrification		Nitrite Oxidation	
	m	μM	SD	nM N d^{-1}	SE	nM N d^{-1}	SE	nM N d^{-1}	SE
Stn 1	126	3.45	0.04	0	0	0	0	10.3	3.2
Stn 1	126	0.47	0.08	3.94	0.6	0	0	0	0
Stn 1	126	0.98	0.12	4.22	1.46	0	0	9.3	1.9
Stn 4	155	4.87	0.10	2.24	0.56	0	0	52.9	4.9
Stn 4	155	4.78	0.14	5.54	0.72	0	0	51.8	1.0
Stn 4	155	9.46	0.17	5.5	2.26	0	0	46.7	3.9
Stn 5	106	0.39	0.19	3.88	0.16	0.66	0.18	11.3	1.1
Stn 5	106	2.76	0.06	1.6	0.2	0.3	0.12	18.6	1.5
Stn 5	106	4.99	0.31	0.54	0.16	0	0	14.4	1.0
Stn 5	156	7.61	0.14	1.16	0.38	0.88	0.26	36.9	2.3
Stn 5	156	1.32	0.11	1.2	0.08	0.4	0.14	46.2	3.4
Stn 5	156	3.09	0.03	3.74	0.96	0.28	0.06	43.3	2.4

Table S3. qPCR primers

Primer Name	Sequence 5' --> 3 '	Annealing Temp ^{o}C	Target Gene	Target Organisms	Efficiency of Standard	Refs
B27F	AGR GTT YGA TYM TGG CTC AG	55	16S rRNA	*Bacteria*	82 - 86 %	[1]
U519R	TTA CCG CGG CKG CTG					[2]
U519F	CAG CMG CCG CGG TAA	63	16S rRNA	SUP05 group	66 - 68 %	[2]
1048R SUP05	CCA TCT CTG GAA AGT TCC GTS T					[3]
B27F	AGR GTT YGA TYM TGG CTC AG	50	16S rRNA	Gammaproteo-bacterial Sulfur Oxidizers	77 - 80 %	[1]
GSO477-R	CTA AAG TTA ACG TCA AGG					[4]
AOA-amoA-f	CTG AYT GGG CYT GGA CAT C	59	Ammonia monooxygenase subunit A	Archaeal nitrifiers (Th *amoA*)	78 - 79 %	[5]
AOA-amoA-r	TTC TTC TTT GTT GCC CAG TA					
cd3aF	GTS AAC GTS AAG GAR ACS GG	58	Nitrite reductase subunit S	Denitrifiers (Den *nirS*)	93 - 94 %	[6]
R3cd	GAS TTC GGR TGS GTC TTG A					
Scnir372F	TGT AGC CAG CAT TGT AGC GT	61	Nitrite reductase subunit S	Scalindua (Sc *nirS*)	86%	[7]
Scnir845R	TCA AGC CAG ACC CAT TTG CT					
nxrB169F	TAC ATG TGG TGG AAC A	57	Nitrite oxidoreductase subunit B	*Nitrospira/ Nitrospina (nxrB)*	88 - 90%	[8]
nxrB638R	CGG TTC TGG TCR ATC A					
aps1F	TGG CAG ATC ATG ATY MAY GG	53	Adenylylsulfate reductase subunit A	diverse	81 - 84 %	[9]
aps4R	GCG CCA ACY GGR CCR TA					

CHAPTER 3

Enhanced nitrogen loss by eddy-induced vertical transport in the offshore Peruvian oxygen minimum zone

Cameron M. Callbeck, Gaute Lavik, Lothar Stramma, Marcel M. M. Kuypers, Laura A. Bristow. (2017) Enhanced nitrogen loss by eddy-induced vertical transport in the offshore Peruvian oxygen minimum zone. PLOS ONE. 12(1): e0170059. doi:10.1371/journal.pone.0170059

Abstract

The eastern tropical South Pacific (ETSP) upwelling region is one of the ocean's largest sinks of fixed nitrogen, which is lost as N_2 via the anaerobic processes of anammox and denitrification. One-third of nitrogen loss occurs in productive shelf waters stimulated by organic matter export as a result of eastern boundary upwelling. Offshore, nitrogen loss rates are lower, but due to its sheer size this area accounts for ~70% of ETSP nitrogen loss. How nitrogen loss and primary production are regulated in the offshore ETSP region where coastal upwelling is less influential remains unclear. Mesoscale eddies, ubiquitous in the ETSP region, have been suggested to enhance vertical nutrient transport and thereby regulate primary productivity and hence organic matter export. Here, we investigated the impact of mesoscale eddies on anammox and denitrification activity using ^{15}N-labelled *in situ* incubation experiments. Anammox was shown to be the dominant nitrogen loss process, but varied across the eddy, whereas denitrification was below detection at all stations. Anammox rates at the eddy periphery were greater than at the center. Similarly, depth-integrated chlorophyll paralleled anammox activity, increasing at the periphery relative to the eddy center; suggestive of enhanced organic matter export along the periphery supporting nitrogen loss. This can be attributed to enhanced vertical nutrient transport caused by an eddy-driven submesoscale mechanism operating at the eddy periphery. In the ETSP region, the widespread distribution of eddies and the large heterogeneity observed in anammox rates from a compilation of stations suggests that eddy-driven vertical nutrient transport may regulate offshore primary production and thereby nitrogen loss.

Oceanic oxygen minimum zones (OMZ) typically occur in regions where upwelling of nutrient rich waters fuels high surface primary productivity. The resulting export of organic matter stimulates microbial respiration, and combined with poor regional ventilation creates low oxygen concentrations (1). Traditionally OMZ boundaries are defined by oxygen concentrations of less than 20μM (2), although, oxygen is regularly observed to be < 10 nM in these regions (3, 4). Under low oxygen concentrations the anaerobic processes anammox and denitrification contribute to nitrogen loss. Specifically, the former catalyzes the anaerobic oxidation of ammonium with nitrite, while the latter is the stepwise reduction of nitrate to N2. An estimated 30-50% of oceanic nitrogen loss occurs in OMZs, which represent roughly 0.1% of the global ocean volume (5). These regions are primarily located within the Arabian Sea, the Bay of Bengal, off the coast of Namibia, the Eastern Tropical North Pacific, and the Eastern Tropical South Pacific (ETSP) (6). In the majority of OMZ studies, anammox has been shown to be the main sink of fixed inorganic nitrogen (NO3-, NO2- and NH4+) (7-12). The main source of inorganic nitrogen substrates for anammox comes from the remineralization of organic matter exported from the photic zone (13). Based on in situ rate measurements, anammox activity is strongest over the upper shelf where the input of organic matter is highest (8, 9, 13). Therefore, organic matter supply places constraints on nitrogen loss (13), which has been attributed to coastal upwelling (1).

The offshore OMZ (defined as >600m water depth following Kalvelage et al., (13)), despite having lower volumetric anammox rates (by an order of magnitude), accounts for two-thirds of ETSP nitrogen loss (13). These rates are heterogeneous and not evenly distributed across the offshore ETSP region (13). Consequently, there must be other mechanisms regulating nitrogen loss and potentially export production in the offshore OMZ (14), where coastal Ekman driven upwelling and the breaking of internal waves is less influential (15). The most compelling suggestion is mesoscale eddies, which occur at a large-scale (50-200 km diameter), can persist for relatively long time periods (weeks to months), and are ubiquitous in the marine environment (16-18).

Eddies mediate vertical advective transport of

nutrients by Ekman and nonlinear Ekman mechanisms. Ekman transport is primarily driven by the eddy-wind interaction and is strongest in the eddy center (19, 20). There are three main types of mesoscale eddies which can be characterized by their isopycnal displacements and the direction of Ekman-driven transport in the eddy center (Fig 1). In cyclonic eddies Ekman transport produces downwelling. In anticyclonic and anticyclonic mode-water eddies this generates upwelling (20-22), these two eddy types are distinguished by their differences in isopycnal displacements. In contrast, nonlinear Ekman transport is driven by the horizontal velocity of the eddy, and operates along density fronts located on the eddy periphery, which is consistent across all eddy types (15, 17) (Fig 1). Nonlinear Ekman transport is also termed submesoscale transport, because it occurs at scales ranging from 0.1 to 10 km. In effect both Ekman and submesoscale vertical transport processes bring nutrients from mid-depths up to sunlit surface waters (23), stimulating primary production. Ekman upwelling within anticyclonic mode-water eddies has been used as a mechanism to explain massive phytoplankton blooms reported in the North Atlantic and elsewhere (24, 25). Eddy-induced enhancement of chlorophyll concentrations at the eddy periphery as a result of submesoscale processes has also been observed (26-28). Comparing the two vertical pumping

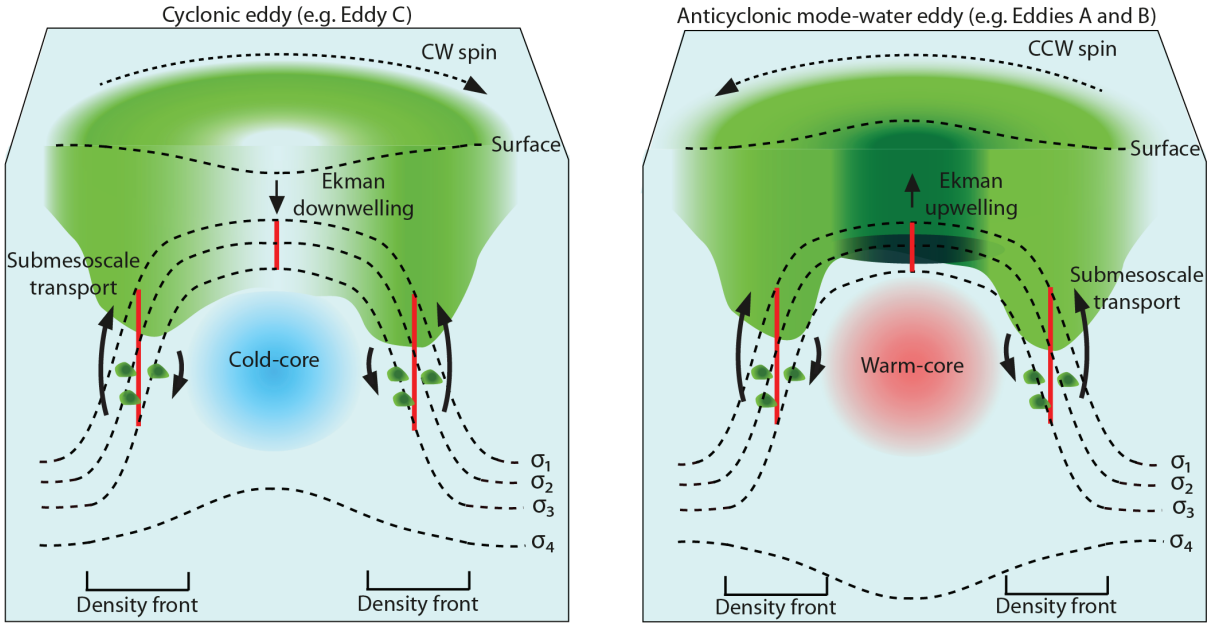

Fig 1. Schematic of isopycnal deformations and vertical transport processes in two eddy types depicted for the southern hemisphere. Shown are a cyclonic (clockwise 'CW' spin) and an anticyclonic mode-water eddy (counterclockwise 'CCW' spin). Both seasonal (dotted lines; $\sigma_{1\text{-}3}$) and main pycnoclines (dotted line; σ_4) are illustrated. At the surface, cyclonic and anticyclonic mode-water eddies cause a negative and positive sea surface height anomaly, respectively. Vertical transport processes in the eddy center can vary in direction and magnitude (20), here, we illustrate the direction of vertical transport in the eddy center derived from eddy-wind interaction Ekman flow. In the center of anticyclonic mode-water eddies, upwelling stimulates chlorophyll accumulation (green), in addition, inward swirling currents concentrate chlorophyll in the eddy center from surrounding waters, also known as eddy entrapment (20). In contrast, cyclonic eddies distribute chlorophyll downwards through the eddy center. In both eddy types submesoscale vertical transport is expected to be enhanced along either side of the density front (i.e. along the tilted isopycnals). This area coincides with an increase in isopycnal spacing (red line) and the eddy horizontal velocity, which can be used to differentiate the eddy periphery from the eddy center. Submesoscale processes drive two-way vertical transport. A net upward transport of nutrients into the euphotic zone stimulates chlorophyll production, while subduction can act to re-distribute chlorophyll over a greater depth, and can cause chlorophyll pockets to form below the surface mixed layer. Submesoscale vertical velocities at the eddy periphery exceed velocities at the center, as represented by the length and thickness of the vertical arrows. This figure represents a synthesis of principles discussed by Mahadevan et al., (36); Omand et al., (32); and McGillicuddy (20).

mechanisms, submesoscale velocities operating on the eddy periphery can reach 10-100 m d^{-1}, several orders of magnitude larger than velocities driven by Ekman transport occurring in the eddy center (0.1-0.4 cm d^{-1}) (24, 29, 30). Additionally, submesoscale processes can act to transport particulate organic carbon and oxygen downwards below the surface mixed layer, referred to as subduction (15, 20, 31-33) and this has recently been suggested to play a pivotal role in the ocean carbon pump (32). Eddies are common throughout all major OMZs (34, 35), but the extent of their regulation over regional chlorophyll and the impact of this on nitrogen loss processes remains understudied.

To date, only a few studies have investigated the effect of eddies on nitrogen cycling processes in OMZs. These studies have used time-integrated records of nitrogen loss, such as natural abundance N-isotopes (14, 37), the nitrogen deficit (N*) (14, 38), and nitrite concentrations (37, 38). All methods show signatures indicative of enhanced nitrogen loss and elevated chlorophyll, in the center of anticyclonic mode-water eddies, and this is referred to as the 'hotspot' theory (14, 37-39). However, the current 'hotspot' theory is debated, because it assumes these chemical signatures originated and were intensified by the eddy, as a result of central Ekman upwelling (14, 37, 38). This theory is contested, as it does not consider the eddy formation history and exchange with surrounding water bodies (40). A study tracking the development of a coastal anticyclonic eddy in the ETSP region found that the eddy naturally entraps coastal water signatures, including coastally derived N* (40). As the eddy continued developing, the signature was enhanced overtime by eddy-induced horizontal advective transport, in effect pulling coastally derived N* inwards towards its center (40). Given that the coastal N* is typically higher than offshore waters (13), as the eddy propagated away from the coast it retained an elevated coastal signature offshore (20, 40). Thomsen et al., (40) highlight that the accumulated biogeochemical signal preserves a record of water mass history, but does not necessarily indicate the presence of ongoing nitrogen loss activity. Likewise, the chlorophyll hotspot observed in anticyclonic mode-water eddies in the ETSP region and elsewhere, conventionally attributed to stimulation induced by central Ekman upwelling (24), could alternatively have accumulated in the eddy center as a result of inward horizontal transport (15, 36). In contrast, recent studies outside of OMZs highlight that the most prevalent nutrient replenishment, and thereby stimulant of primary productivity, is occurring on the eddy periphery due to submesoscale dynamics (15, 26, 36, 41, 42).

We investigated the spatial distribution of nitrogen loss rates and chlorophyll across mesoscale eddies in the ETSP region. Specifically, we attempt to better resolve which vertical transport mechanisms regulate nitrogen loss and chlorophyll concentrations within eddies. In this study we provide the first *in situ* rate measurements of nitrogen loss across an eddy. Our analysis further expands our understanding of system wide patterns of offshore chlorophyll and the regulation of nitrogen loss as a result of the widespread distribution of eddies in the ETSP region.

Results and Discussion

Eddy hydrodynamics and station definition

During the M90 research cruise in November 2012, eddies A, B and C, were readily observable from satellite sea surface height altimetry (SSHA), and were sampled along the 16.45° S transect (Fig 2A). Eddies A, B and C extended vertically from surface waters down to between 600-950 m depth (38). At the time of sampling, eddy A was still forming over the upper shelf, whereas eddies B and C were detached from the coast and had propagated westward. Based on satellite altimetry tracking, eddy A was the youngest, followed by eddies C and B at 2, 3 and 5 months old, respectively (38). Eddies A and B, based on isopycnal profiles were by definition anticyclonic mode-water eddies because they had uplifted seasonal pycnoclines and depressed main pycnoclines, whereas eddy C was cyclonic because it had upward shoaling of both seasonal and main pycnoclines ((24); Figs 1 and 2B).

We define the location of our stations within

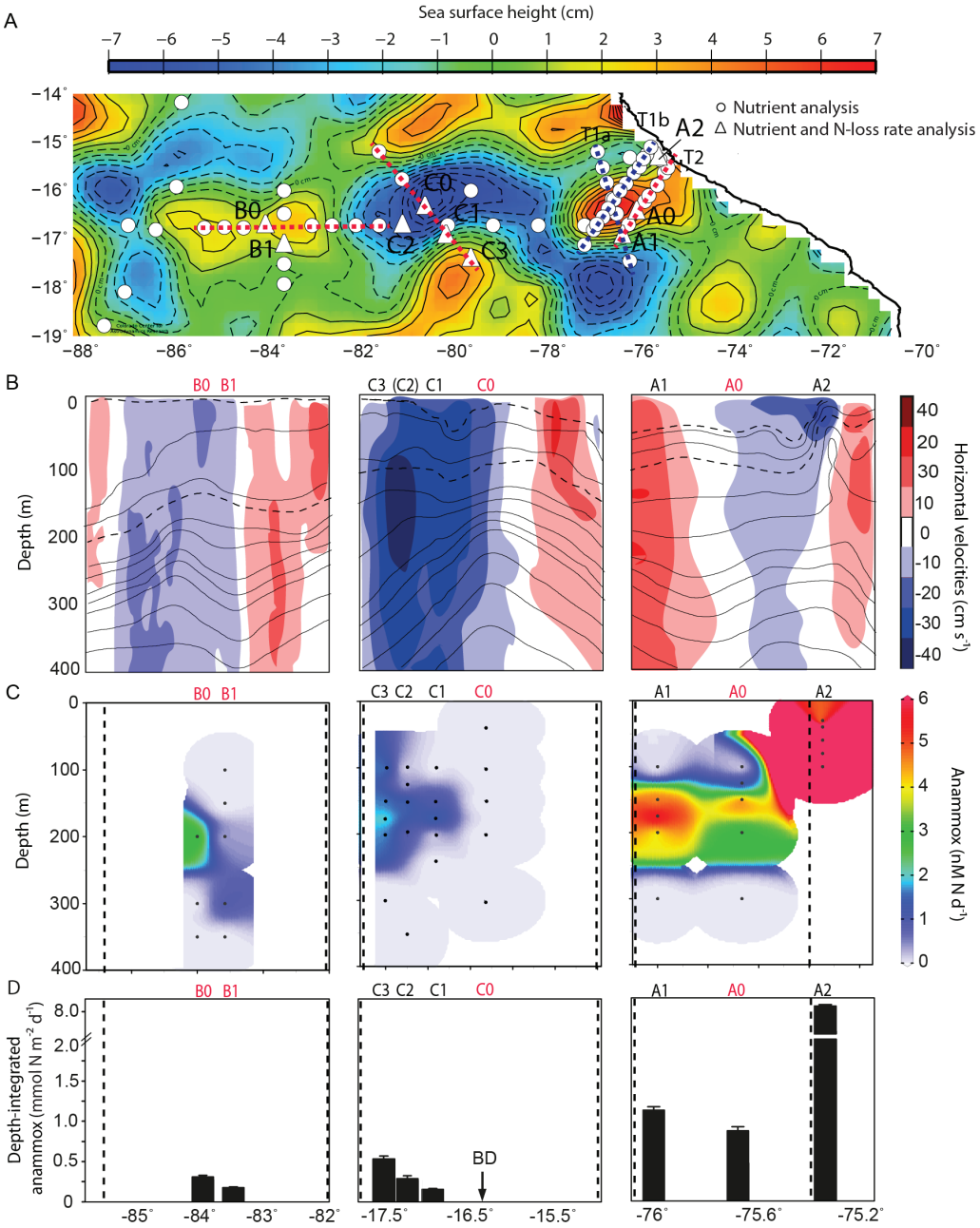

Fig 2. Distribution of anammox activity across eddies A, B and C in the ETSP region. (A) Sea surface height altimetry (SSHA) of sampled eddies A, B and C during the M90 cruise, November 22nd, 2012. The approximate locations of sampled stations within the eddy are shown, please note that the eddies propagated westward over the sampling period. Stations sampled for nutrients only (open circles) and nutrients plus nitrogen loss rates (open triangles with station numbers) are indicated. The red and blue dotted lines indicate transects sampled across eddies A, B and C, note that three defined transects were performed across eddy A (T1a/b in blue and T2 in red). Transects shown in panels B-D represent red dotted lines, whereas additional transects T1a (blue) are shown in S2-S4 Figs. (B) Horizontal velocity depth profiles are adapted from Stramma et al., (38). Isopycnal contours are indicated by black lines, while reference isopycnals 25.4 and 26.0 kg m^{-3} are highlighted by black dotted lines. (C, D) Indicate volumetric and depth-integrated anammox rates for $^{15}N\text{-}NH_4^+$ experiments. Error bars for depth-integrated anammox rates represent the standard error. BD indicates below the limit of detection. Stations numbered in red (B0, B1, C0, and A0) were sampled in or near the eddy center while stations with black numbers (C3, C2, C1, and A1) were sampled on the eddy periphery, identified according to eddy-induced horizontal velocities, density fronts, and SSHA, shown in panels a and b. Note that the center of eddy C, based on SSHA and supported by horizontal velocities, is at -16.25 °N, -80.38 °E 14 km northeast of station C0. Note that data from station C2 is not included in the transect profiles shown in panel B (indicated by (C2)), but is shown in panels C, D. The coastal upwelling station is indicated by 'A2'. The vertical black dotted lines in panels C and D indicate the edge of the respective eddies.

the eddy according to two characteristic features: horizontal velocities for transects across individual eddies, and isopycnal spacing for system wide trends. 1) Horizontal velocities induced by the eddy vary across its diameter. Inherently, the center of the eddy has low or near-stagnant horizontal velocities that increase moving away in either direction from the center (Fig 2B). Horizontal velocities eventually peak and then decrease at the outer limits of the eddy. Generally, the center exhibits flat isopycnals that begin to tilt moving away in either direction from the center. The tilting of the isopycnals, otherwise referred to as the density front, coincides with an increase in eddy horizontal velocity (Fig 1). Unless specified we use the terms, "center" to describe the area of the eddy having the lowest horizontal velocity, and "periphery" referring broadly to the density front, which also coincides with higher eddy horizontal velocities. 2) For the analysis of system-wide trends, and specifically when horizontal velocity data was unavailable, stations were instead located according to the isopycnal spacing, following a similar concept as Strass (42). In principle, on either side of each density front, isopycnals begin to flatten; notably, the center characteristically exhibits a smaller distance between individual isopycnals than the eddy periphery (Fig 1). Thereby, isopycnal spacing can be used to determine the relative location of sampled stations within an eddy (i.e. periphery versus center). Here, we use reference isopycnals, 25.4 and 26.0 kg m^{-3}, to calculate isopycnal spacing. Isopycnals 25.4 and 26.0 kg m^{-3} located near the surface and oxycline, respectively, were chosen because they were representative of uplifted seasonal pycnoclines in eddies A, B and C (Fig 2B).

Distribution of chemical parameters

Eddies A, B and C penetrated vertically through the OMZ core, which was observed between 100 and 500 m depths, using a cutoff of 20 μM oxygen (S1 Fig). These eddies had a distinct effect on the distribution of oxygen and nutrients (originally discussed by Stramma et al., (38)). For cyclonic eddy C, the center, had undetectable nitrite concentrations and an N* of -17 μM (S2 Fig). Chlorophyll concentrations were between 2-2.5 μg L^{-1} from 20 to 40 m depth, and oxygen concentrations were notably high, reaching more than 5 μM in the center from 200-350 m depth (S1-S3 Figs). At the periphery, chlorophyll concentrations were slightly lower (0.5-2 μg L^{-1}) relative to the center, however, chlorophyll had a deeper penetration (down to 150 m) through the water column along the density front (S3 Fig). Increases in nitrite, N*, and a decrease in oxygen were observed moving away from the center along the density front. Furthermore, elevated concentrations and low oxygen waters (<3 μM) were observed over a larger depth range relative to the center. At the periphery, N* and nitrite concentrations were most pronounced, with values reaching -40 μM and 11 μM, respectively. Here it is important to note that these parameters (N* and nitrite concentrations) are traditionally thought of as chemical signatures of active nitrogen loss, but it has been shown that no quantitative correlation exists between them and ongoing nitrogen loss activity (8, 13, 43). For eddy C, Stramma et al., (38) attributed the increase in nitrite and N* occurring along the periphery to an impinging anticyclonic eddy (seen in Fig 2A). An alternative interpretation is that strong upward directed transport of nutrients along the density front stimulated primary productivity, in agreement with modeling studies (36, 41). The enhanced organic matter supply and subsequent remineralization decreased oxygen concentrations, and could potentially promote nitrogen loss activity.

For anticyclonic mode-water eddies A and B, nutrient and oxygen distributions across the eddy differed relative to eddy C. The center of eddy A had oxygen concentrations less than 3 μM between 140 and 400 m depth and a maximum chlorophyll concentration of 6.1 μg L^{-1} at 50 m depth (S2 and S3 Figs; Stramma et al., (38)). For eddy B, the maximum chlorophyll concentration was half that (2.5 μg L^{-1}) of eddy A (S3 Fig), and oxygen-depleted (<3 μM) waters at the center were observed between 200 and 400 m depth (S1 and S2 Figs; (38)). N* and nitrite concentrations were most pronounced in the centers of eddies A and B, a strong contrast to eddy C (S2 Fig; (38)). Eddies A and B, exhibited a strong N* between 175-250 m depth of -30 μM, and nitrite concentrations

up to 8 μM (S2 Fig). Moving away from the center of eddies A and B there was a decrease in nitrite and N*concentrations, as well as an increase in oxygen concentrations, indicating an opposite cross-eddy pattern between sampled cyclonic and anticyclonic mode-water eddies. Maximum chlorophyll concentrations also decreased moving towards the periphery, however, chlorophyll was distributed over a larger depth range, with lateral intrusions and/or deep penetrating pockets of chlorophyll being observed along the density front (S3 Fig; (38)). Similar features, occurring along the eddy periphery, have been observed in anticyclonic eddies in the North Atlantic, which were indicative of eddy-induced peripheral submesoscale transport processes (32). In the study by Omand et al., (32) submesoscale vertical transport resulted in over half of the springtime bloom being exported below the surface mixed layer. Subducted chlorophyll in eddies A and B along the periphery could be considered evidence of active submesoscale driven transport, which may directly supply organic matter for nitrogen loss processes in the OMZ. Moreover in the ETSP region and elsewhere, submesoscale processes have been shown to introduce oxygen below the surface mixed layer (32, 33). Consequently this could potentially fuel microaerobic activity that has been shown to be an important process in supplying ammonium for anammox bacteria (44).

Distribution of nitrogen loss rates

To determine anammox and denitrification activity across each eddy we performed incubation experiments with $^{15}N\text{-}NH_4^+$ and $^{15}N\text{-}NO_2^-$ additions. Denitrification was below detection at all of the stations, which is in line with previous studies in the ETSP region, which have shown denitrification rates to be highly patchy (45). Anammox activity dominated at the sampled stations, which is consistent with previous studies, suggesting anammox as the main microbial nitrogen loss pathway in the ETSP region (9, 13). Volumetric anammox rates from the two incubation experiments were generally comparable to each other (S1 Fig). Over depth, the highest volumetric anammox rates generally corresponded with both N* and nitrite maximums, which also corresponded to the depths just below where oxygen dropped below 20 μM. Our volumetric anammox rates for two offshore stations and eddies A, B and C ranged from below detection to 8 nM N d^{-1}, and for the coastal station ranged from below detection to 57 nM N d^{-1} (S1 Fig). These are comparable to previously reported anammox rates for coastal and offshore OMZ environments (9-13, 45). Moreover, our volumetric rates followed the same longitudinal trend as Kalvelage et al., (13) indicating highest anammox activity over the shelf followed by a decrease of an order of magnitude at offshore stations. Although these volumetric rates are lower in the offshore OMZ, they exhibit large variability that is not related to the distance from the shelf (13).

To compare anammox activity across each eddy we will focus on the maximal volumetric and depth-integrated rates observed at each station, based on $^{15}N\text{-}NH_4^+$ incubations. For cyclonic eddy C, rates of anammox activity varied across the eddy transect, in total four stations were available for comparison. The center station (C0), which had the lowest horizontal velocity of the four stations, had non-detectable anammox activity (Fig 2C). The remaining three stations were sampled along the density front. The second (C1) and third (C2) closest stations to the center, located nearest to the highest horizontal velocity had anammox rates up to 1.55 and 1.71 nM N d^{-1} at 150 m depth. At the station furthest from the center (C3), activity increased to 2.11 nM N d^{-1}, and had consistently high rates of 1.75 to 2.11 nM N d^{-1} between 100 and 200 m depth; this station corresponded to the outer edge of the density front where horizontal velocities began to decrease. The same trend is further highlighted when looking at the depth-integrated anammox rates, where we observed a transition from lowest to highest anammox rates moving from the center towards the periphery of the eddy, 0.00 to 0.53 ± 0.04 mmol N m^{-2} d^{-1} (Fig 2D). These findings indicate a tendency for anammox activity to increase moving away from the center across the eddy density front, and towards higher horizontal velocities.

For anticyclonic mode-water near-coastal eddy A volumetric anammox rates increased from 4.95 ±

0.50 nM N d^{-1} to 5.97 ± 0.50 nM N d^{-1}, moving from the eddy center towards the periphery (Fig 2C), suggesting no across-eddy differences. However, depth-integrated anammox rates show a pattern identical to that of eddy C with lower activity in the eddy center (0.86 ± 0.05 mmol N m^{-2} d^{-1}) relative to the periphery (1.12 ± 0.04 mmol N m^{-2} d^{-1}; Fig 2D). Elevated anammox activity at the periphery coincided with the strongest horizontal velocities (Fig 2B). Anticyclonic mode-water eddy B, the weakest of the eddies based on its horizontal velocity, had nitrogen loss rates up to 3.04 nM N d^{-1}, at two stations in close proximity to the eddy center (Fig 2B, C). With only center stations available it was not possible to determine if anammox rates were higher at the eddy periphery as observed for eddies A and C. Though, depth-integrated anammox activity in the center of eddy B was similar to that of an offshore station sampled at the same longitude (0.30 ± 0.02 and 0.39 ± 0.05 mmol N m^{-2} d^{-1} respectively, Fig 2D). This is notable, because the center of eddy B has previously been suggested as a 'hotspot' for nitrogen loss due to its elevated concentrations of N* and nitrite (38), but the direct measurements of ongoing activity measured here seem to disagree with this, as anammox rates were not higher in the center of eddy B.

The centers of cyclonic and anticyclonic mode-water eddies exhibited differences not only in nitrogen loss activity but also in nutrients. For cyclonic eddy C, anammox activity, nitrite, N*, and chlorophyll were lower at the center compared to the centers of eddies A and B. This difference in activity and nutrient distributions between eddies could potentially be explained by the direction of Ekman driven vertical transport at the eddy center. Anticyclonic mode-water eddies which produce upwelling would be expected to generate higher primary production and thereby higher organic matter export in the center than cyclonic eddies which drive nutrient downwelling (24). Enhanced organic matter export could have fueled higher anammox activity in the centers of anticyclonic mode-water eddies A and B compared to cyclonic eddy C. Moreover, in eddy C, downwelling of oxygenated waters may have ventilated the eddy center, which could explain why oxygen concentrations never fell below 5 μM, while in eddies A and B concentrations were generally below the detection limit (3 μM). Recent studies quantifying the oxygen sensitivity of anammox have found 50% inhibition concentrations of 1 to 10 μM oxygen (46, 47), which could be a potential explanation of why lower anammox activity was observed in the center of eddy C. Thus we suggest that the direction of Ekman driven vertical transport in the center plays a role in regulating nitrogen loss by controlling export production and oxygen supply.

While rates of nitrogen loss in the centers of eddies A and B were moderate, they were lower or comparable to rates observed at the periphery or other offshore stations, despite having elevated chlorophyll, N* and nitrite concentrations (38). To date these enhanced chemical signatures of nitrogen loss (N*, nitrite concentrations and natural abundance N-isotopes) have been the basis for the hotspot theory, proposing Ekman upwelling as the main driver of nitrogen loss at the eddy center (14, 37, 38, 48). However, as a consequence of how eddies form, mixing with adjacent waters could explain the majority of the nutrient and low oxygen concentrations. Indeed, salinity characteristics in the centers of eddies A and B were of a similar range to values measured for the coastal Peruvian-Chilean undercurrent (PCUC), ranging between 34.8-35.9 from 50 to 200 m water depth (38). The coastal PCUC waters can vary in terms of nutrient chemistry, but generally have concentrations of nitrite, N*, and chlorophyll ranging between 6-9 μM, ~25-28 μM, >6 μg L^{-1}, respectively (13, 38, 40), as well as oxygen concentrations below 10 nM (3). Conserved nutrient chemistry and salinity characteristics between the centers of eddies A and B and the PCUC would suggest that nutrients in the centers of eddies A and B originated from the coast. A similar finding was reported for another anticyclonic eddy occurring in the same region tracked over its formation history (40). Thomsen et al (40), showed snapshots of nutrient concentrations before, during and after the eddy formation to reveal increasing nitrite and N* concentrations in the eddy center and decreasing oxygen over this period. After formation the eddy center had comparable nutrient concentrations to the PCUC. Moreover nutrient gradients

(nitrate, nitrite and oxygen) formed along isopycnals between the eddy and the coast, diagnostic of eddy-induced horizontal advection (40). In the ETSP region eddy-induced horizontal advection of coastal nutrients and productivity offshore lowers the overall productivity of the coastal upwelling region (49).

Contrary to the hotspot theory, our findings show that nitrogen loss activity at the periphery of eddies A and C is greater than activity at the eddy center (Fig 2). For eddy C, the increase in anammox activity along the periphery was also paralleled by increases in nitrite, N*, and chlorophyll as well as a decrease in oxygen concentrations (38). Moreover, N_2O, an intermediate of the denitrification pathway accumulated on the periphery of eddies A, B and C [38]. In high-resolution eddy models the periphery is the site of enhanced vertical nutrient replenishment, which by far exceeds vertical transport velocities induced by Ekman upwelling in the eddy center (15, 36). The horizontal velocity of the eddy drives submesoscale transport that is predicted to occur along either side of the density front (15, 17). Given that nitrogen loss is correlated with organic matter export (13), our nitrogen loss rates support the idea that for eddies A, and C the periphery is an important site supporting primary productivity and a supply of organic matter, which as a whole is driven by submesoscale transport, a previously unrecognized process regulating nitrogen loss.

Large-scale trends: correlation of chlorophyll with eddy isopycnal spacing

Isopycnal spacing, as previously mentioned, can be used to determine the relative position within an eddy (Fig 1). In general, isopycnal spacing is smallest at the eddy center and increases moving away in either direction along the density front (i.e. towards the eddy periphery; Fig 1). Thereby, we can use the relationship between isopycnal spacing and chlorophyll to identify patterns across an eddy. Additionally, isopycnal spacing conveys the approximate distance from the coast (plotted verses longitude in Fig 3A). Stations related to eddies A, B, and C group successively along this trend line with coastal and offshore stations found at either longitudinal extreme ($R = 0.91$, $p < 0.05$). This relationship with isopycnal spacing therefore provides an approximate location of the eddy across the longitudinal transect and the position within an eddy i.e. center vs. periphery.

In high-resolution chlorophyll profiles, mesopelagic intrusions and deep pockets can be seen extending into the surface mixed layer of all eddies, often occurring along the density front (38) (S3 Fig). Therefore, chlorophyll was depth-integrated at each

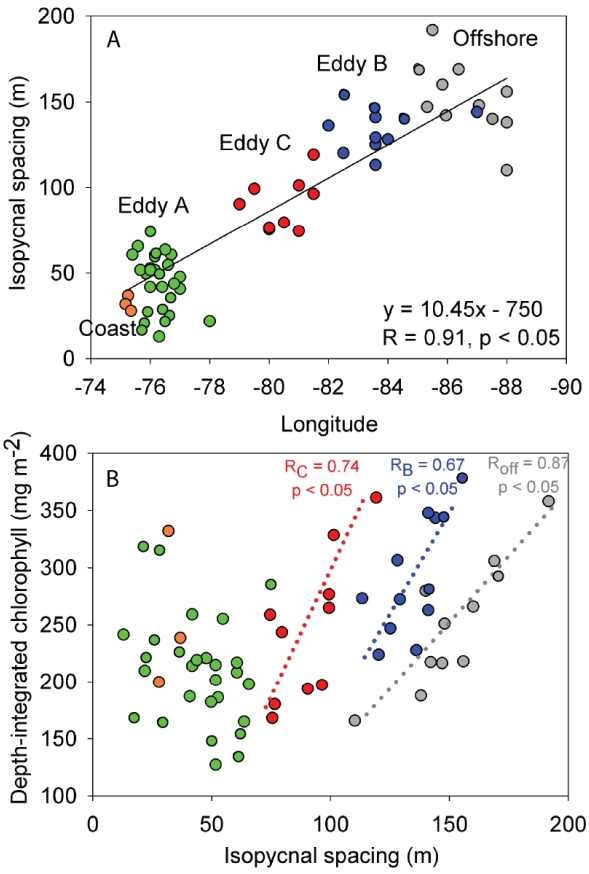

Fig 3. Relationship between isopycnal spacing and chlorophyll. (A) Correlation of isopycnal spacing versus longitude for eddies A (green), B (blue), and C (red), alongside coastal upwelling stations (orange) and offshore stations extending past eddy B (grey). (B) Correlation of isopycnal spacing versus depth-integrated chlorophyll. Chlorophyll at all stations was depth-integrated down to 300 m depth, except for coastal stations which were depth-integrated down to 200 m. Dotted linear regression lines indicate eddy specific trends (R_C = eddy C, R_B = eddy B and R_{off} = offshore). Pearson correlation values are indicated in each panel (p-values).

station because of its broad vertical distribution. For offshore eddies C and B; depth-integrated chlorophyll was positively correlated with isopycnal spacing (Fig 3b; eddy C, $R = 0.74$, $p < 0.05$; eddy B, $R = 0.67$, $p < 0.05$). Interestingly, if we include in our analysis a range of offshore stations sampled along undefined transects past eddy B (Fig 3: grey circles), we find offshore stations produce a similar pattern to eddy C and B, signifying higher overall chlorophyll content with increasing isopycnal spacing ($R = 0.87$, $p < 0.05$). A different pattern emerged for the coastal anticyclonic mode-water eddy A, where no relationship was found between depth-integrated chlorophyll and isopycnal spacing. In other words no distinct pattern was observed in eddy A as stations grouped tightly together indicating that chlorophyll was evenly distributed across both the periphery and center of the mesoscale eddy (Fig 3b). Given the proximity of eddy A to the coast and our current understanding of horizontal advection induced by eddies (40), the lack of discernible difference in chlorophyll across eddy A could be ascribed to a masking effect caused by coastal-derived chlorophyll.

Plotting depth-integrated chlorophyll as a function of distance from the center of eddies A, B and C, based on SSHA also reveals depth-integrated chlorophyll to increase at the eddy periphery (S4 Fig; $R = 0.50$, $p < 0.05$). Notably, however, SSHA is not necessarily congruent with the subsurface properties of the eddy including the eddy horizontal velocity or isopycnal spacing (38, 40). Arguably the more robust and less subjective method is to analyze depth-integrated chlorophyll as a function of isopycnal spacing. The finding of enhanced chlorophyll along the density front in this study (Fig 3 and S4 Fig), is also in agreement with high-resolution modeling studies, which demonstrate that submesoscale dynamics operate non-uniformly along the eddy density front creating pockets of upwelling and subduction (15, 17, 30, 36, 41). An observational study by Strass, (42) has shown in a 2000 km transect across the North Atlantic a tendency for higher chlorophyll along the eddy density front where isopycnal spacing was largest and conversely lower chlorophyll concentrations when spacing was smallest. Evidence in this study indicates that peripheral chlorophyll extends deeper into the OMZ than at the center, as demonstrated by the appearance of lateral intrusions and deep chlorophyll pockets observed in eddy transect profiles ((38); S3 Fig). Submesoscale processes may likewise play an important role in actively supplying organic matter in the offshore OMZ (33).

In addition to the coastally derived chlorophyll background (e.g. eddy C versus eddy A) our data further suggests that submesoscale peripheral processes have the potential to generate new chlorophyll. If we use chlorophyll as a proxy for primary production, then enhanced organic matter at the periphery, exported as either sinking particles or by subduction, could fuel measured anammox activity (Fig 3 and S3 Fig). Unfortunately, there is insufficient data available to perform a similar comparison of isopycnal spacing with depth-integrated anammox rates. Nevertheless, the relationship of chlorophyll with isopycnal spacing established over a large number of offshore stations, including stations sampled along undefined transects past eddy B is intriguing (Fig 3B). Why this holds could be attributed to the ubiquity of mesoscale eddies and submesoscale fronts, which have been shown to cause enhanced vertical transport in ETSP waters (33). The combination of these processes, and their influence over vertical transport, could strongly regulate the distribution of chlorophyll in the ETSP region and thereby microbial nitrogen loss processes.

Aerial sea surface height analysis highlights the widespread distribution of mesoscale eddies in the ETSP region. If we overlay depth-integrated anammox rates over sea surface height for stations sampled across eddies A, B and C, we find that nitrogen loss is heterogeneous (Fig 4). Similar heterogeneity in both nitrogen loss rates and the distribution of eddies was observed in previous ETSP sampling campaigns in January and February 2009 (Fig 4; M77-3 and -4; (13)), suggesting that eddies may drive much of the vertical nutrient transport and thereby primary productivity in the offshore OMZ. Previous studies in the ETSP region and elsewhere have shown that submesoscale transport is an important process, not only fueling enhanced primary productivity (36, 41), but also contributing to the subduction of organic

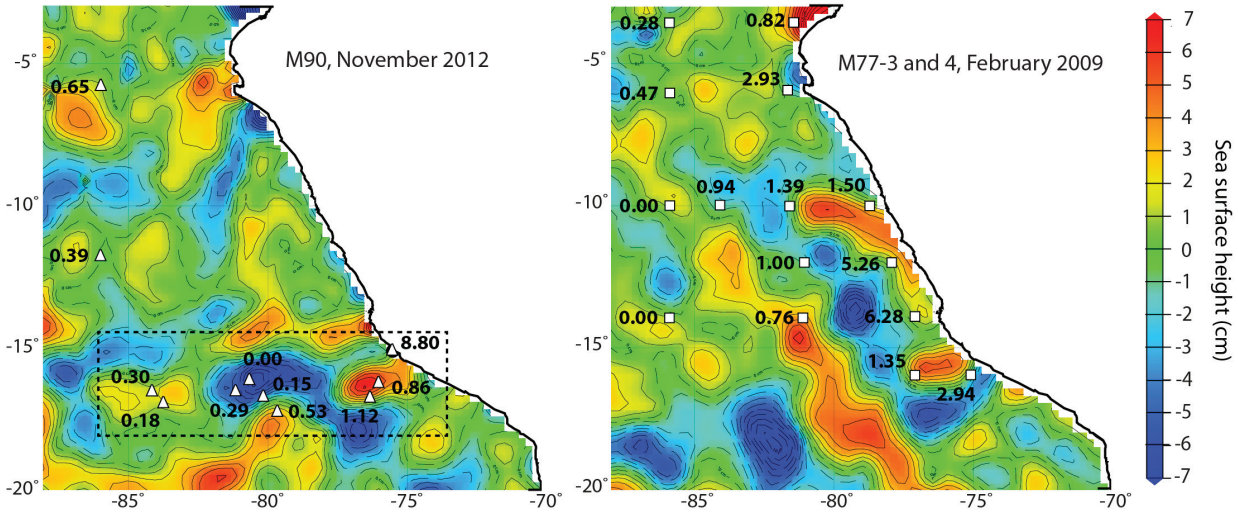

Fig 4. Widespread distribution of mesoscale eddies and the heterogeneity of anammox rates in the offshore ETSP region. Aerial sea surface height during the M90 (November 22nd, 2012) and the M77-4 (February 5th, 2009) research cruises. Eddies A, B and C shown in Fig 2A are highlighted by the dashed box in the left panel. Overlaid are depth integrated anammox rates (mmol N m^{-2} d^{-1}) from ^{15}N-incubation experiments from this study (left panel), and rates from the M77-3 and M77-4 research expeditions (right panel) (13). Anammox rates are depth integrated over the OMZ at a cutoff of 20 μM oxygen.

matter below the surface mixed layer (32, 33). Based on our findings we suggest that eddy-driven submesoscale vertical transport of nutrients and organic matter may be a major regulator of offshore ETSP nitrogen loss, which by volume represents the largest regional sink of fixed nitrogen.

Summary and Conclusions

In this study we provide the first rate measurements of nitrogen loss processes across cyclonic and anticyclonic mode-water eddies in the ETSP. Contrary to the recent 'hotspot' studies, which have suggested that the highest activity occurs in the eddy center (14, 37-39, 48), our ^{15}N-labelling incubation experiments revealed that nitrogen loss activity was greatest at the periphery of mesoscale eddies. Although, highest chlorophyll concentrations were observed in the center (38), depth-integrated chlorophyll content was also highest at the eddy periphery. The observed lateral intrusions and deep chlorophyll pockets occurring along the eddy periphery (38), suggest that this area of the eddy was active in the generation and export of organic matter, in agreement with modeling studies (36, 41).

Our findings, which indicate enhanced anammox activity and chlorophyll along the eddy periphery, appear to be consistent with these features being regulated by a submesoscale nutrient transport mechanism. The periphery of the eddy, as defined here and elsewhere, represents the eddy density front where isopycnals tilt and the spacing between isopycnals increases relative to the center. Specifically, submesoscale processes operate on either side of the density front, where the highest horizontal velocities occur (15, 17). In other regions, eddy-induced submesoscale processes have been shown to be significant drivers of vertical nutrient transport along the eddy periphery, thereby providing a supply of organic matter below the surface mixed layer (32, 41), which then has the potential to fuel microbial nitrogen loss activity in OMZs. Observations from two additional sampling campaigns in the ETSP OMZ demonstrate heterogeneity in both mesoscale eddy activity and nitrogen loss rates. Together this is suggestive that eddy-driven vertical transport of nutrients may regulate offshore nitrogen loss.

On a global scale mesoscale eddies contribute to an estimated vertical water column nutrient flux of 0.12 mol N m^{-2} yr^{-1} (23, 50). This estimation roughly

doubles if global biogeochemical model simulations resolve for submesocale processes within eddies (51). Current regional biogeochemical models, which have limited spatial resolution, do not yet include small-scale submesoscale features (52). Parameterization of vertical mixing processes may thus help to improve biogeochemical models and provide a more realistic assessment of the marine OMZ nitrogen budget.

Material and Methods

Ethics statement

Permission for the sampling campaign was obtained from the Peruvian authorities.

Nutrient and hydrography analysis

Sampling was undertaken on the M90 research expedition onboard the *R/V Meteor* from October 31st to November 26th, 2012. Eddies A, B and C were sampled along the 16.45'S transect (Fig 2A). Onboard, eddies were first identified and tracked by real-time SSHA data obtained from AVISO satellite altimetry. Transects through these eddies were made according to SSHA data. Horizontal velocities of the eddy were measured by acoustic Doppler current profiling (ADCP). A 75 and 38 kHz ADCP systems measured velocities down to 700 and 1200 m depth, respectively, detailed by Stramma et al., (38). In this study we define eddy boundaries according to ADCP profiles and not specifically by SSHA.

Complete details of methods used to measure and analyze eddy nutrient chemistry are described elsewhere (38). Briefly, a Seabird CTD-rosette equipped with 10L Niskin bottles was used to sample waters at depth. Chlorophyll, temperature, salinity, and oxygen were recorded by CTD sensors on both up and down casts. The oxygen sensor was calibrated by Winkler titration (53), with a detection limit of approximately 3 μM. Chlorophyll was calibrated according to the company specifications, with sensitivity down to 0.025 μg L^{-1}. No shipboard chlorophyll calibration was applied, because of this, Stramma et al., (38) note that absolute numbers may have uncertainties; nevertheless, gradient trends observed across the eddy are accurate. Nutrient samples were taken to measure nitrate, nitrite, and phosphate onboard by a QuAAtro auto-analyzer (Seal Analytical), with precisions of ± 0.1 μmol L^{-1}, ± 0.1 μmol L^{-1}, and ± 0.02 μmol L^{-1}, respectively. The N*, commonly used as a general measure of nitrogen loss, estimates from a given water mass chemistry the deviation of inorganic nitrogen pools from Redfield stoichiometry, was calculated according to the following equation $N^* = (NO_3^- + NO_2^-) - 16PO_4^{3-}$ (originally defined by (54), later modified by (14, 38)).

^{15}N incubation experiments

In situ ^{15}N-labelling incubation experiments were performed according to Holtappels et al., (55). In brief, waters were sampled directly from the Niskin bottle into 250 mL glass serum bottles. Bottles were overflowed 2-3 times their volume and sealed headspace free with a butyl rubber stopper, that had been stored under helium for 2 days prior to use, to avoid oxygen contamination. Once filled, glass serum bottles were stored at in situ temperature in the dark until all depths were sampled. Each serum bottle was purged for a total of 15 min with helium; ^{15}N-labeled isotopes were added with a gas-tight syringe after 5 min of purging to allow mixing. The experiments included the following additions: exp1: $^{15}N\text{-}NO_2^- + {}^{14}N\text{-}NH_4^+$, and exp2: $^{15}N\text{-}NH_4^+ + {}^{14}N\text{-}NO_2^-$. The concentration of added substrates was 5 μM. After degassing, exetainers (12 mL, Labco, UK) were filled off and capped headspace free. Caps were degassed with a vacuum, followed by purging with helium three times and then stored 2-3 days before use, to reduce oxygen contamination (56). Samples were incubated in the dark at in situ temperature. Exetainers were terminated at 0, 6, 12, 24 and 48 hours with 100 μL $HgCl_2$ after inserting a 2 mL helium headspace. Terminated samples were stored in the dark at ambient temperature cap side down until further processing.

Isotope products $^{14}N^{15}N$ and $^{15}N^{15}N$ were measured by a gas-chromatography isotope-ratio mass spectrometer (GC-IRMS; VG Optima, Manchester, UK). The rates of N_2 production from $^{15}N\text{-}NH_4^+$ and

$^{15}N\text{-}NO_2^-$ incubation experiments were determined from the slope of the linear regression as a function of time. Anammox and denitrification rates were calculated according to the equations of Thamdrup and Dalsgaard, (57). A t-test was used to determine whether rates were significantly different from zero ($p < 0.05$). Detection limits were estimated from the median of the standard error of the slope, multiplied by the t-value for $p = 0.05$, thus the detection limits for anammox were 0.68 and 0.66 nM N d^{-1} for $^{15}N\text{-}NH_4^+$ and $^{15}N\text{-}NO_2^-$ incubation experiments, respectively. The majority of our analysis is based on the $^{15}N\text{-}NH_4^+$ incubations, due to the potential caveats of using $^{15}N\text{-}NO_2^-$ to determine anammox rates; nitrogen isotope exchange between the nitrate and nitrite pools (58), and 'nitrite shunting' (59).

Anammox rates were depth integrated from the base of the upper oxycline down to the bottom oxycline (using an oxygen cutoff of 20 μM), analogous to depth integrated rates reported by Kalvelage et al., (13). At all offshore stations chlorophyll was depth-integrated down to 300 m depth, which was the deepest depth reported for anammox activity in eddies A and C. At coastal stations chlorophyll was depth-integrated down to 200 m. Isopycnal spacing was calculated for each station by subtracting the distance between reference densities 25.4 and 26.0 kg m^{-3}. Pearson correlation statistics were applied to determine if relationships were significant ($p < 0.05$).

Author contributions

Conceptualization: C.M.C., G.L., L.S., M.M.M.K., L.A.B. Data curation: C.M.C., L.S. Formal analysis: C.M.C., G.L., L.A.B. Funding acquisition: M.M.M.K. Investigation: C.M.C. Project administration: L.S., M.M.M.K. Resources: L.S., M.M.M.K. Visualization: C.M.C. Writing – original draft: C.M.C. Writing – review & editing: G.L., L.S., M.M.M.K., L.A.B.

Acknowledgements

We thank the Peruvian authorities for access to national waters as well as the crew of the *RV Meteor* for assistance onboard the M90 research expedition as well as co-chief scientist M. Frank. We would also like to thank C. Schelten for administrative support; technical assistance by T. Kalvelage; proof reading of the manuscript by H. Marchant and the editor and two anonymous reviewers for constructive feedback.

References

1. *Karstensen J, Stramma L, & Visbeck M (2008) Oxygen minimum zones in the eastern tropical Atlantic and Pacific oceans. Progress in Oceanography 77(4):331-350.*
2. *Lam P & Kuypers MMM (2011) Microbial nitrogen cycling processes in oxygen minimum zones. Ann Rev Mar Sci 3:317-345.*
3. *Tiano L, et al. (2014) Oxygen distribution and aerobic respiration in the north and south eastern tropical Pacific oxygen minimum zones. Deep Sea Research Part I: Oceanographic Research Papers 94:173-183.*
4. *Thamdrup B, Dalsgaard T, & Revsbech NP (2012) Widespread functional anoxia in the oxygen minimum zone of the Eastern South Pacific. Deep Sea Research Part I: Oceanographic Research Papers 65:36-45.*
5. *Codispoti LA, et al. (2001) The oceanic fixed nitrogen and nitrous oxide budgets: Moving targets as we enter the anthropocene? Scientia Marina 65(S2):85-105.*
6. *Ulloa O, Canfield DE, DeLong EF, Letelier RM, & Stewart FJ (2012) Microbial oceanography of anoxic oxygen minimum zones. Proceedings of the National Academy of Sciences of the United States of America 109(40):15996-16003.*
7. *Kuypers MM, et al. (2005) Massive nitrogen loss from the Benguela upwelling system through anaerobic ammonium oxidation. Proceedings of the National Academy of Sciences of the United States of America 102(18):6478-6483.*
8. *Jensen MM, et al. (2011) Intensive nitrogen loss over the Omani Shelf due to anammox coupled with dissimilatory nitrite reduction to ammonium. The ISME journal 5(10):1660-1670.*
9. *Hamersley MR, et al. (2007) Anaerobic ammonium oxidation in the Peruvian oxygen minimum zone. Limnology and Oceanography 52(3):923-933.*
10. *Lam P, et al. (2009) Revising the nitrogen cycle in the Peruvian oxygen minimum zone. Proceedings of the National Academy of Sciences of the United States of*

America 106(12):4752-4757.

11. Thamdrup B, et al. (2006) Anaerobic ammonium oxidation in the oxygen-deficient waters off northern Chile. Limnology and Oceanography 51(5):2145-2156.

12. Galán A, et al. (2009) Anammox bacteria and the anaerobic oxidation of ammonium in the oxygen minimum zone off northern Chile. Deep Sea Research Part II: Topical Studies in Oceanography 56(16):1021-1031.

13. Kalvelage T, et al. (2013) Nitrogen cycling driven by organic matter export in the South Pacific oxygen minimum zone. Nature Geosci 6(3):228-234.

14. Altabet MA, et al. (2012) An eddy-stimulated hotspot for fixed nitrogen-loss from the Peru oxygen minimum zone. Biogeosciences 9(12):4897-4908.

15. Mahadevan A (2016) The Impact of Submesoscale Physics on Primary Productivity of Plankton. Annual Review of Marine Science 8(1).

16. Chelton DB, Schlax MG, Samelson RM, & de Szoeke RA (2007) Global observations of large oceanic eddies. Geophysical Research Letters 34(15).

17. Klein P & Lapeyre G (2009) The Oceanic Vertical Pump Induced by Mesoscale and Submesoscale Turbulence. Annual Review of Marine Science 1(1):351-375.

18. Johannessen JA, et al. (1996) Coastal ocean fronts and eddies imaged with ERS 1 synthetic aperture radar. Journal of Geophysical Research: Oceans 101(C3):6651-6667.

19. Niiler PP (1969) On the Ekman divergence in an oceanic jet. Journal of Geophysical Research 74(28):7048-7052.

20. McGillicuddy DJ, (2016) Mechanisms of Physical-Biological-Biogeochemical Interaction at the Oceanic Mesoscale. Annual Review of Marine Science 8(1):125-159.

21. Gaube P, Chelton DB, Samelson RM, Schlax MG, & O'Neill LW (2015) Satellite Observations of Mesoscale Eddy-Induced Ekman Pumping. Journal of Physical Oceanography 45(1):104-132.

22. Gaube P, Chelton DB, Strutton PG, & Behrenfeld MJ (2013) Satellite observations of chlorophyll, phytoplankton biomass, and Ekman pumping in nonlinear mesoscale eddies. Journal of Geophysical Research: Oceans 118(12):6349-6370.

23. McGillicuddy DJ, et al. (1998) Influence of mesoscale eddies on new production in the Sargasso Sea. Nature 394(6690):263-266.

24. McGillicuddy DJ, et al. (2007) Eddy/Wind Interactions Stimulate Extraordinary Mid-Ocean Plankton Blooms. Science 316(5827):1021-1026.

25. Li J, Qi Y, Jing Z, & Wang J (2014) Enhancement of eddy-Ekman pumping inside anticyclonic eddies with wind-parallel extension: Satellite observations and numerical studies in the South China Sea. Journal of Marine Systems 132:150-161.

26. Mizobata K, et al. (2002) Bering Sea cyclonic and anticyclonic eddies observed during summer 2000 and 2001. Progress in Oceanography 55(1–2):65-75.

27. Lévy M & Klein P (2004) Does the low frequency variability of mesoscale dynamics explain a part of the phytoplankton and zooplankton spectral variability? Proceedings of the Royal Society of London A: Mathematical, Physical and Engineering Sciences 460(2046):1673-1687.

28. Kahru M, Mitchell BG, Gille ST, Hewes CD, & Holm-Hansen O (2007) Eddies enhance biological production in the Weddell-Scotia Confluence of the Southern Ocean. Geophysical Research Letters 34(14): L14603.

29. Ledwell JR, McGillicuddy Jr DJ, & Anderson LA (2008) Nutrient flux into an intense deep chlorophyll layer in a mode-water eddy. Deep Sea Research Part II: Topical Studies in Oceanography 55(10–13):1139-1160.

30. Martin AP & Richards KJ (2001) Mechanisms for vertical nutrient transport within a North Atlantic mesoscale eddy. Deep Sea Research Part II: Topical Studies in Oceanography 48(4–5):757-773.

31. Fielding S, et al. (2001) Mesoscale subduction at the Almeria–Oran front: Part 2. Biophysical interactions. Journal of Marine Systems 30(3–4):287-304.

32. Omand MM, et al. (2015) Eddy-driven subduction exports particulate organic carbon from the spring bloom. Science 348(6231):222-225.

33. Thomsen S, et al. (2016) Do submesoscale frontal processes ventilate the oxygen minimum zone off Peru? Geophysical Research Letters 43(15):8133-8142.

34. Chaigneau A, Gizolme A, & Grados C (2008) Mesoscale eddies off Peru in altimeter records: Identification algorithms and eddy spatio-temporal patterns. Progress in Oceanography 79(2–4):106-119.

35. Chaigneau A, Eldin G, & Dewitte B (2009) Eddy activity in the four major upwelling systems from satellite

altimetry (1992–2007). Progress in Oceanography 83(1–4):117-123.

36. *Mahadevan A, Thomas LN, & Tandon A (2008) Comment on "Eddy/Wind Interactions Stimulate Extraordinary Mid-Ocean Plankton Blooms". Science 320(5875):448-448.*

37. *Bourbonnais A, et al. (2015) N-loss isotope effects in the Peru oxygen minimum zone studied using a mesoscale eddy as a natural tracer experiment. Global Biogeochemical Cycles 29(6):793-811.*

38. *Stramma L, Bange HW, Czeschel R, Lorenzo A, & Frank M (2013) On the role of mesoscale eddies for the biological productivity and biogeochemistry in the eastern tropical Pacific Ocean off Peru. Biogeosciences 10(11):7293-7306.*

39. *Löscher CR, et al. (2015) N2 fixation in eddies of the eastern tropical South Pacific Ocean. Biogeosciences Discuss. 12(22):18945-18972.*

40. *Thomsen S, et al. (2016) The formation of a subsurface anticyclonic eddy in the Peru-Chile Undercurrent and its impact on the near-coastal salinity, oxygen, and nutrient distributions. Journal of Geophysical Research: Oceans. 476-501.*

41. *Brannigan L (2016) Intense submesoscale upwelling in anticyclonic eddies. Geophysical Research Letters:n/a-n/a.*

42. *Strass VH (1992) Chlorophyll patchiness caused by mesoscale upwelling at fronts. Deep Sea Research Part A. Oceanographic Research Papers 39(1):75-96.*

43. *Lam P, et al. (2011) Origin and fate of the secondary nitrite maximum in the Arabian Sea. Biogeosciences 8(6):1565-1577.*

44. *Kalvelage T, et al. (2015) Aerobic Microbial Respiration In Oceanic Oxygen Minimum Zones. PloS one 10(7):e0133526.*

45. *Dalsgaard T, Thamdrup B, Farías L, & Revsbech NP (2012) Anammox and denitrification in the oxygen minimum zone of the eastern South Pacific. Limnology and Oceanography 57(5):1331-1346.*

46. *Dalsgaard T, et al. (2014) Oxygen at Nanomolar Levels Reversibly Suppresses Process Rates and Gene Expression in Anammox and Denitrification in the Oxygen Minimum Zone off Northern Chile. mBio 5(6).*

47. *Kalvelage T, et al. (2011) Oxygen Sensitivity of Anammox and Coupled N-Cycle Processes in Oxygen Minimum Zones. PloS one 6(12):e29299.*

48. *Arévalo-Martínez DL, et al. (2015) Influence of mesoscale eddies on the distribution of nitrous oxide in the eastern tropical South Pacific. Biogeosciences Discuss. 2015:9243-9273.*

49. *Gruber N, et al. (2011) Eddy-induced reduction of biological production in eastern boundary upwelling systems. Nature Geosci 4(11):787-792.*

50. *McGillicuddy DJ, Anderson LA, Doney SC, & Maltrud ME (2003) Eddy-driven sources and sinks of nutrients in the upper ocean: Results from a 0.1° resolution model of the North Atlantic. Global Biogeochemical Cycles 17(2):n/a-n/a.*

51. *Lapeyre G & Klein P (2006) Impact of the small-scale elongated filaments on the oceanic vertical pump. Journal of Marine Research 64(6):835-851.*

52. *Nagai T, et al. (2015) Dominant role of eddies and filaments in the offshore transport of carbon and nutrients in the California Current System. Journal of Geophysical Research: Oceans 120(8):5318-5341.*

53. *Winkler LW (1888) Die Bestimmung des im Wasser gelösten Sauerstoffes. Berichte der deutschen chemischen Gesellschaft 21(2):2843-2854.*

54. *Gruber N & Sarmiento JL (1997) Global patterns of marine nitrogen fixation and denitrification. Global Biogeochemical Cycles 11(2):235-266.*

55. *Holtappels M, Lavik G, Jensen MM, & Kuypers MMM (2011) 15N-labeling experiments to dissect the contributions of heterotrophic denitrification and anammox to nitrogen removal in the OMZ waters of the ocean. Methods in Enzymology, ed Martin GK (Academic Press), Vol Volume 486, pp 223-251.*

56. *De Brabandere L, Thamdrup B, Revsbech NP, & Foadi R (2012) A critical assessment of the occurrence and extend of oxygen contamination during anaerobic incubations utilizing commercially available vials. Journal of microbiological methods 88(1):147-154.*

57. *Thamdrup B & Dalsgaard T (2002) Production of N2 through anaerobic ammonium oxidation coupled to nitrate reduction in marine sediments. Applied and environmental microbiology 68(3):1312-1318.*

58. *Brunner B, et al. (2013) Nitrogen isotope effects induced by anammox bacteria. Proceedings of the National Academy of Sciences 110(47):18994-18999.*

59. *De Brabandere L, et al. (2014) Vertical partitioning of*

nitrogen-loss processes across the oxic-anoxic interface of an oceanic oxygen minimum zone. Environmental microbiology 16(10):3041-3054.

Supporting information

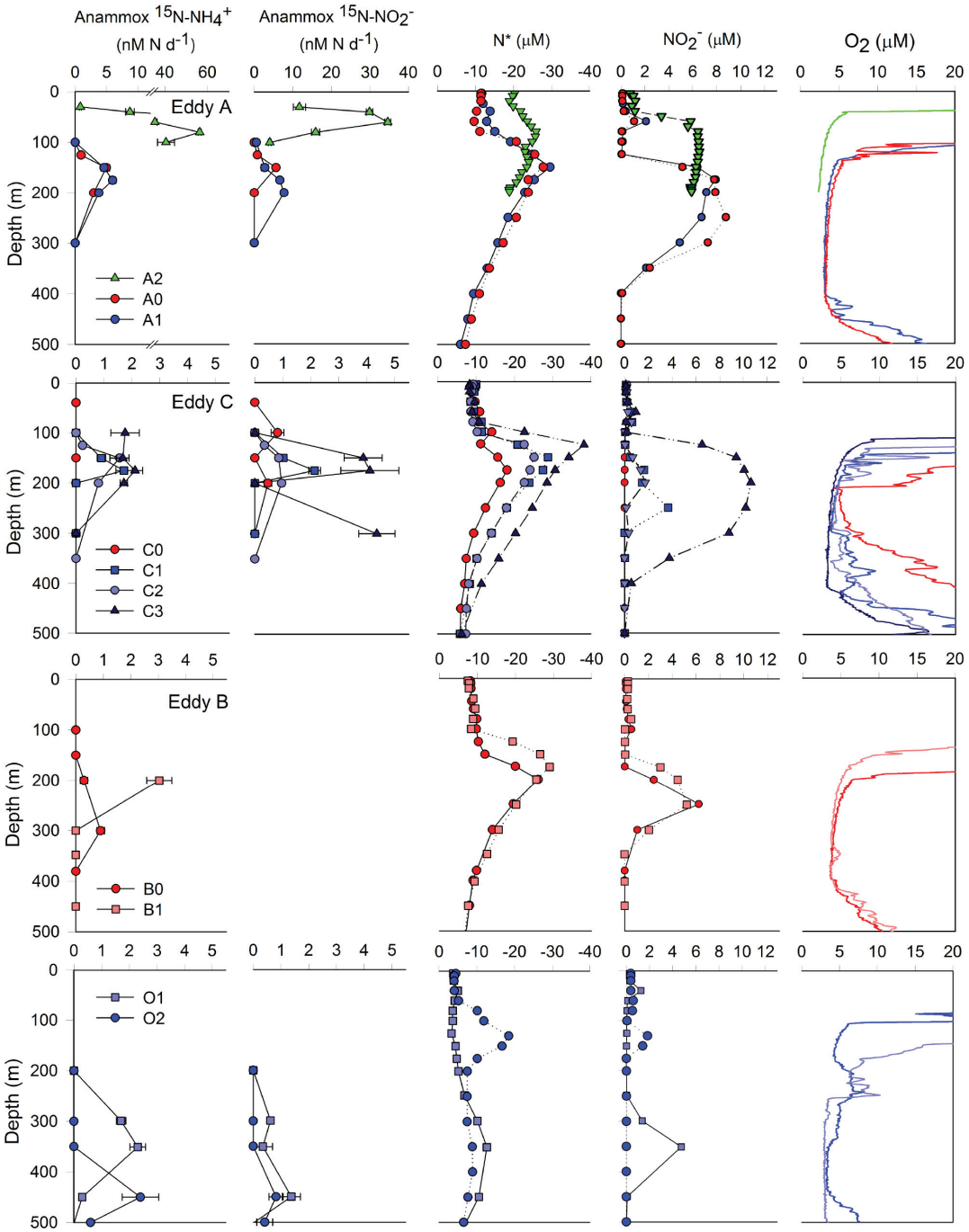

S1 Fig. Depth profiles of anammox activity, nutrient, and oxygen concentrations at stations sampled within eddies A, B and C, and two offshore stations. The location of stations is indicated in Fig 2A and S1 Table. Anammox activity for 15N-NH4+ and 15N-NO2- experiments are indicated in separate panels. For stations B0 and B1 (eddy B) anammox rates from 15N-NO2- experiments were not determined. Error bars for anammox rates represent the standard error. The N-deficit was calculated according to Stramma et al., [37], see material and methods section.

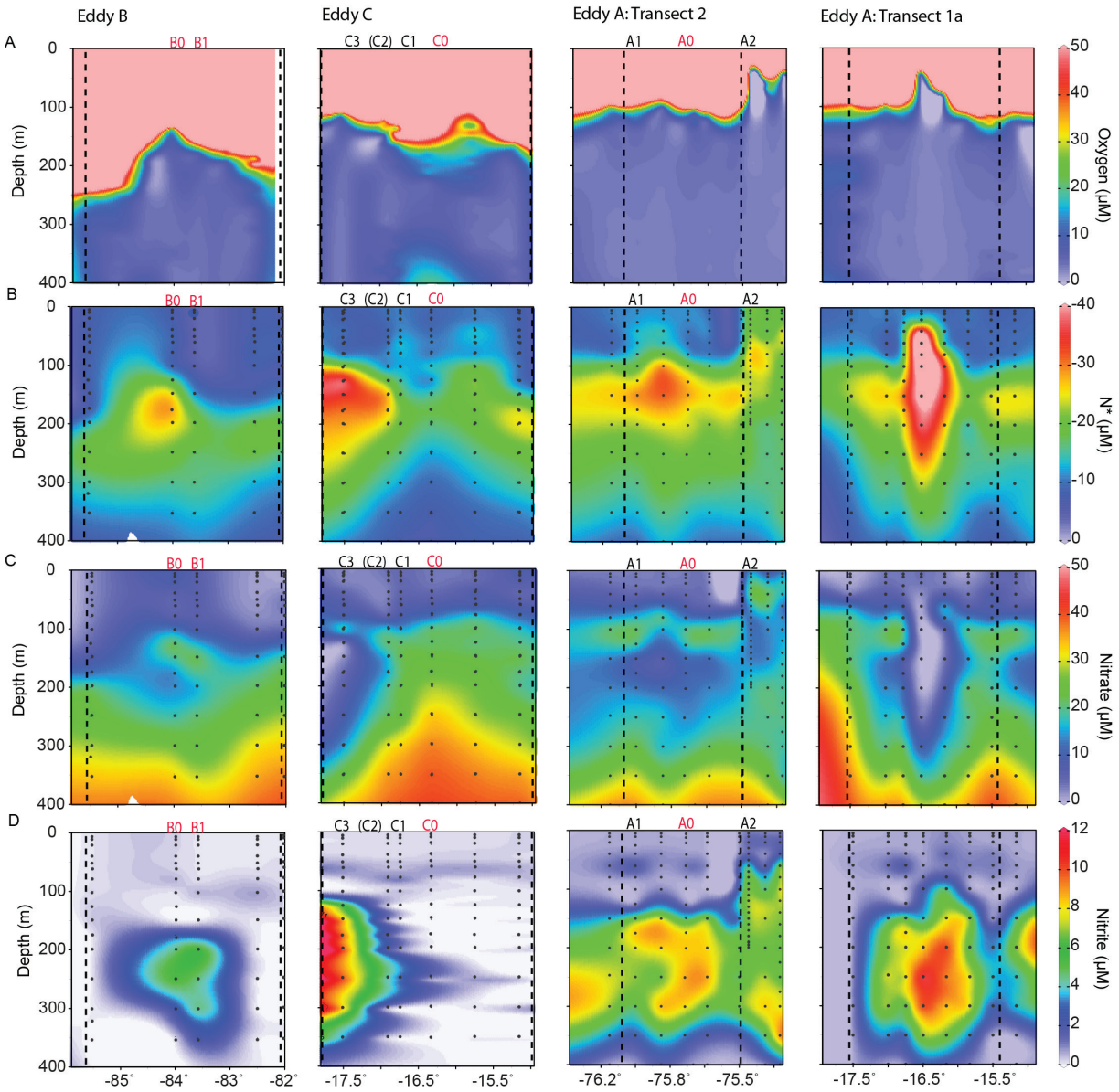

S2 Fig. Distribution of oxygen, N*, and nutrients across eddies A, B and C in the ETSP region. The cross eddy transects are shown in Fig 2A. Note that both oxygen, N*, and nutrients transects of eddy A are indicated (see Fig 2A for transect stations: T1a (blue dotted lines) and T2 (red dotted lines)). Stations numbered in red (B0, B1, C0, and A0) were sampled in the eddy center while stations with black numbers (C3, C2, C1, and A1) were sampled on the eddy periphery, identified according to eddy-induced horizontal velocities and density fronts, shown in Fig 2. Note that data from station C2 is not included in the transect profiles shown (indicated by (C2)). The coastal upwelling station is indicated by 'A2'. The vertical black dotted lines in panels A-D represent the outer periphery of the respective eddies. Data shown is adapted from Stramma et al., [37].

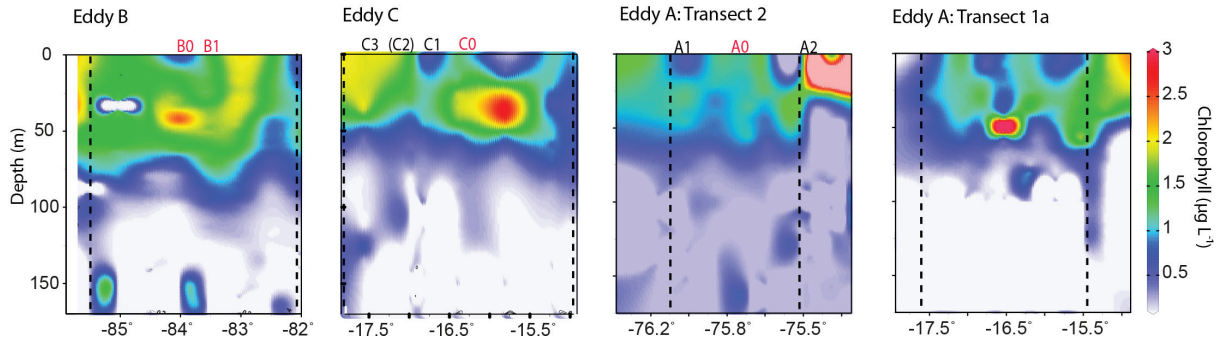

S3 Fig. Distribution of chlorophyll across eddies A, B and C in the ETSP region. The cross eddy transects are shown in Fig. 2A. Note that both chlorophyll transects of eddy A are indicated (see Fig 2A for transect stations: T1a (blue dotted lines) and T2 (red dotted lines)). Stations numbered in red (B0, B1, C0, and A0) were sampled in the eddy center while stations with black numbers (C3, C2, C1, and A1) were sampled on the eddy periphery, identified according to eddy-induced horizontal velocities and density fronts, shown in Fig 2. Note that data from station C2 is not included in the transect profiles shown (indicated by (C2)). The coastal upwelling station is indicated by 'A2'. The vertical black dotted lines in each panel represent the outer periphery of the respective eddies. Data shown is adapted from Stramma et al., [37].

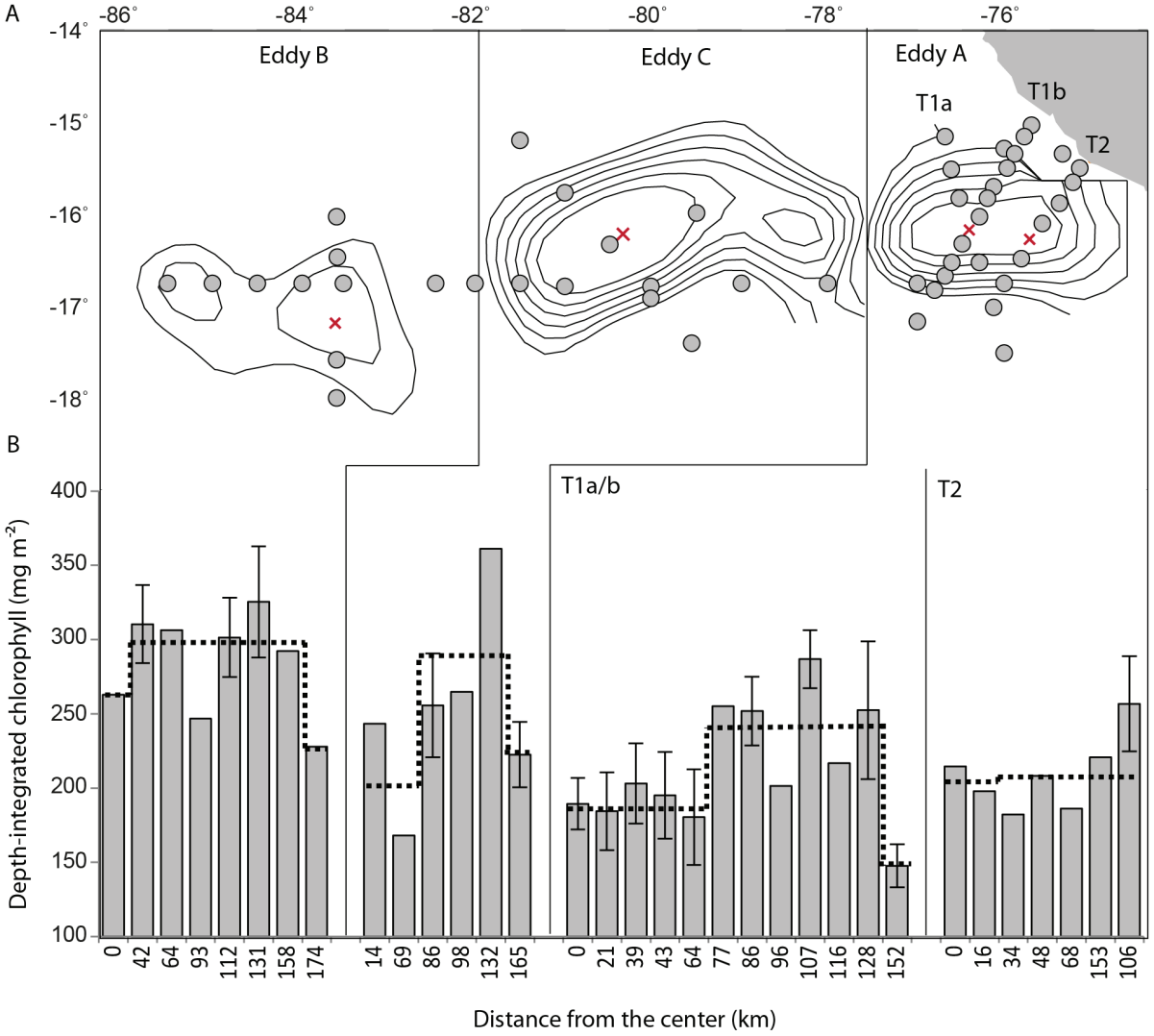

S4 Fig. Distribution of depth-integrated chlorophyll across eddies A, B and C in the ETSP region based on satellite sea surface height altimetry (SSHA). (A) Aerial SSHA snapshot of eddies A, B and C. The eddy center is marked by the red cross, determined based on SSHA and the stations indicated are the same stations as those used in Fig 3 (offshore stations are not included). Note that eddy A is subdivided into three distinct transects (T1a/b and T2), with transects 1 and 2 having a different eddy center (red cross) as the transects were sampled approximately 5 days apart, and the eddy had propagated westward during this time. (B) Depth-integrated chlorophyll plotted as a function of distance from the eddy center. Depth-integrated chlorophyll of stations located a similar distance from the center (±2 km) were averaged, as indicated by the error bars (the standard error is shown). The overlaid dotted lines indicate the average depth-integrated chlorophyll for the eddy center, periphery and outside the eddy. Chlorophyll at all stations was depth-integrated down to 300 m depth, except for coastal stations which were depth-integrated down to 200 m. Plotting depth-integrated chlorophyll in panel B as a function of distance from the eddy center for all eddy stations (excluding the outside eddy stations) indicates a significant positive correlation ($R = 0.50$, $p < 0.05$).

S1 Table. List of stations sampled for anammox rates during the M90 research cruise November 2012.

Abbreviated station name (used in text)	M90 station name	Latitude (°N)	Longitude (°E)
B0	1639	-16.75	-84.00
B1	1646	-17.17	-83.58
C0	1659	-16.33	-80.50
C1	1660	-16.92	-80.00
C2	1652	-16.75	-81.00
C3	1661	-17.50	-79.50
A0	1672	-16.23	-75.67
A1	1668	-16.74	-76.00
A2	1679	-15.33	-75.35
O1	1581	-6.00	-85.83
O2	1604	-12.00	-85.83

CHAPTER 4

Sulfur cycling associated with oxygen minimum zone waters

Cameron M. Callbeck, Donald E. Canfield, Marcel M. M. Kuypers, Pelin Yilmaz, Gaute Lavik, Bo Thamdrup, Laura A. Bristow. (2017) Sulfur cycling associated to oxygen minimum zones waters. In review *Limnology and oceanography*

Abstract

Oxygen minimum zones (OMZs) are active regions of nitrogen (N) loss and support a tightly coupled but hardly explored microbial sulfur cycle. A number of OMZ studies have revealed that this sulfur cycle generates the full spectrum of oxidized and reduced fixed N species and thus contributes either directly or indirectly to N-loss, and to the production of the greenhouse gas N_2O. Sulfur cycling is most prominent in highly productive coastal OMZ waters depleted in oxygen and nitrate, where sulfide accumulates in bottom waters during sulfidic events. Such phenomena, which occur in all major OMZs, can cover vast expanses of upper shelf waters, impacting shelf biogeochemistry with detrimental consequences on marine life. The accumulation of sulfide in these waters is regulated not only by the benthic-pelagic coupling of sulfate-reducing and sulfide-oxidizing bacteria, but also by the interplay of various physical mechanisms. Recent evidence indicates that sulfur cycling processes may also occur in nitrate-rich offshore OMZ waters. These offshore waters ubiquitously host a community of sulfate-reducing and sulfide-oxidizing bacteria, including poorly characterized heterotrophic sulfide-oxidizing bacterial clades that potentially thrive from the turnover and oxidation of organosulfonate compounds. In this review, we summarize our current understanding of OMZ sulfur cycling dynamics, key microbial community players, and open questions that persist moving forward.

Large-scale thermo-haline circulation maintains a well-oxygenated ocean, with the exception of eutrophic regions called oxygen minimum zones (OMZ). OMZs occur at tropical latitudes along continental margins where coastal upwelling of nutrient rich waters causes intensified primary productivity in surface waters (1). As a result, the downward settling flux of organic matter stimulates microbial respiration that lowers dissolved oxygen concentrations in the underlying water column. Most waters typically have lower oxygen concentrations below the euphotic zone; however, in OMZs this deficit is exacerbated by poor regional ventilation resulting in oxygen concentrations below the detection limit (a few nanomoles per litre) of the highly sensitive STOX oxygen sensor (2-4). The major OMZs are located in the eastern tropical South Pacific (ETSP), the eastern tropical North Pacific (ETNP), the eastern tropical South Atlantic (ETSA), the Arabian Sea and the Bay of Bengal (Fig. 1). At an oxygen cutoff of 20 μM, OMZs together comprise ~1% of the global ocean volume (5).

OMZ waters, especially those with low nanomolar to no detectable oxygen, host a diverse assemblage of anaerobic microorganisms. These organisms thrive in the absence of oxygen using electron acceptors such as nitrate, leading to substantial fixed nitrogen loss in OMZ waters, strongly impacting the marine nitrogen budget (6-8). Following the redox tower, nitrate reduction is followed by manganese reduction, iron reduction and then sulfate reduction (9). Even though sulfate reduction holds one of the lowest positions on the redox tower, the potential for heterotrophic sulfate-reduction in OMZ waters is large. Modern day sulfate concentrations, which stand at 28 mM, are much higher than concentrations of other more favorable electron acceptors, which are found in nanomoles to micromoles per liter. The large sulfate pool, in combination with the enhanced particle load of OMZs, theoretically provides a nearly inexhaustible supply of substrate for heterotrophic sulfate-reducing bacteria. This is hypothesized to be the basis of the OMZ sulfur cycle and generates sulfide that in turn fuels sulfide-oxidizing bacteria and the production of other reduced sulfur intermediates (Fig. 2). The large sulfate pool also potentially supports an extensive microbial organic-sulfur based cycle that stems from the assimilation of sulfate into sulfur-containing compounds (10). This, in turn, fuels heterotrophic sulfide-oxidizing bacteria that thrive from organic matter sulfidogenesis, or the breakdown of organic sulfur-containing compounds to reduced sulfur species, sulfide, thiosulfate and sulfite (11, 12). This review provides a synthesis of our current, but rudimentary

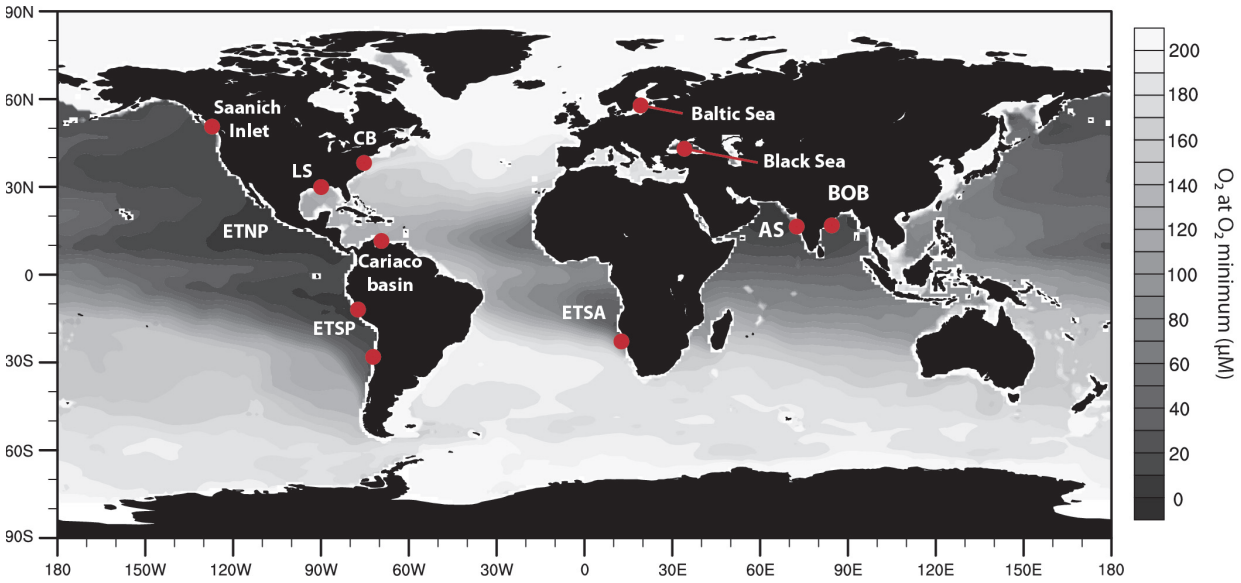

Fig. 1. Location of oxygen minimum zone waters and sulfidic marine environments. Plotted is the minimum O_2 concentration in the water column, based on World Atlas data 2013. Red circles indicate regions with documented sulfidic waters. Abbreviations indicated stand for: Eastern Tropical South Pacific (ETSP), Eastern Tropical North Pacific (ETNP), Eastern Tropical South Atlantic, Arabian Sea (AS), Bay of Bengal (BOB), Chesapeake Bay (CB) and Louisiana Shelf (LS).

understanding of sulfur cycling in modern OMZs, with a specific focus on the pelagic water column and its interactions with the sediment.

Sulfur cycling in modern OMZs

The intensified input of organic matter along coastal upwelling regions has the potential to fuel an enhanced sulfur cycle in sediments underlying OMZ shelf waters. During severe oxygen and nitrate depletion, episodic occurrences of hydrogen sulfide release have been reported, termed sulfidic events (13-16). A prerequisite for a sulfidic event is the formation of stagnant and stratified bottom waters that result in the consumption of water column oxygen and, subsequently, nitrate, ultimately releasing benthic hydrogen sulfide, produced by the activities of heterotrophic sulfate reducing bacteria (13, 17, 18). In seawater (pH 7-8), H_2S is mainly in the form of HS^- ($H_2O + H_2S \rightarrow H_3O^+ + HS^-$, pK_a=6.88) (19), but for simplicity, we refer to 'sulfide' as comprising both the aqueous HS^- and its gaseous form H_2S. Part of the sulfide that escapes immediate removal in sediments (e.g. by pyrite formation or by mat-forming sulfide-oxidizing bacteria, (20)) is released into the water column via passive molecular diffusion (21). This release can be further facilitated by ebullition with methane bubbles (22, 23), or in rare cases, sulfide is released in catastrophic eruptions following the collapse of gas-charged pockmarks (21). Generally, sulfide accumulates to low micromolar concentrations in shelf bottom waters over the course of days (24). Sulfidic events are generally contained and terminated in OMZ bottom waters by oxidation coupled to the reduction of nitrate supplied from the overlying water, catalyzed by a consortium of sulfide/sulfur-oxidizing bacteria (13). However, sulfide that escapes oxidation, reaching oxic waters (e.g. by sudden eruptions or by advection), can have detrimental impacts on marine life resulting in mass migrations and die-offs of regional fish and invertebrate stocks (25, 26).

Oceanic sulfidic events have been observed as far back as the 19th century, many being detected by the smell of "rotten eggs" – the most recognizable characteristic of hydrogen sulfide (H_2S). It was not until the late 1970's when sulfide events (detected by smell) were shown to be associated with nitrate-depleted waters, implicating sulfide-driven nitrate reduction (27). In the past decade, advances in remote sensing technology have offered improved spatial and

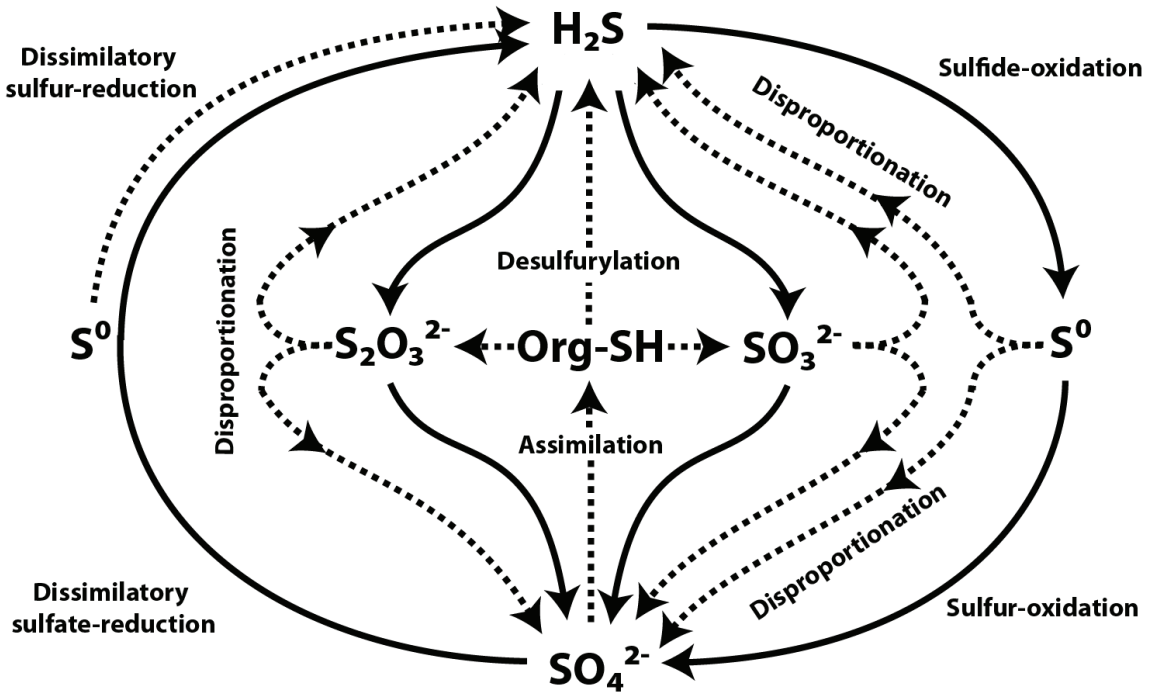

Fig. 2. The microbial sulfur cycle in oxygen minimum zones. Sulfate-reduction produces sulfide (H_2S), whereas sulfide oxidation generates intermediate sulfur species that include elemental sulfur (S^0), thiosulfate ($S_2O_3^{2-}$) and sulfite (SO_3^{2-}). Sulfide, including produced intermediates, can be oxidized to sulfate, thus complementing sulfate reduction. Produced sulfur intermediates can also be disproportionated to yield sulfide and sulfate. Sulfur-containing organic matter is produced from the assimilation of sulfate into biomass. Reduced sulfur intermediates, thiosulfate, sulfite and sulfide can be generated from the degradation of organic sulfur-containing compounds (Org-SH), referred to as organic matter sulfidogenesis. Produced sulfur species can be oxidized to sulfate via the pathways indicated. Solid lines represent processes that are known to occur in OMZ waters, while pathways shown in dotted lines are expected to occur in OMZ waters but that have limited evidence.

temporal resolution of sulfidic events by observation of sulfur plumes (28). Sulfur, a common by-product of microbial sulfide oxidation, scatters light giving the water a milky-turquoise discoloration with a maximum wavelength reflectance at 560 nm (29). Sulfidic events have been detected in shelf waters of all major OMZs by remote sensing of sulfur plumes and/or by ship-based sulfide measurements (using the highly sulfide sensitive methylene blue assay; (30)) (Fig. 1).

In ETSA waters, sulfidic events based on remote sensing of sulfur plumes, have been observed to form and dissipate within days along the Namibian coastline (Fig. 3a) (13, 29, 31). Singular events can cover a shelf area ranging from 800 to 1600 km^2 (29), with some events reported over 20,000 km^2 (albeit using a less conservative spectral analysis, which may include offshore plumes outside the immediate upwelling area generated by coccolithophore blooms) (31, 32) (Fig. 3a). The largest events are primarily reported in April and May but occur frequently from January to July approximately once every 1-2 weeks, whereas smaller sized events occur from September to November (13, 29). Additionally, sulfide has been detected in bottom waters on a number of ship-based sampling campaigns (13, 21). ETSP shelf waters are similarly prone to sulfidic events, which occur frequently along the Peruvian and Chilean coastline, based on the remote sensing of sulfur plumes (Fig. 3b). In accordance, ship-based sampling campaigns have documented sulfidic events in bottom waters off the coast of Peru and Chile (14, 16). In the monsoonal driven upwelling regions of the Arabian Sea and Bay of Bengal, cloud coverage can hinder regional remote sensing of sulfidic events. Nonetheless, sulfide accumulation in bottom waters has been documented spanning the Western shelf of India as well as in the Bay of Bengal (15, 33-35).

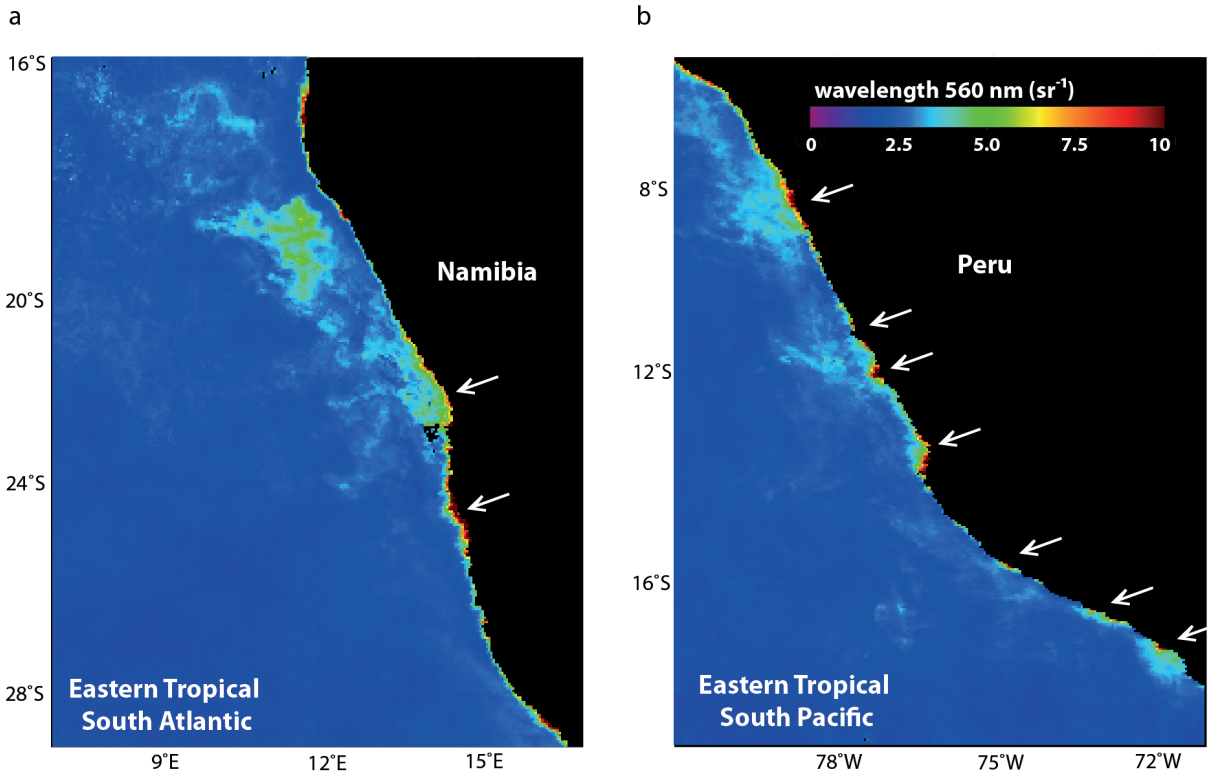

Fig. 3. Spatial distribution of sulfur plumes in the ETSA and ETSP regions. (a, b) Remote sensing image of sulfur events (highlighted by the white arrows) at a reflectance wavelength of 560 nm, the images shown are seasonal composites from 21 December to 20 March, 2004-2005. The images were acquired by Moderate Resolution Imaging Spectroradiometer (MODIS) downloaded from the NASA Ocean Colour Database and processed using SeaDas software (www.seadas.gsfc.nasa.gov/).

In contrast to the ETSA off Namibia and the ETSP off Peru, which receive little freshwater runoff, these areas are heavily impacted by anthropogenic riverine input, which may thus contribute to eutrophication and stratification in these regions (33, 36). However, despite the advantages of remote sensing technology for the detection of sulfidic events, in many cases, the sulfur may be oxidized in subsurface waters before a visible plume is formed (13). Therefore the number of sulfidic events in OMZs is likely underestimated by remote sensing.

Sulfidic events are prone to develop during periods of intensified upwelling and/or during seasonal windows of enhanced or shoaling water-column anoxia. In ETSA shelf waters anoxia is regulated by two opposing water masses, each dominating the shelf at different times. Shelf anoxia ensues when the oxygen-poor water mass dominates the upper shelf, which begins in December (austral summer) and peaks in June (early winter) (37, 38). This leads to an increase in the number of sulfidic events (13, 29), and mass die-offs of fish and invertebrates (37, 39, 40). A distinctly different and more oxygenated water mass dominate upper shelf waters from late winter to early summer, decreasing sulfidic event frequency and intensity (38). The movements of these water masses are independently governed by remote wind-forcing that vary not only seasonally but on interannual timescales (37).

On the Pakistan and West Indian shelf of the Arabian Sea, a period of water-column anoxia follows after the heavy rainfall of the southwest monsoon, which creates a fresh/warm water lens overtop of saline/cold upwelled waters, isolating the bottom water mass and prompting water column stratification (26). Sulfidic events have been reported to occur thereafter, once oxygen and nitrate have been consumed in the bottom waters (15, 33). In the ETSP region, which

is more or less permanently oxygen-free, nitrate-rich waters function as the barrier to the release of benthic sulfide year-round. Nitrate concentrations appear to be most depleted during the enhanced upwelling period from November to March and sulfidic events have been observed during this period from ship-based measurements (14, 16). A larger monitoring effort is required to better resolve sulfidic event seasonality in ETSP waters. A common thread across OMZs is that sulfidic events form in sporadic pockets along the coast, which suggest that local hydrodynamic factors on shorter timescales may additionally play a role in regulating these phenomena including regional oxygen and nitrate dynamics.

Aside from active sulfur cycling in benthic influenced coastal OMZ waters, recent evidence indicates that a sulfur cycle exists in the nitrate-rich offshore waters of the ETSP region detached from benthic processes (41). Canfield et al., (41) reported significant rates of sulfate reduction at two stations over 23 km from the ETSP coast. The production of sulfide by sulfate-reducing bacteria is inferred to be tightly coupled to its consumption by sulfide-oxidizing bacteria, and therefore sulfide does not accumulate – a phenomenon termed the "cryptic" sulfur cycle (41). How cryptic sulfur cycling occurs in ETSP waters under nitrate-rich conditions is ambiguous, as sulfate reduction should be outcompeted by nitrate reduction based on energetic considerations. The hypothesis is that the microbes that carry out sulfate-reduction and sulfide-oxidation are housed within marine snow aggregates (42). Such aggregates would theoretically act as both a source of organic matter and a substrate for attachment (43-45), and nitrate could potentially be depleted internally due to diffusional limitation (46). Whether sinking aggregates provide a microniche for the cryptic sulfur cycle in nitrate-rich OMZ waters remains an open question. In addition, the full extent of the offshore cryptic sulfur cycle remains poorly understood. However, a sulfur-based community comprising of sulfide/thiosulfate-oxidizing and sulfate-reducing bacteria has been consistently found in ETSP microbial community surveys, as well as in other OMZs (41, 47-50), suggestive of a widespread OMZ sulfur cycle (41).

Microbial sulfur cycling pathways

Dissimilatory sulfate-reduction

Dissimilatory sulfate reduction is an intracellular pathway that uses sulfate as the terminal electron acceptor to gain energy for growth, producing sulfide. Sulfate reduction is carried out by both *Bacteria* and *Archaea*, hereafter we use the generic term sulfate-reducing bacteria (SRB) rather than differentiating between the two prokaryote domains. The activity levels of heterotrophic SRB depend on the quantity and quality of available organic matter. Preferred organic matter substrates include volatile fatty acids, as well as more complex carbon sources such as hydrocarbons, monocaboxylic acids, alcohols, amino acids, sugars, and aromatic compounds (10, 51). The oxidation of these organic substrates via substrate-level phosphorylation can be subdivided into two distinct metabolisms: the incomplete oxidation of organics producing acetate, or the complete oxidation to CO_2 (52).

In dissimilatory sulfate reduction, once sulfate is transported into the cell, it is activated with ATP sulfurylase (Sat) generating APS (adenosine-5'-phosphosulfate). APS is reduced by the soluble APS reductase to sulfite with two electrons (53) and then further to sulfide with six-electrons catalyzed by dissimilatory sulfite reductase (dsr) (54). Notably, the soluble reductase enzymes are coupled to membrane-bound complexes for energy conservation: AprAB-QmoABC and DsrABC-MKJOP complexes. The Dsr pathway is highly conserved among SRB and is currently found in five bacterial and two archaeal lineages (51), although the vast majority of sulfate- and sulfur-reducing bacteria are affiliated with the deltaproteobacterial lineage (55).

Dissimilatory sulfate-reduction in OMZs

Most SRB species identified by culture-independent techniques or cultivated from OMZs are affiliated with the deltaproteobacteria class. Two novel SRB strains within Desulfovibrio oceani have been isolated from OMZ waters off the Peruvian coast (56).

Finster and Kjeldsen, (56) demonstrated that the D. oceani strains couple organic matter oxidation (e.g. using lactate, malate, fumarate) to sulfate, sulfite, thiosulfate, or taurine reduction. The strains, during sulfate reduction, also showed a high oxygen tolerance characteristic of many Desulfovibrio spp. (57), suggestive that D. oceani is perhaps adapted to fluctuations in oxygen concentrations introduced by horizontal and vertical mixing processes (56). Other SRB have been identified from functional and phylogenetic gene marker surveys in ETSP waters including Desulfobacca, Desulfatibacillum, Desulfobacterium, Desulfococcus, and Syntrophobacter species (41, 58). Desulfobacterium autotrophicum, a versatile SRB capable of oxygen detoxification as well as mixotrophic growth (59), has been shown to be one of the most abundant microorganisms in sulfidic ETSP shelf waters (14, 59).

Sulfide accumulation in bottom waters (i.e. during a sulfidic event) is generally attributed to the benthic sulfide flux rather than water-column sulfate reduction as in the Black Sea (21, 60). For example, even at the highest sulfate reduction rate reported in ETSA shelf waters (<200 m water depth; 0.2-6.8 nmol L^{-1} d^{-1}) it would take 147 days to produce 1 μM of sulfide (13, 21), whereas the benthic sulfide flux to these nitrate free shelf waters has been shown to match the sulfide accumulation (13). OMZ sulfate reduction rates are highest (up to 120 nmol cm^{-3} d^{-1}) in upper-shelf sediments due to high accumulation rates of organic matter (17, 18, 61, 62). Benthic rates of sulfate-reduction, as well as the benthic sulfide fluxes, decrease with distance from the coastal upwelling (20, 63). In shallow OMZ shelf waters, as in other upper shelf marine settings, benthic SRB activity dominates the remineralization of organic matter (10, 17, 18, 61, 62, 64). Ammonium is a product of this activity, and an important electron donor for anammox bacteria. In the ETSP region, the benthic ammonium flux satisfies approximately 50% of the ammonium requirements for anammox bacteria (65, 66).

The offshore cryptic sulfur cycle has similar biogeochemical implications for the OMZ nitrogen cycle. At a station located 23 km from the coast in northern Chile, sulfate-reduction (12 ± 5 nmol L^{-1} d^{-1}) accounted for 33% of organic carbon mineralization (41). Using Redfieldian C:N ratios, the measured sulfate-reduction rate could yield up to 0.30 mmol NH_4^+ m^{-2} d^{-1}, roughly 22% of the ammonium needed to sustain offshore anammox activity (41). At a station located 44 km from the coast, which had lower average sulfate-reduction rates (1.3 ± 0.6 nmol L^{-1} d^{-1}), sulfate reduction accounted for 8% of anammox ammonium requirements (41). Despite the variability in offshore rates, these data indicate that offshore sulfate reduction (in consortium with fermenting bacteria) could be a potentially significant supply of ammonium for anammox bacteria in the offshore OMZ. However, these are, to our knowledge, the only process rate measurements of sulfate reduction in offshore OMZ waters to date.

Time-integrated indicators of sulfate-reduction have been studied in an attempt to quantify cryptic sulfur cycling processes in offshore ETSP waters. Sulfate reduction imparts natural abundance isotope signatures of sulfur ($^{33}S/^{32}S$, $^{34}S/^{32}S$) and oxygen ($^{18}O/^{16}O$) (67) and the isotope composition of sulfate was analyzed to constrain dissimilatory sulfate reduction processes in the ETSP region. However, no clear signature of water column sulfur cycling was observed. The lack of a signature in ETSP waters does not necessarily preclude a cryptic sulfur cycle operating in offshore waters, as observed experimentally, because the time-integrated maximum rates of sulfate reduction as constrained by the ^{18}O sulfate data (6.4 – 64 nmol L^{-1} d^{-1} depending on the assumed water residence time) were at or above the mean rate directly measured by Canfield et al., (41), demonstrating that the ^{18}O sulfate method is not yet sensitive enough to respond to the cryptic sulfur cycle.

Sulfide oxidation

Complementing sulfate reduction are sulfide-oxidizing bacteria (SOB) that gain energy from the oxidation of sulfide to sulfate, or from the oxidation of other intermediate species such as sulfur, thiosulfate and sulfite (Fig. 2). SOB are a taxonomically diverse group spread across various phyla including alpha, beta, gamma, and epsilon subdivisions of the

Proteobacteria as well as the order Sulfolobales in the *Archaea* (10, 68). Most SOB grow as either strict or facultative aerobes, capable of switching between oxygen or nitrate as the electron acceptor. Like heterotrophic denitrification, sulfide-dependent denitrification is the stepwise reduction of nitrate to N_2 via intermediates NO_2^-, NO, and N_2O. Moreover sulfide-dependent dissimilatory NO_3^-/NO_2^- reduction to NH_4^+ (DNRA) produces ammonium from the oxidation of sulfide/sulfur, which is generally catalyzed by large sulfur bacteria in sediments (63, 69-72). As a carbon source, SOB either fix CO_2 into biomass or assimilate organic carbon for growth (e.g. acetate), designated as chemolithoautrophy and chemolithoheterotrophy, respectively, though the latter is poorly understood and sometimes loosely defined as heterotrophic sulfur-oxidizing bacteria (73, 74).

Two predominant sulfide oxidation pathways exist in SOB: the multienzyme Sox system and the "reverse" siroheme-containing sulfite reductase (rDsr) pathway. The rDsr pathway can, in some variations, involve similar enzymes as dissimilatory sulfate reduction, however, operating in the reverse direction. The rDsrAB enzyme that catalyzes the oxidation of sulfide to sulfite is homologous to but phylogenetically distinct from DsrAB (10, 75, 76). The oxidation of sulfite to sulfate involves APS reductase and ATP sulfurylase, similar to dissimilatory sulfate reduction acting in the reverse direction. When sulfide concentrations exceed those of available electron acceptors (e.g. nitrate) then elemental sulfur is the typical end-product (77). As mentioned above, elemental sulfur has been detected both in situ and by remote sensing of OMZ sulfidic events (13, 28, 29, 31). Similarly to rDSR, the periplasmic sulfur-oxidizing multienzyme system (SoxABCDXYZ), operating in conjunction with the sulfide-quinone oxidoreductase (Sqr) or flavocytochrome C (Fcc) oxidoreductase, is capable of oxidizing various reduced sulfur species to sulfate, including sulfide, elemental sulfur, thiosulfate, and sulfite (68, 78-80). Some sulfide-oxidizing bacteria, including SOB identified in OMZs, have both Sox and rDsr pathways with an important distinction; the sox pathway is truncated, missing the SoxCD genes (80-82). In cultivated SOB, a truncated sox pathway is correlated with the formation of intracellular sulfur deposits that are oxidized further via the rDsr pathway (82). This 'two-stage' Sox and rDsr pathway operates in both phototrophic and non-phototrophic sulfide oxidizers (80). The ability to metabolize stored sulfur reserves enables survival under sulfide-poor conditions (83), and thereby may allow greater versatility in dynamic OMZ shelf conditions..

Sulfide-oxidation in OMZs

OMZs harbor a large diversity and an appreciable abundance of SOB, and a number of these SOB serve as key identifiers of water column anoxia and sulfidic event detoxification. Under highly sulfidic conditions in OMZ shelf waters, SOB taxa such as *Arcobacter*, *Sulfurovum* and *Sulfurimonas spp.* within the Epsilonproteobacteria dominate (13, 14, 42, 84, 85). When sulfidic conditions subside, the community shifts from Epsilonproteobacteria-dominated to an increase in the prevalence of gammaproteobacterial sulfide-oxidizing bacteria (GSO) (13, 14, 42, 84, 85). Most commonly identified GSO members in OMZ waters include the two closely related sister clades, SUP05 and Arctic96BD-19. The former comprises planktonic (e.g. '*Candidatus* Thioglobus autotrophicus' (86)) and symbiont associated (e.g. '*Candidatus* Ruthia magnifica'; (87)) chemolithoautotrophic SOB, while the latter contains free-living (e.g. '*Candidatus* Thioglobus singularis': (88)) mixotrophic/heterotrophic SOB. Both clades have the capacity to oxidize various reduced sulfur species (14, 81, 89, 90). For example, SUP05 bacteria contain the two-stage Sox and rDsr pathways that enable the oxidation of sulfide, sulfur and thiosulfate, and allow for the storage of intracellular sulfur (14, 81, 91, 92). For Arctic96BD-19 bacteria the energy derived from the oxidation of reduced sulfur species is coupled to oxygen respiration (89, 93, 94), while in SUP05 bacteria, sulfide oxidation is coupled to either oxygen respiration or to nitrate reduction via denitrification (14, 81, 94).

In accordance with genome studies, SUP05 bacteria predominately thrive at the nitrate- or oxygen-sulfide redoxcline of OMZs and stratified basins (13, 41, 42, 47, 48, 95-98). However, SUP05 bacteria also

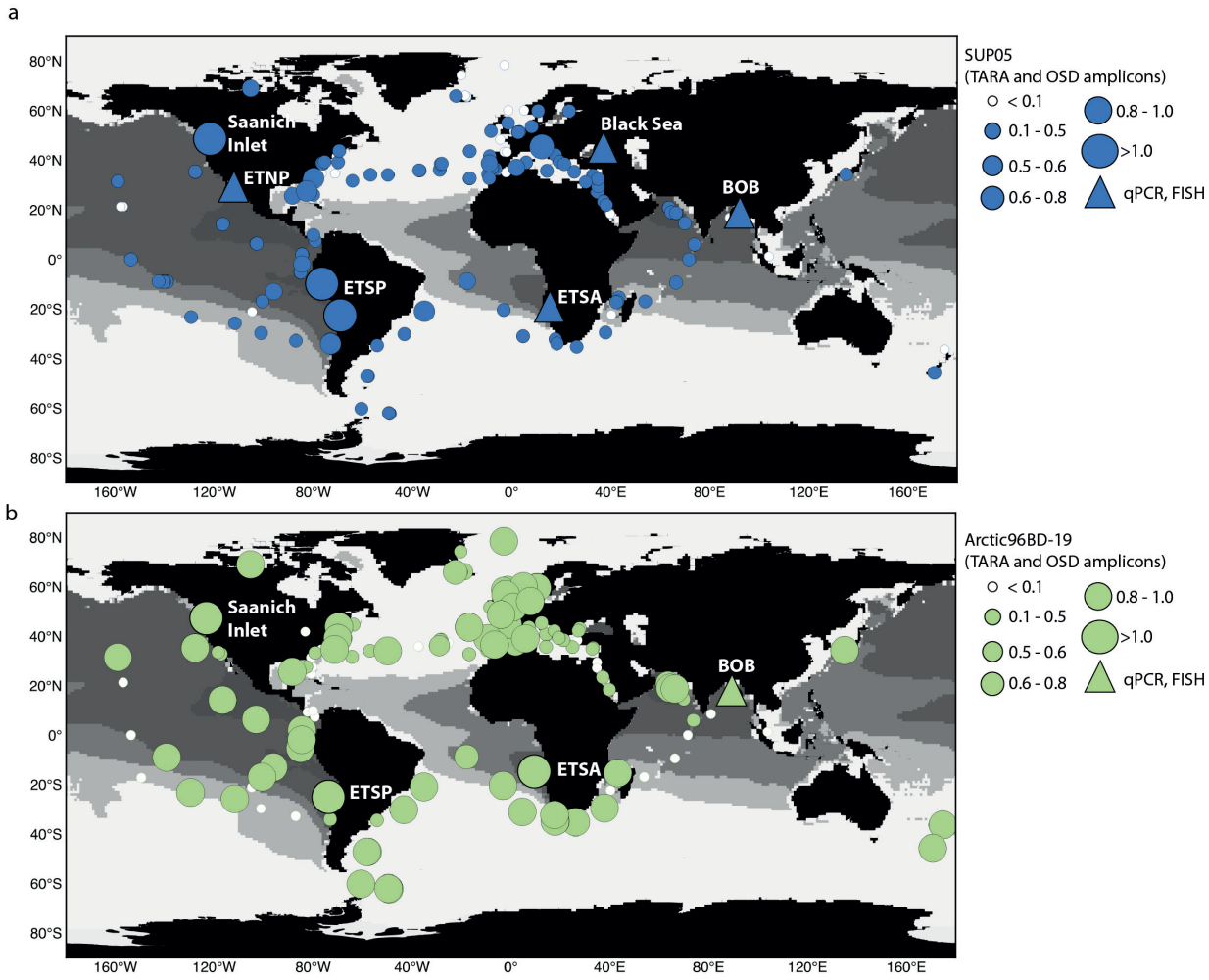

Fig. 4. Distribution of SUP05 and Arctic96BD-19 clades. SUP05 (a) and Arctic96BD-19 (b) abundances are represented as the percentage of associated 16S rRNA sequences in metagenomic and amplicon sequencing datasets from TARA Ocean and OSD, Ocean Sampling Day 2014 (OSD2014) as well as from other OMZ metagenomic datasets (14, 41, 42, 81). The highest reported SUP05 and Arctic96BD-19 abundances at each station are indicated. Note that studies using qPCR (49, 50) and FISH (13, 96) based approaches to quantify SUP05 and Arctic96BD-19 bacteria are highlighted with blue triangles. Mapping of 16S rRNA gene sequence reads from the TARA Ocean and OSD datasets was performed according to Martínez-Pérez et al., (136). Near full-length published and unpublished 16S rRNA gene sequences from previously identified SUP05 and Arctic96BD-19 species were used as a BLASTn classification reference database. A cutoff of (percent query coverage + percent alignment identity)/2 > 98% was used to assign either SUP05 or Arctic96BD-19 identity to a read.

persist outside of sulfidic waters (i.e. in the offshore OMZ), but at low to moderate relative cell abundances based on functional and phylogenetic gene surveys (41, 42, 47, 48, 95, 97) (Fig. 4a). The persistence of SUP05 bacteria in the offshore OMZ waters has been attributed to a cryptic sulfur cycle, where the sulfide needed for their energy metabolism is produced from closely coupled sulfate-reducing bacteria (41). On the other hand, Arctic96BD-19 bacteria are more widespread to oxygenated surface- and deep-waters of OMZ regions as well as other marine environments (Fig. 4b). In addition, Arctic96BD-19 bacteria possess gene pathways necessary for organic sulfur degradation, which could be an important supply of reduced sulfur equivalents supporting growth (86, 88, 89). This raises a number of questions regarding the metabolic capacity of Arctic96BD-19 bacteria in offshore waters (discussed below).

Other prominent, though poorly characterized, SOB bacteria identified in offshore OMZ waters include SAR324 (Marine Group B) within the Deltaproteobacteria, and Marinimicrobia, previously known as SAR406 (Marine Group A), which both form deep-branching uncultivated lineages (99). Members of these groups are strongly associated to low-oxygen concentrations and have been found ubiquitously throughout all major OMZs as well as in permanently/seasonally anoxic basins, showing some overlap with the distribution of SUP05 bacteria (42, 47, 95, 98, 100-102). The metagenome of SAR324 reveals various encoded pathways for organic matter degradation, as well as for chemolithoautotrophic processes involved in carbon fixation and sulfide oxidation (89, 103). Partial gene fragments and draft genomes of Marinimicrobia recovered from oxygen deficient waters also find adaptions for low oxygen and genes encoding for a polysulfide reductase (102, 104). The encoded polysulfide reductase is potentially involved in sulfur oxidation or in polysulfide reduction to sulfide (104, 105). In addition, nitrate may also serve as an electron acceptor for Marinimicrobia, which is predicted to be capable of DNRA (102). Hence, Marinimicrobia and SAR324 serve an ambiguous, though putative role in the OMZ nitrogen and sulfur cycle.

Chemolithoautotrophic SOB contribute not only to the detoxification of sulfidic events but have an important influence over other element cycles including nitrogen and carbon. Nitrate is primarily used to oxidize sulfide from sulfidic bottom waters, and thereby SOB contribute directly to the removal of fixed nitrogen in OMZs via sulfide-dependent denitrification. In the ETSP and ETSA regions, rates of sulfide-dependent denitrification to N_2 for various sulfidic events have been observed up to 0.5-2.4 µmol N L^{-1} d^{-1}. These rates are, considerably higher than anammox rates reported in the same waters (0.1-1.0 µmol N L^{-1} d^{-1}) (13, 14, 16, 65).

The free energy yield from sulfide oxidation to sulfur with nitrate (Gibbs free energy [$\Delta G°$] = -1260 kJ mol^{-1}) is far more favorable than anammox ($\Delta G°$ = -358 kJ mol^{-1}) (6). Likewise, doubling times for SOB (0.04-0.67 days, under optimal conditions; (106)) are substantially greater than for anammox bacteria (~11 days, under optimal conditions; (107)). Regardless of these energetic differences, both anammox and sulfide-dependent denitrification activities significantly overlap in OMZ shelf waters; for example, both tend to show enhanced activity near the nitrate-sulfide redoxcline and in shallow shelf bottom waters closely coupled to sediment processes (13, 16, 65, 108). Nitrite and ammonium, substrates required by anammox bacteria, can be jointly supplied by sulfide-dependent nitrate reduction and DNRA activity, respectively. In accordance, Russ et al., (109) demonstrated that in co-culture bioreactor experiments, SOB and anammox activity are tightly coupled. Thus, when supplied with nitrate, ammonium and sulfide, the SOB generated the nitrite required to fuel anammox activity, accounting for 65-75% of nitrogen loss (109).

In the ETSP region under sulfidic conditions, elevated rates of nitrate reduction to nitrite (up to 2.5 µmol N L^{-1} d^{-1}) have been observed (14), suggesting that during sulfidic events sulfide oxidation could be an important supply of water column nitrite. Several SOB have been identified in these waters with the potential to reduce nitrate to nitrite including SUP05, *V. okutanii* and *Sulfurovum* (14, 110). While the ammonium needed to fuel anammox, can be in part supplied via the activities of sulfide-dependent DNRA in sulfidic bottom waters (14) or in the benthos catalyzed via giant sulfur bacteria (63, 66). This along with the ammonium released during remineralisation of organic matter by SRB, means that the benthic ammonium flux can account for approximately 50% of the ammonium requirements for anammox bacteria in ETSP shelf waters (65).

ETSP waters experience massive emissions of N_2O (111), and a number of in situ incubation experiments performed in these waters suggest that SOB may contribute in part to this production (16, 41, 112). For example, Dalsgaard et al., (112) showed that the addition of sulfide (1 µM) to incubation experiments with ETSP waters caused an increase in net N_2O production of more than 4.5 fold (up to ~120 nmol L^{-1} d^{-1}) relative to non-sulfide amended experiments. Galan et al., (16) performed similar experiments, except with 5 µM sulfide, and observed

a net N_2O production of 12-29 nmol L^{-1} d^{-1}, with no N_2O production observed in sulfide-free controls. A potential contributor to shelf water N_2O production is the SUP05 clade. Omic-based approaches indicate that a number of SUP05 strains identified in ETSP waters and in the Saanich Inlet OMZ can reduce nitrate to N_2O. These SUP05 strains, however, lack the gene (*nosZ*) necessary for N_2O reduction to N_2 (81).

Many SOB fix CO_2 into biomass and thereby contribute to rates of 'dark' carbon fixation (carbon fixation occurring in the absence of light) in OMZs. For example, the sulfidic event reported by Schunck and colleagues in ETSP waters in May 2009 supported some of the highest rates of dark fixation in the ocean of 0.9 to 1.4 μmol C L^{-1} d^{-1} (14). Assuming that the total amount of sulfide contained in these waters was oxidized for growth by chemolithoautotrophic bacteria, then this singular event represented up to ~30% of the photoautotrophic carbon fixation (14). This fraction of carbon fixation is of a similar magnitude to the amount of photosynthetic surface production exported below the photic zone that in part fuels heterotrophic bacteria. Similarly elevated rates of dark carbon fixation have been reported during sulfidic conditions in the Chilean upwelling region (16). Key taxa that potentially mediate dark carbon fixation, as either mixotrophs or obligate autotrophs, include the SUP05/Arctic96BD-19 clade, *Arcobacter*, *Sulfurovum* and SAR324 species.

Disproportionation

Sulfur compound disproportionation is a chemolithoautrophic mode of microbial growth that catalyzes the inorganic 'fermentation' of intermediate sulfur compounds to produce sulfide and sulfate (Fig. 2). Specifically, inorganic sulfur intermediate compounds such as elemental sulfur, thiosulfate and sulfite act as both the electron acceptor and electron donor. These intermediate compounds, which are important shunts in the sulfur cycle, are produced from the oxidation of sulfide and hence are often found to accumulate at the redoxcline of anoxic water columns (113-115). These sulfur intermediates can be oxidized or reduced by SOB and SRB, respectively, and can also be disproportionated to regenerate sulfide and sulfate. Of the known disproportionating bacteria, most occur within the Deltaproteobacteria class (116) with exception of a haloalkaliphilic member of the Clostridia (117). The thermodynamics of disproportionation are near the energetic limit which perhaps explains why not all disproportionating bacteria grow by this reaction; instead some perform both sulfate-reduction and disproportionation (116). Microbes that grow solely by disproportionation are restricted to only a few genera.

The pathway for thiosulfate disproportionation has been characterized by work done with *Desulfocapsa sulfoexigens* (116). Notably, the genes involved in thiosulfate disproportionation are largely indistinguishable from genes required for sulfate-reduction, which makes it nearly impossible to detect disproportionation solely from culture-independent approaches. Other methods of detecting disproportionation include cultivation or by natural abundance sulfur isotopes. To our knowledge, only two SRB strains have been isolated from OMZs and none were capable of disproportionating reduced sulfur intermediates (56). Natural abundance sulfur isotope signatures, however, indicate that disproportionation is occurring in the redoxclines of some permanent and seasonally stratified basins (118, 119), which resemble conditions in OMZs. However, it remains untested whether disproportionation is a significant process operating in the redoxcline of OMZ sulfidic events, as well as the distribution and concentration of intermediate sulfur species.

Sulfur assimilation and organic matter sulfidogenesis

Sulfate assimilation is the incorporation of inorganic sulfur into biomass and occurs ubiquitously across aerobic and anaerobic microbes (10). The cycling of sulfur through assimilation / mineralization in both oxic and anoxic environments though, remains poorly understood (120). In the absence of sulfide, sulfate is assimilated through assimilatory sulfate reduction (ASR), which shares the first two steps with dissimilatory sulfate reduction and produces sulfide, which

is then incorporated into organic sulfur-containing compounds. This ASR requires eight electrons and ATP, which makes this pathway energetically expensive (10). The sulfur contained in these organic molecules is at various redox states. Thus their degradation can yield various sulfur intermediates including sulfide, thiosulfate, and sulfite, a process known as organic matter sulfidogenesis. For example, the desulfurylation of arylsulfonates, alkylsulfonates and taurine (2-aminoethanesulfonate) will produce sulfite (121-123). Other compounds like cysteine produce sulfide when degraded, whereas the fermentation of taurine can yield thiosulfate and sulfide (11, 124).

Organosulfonate compounds such as taurine are readily abundant in marine environments (125, 126) and some microbes depend on these compounds and their degradation products for assimilable carbon, nitrogen and sulfur. For example, ASR is thought to be almost universal in aerobic bacteria, but the ubiquitous and highly abundant SAR11 have been shown to be deficient in ASR genes and instead seem to rely exclusively on reduced sulfur compounds for growth, such as dimethylsulfoniopropionate and thiosulfate (127, 128). Within OMZ environments, SAR11 are often one of the most abundant organisms and have been shown to have adapted to life without oxygen, including having genes for the nitrite producing first step of denitrification (129), but whether this requirement for reduced sulfur can be extended to OMZ SAR11 lineages remains to be determined. Other microorganisms may oxidize organosulfonate produced sulfur species, sulfide, thiosulfate, and sulfite for energy gain via the Sox and rDsr pathways or by sulfite oxidizing enzymes. The family of molybdenum-containing sulfite oxidizing enzymes YedYZ and SorAB are widespread in SOB and organosulfonate degrading heterotrophs (130).

Outside of anoxic/sulfidic environments, organosulfonates are believed to be an important source of inorganic sulfur fueling the diversity of heterotrophic SOB in the open ocean (11, 12, 131), and presumably the same holds true in OMZ waters. Recent work in the Canary and Benguela upwelling systems supports this and suggests that OMZs may be active areas of remineralisation of dissolved organic sulfur-containing compounds, although the relationship to oxygen concentrations was not explored (120). The widely distributed heterotrophic SOB such as Arctic96BD-19 and SAR324, found also ubiquitously in OMZs (Fig. 4b) (42, 47, 95, 98, 100-102), may thrive from the oxidation of organic sulfur-containing compounds. For instance, Arctic96BD-19, a sister clade to SUP05, harbors genes for carbon fixation, as well as pathways for organic matter uptake and respiration, including genes involved in the degradation of taurine (TauD) (86, 88, 89). TauD is a dioxygenase that catalyzes the conversion of taurine to sulfoacetaldehyde releasing sulfite (132), although within the anoxic waters of an OMZ the potential and pathway for the degradation of taurine by Arctic96BD-19 remains unclear. Arctic96BD-19 also contains a number of putative dissimilatory sulfite oxidizing enzymes as well as a Sox sulfide oxidizing pathway (88, 93, 94). The presence of these genes indicates that sulfite or other reduced sulfur species produced from the desulfurylation of organosulfonate compounds might be an additional energy source. Similarly, metatranscriptomic data reveals SAR324 genes involved in alkanesulfonate degradation and organosulfonate transport, and encodes for pathways involved in sulfide oxidation via a complete rDsr system (89, 103). Hence, the scavenging of organosulfonate compounds and the oxidation of reduced sulfur produced from organic matter sulfidogenesis may support heterotrophic SOB such as SAR324 and Arctic96BD-19 bacteria in OMZs and other marine environments.

Summary and open questions for future research

Organic matter is the principal driver of sulfate reduction, which constitutes the basis of the OMZ sulfur cycle. The oxidation of produced sulfide yields important sulfur intermediate compounds including, sulfur, and putatively thiosulfate and sulfite. Collectively, a diverse assemblage of microbes mediates the turnover of these reduced sulfur species. The sulfur cycle is tightly coupled to the activities of other biogeochemical cycles including oxygen, nitrogen and carbon. Products of the sulfur cycle generate the full spectrum

of oxidized and reduced intermediates of the nitrogen cycle (NH_4^+, N_2, N_2O, and NO_2^-,). These intermediates directly or indirectly contribute to nitrogen loss and greenhouse gas production in OMZs, which is most evident in shelf waters. The finding of a cryptic sulfur cycle in OMZ waters detached from benthic processes indicates potential for a large-scale offshore sulfur cycle. The abundant community of heterotrophic SOB in offshore waters may also be in part fueled by organic matter sulfidogenesis. Our understanding of sulfur cycling dynamics in OMZs is still rudimentary; caveats and gaps in our knowledge remain as outlined below. Most of these emerging questions can be addressed with technologies already in hand through multidisciplinary efforts.

1 Shipboard and remote sensing observations indicate that sulfidic events are more frequent than previously recognized (Fig. 3) (13-16, 21, 27, 29, 31). Moreover, the expansion of OMZs in a global warming scenario in combination with anthropogenic riverine runoff is expected to lead to an increase in the frequency and intensity of sulfidic events (13, 35, 133). Despite the documented prevalence of sulfidic events in OMZ waters very little is known of their regulation. Sulfidic events occur during periods of shelf anoxia; however, their distribution along the coastline at any given time appears sporadic (Fig. 3). Other local hydrodynamics factors such as mesoscale eddies may be at play, tightly regulating the initiation and termination of these events. To better understand the regulation of these phenomena we need to employ long-term OMZ monitoring programs that integrate water column fluxes, process rate measurements, remote sensing in combination with hydrodynamic observations (e.g. moorings and autonomous gliders). Understanding the regulation of sulfidic events may even enable forecasting of these phenomena in the future.

2 Despite the potential for cryptic sulfur cycling in offshore waters very few rates of sulfate reduction and sulfide oxidation exist for OMZ waters. To explore the full extent and spatial-temporal dynamics of offshore sulfur cycling more process rate measurements are needed across OMZs, coupled with single-cell techniques (nanoSIMS) to determine cell specific activity, thereby directly linking function and identity. These should be supplemented with high-sensitivity analyses of the distribution of sulfide and intermediate sulfur species.

3 How a cryptic sulfur cycle is manifested under nitrate-rich conditions in offshore OMZ waters is an enigma. The current hypothesis is that cryptic sulfur cycling could be housed inside particles, which permit the close spatial coupling of SRB and SOB activity (42, 95). In the environment SUP05 demonstrates an affinity for growth in association to particles (41, 95), whereas SAR324 and Marine Group A appear to favor a planktonic lifestyle (134). More work is needed to address the role of particles in the OMZ sulfur cycle and to disentangle rates of sulfur transformation processes therein.

4 Very few cultivated representatives of SOB and SRB exist for OMZs. In microbiology in general, there is a widening gap between the number of microbes identified by molecular techniques to those actually cultivated. Cultivation-dependent experiments still stand as the most effective method of resolving a microbe's physiology and how it adapts to changing environmental conditions. Clades that putatively serve a function in the sulfur cycle, but that still elude cultivation, include SAR324 and Marine Group A. Additionally, many SOB and SRB may have multiple roles in the sulfur cycle. For example, some SRB are able to perform disproportionation (116). Cultivation-dependent techniques would help to disentangle the multi-functionality of microbes in OMZ waters and may further serve to verify omic-based metabolic models.

5 Anoxygenic photosynthesis contributes substantially to the oxidation of sulfide in the chemolines of stratified basins (135). Little is known of the role of anoxygenic photosynthesizing bacteria in OMZs. Some evidence from functional and phylogenetic gene surveys have identified green sulfur bacteria closely affiliated to *Chlorobium limicola* and *Chlorobium*

Table 1: Key genes and processes hypothesized to be associated with OMZ sulfur cycling.

Process	Gene	Encoding enzyme and function
Dissimilatory sulfate reduction	*sat*	ATP sulfurylase: activates sulfate to from APS (adenosine-5'-phosphosulfate)
	aprAB	Soluble APS reductase, forms membrane bound complex with QmoABC
	dsrABC	Dissimilatory sulfite reductase, forms membrane bound complex with DsrMKJOP
Assimilatory sulfate reduction	*Sat, or CysDN*	ATP sulfurylase: activates sulfate to from APS (adenosine-5'-phosphosulfate)
	CysC	APS kinase, APS is phosphatized with ATP producing PAPS (adenosine 3'-phosphate-5'-phosphosulfate)
Sulfide oxidation (rDsr)	*rdsrAB*	Reverse dissimilatory sulfite reductase
	aprAB	Soluble APS reductase, forms membrane bound complex with QmoABC
	sat	ATP sulfurylase: activates sulfate to from APS (adenosine-5'-phosphosulfate)
Sulfide oxidation (Sox)	*soxXA*	Heterodimeric c-type cytochrome
	soxYZ	Heterodimeric protein that binds thiosulfate
	soxCD	Heterotetramer protein comprising of a molybdenum cofactor-containing subunit (SoxC), and a diheme c-type cytochrome (SoxD)
	soxB	Monomer containing manganese
	Sqr or fccC	Sulfide-quinone oxidoreductase or flavocytochrome C oxidoreductase
Sulfite oxidation	*YedYZ, SorAB*	Molybdenum-containing sulfite oxidizing enzyme (SOE) family
Taurine and organosulfonates oxidation	*tauXY*	Taurine dehydrogenase, produces sulfoacetaldehyde from taurine
	tauD	Taurine dioxygenase, produces sulfoacetaldehyde and sulfite from taurine
	xsc	Sulfoacetaldehyde acetyltransferase, produces acetyl phosphate and sulfite from sulfoacetaldehyde
	eutD	Phosphate acetyltransferase, produces acetyl-CoA from acetyl phosphate
	SsuD and SsuE	Two-part alkanesulfonate monoxygenase

tepdium in ETSP waters (14, 97). Whether sufficient sulfide concentrations can penetrate the photic zones of OMZ shelf waters to support green and purple sulfur bacteria is unknown.

6 There is mounting metagenomic and metatranscriptomic evidence that organosulfonate sulfidogenesis could play a role in the offshore OMZ sulfur cycle. For example abundant OMZ taxa, such as SAR324 and Arctic96BD-19, harbor genes for organosulfonate degradation pathways, including genes for sulfide, thiosulfate and sulfide oxidation (86, 103). The significance of organosulfonate sulfidogenesis as source of reducing equivalents for SOB in the offshore OMZ remains un-quantified, as does its potential linkage to the nitrogen cycle or other elemental cycles.

Author contributions

C.M.C., and L.A.B. designed the study; C.M.C., and P. Y. performed experiments; C.M.C., and P.Y. analysed data; C.M.C. wrote the original draft; D.E.C., M.M.M.K., P.Y., G.L., B.T., and L.A.B. reviewed and edited the manuscript

Acknowledgements

The authors would like to thank Gesa Eirund for plotting of the World Ocean Atlas data 2013. This work was supported by the MPG and the Sonderforschungsbereich (SFB754) GEOMAR, Kiel as well as the Villum Foundation and the Danish Council for Independent Research (Grant no. xxx). The stipend of C.M.C was also supported by a Natural Sciences and Engineering Research Council of Canada (NSERC) scholarship.

References

1. *Carr M-E (2001) Estimation of potential productivity in Eastern Boundary Currents using remote sensing. Deep Sea Research Part II: Topical Studies in Oceanography 49(1–3):59-80.*

2. *Karstensen J, Stramma L, & Visbeck M (2008) Oxygen minimum zones in the eastern tropical Atlantic and Pacific oceans. Progress in Oceanography 77(4):331-350.*

3. *Revsbech NP, et al. (2009) Determination of ultra-low oxygen concentrations in oxygen minimum zones by the STOX sensor. Limnology and Oceanography: Methods 7(5):371-381.*

4. *Tiano L, et al. (2014) Oxygen distribution and aerobic respiration in the north and south eastern tropical Pacific oxygen minimum zones. Deep Sea Research Part I: Oceanographic Research Papers 94:173-183.*

5. *Lam P & Kuypers MMM (2011) Microbial Nitrogen Cycling Processes in Oxygen Minimum Zones. Annual Review of Marine Science 3(1):317-345.*

6. *Lam P & Kuypers MMM (2011) Microbial nitrogen cycling processes in oxygen minimum zones. Ann Rev Mar Sci 3:317-345.*

7. *Codispoti LA, et al. (1986) High nitrite levels off Northern Peru: A signal of instability in the marine denitrification rate. Science 233(4769):1200-1202.*

8. *Ulloa O, Canfield DE, DeLong EF, Letelier RM, & Stewart FJ (2012) Microbial oceanography of anoxic oxygen minimum zones. Proceedings of the National Academy of Sciences of the United States of America 109(40):15996-16003.*

9. *Froelich PN, et al. (1979) Early oxidation of organic matter in pelagic sediments of the eastern equatorial Atlantic: suboxic diagenesis. Geochimica et Cosmochimica Acta 43(7):1075-1090.*

10. *Canfield DE, Erik K, & Bo T (2005) The Sulfur Cycle. Advances in Marine Biology, eds Donald E. Canfield EK & Bo T (Academic Press), Vol Volume 48, pp 313-381.*

11. *Denger K, Laue H, & Cook MA (1997) Thiosulfate as a metabolic product: the bacterial fermentation of taurine. Archives of Microbiology 168(4):297-301.*

12. *Cook AM & Denger K (2006) Metabolism of taurine in microorganisms. Taurine 6, eds Oja SS & Saransaari P (Springer US, Boston, MA), pp 3-13.*

13. *Lavik G, et al. (2009) Detoxification of sulphidic African shelf waters by blooming chemolithotrophs. Nature 457(7229):581-584.*

14. *Schunck H, et al. (2013) Giant hydrogen sulfide plume in the oxygen minimum zone off Peru supports chemolithoautotrophy. PloS one 8(8):e68661.*

15. *Naqvi SWA, et al. (2000) Increased marine production of N2O due to intensifying anoxia on the Indian continental shelf. Nature 408(6810):346-349.*

16. Galán A, Faúndez J, Thamdrup B, Santibáñez JF, & Farías L (2014) Temporal dynamics of nitrogen loss in the coastal upwelling ecosystem off central Chile: Evidence of autotrophic denitrification through sulfide oxidation. Limnology and Oceanography 59(6):1865-1878.

17. Fossing H (1990) Sulfate reduction in shelf sediments in the upwelling region off Central Peru. Continental Shelf Research 10(4):355-367.

18. Ferdelman TG, Fossing H, Neumann K, & Schulz HD (1999) Sulfate reduction in surface sediments of the southeast Atlantic continental margin between 15°38'S and 27°57'S (Angola and Namibia). Limnology and Oceanography 44(3):650-661.

19. Fonselius S, Dyrssen D, & Yhlen B (1999) Determination of hydrogen sulphide. Methods of Seawater Analysis., eds Grasshoff K, Ehrhardt M, & Kremling K (WILEY-VCH Verlag GmbH), Vol 14, pp 91-100.

20. Brüchert V, et al. (2003) Regulation of bacterial sulfate reduction and hydrogen sulfide fluxes in the central namibian coastal upwelling zone. Geochimica et Cosmochimica Acta 67(23):4505-4518.

21. Brüchert V, et al. (2006) Biogeochemical and physical control on shelf anoxia and water column hydrogen sulphide in the Benguela upwelling system of Namibia Past and Present Water Column Anoxia, ed Neretin NL (Springer Netherlands, Dordrecht), pp 161-193.

22. Martens CS, Albert DB, & Alperin MJ (1998) Biogeochemical processes controlling methane in gassy coastal sediments—Part 1. A model coupling organic matter flux to gas production, oxidation and transport. Continental Shelf Research 18(14):1741-1770.

23. Martens CS & Val Klump J (1980) Biogeochemical cycling in an organic-rich coastal marine basin—I. Methane sediment-water exchange processes. Geochimica et Cosmochimica Acta 44(3):471-490.

24. Kasten S & Jørgensen BB (2000) Sulfate Reduction in Marine Sediments. Marine Geochemistry, eds Schulz HD & Zabel M (Springer Berlin Heidelberg, Berlin, Heidelberg), pp 263-281.

25. Copenhagen WJ (1954) The periodic mortality of fish in the Walvis region. S Afr Med J 28(18):381.

26. Levin LA, et al. (2009) Effects of natural and human-induced hypoxia on coastal benthos. Biogeosciences 6(10):2063-2098.

27. Dugdale RC, Goering JJ, Barber RT, Smith RL, & Packard TT (1977) Denitrification and hydrogen sulfide in the Peru upwelling region during 1976. Deep Sea Research 24(6):601-608.

28. Weeks SJ, Currie B, & Bakun A (2002) Satellite imaging: Massive emissions of toxic gas in the Atlantic. Nature 415(6871):493-494.

29. Ohde T, Siegel H, Reißmann J, & Gerth M (2007) Identification and investigation of sulphur plumes along the Namibian coast using the MERIS sensor. Continental Shelf Research 27(6):744-756.

30. Cline JD (1969) Spectrophotometric determination of hydrogen sulfide in natural waters Limnology and Oceanography 14(3):454-458.

31. Weeks SJ, Currie B, Bakun A, & Peard KR (2004) Hydrogen sulphide eruptions in the Atlantic Ocean off southern Africa: implications of a new view based on SeaWiFS satellite imagery. Deep Sea Research Part I: Oceanographic Research Papers 51(2):153-172.

32. Siegel H, Ohde T, Gerth M, Lavik G, & Leipe T (2007) Identification of coccolithophore blooms in the SE Atlantic Ocean off Namibia by satellites and in-situ methods. Continental Shelf Research 27(2):258-274.

33. Naqvi SAW, Naik H, Jayakumar DA, Shailaja MS, & Narvekar PV (2006) Seasonal oxygen deficiency over the western continental shelf of India Past and Present Water Column Anoxia, ed Neretin NL (Springer Netherlands, Dordrecht), pp 195-224.

34. Ivanenkov VN & Rozanov AG (1961) Hydrogen sulphide contamination of the intermediate water layers of the Arabian Sea and the Bay of Bengal. Okeanologiya 1(13):443-449.

35. Diaz RJ & Rosenberg R (2008) Spreading dead zones and consequences for marine ecosystems. Science 321(5891):926-929.

36. Jickells TD, et al. (2017) A reevaluation of the magnitude and impacts of anthropogenic atmospheric nitrogen inputs on the ocean. Global Biogeochemical Cycles 31(2):2016GB005586.

37. Monteiro PMS, van der Plas AK, Mélice JL, & Florenchie P (2008) Interannual hypoxia variability in a coastal upwelling system: Ocean–shelf exchange, climate and ecosystem-state implications. Deep Sea Research Part I: Oceanographic Research Papers 55(4):435-450.

38. *Monteiro PMS, et al. (2006) Variability of natural hypoxia and methane in a coastal upwelling system: Oceanic physics or shelf biology? Geophysical Research Letters 33(16):n/a-n/a.*

39. *Hamukuaya H, O'Toole MJ, & Woodhead PMJ (1998) Observations of severe hypoxia and offshore displacement of Cape hake over the Namibian shelf in 1994. South African Journal of Marine Science 19(1):57-59.*

40. *Cockcroft AC (2002) Jasus lalandii "walkouts" or mass strandings in South Africa during the 1990's: an overview. Marine and Freshwater Research 52(8):1085-1093.*

41. *Canfield DE, et al. (2010) A cryptic sulfur cycle in oxygen-minimum-zone waters off the Chilean coast. Science 330(6009):1375-1378.*

42. *Wright JJ, Konwar KM, & Hallam SJ (2012) Microbial ecology of expanding oxygen minimum zones. Nature reviews. Microbiology 10(6):381-394.*

43. *Alldredge AL & Cohen Y (1987) Can microscale chemical patches persist in the sea? Microelectrode study of marine snow, fecal pellet. Science 235(4789):689-691.*

44. *Woebken D, Fuchs BM, Kuypers MMM, & Amann R (2007) Potential interactions of particle-associated anammox bacteria with bacterial and archaeal partners in the Namibian upwelling system. Applied and environmental microbiology 73(14):4648-4657.*

45. *Karl DM, Knauer GA, Martin JH, & Ward BB (1984) Bacterial chemolithotrophy in the ocean is associated with sinking particles. Nature 309(5963):54-56.*

46. *Stief P, Kamp A, Thamdrup B, & Glud RN (2016) Anaerobic nitrogen turnover by sinking diatom aggregates at varying ambient oxygen levels. Frontiers in microbiology 7:98.*

47. *Stevens H & Ulloa O (2008) Bacterial diversity in the oxygen minimum zone of the eastern tropical South Pacific. Environmental microbiology 10(5):1244-1259.*

48. *Fuchs BM, Woebken D, Zubkov MV, Burkill P, & Amann R (2005) Molecular identification of picoplankton populationsin contrasting waters of the Arabian Sea. Aquatic Microbial Ecology 39(2):145-157.*

49. *Carolan M & Beman JM (2015) Transcriptomic evidence for microbial sulfur cycling in the eastern tropical North Pacific oxygen minimum zone. Frontiers in microbiology 6.*

50. *Bristow LA, et al. (2017) N2 production rates limited by nitrite availability in the Bay of Bengal oxygen minimum zone. Nature Geosci 10(1):24-29.*

51. *Muyzer G & Stams AJM (2008) The ecology and biotechnology of sulphate-reducing bacteria. Nat Rev Micro 6(6):441-454.*

52. *Widdel F (1988) Microbiology and ecology of sulfate- and sulfur-reducing bacteria. Biology of Anaerobic Organisms, ed Zehnder AJB (John Wiley, New York), pp 469-585.*

53. *Ramos A, Keller K, Wall J, & Pereira IA (2012) The membrane QmoABC complex interacts directly with the dissimilatory adenosine 5´-phosphosulfate reductase in sulfate reducing bacteria. Frontiers in microbiology 3(137).*

54. *Santos AA, et al. (2015) A protein trisulfide couples dissimilatory sulfate reduction to energy conservation. Science 350(6267):1541-1545.*

55. *Wagner M, Roger AJ, Flax JL, Brusseau GA, & Stahl DA (1998) Phylogeny of dissimilatory sulfite reductases supports an early origin of sulfate respiration. Journal of bacteriology 180(11):2975-2982.*

56. *Finster KW & Kjeldsen KU (2010) Desulfovibrio oceani subsp. oceani sp. nov., subsp. nov. and Desulfovibrio oceani subsp. galateae subsp. nov., novel sulfate-reducing bacteria isolated from the oxygen minimum zone off the coast of Peru. Antonie van Leeuwenhoek 97(3):221-229.*

57. *Cypionka H (2000) Oxygen respiration by Desulfovibrio species. Annual review of microbiology 54(1):827-848.*

58. *Stewart FJ, Ulloa O, & DeLong EF (2012) Microbial metatranscriptomics in a permanent marine oxygen minimum zone. Environmental microbiology 14(1):23-40.*

59. *Strittmatter AW, et al. (2009) Genome sequence of Desulfobacterium autotrophicum HRM2, a marine sulfate reducer oxidizing organic carbon completely to carbon dioxide. Environmental microbiology 11(5):1038-1055.*

60. *Albert DB, Taylor C, & Martens CS (1995) Sulfate reduction rates and low molecular weight fatty acid concentrations in the water column and surficial sediments of the Black Sea. Deep Sea Research Part I: Oceanographic Research Papers 42(7):1239-1260.*

61. *Ferdelman TG, et al. (1997) Sulfate reduction and*

methanogenesis in a Thioploca-dominated sediment off the coast of Chile. Geochimica et Cosmochimica Acta 61(15):3065-3079.

62. *Fossing H, et al. (1995) Concentration and transport of nitrate by the mat-forming sulphur bacterium Thioploca. Nature 374(6524):713-715.*

63. *Sommer S, et al. (2016) Depletion of oxygen, nitrate and nitrite in the Peruvian oxygen minimum zone cause an imbalance of benthic nitrogen fluxes. Deep Sea Research Part I: Oceanographic Research Papers 112:113-122.*

64. *Thamdrup B & Canfield DE (1996) Pathways of carbon oxidation in continental margin sediments off central Chile. Limnology and Oceanography 41(8):1629-1650.*

65. *Kalvelage T, et al. (2013) Nitrogen cycling driven by organic matter export in the South Pacific oxygen minimum zone. Nature Geosci 6(3):228-234.*

66. *Bohlen L, et al. (2011) Benthic nitrogen cycling traversing the Peruvian oxygen minimum zone. Geochimica et Cosmochimica Acta 75(20):6094-6111.*

67. *Johnston DT, et al. (2014) Placing an upper limit on cryptic marine sulphur cycling. Nature 513(7519):530-533.*

68. *Friedrich CG, Rother D, Bardischewsky F, Quentmeier A, & Fischer J (2001) Oxidation of Reduced Inorganic Sulfur Compounds by Bacteria: Emergence of a Common Mechanism? Applied and environmental microbiology 67(7):2873-2882.*

69. *Hogslund S, et al. (2009) Physiology and behaviour of marine Thioploca. The ISME journal 3(6):647-657.*

70. *Sayama M, Risgaard-Petersen N, Nielsen LP, Fossing H, & Christensen PB (2005) Impact of bacterial NO3– transport on sediment biogeochemistry. Applied and environmental microbiology 71(11):7575-7577.*

71. *Otte S, et al. (1999) Nitrogen, Carbon, and Sulfur Metabolism in NaturalThioploca Samples. Applied and environmental microbiology 65(7):3148-3157.*

72. *Preisler A, et al. (2007) Biological and chemical sulfide oxidation in a Beggiatoa inhabited marine sediment. ISME J 1(4):341-353.*

73. *Roberston LA & Kuenen JG (2013) The colorless sulfur bacteria. The Prokaryotes, eds Rosenberg R, Delong EF, Lory S, Stackebrandt E, & Thompson F (Springer-Verlag, New York), 4 Ed Vol 2, pp 985-1011.*

74. *Teske A, et al. (2000) Diversity of thiosulfate-oxidizing bacteria from marine sediments and hydrothermal vents. Applied and environmental microbiology 66(8):3125-3133.*

75. *Loy A, et al. (2009) Reverse dissimilatory sulfite reductase as phylogenetic marker for a subgroup of sulfur-oxidizing prokaryotes. Environmental microbiology 11(2):289-299.*

76. *Molitor M, et al. (1998) A dissimilatory sirohaem-sulfite-reductase-type protein from the hyperthermophilic archaeon Pyrobaculum islandicum. Microbiology 144(2):529-541.*

77. *Cardoso RB, et al. (2006) Sulfide oxidation under chemolithoautotrophic denitrifying conditions. Biotechnology and bioengineering 95(6):1148-1157.*

78. *Friedrich CG, Bardischewsky F, Rother D, Quentmeier A, & Fischer J (2005) Prokaryotic sulfur oxidation. Current Opinion in Microbiology 8(3):253-259.*

79. *Schütz M, Maldener I, Griesbeck C, & Hauska G (1999) Sulfide-quinone reductase from Rhodobacter capsulatus: Requirement for growth, periplasmic localization, and extension of gene sequence analysis. Journal of bacteriology 181(20):6516-6523.*

80. *Ghosh W & Dam B (2009) Biochemistry and molecular biology of lithotrophic sulfur oxidation by taxonomically and ecologically diverse bacteria and archaea. FEMS Microbiology Reviews 33(6):999-1043.*

81. *Walsh DA, et al. (2009) Metagenome of a versatile chemolithoautotroph from expanding oceanic dead zones. Science 326(5952):578-582.*

82. *Dahl C, et al. (2005) Novel genes of the dsr gene cluster and evidence for close interaction of Dsr proteins during sulfur oxidation in the phototrophic sulfur bacterium Allochromatium vinosum. Journal of bacteriology 187(4):1392-1404.*

83. *Berg JS, Schwedt A, Kreutzmann A-C, Kuypers MMM, & Milucka J (2014) Polysulfides as intermediates in the oxidation of sulfide to sulfate by Beggiatoa spp. Applied and environmental microbiology 80(2):629-636.*

84. *Grote J, et al. (2012) Genome and physiology of a model Epsilonproteobacterium responsible for sulfide detoxification in marine oxygen depletion zones PNAS 109(2):506-510.*

85. *Grote J, Jost G, Labrenz M, Herndl GJ, & Jurgens K (2008) Epsilonproteobacteria represent the major*

portion of chemoautotrophic bacteria in sulfidic waters of pelagic redoxclines of the Baltic and Black Seas. Applied and environmental microbiology 74(24):7546-7551.

86. *Shah V & Morris RM (2015) Genome sequence of "Candidatus Thioglobus autotrophica" Strain EF1, a Chemoautotroph from the SUP05 Clade of marine Gammaproteobacteria. Genome Announcements 3(5):e01156-01115.*

87. *Roeselers G, et al. (2010) Complete genome sequence of Candidatus Ruthia magnifica. Standards in genomic sciences 3(2):163-173.*

88. *Marshall KT & Morris RM (2015) Genome sequence of "Candidatus Thioglobus singularis" Strain PS1, a mixotroph from the SUP05 clade of marine Gammaproteobacteria. Genome Announcements 3(5).*

89. *Swan BK, et al. (2011) Potential for chemolithoautotrophy among ubiquitous bacteria lineages in the dark ocean. Science 333(6047):1296-1300.*

90. *Murillo AA, RamÃrez-Flandes S, DeLong EF, & Ulloa O (2014) Enhanced metabolic versatility of planktonic sulfur-oxidizing gammaproteobacteria in an oxygen-deficient coastal ecosystem. Frontiers in Marine Science 1.*

91. *Kuwahara H, et al. (2007) Reduced genome of the thioautotrophic intracellular symbiont in a deep-sea clam, Calyptogena okutanii. Current Biology 17(10):881-886.*

92. *Newton IL, et al. (2007) The Calyptogena magnifica chemoautotrophic symbiont genome. Science 315(5814):998-1000.*

93. *Mattes TE, et al. (2013) Sulfur oxidizers dominate carbon fixation at a biogeochemical hot spot in the dark ocean. The ISME journal 7(12):2349-2360.*

94. *Marshall KT & Morris RM (2013) Isolation of an aerobic sulfur oxidizer from the SUP05/Arctic96BD-19 clade. The ISME journal 7(2):452-455.*

95. *Fuchsman CA, Kirkpatrick JB, Brazelton WJ, Murray JW, & Staley JT (2011) Metabolic strategies of free-living and aggregate-associated bacterial communities inferred from biologic and chemical profiles in the Black Sea suboxic zone. FEMS microbiology ecology 78(3):586-603.*

96. *Glaubitz S, Kiesslich K, Meeske C, Labrenz M, & Jurgens K (2013) SUP05 dominates the Gammaproteobacterial sulfur oxidizer assemblages in pelagic redoxclines of the central Baltic and Black Seas. Applied and environmental microbiology 79(8):2767-2776.*

97. *Stewart FJ (2011) Dissimilatory sulfur cycling in oxygen minimum zones: an emerging metagenomics perspective. Biochemical Society transactions 39(6):1859-1863.*

98. *Hawley AK, Brewer HM, Norbeck AD, Pasa-Tolic L, & Hallam SJ (2014) Metaproteomics reveals differential modes of metabolic coupling among ubiquitous oxygen minimum zone microbes. Proceedings of the National Academy of Sciences of the United States of America 111(31):11395-11400.*

99. *Yilmaz P, Yarza P, Rapp JZ, & Glöckner FO (2016) Expanding the World of Marine Bacterial and Archaeal Clades. Frontiers in microbiology 6(1524).*

100. *Allers E, et al. (2013) Diversity and population structure of Marine Group A bacteria in the Northeast subarctic Pacific Ocean. The ISME journal 7(2):256-268.*

101. *Beman JM & Carolan MT (2013) Deoxygenation alters bacterial diversity and community composition in the ocean's largest oxygen minimum zone. Nature Communications 4:2705.*

102. *Thrash JC, et al. (2016) Decoding bacterioplankton metabolism in the northern Gulf of Mexico Dead Zone. bioRxiv.*

103. *Sheik CS, Jain S, & Dick GJ (2014) Metabolic flexibility of enigmatic SAR324 revealed through metagenomics and metatranscriptomics. Environmental microbiology 16(1):304-317.*

104. *Wright JJ, et al. (2014) Genomic properties of Marine Group A bacteria indicate a role in the marine sulfur cycle. The ISME journal 8(2):455-468.*

105. *Hedderich R, et al. (1998) Anaerobic respiration with elemental sulfur and with disulfides. FEMS Microbiology Reviews 22(5):353-381.*

106. *Takai K, et al. (2006) Sulfurimonas paralvinellae sp. nov., a novel mesophilic, hydrogen- and sulfur-oxidizing chemolithoautotroph within the Epsilonproteobacteria isolated from a deep-sea hydrothermal vent polychaete nest, reclassification of Thiomicrospira denitrificans as Sulfurimonas denitrificans comb. nov. and emended description of the genus Sulfurimonas. International Journal of Systematic and Evolutionary Microbiology 56(8):1725-1733.*

107. Strous M, Heijnen JJ, Kuenen JG, & Jetten MSM (1998) The sequencing batch reactor as a powerful tool for the study of slowly growing anaerobic ammonium-oxidizing microorganisms. Applied microbiology and biotechnology 50(5):589-596.

108. Kuypers MM, et al. (2005) Massive nitrogen loss from the Benguela upwelling system through anaerobic ammonium oxidation. Proceedings of the National Academy of Sciences of the United States of America 102(18):6478-6483.

109. Russ L, Speth DR, Jetten MSM, Op den Camp HJM, & Kartal B (2014) Interactions between anaerobic ammonium and sulfur-oxidizing bacteria in a laboratory scale model system. Environmental microbiology 16(11):3487-3498.

110. Shah V, Chang BX, & Morris RM (2016) Cultivation of a chemoautotroph from the SUP05 clade of marine bacteria that produces nitrite and consumes ammonium. The ISME journal.

111. Arevalo-Martinez DL, Kock A, Loscher CR, Schmitz RA, & Bange HW (2015) Massive nitrous oxide emissions from the tropical South Pacific Ocean. Nature Geosci 8(7):530-533.

112. Dalsgaard T, et al. (2014) Oxygen at Nanomolar Levels Reversibly Suppresses Process Rates and Gene Expression in Anammox and Denitrification in the Oxygen Minimum Zone off Northern Chile. mBio 5(6).

113. Li X, Taylor GT, Astor Y, & Scranton MI (2008) Relationship of sulfur speciation to hydrographic conditions and chemoautotrophic production in the Cariaco Basin. Marine Chemistry 112(1–2):53-64.

114. Zopfi J, Ferdelman TG, Jorgensen BB, Teske A, & Thamdrup B (2001) Influence of water column dynamics on sulfide oxidation and other major biogeochemical processes in the chemocline of (Mariager Fjord Denmark). Marine Chemistry 74:29-51.

115. Hayes MK, Taylor GT, Astor Y, & Scranton MI (2006) Vertical distributions of thiosulfate and sulfite in the Cariaco Basin. Limnology and Oceanography 51(1):280-287.

116. Finster K (2011) Microbiological disproportionation of inorganic sulfur compounds. Journal of Sulfur Chemistry 29(3-4):281-292.

117. Poser A, et al. (2013) Disproportionation of elemental sulfur by haloalkaliphilic bacteria from soda lakes. Extremophiles 17(6):1003-1012.

118. Sørensen KB & Canfield DE (2004) Annual fluctuations in sulfur isotope fractionation in the water column of a euxinic marine basin. Geochimica et Cosmochimica Acta 68(3):503-515.

119. Neretin LN, Böttcher ME, & Grinenko VA (2003) Sulfur isotope geochemistry of the Black Sea water column. Chemical Geology 200(1-2):59-69.

120. Ksionzek KB, et al. (2016) Dissolved organic sulfur in the ocean: Biogeochemistry of a petagram inventory. Science.

121. Johnston JB, Murray K, & Cain RB (1975) Microbial metabolism of aryl sulphonates A re-assessment of colorimetric methods for the determination of sulphite and their use in measuring desulphonation of aryl and alkylbenzene sulphonates. Antonie van Leeuwenhoek 41(1):493-511.

122. Thysse GJE & Wanders TH (1974) Initial steps in the degradation of n-alkane-1-sulphonates by Pseudomonas. Antonie van Leeuwenhoek 40(1):25-37.

123. Kondo & Ishimoto M(1972) Enzymatic formation of sulfite and acetate from sulfoacetaldehyde, a degradation product of taurine. Journal of Biochemistry 72(2):487-489.

124. Lie TJ, Clawson ML, Godchaux W, & Leadbetter ER (1999) Sulfidogenesis from 2-aminoethanesulfonate (taurine) fermentation by a morphologically unusual sulfate-reducing bacterium, Desulforhopalus singaporensis sp. nov. Applied and environmental microbiology 65(8):3328-3334.

125. Tevatia R, et al. (2015) The taurine biosynthetic pathway of microalgae. Algal Research 9:21-26.

126. Flynn KJ, Jones KJ, Raine R, Richard J, & Flynn K (1994) Use of intracellular amino acid analysis as an indicator of the physiological status of natural dinoflagellate populations. Marine Ecology Progress Series 103(1-2):175-186.

127. Tripp HJ, et al. (2008) SAR11 marine bacteria require exogenous reduced sulphur for growth. Nature 452(7188):741-744.

128. Sun J, et al. (2016) The abundant marine bacterium Pelagibacter simultaneously catabolizes dimethylsulfoniopropionate to the gases dimethyl sulfide and methanethiol. 1:16065.

129. Tsementzi D, et al. (2016) SAR11 bacteria

linked to ocean anoxia and nitrogen loss. Nature 536(7615):179-183.

130. *Kappler U (2008) Bacterial sulfite-oxidizing enzymes – enzymes for chemolithotrophs only? Microbial Sulfur Metabolism, eds Dahl C & Friedrich CG (Springer Berlin Heidelberg, Berlin, Heidelberg), pp 151-169.*

131. *Williams TJ, et al. (2012) A metaproteomic assessment of winter and summer bacterioplankton from Antarctic Peninsula coastal surface waters. The ISME journal 6(10):1883-1900.*

132. *van der Ploeg JR, et al. (1996) Identification of sulfate starvation-regulated genes in Escherichia coli: a gene cluster involved in the utilization of taurine as a sulfur source. Journal of bacteriology 178(18):5438-5446.*

133. *Stramma L, Johnson GC, Sprintall J, & Mohrholz V (2008) Expanding oxygen-minimum zones in the tropical oceans. Science 320(5876):655-658.*

134. *Ganesh S, Parris DJ, DeLong EF, & Stewart FJ (2014) Metagenomic analysis of size-fractionated picoplankton in a marine oxygen minimum zone. The ISME journal 8(1):187-211.*

135. *Overmann J & Manske AK (2006) Anoxygenic phototrophic bacteria in the Black Sea chemocline. Past and Present Water Column Anoxia, ed Neretin LN (Springer Netherlands, Dordrecht), pp 523-541.*

136. *Martínez-Pérez C, et al. (2016) The small unicellular diazotrophic symbiont, UCYN-A, is a key player in the marine nitrogen cycle. Nature Microbiology 1:16163.*

CHAPTER 5

Oxygen minimum zone cryptic sulfur cycling sustained by offshore transport of key oxidizing bacteria

Cameron M. Callbeck, Gaute Lavik, Timothy G. Ferdelman, Bernhard Fuchs, Harald Gruber-Vodicka, Philipp F. Hach, Sten Littmann, Niels J. Schoffelen, Tim Kavelage, Sören Thomsen, Harald Schunck, Carolin Löscher, Ruth A. Schmitz, and Marcel M. M. Kuypers. (2017) Oxygen minium zone cryptic sulfur cycling sustained by offshore transport of key oxidizing bacteria. In review *Nature Communications*

Abstract

The chemolithoautotrophic gammaproteobacterial clade SUP05 couples water column sulfide oxidation to nitrate reduction in coastal oxygen minimum zones (OMZs). Reports of SUP05 distributions in offshore OMZ waters where dissolved sulfide is not detected has led to the suggestion that a cryptic sulfur cycle involving SUP05 exists. We examined the distribution and metabolic capacity of SUP05 in Peru Upwelling waters, as well as nitrogen, sulfur and carbon turnover in bulk samples and at the SUP05 single-cell level. High rates of SUP05 CO_2 assimilation were measured in offshore waters containing elevated concentrations of elemental sulfur that had been transported offshore by a mesoscale eddy. Genome analysis indicated that the Peru Upwelling SUP05 ("*Candidatus* Thioglobus perditus") can perform complete denitrification. Its capacity to couple denitrification with elemental sulfur oxidation enables the survival of Peru Upwelling SUP05 in the absence of dissolved sulfide underpins reports of offshore sulfur cycling and fixed nitrogen loss in OMZs.

Oxygen Minimum Zones (OMZs), where dissolved oxygen concentrations fall below 20 μmol kg^{-1}, are responsible for large losses of fixed nitrogen from the ocean, although they occupy less than 1% of the global ocean volume (1-3). In OMZs, such as those found in the Eastern Tropical South Pacific (ETSP), the Eastern Tropical South Atlantic, and the Arabian Sea, high rates of primary productivity coupled with poor ventilation of OMZ shelf waters can furthermore lead to the recurrent accumulation of dissolved hydrogen sulfide within these waters (4-7). Such "sulfidic events" often generate episodic plumes of particulate elemental sulfur in surface waters that are visible from space (6, 8-10). Closely associated with these sulfidic events are bacteria from the gammaproteobacterial clade known as SUP05 (5, 6, 11, 12). As a nitrate-reducing, sulfide-oxidizing chemolithoautotroph, SUP05 may substantially contribute to the loss of fixed N from productive upwelling regions, the production of climate relevant N_2O, and dark carbon fixation in the sub-euphotic water column (5, 6, 11, 13).

Gene sequences associated to the SUP05 clade are frequently found not only in sulfidic shelf waters (5, 6), but in OMZ waters on the outer shelf and offshore waters where dissolved hydrogen sulfide concentrations fall below typical detection levels (<1 μM)(14-18). Offshore OMZs also harbor diverse assemblages of putative sulfate-reducing bacteria (13, 15-17), and it has been proposed that SUP05 and sulfate-reducing bacteria may be involved in a so-called "cryptic sulfur cycle" (13). Cryptic sulfur cycling refers to the simultaneous activity of sulfate-reducing and sulfide-oxidizing pathways in a closely defined space such as a marine particle aggregate, in that produced sulfide from sulfate-reducing bacteria is immediately oxidized back to elemental sulfur or sulfate by sulfide-oxidizing bacteria (13). Cryptic sulfur cycling in OMZ waters may have major implications for nitrogen cycling. For instance, organic matter mineralization mediated by microbial fermentation coupled to sulfate reduction yields ammonium that can drive anaerobic ammonium oxidation (anammox) (13). Sulfide oxidation, via nitrate reduction mediated by SUP05, may in turn contribute to the loss of fixed N and to the production of N_2O (13).

SUP05 thus appears to play a key role linking nitrogen and sulfur cycling in OMZ waters. Nevertheless, several important questions regarding the distribution, metabolic capabilities and actual activities of SUP05 persist. For instance, the fluorescent in situ hybridization (FISH) probe previously employed to identify sulfide-oxidizing gammaproteobacteria bacteria, based on the 16S rRNA marker gene, also broadly covers the closely related heterotrophic sulfide-oxidizing bacteria, Arctic96BD-19 clade (Fig. S1). Owing to the phylogenetic breadth of the SUP05 clade it is not clear whether the SUP05 bacteria identified offshore are indeed the same species as the SUP05 bacteria identified in near-shore sulfidic environments. Furthermore, the metabolic capacities of the SUP05 clade, especially those of the

marine Peru Upwelling region are not completely understood. A nitrous oxide reductase gene, *nosZ*, has not been found in SUP05 genomes (5, 11, 19), and it has been suggested that other bacteria associated with SUP05 perform the final denitrification step of N_2O reduction to N_2 (20). Lastly, despite the persistence of apparent sulfur-based metabolic capacities throughout OMZ waters (13-18), the actual metabolic activity of organisms corresponding with these gene sequences may be diminished in offshore waters. Geochemical evidence that would point to substantial rates of microbial sulfate reduction in offshore waters has not been found in the ETSP (21). In the ETSP region and in other OMZs, mesoscale eddies forming close to the coast are known to facilitate the rapid horizontal advection of coastal biogeochemical signals offshore (22-24). Therefore, the observed presence of the offshore SUP05 and sulfate-reducing bacterial communities may simply reflect the advection of sulfur rich shelf waters into the open ocean as suggested previously (15).

The chemical and hydrographic conditions in the continental Peru Margin waters of the ETSP in late austral summer 2013 provided a framework for examining the distribution and activity of SUP05 organisms (Fig. 1). Under normal flow conditions

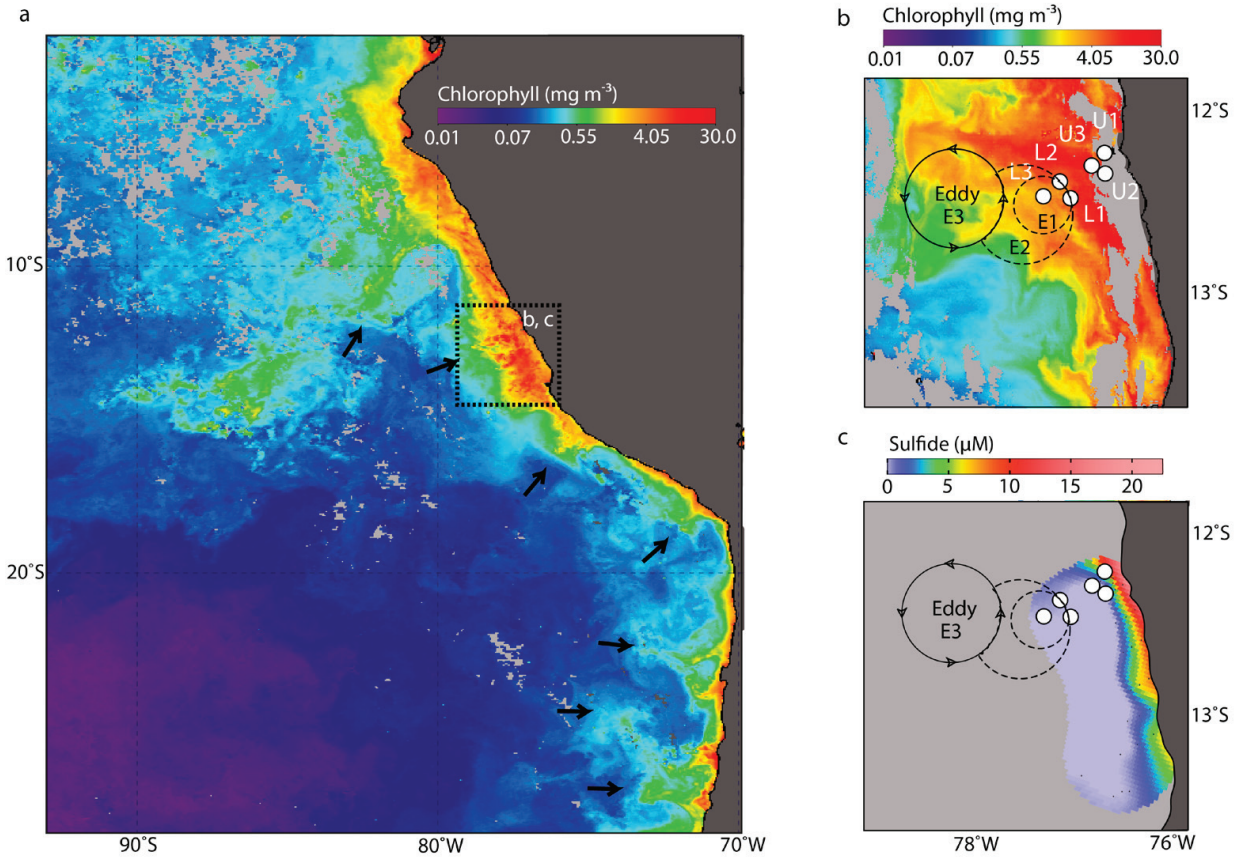

Fig. 1. Station and mesoscale eddy location relative to near-surface chlorophyll a and maximum dissolved sulfide concentrations: (a) Monthly composite MODIS image (see Methods for source) showing near-surface chlorophyll concentrations for March 2013, where the black arrows indicate cross-shelf advected filaments. (b) MODIS image of near-surface chlorophyll concentrations for February 24, 2013. Main water column sampling stations are marked with white circles. Times of station sampling are provided in Table S1. Formation and propagation of the eddy westward occurring over time is indicated: E1 represents the initial eddy formation from Jan 28th to Feb 3rd, E2 shows the expansion of the eddy (Feb. 7-12, 2013), and E3 is the location of the eddy when the image was taken (Feb. 24, 2013). (c) Maximum sulfide concentration reported for water masses with densities between 26.1 and 26.2 kg m^{-3}. White circles show main sampling stations as in panel 1b; stations sampled for sulfide are shown in Fig. S3.

at the Peru Margin, Ekman transport of the surface, equator-ward flowing Peru Coastal Current results in near shore upwelling of the oxygen-poor and nutrient-rich water derived from the poleward flowing Peru-Chile Undercurrent (25). Instabilities in the Peru-Chile Undercurrent possibly triggered by sharp variations in shoreline topography (24) lead to the formation of offshore sub-surface anticyclonic eddies (24, 26-28) (Fig. S2b). Thus, in addition to the typical near-shore and offshore ETSP waters, we obtained samples at the offshore site during a period of time when the formation of a sub-surface anticyclonic eddy drove cross-shelf, offshore transport of sulfur-rich shelf waters. To quantitatively discriminate dominant Peru Upwelling SUP05 bacteria from close relatives of the SUP05 clade, we designed and applied a more stringent SUP05 probe. Based on a near complete metagenomics bin we reconstructed the metabolic capabilities of the Peru Upwelling SUP05 bacteria. Finally, we specifically determined the single-cell C uptake activity of SUP05 bacteria via isotope labeling experiments combined with nanoscale secondary ion mass spectrometry (nanoSIMS) analysis. This allowed us to evaluate the contribution of SUP05 activity to carbon, nitrogen and sulfur cycling both in near-shore and in offshore ETSP OMZ waters.

Results and Discussion

Biogeochemical characterization of shelf and offshore waters

Waters from the ETSP region off the coast of Peru (12°S' 78.5°W and 13.5°S'77°W) were sampled from February 8th to March 4th, 2013 onboard the RV *Meteor* (Expedition M93; Table S1). At the beginning of the sampling period in February 2013, an anticyclonic mesocale eddy had formed approximately 50 km from the coast (Fig. 1; S2b). During the course of our experiments and sampling, the subsurface eddy expanded and propagated in south-southwesterly direction, eventually curling in a westerly direction (Fig. 1b; S2c-f). By March 2013, the eddy had caused a filament of surface shelf water moving along the northern rim of the eddy to extend to nearly 330 km offshore (Fig. 1b). Sub-surface waters at stations U2, U3, L1 and L3 were impacted by the resulting cross-shelf transport of shelf waters during and after the eddy formation (24). Station L2, on the other hand, was sampled after the eddy had travelled already further westwards and caused the onshore advection of offshore water masses along its southern rim(24). Thus, station L2 referred here to "non-eddy" for simplicity, exhibited temperature-salinity characteristics typical of offshore waters, which are clearly separated in the temperature and salinity space from the stations impacted by coastal waters (Fig. S4).

Station U1 on the shelf was also sampled in early March when normal (non-eddy) flow conditions prevailed (Fig. S2). The near-shore, shelf waters at station U1 were characterized by extreme depletion of dissolved oxygen (below 10 m) and nitrate (below 30 m), and the presence of free dissolved hydrogen sulfide (up to 7 μM) and ammonium (up to 6 μM) (Fig. 2; S5). Nitrate-depleted, sulfide and elemental sulfur rich bottom waters covered the entire near-shore Peruvian shelf between 12°S 78.3°W and 13.3°S 77°W (Fig. 1; S3). The reduced sulfur inventories in February-March, 2013 (1.6 x 10^9 moles H_2S and 7.0 x 10^8 moles elemental sulfur) were more than twice as large as for the sulfidic event reported for the same area in 2009 (5).

A nitrate-sulfide chemocline in the inner shelf waters at 25-35 m water depth (hereafter simply referred to as the chemocline) coincided with peaks of nitrite and elemental sulfur (Fig. 2; S5). An intermediate product of biotic and abiotic sulfide oxidation, elemental sulfur reached concentrations of up to 6 μM within the chemocline and persisted at μM concentrations in the deeper, sulfidic waters (Fig. 2; S5). Elemental sulfur likely formed at 30-35 meters as chemolithotrophic organisms used downward mixed nitrate to oxidize hydrogen sulfide. Under the denitrifying conditions found at the base of the chemocline, elemental sulfur is the first product of sulfide oxidation (29) as depicted in Equation 1:

$$5H_2S + 2NO_3^- + 2H^+ \rightarrow 5S^0 + N_2 + 6H_2O \quad [Eq.1]$$

Elemental sulfur, transported through eddy

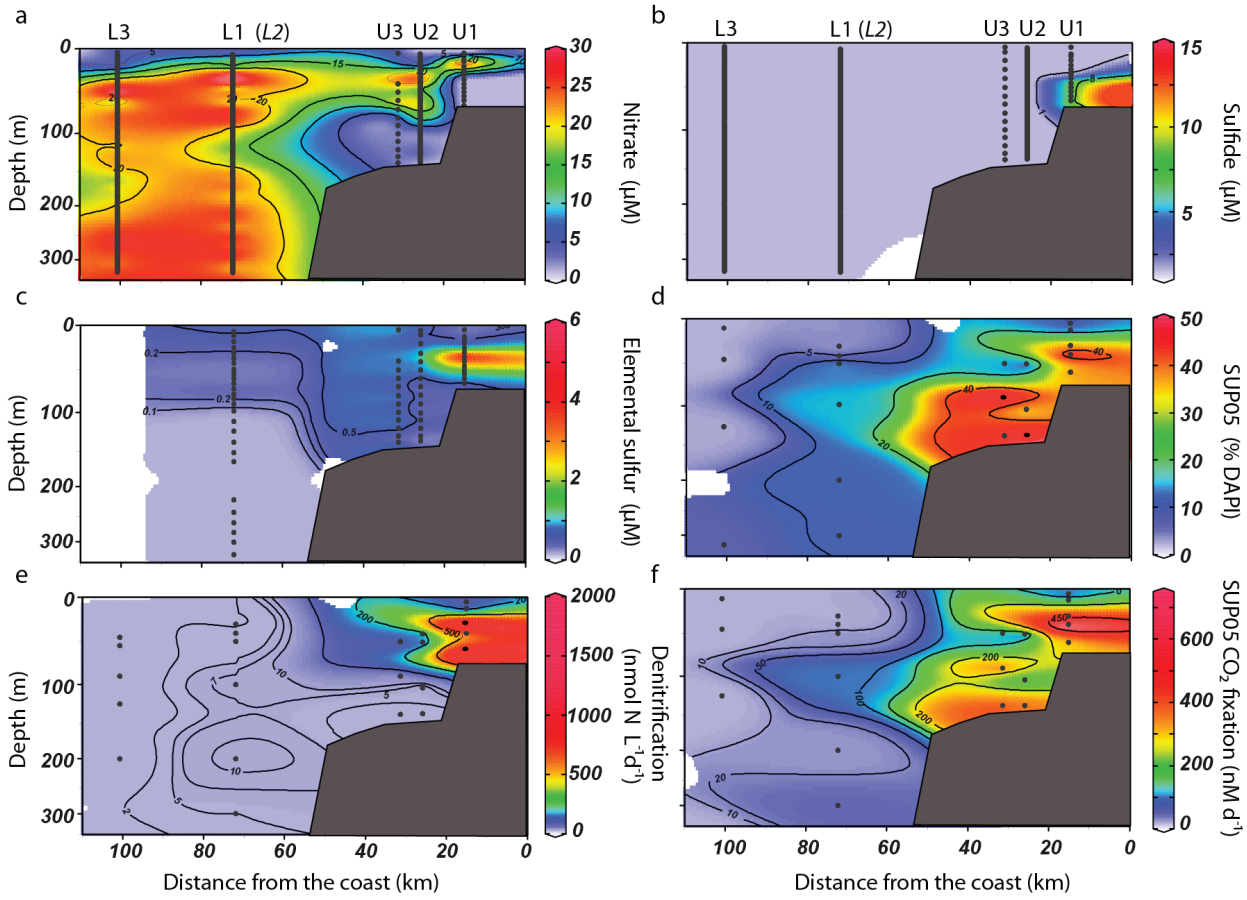

Fig. 2. Distribution of concentrations, abundances and bulk and single cell activities in the Peru Upwelling OMZ as a function of distance from the coast. The composite plots show depth and cross-shelf distribution (a) nitrate, (b) dissolved sulfide, (c) elemental sulfur, (d) % total bacteria (DAPI) identified as SUP05, (e) bulk rates of denitrification, and (f) single-cell determined rates of CO_2 fixed by SUP05. Black dots indicate sample depths at each station included in the composite plots.

diffusion further to the top of the chemocline, may fuel further nitrate consumption via denitrification as shown in Equation 2.

$$5S^0 + 6NO_3^- + 2H_2O \rightarrow 5SO_4^{2-} + 3N_2 + 4H^+ \quad [Eq.\ 2]$$

Overall, as estimated from nitrate and sulfide concentration gradients and employing an eddy diffusion coefficient (Table 1) the downward nitrate flux into the chemocline (17 mmol S m^{-2} d^{-1}) was more than sufficient to oxidize the upward flux of sulfide (-7.6 mmol S m^{-2} d^{-1}) completely to sulfate via denitrification (combined equations 1 and 2 as shown in Eq. 3)

$$5H_2S + 8NO_3^- \rightarrow 5SO_4^{2-} + 4N_2 + 4H_2O + 2H^+ \quad [Eq.\ 3]$$

Up to 70% of the total nitrate flux could be attributed to the oxidation of sulfide within the chemocline at station U1. Microorganisms, such as SUP05, that can couple dissolved sulfide oxidation to nitrate reduction should, therefore, dominate this interface between deep sulfidic waters and overlying nitrate.

Distribution of SUP05 in Peru Upwelling Waters

A new FISH probe, GSO131, was designed to clearly distinguish Peru upwelling SUP05 clade bacteria from near relatives within the Gammaproteobacterial sulfide oxidizer (GSO) clade (e.g. Arctic96BD-19 bacteria) (Fig. S1; Table S2 and S3). Peru Upwelling SUP05 bacteria as quantified using the GSO131 probe

Table 1: SUP05 contribution to CO_2-fixation, sulfide oxidation and denitrification. See Methods for details regarding single-cell calculations.

	Station U1	Station L1	Station L2
[a] ***SUP05 cell abundance (cells L^{-1})***	1.7 x 10^9 (30 m)	7.3 x 10^7 (50 m)	2.9 x 10^7 (200 m)
[b]***Single-cell carbon fixation rates***			
Number of SUP05 cells analyzed	107	67	23
Cell size (μm)	0.81 ± 0.02	1.00 ± 0.03	0.86 ± 0.05
Cell carbon content (*pmols C cell^{-1}*)	6.42 x 10^{-3}	8.46 x 10^{-3}	6.99 x 10^{-3}
Per cell fixation rate (*fmol C cell^{-1} d^{-1}*)	0.24 ± 0.03	0.22 ± 0.05	0.07 ± 0.02
[c]***SUP05 contribution to CO_2 fixation***			
Volumetric SUP05 CO_2 fixation rate rates (*nmol C L^{-1} d^{-1}*)	409 (30 m);	16 (50 m);	2 (200 m)
Depth-integrated SUP05 CO_2 fixation rate (*mmol C m^{-2} d^{-1}*)	17.1 ± 1.4 (8.6 ± 0.7)	10.7 ± 1.5	0.37 ± 0.08
Bulk depth-integrated Dark CO_2 fixation: (mmol C m^{-2} d^{-1})	26.2 ± 2.0	8.0 ± 1.0	4.5 ± 0.6
Nitrate-sulfide redoxcline:			
Sulfide flux (*mmol S m^{-2} d^{-1}*)	-7.6	NA	NA
Sulfur flux (*mmol S m^{-2} d^{-1}*)	-6.6	NA	NA
Nitrate flux (*mmol N m^{-2} d^{-1}*)	17.6	NA	NA
Bulk denitrification rates			
Depth-integrated rates (*mmol N m^{-2} d^{-1}*)	62.3 ± 6.00	3.1 ± 0.6	0.23 ± 0.02
Volumetric rates (*nmol N L^{-1} d^{-1}*)	2044 (30 m);	5.4 (50 m)	BD (200 m)
Environmental Growth Factor			
mol CO_2 assimilated per mol nitrate reduced	0.2-0.29		
mol CO_2 assimilated per mol sulfide oxidized	0.33-0.49		
[d]***SUP05 contribution to H_2S and NO_3^- turnover***			
H_2S oxidation rate to SO_4^{2-} (*mmol S m^{-2} d^{-1}*)	7.8 ± 1.8	3.6 ± 1.0	0.12 ± 0.04
Denitrification rate (*mmol N m^{-2} d^{-1}*)	4.7 ± 1.3	2.2 ± 0.7	0.07 ± 0.03

[a]SUP05 abundances (and associated water depth) used for single-cell CO_2 uptake calculations.
[b]Rates and abundances are from Stations and depths nanoSIMS measurements were performed: Station U1 (30 and 60 m), station L1 (50 and 200 m) and station L2 (200 m).
[c] Dark CO_2 fixation rates integrated for station U1 over 30-65 m and (12-35 m), L1 over 100-300 m, and L2 over 125-320 m.
[d]Depth-integrations were performed for station U1 from 5-65 m and for the offshore station L1 from 6-300 m, and station L2 from 10-320 m depth.

composed up to 50% (1.7-3.2 x 10^6 cells^{-1} ml^{-1}) of the total microbial community within the chemocline at station U1 (Fig. 2; S5). Similar cell densities using a less specific SUP05 FISH probe have been reported for the Namibian shelf region where sulfidic conditions prevailed (6). At station U1, peak SUP05 cell densities within the chemocline coincided with peak rates of denitrification (2000 nmol N L^{-1} d^{-1}) (Fig. 2; S5) and dark carbon fixation (600 - 1000 nmol C L^{-1} d^{-1}) (Fig. S5). These results reaffirm earlier conclusions that SUP05 is a dominant taxon mediating sulfide-driven denitrification at the chemocline in such sulfidic, upwelling shelf waters (5, 6).

In contrast to the sulfide-rich, nitrate-deplete waters on the inner shelf, total dissolved sulfide concentrations dropped below detection (< 1 μM) on the outer shelf (stations U2 and U3; Fig. 2) and offshore beyond the outer shelf break. Elemental

sulfur remained detectable at 100 to 1000 nM in the oxygen and nitrate depleted deep waters of outer shelf stations U2 and U3, and more interestingly, persisted in the offshore eddy-influenced waters of station L1 where dissolved sulfide was not detected (Fig. 2; S5). At station L1, elemental sulfur concentrations ranged between 50-750 nM from 5 to 100 m depth, and coincided with a nitrate minimum (Fig. 2; S5). Temperature-salinity properties at station L1 suggest that nitrate-depleted coastal waters containing elemental sulfur were transported offshore along isopycnals up to 80 km from the coast (Fig. 2a, c; S4). After the eddy had moved further offshore, elemental sulfur was restricted to a narrow band near the surface with concentrations of <300 nM as seen at station L2 (Figs. 2, S4 and S5).

Large cell densities of SUP05 up to 4.5 x 10^5 cells ml^{-1} persisted at station L1 coincident to the passage of a nearly formed anticyclonic eddy through this offshore site (Fig. 2; S5). Even in the absence of dissolved sulfide, SUP05 comprised a significant fraction (up to 17%) of the microbial community in these eddy-influenced offshore waters. Rates of nitrate reduction to N_2 at L1 ranged from 5 to 16 nmol N L^{-1} d^{-1} (Fig. 2; S5), and dark carbon fixation of 9-130 nmol C L^{-1} d^{-1} (Fig. S5) were much lower than those at station U1 on the inner shelf. Nonetheless, rates of denitrification and dark carbon fixation at station L1 under the influence of the eddy and cross-shelf transport exceeded those observed under "non-eddy" conditions (L2). At station L2 we measured reduced rates of denitrification (<0.13 to 4.3 nmol N L^{-1} d^{-1}) and dark carbon fixation (11 to 51 nmol C L^{-1} d^{-1}; Fig. 2; S5). Correspondingly, SUP05 abundances at L2 were one order of magnitude lower than at station L1 and comprised only a minor fraction (0-2%) of the microbial community. Thus, even offshore, SUP05 cell densities appear to correlate with the bulk denitrification rates.

Single-cell activities of SUP05 Bacteria

Despite such correlation, the presence and abundance of an organism in any given environmental setting, for instance SUP05 distributions in eddy influenced offshore waters, yields only limited information on the activity of the organism and its potential impact on the chemistry of the environment. To address the impact of SUP05 on the cycling and fate of sulfur and nitrogen in ETSP waters, we compared the SUP05 specific biogeochemical activity in the chemocline at station U1, where SUP05 plays a dominant role in coupling sulfide oxidation with denitrification, with SUP05 specific activities at the eddy influenced offshore (L1) and "non-eddy" station (L2) stations. We quantified the specific contribution of SUP05 bacteria to dark carbon fixation by measuring the assimilation of ^{13}C-bicarbonate into SUP05 biomass at the single-cell level using nanoSIMS technology. In experiments from station U1 and in the presence of close to ambient concentrations of sulfide, elemental sulfur and nitrate, SUP05 fixed CO_2 at cell specific rate of 0.24 ± 0.03 fmol C $cell^{-1}$ d^{-1} (averaged from 30 and 60 m depths; Fig. 3, Table 1). From the SUP05 cell densities this yielded a SUP05 C fixation volumetric rate at the chemocline (30 m) of 409 ± 50 nmol C L^{-1} d^{-1} (Table 1). Consistent with the premise that SUP05 is the main denitrifying chemoautotroph in the chemocline, comparing integrated SUP05 C fixation rates over depth with total dark CO_2 fixation showed that SUP05 contributed to ~65% of the bulk dark C fixation rates in the sub-euphotic water column at station U1.

The depth-integrated CO_2 uptake attributed to SUP05 (10.7 ± 1.5 mmol C m^{-2} d^{-1}) at station L1 likewise accounted for the majority of dark carbon fixation (Table 1). More significantly, the average SUP05 CO_2 fixation rate of 0.22 ± 0.05 fmol C $cell^{-1}$ d^{-1} was comparable (ANOVA, p = 0.14, no statistical difference) to the specific CO_2 fixation rate determined at station U1 (Fig. 3). Thus, SUP05 bacteria were active in waters transported offshore from the shelf despite the lack of any obvious or measurable dissolved sulfide gradients. In contrast, at station L2 SUP05 bacteria exhibited much lower specific carbon fixation rates of 0.07 ± 0.02 fmol C $cell^{-1}$ d^{-1} rates (Fig. 3) (ANOVA, p = <0.001). In these offshore waters that are not affected by shelf water, SUP05 C fixation rates were <2.1 nmol C L^{-1} d^{-1}. The overall contribution of SUP05 to dark carbon fixation was small (8%).

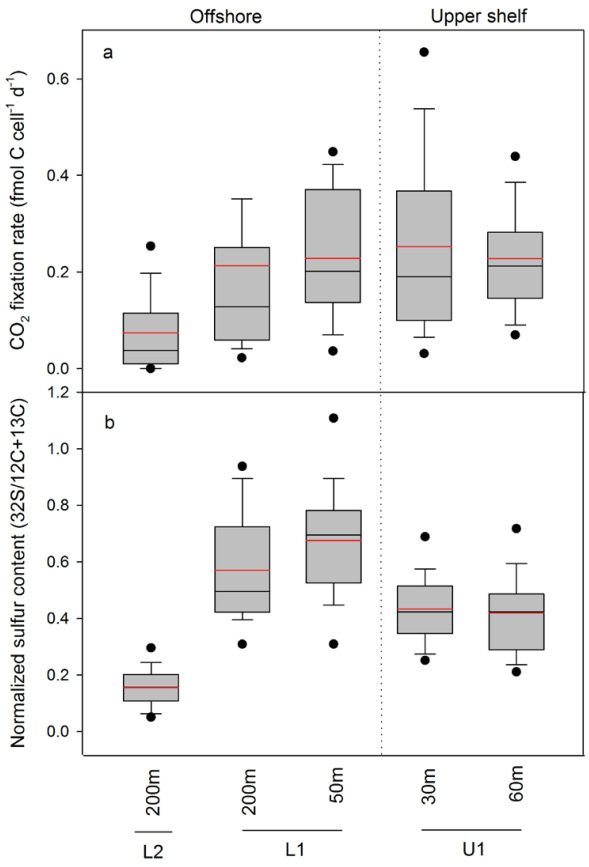

Fig. 3: SUP05 single-cell activity and sulfur content of ETSP SUP05 bacteria. (a) Rates of CO_2 fixation rates based on ^{13}C-bicarbonate uptake into SUP05 cells. (b) Normalized single-cell sulfur content. The mean (red line) and median (black line) are indicated. The boxes represent the distribution of data with 95th and 5th percentiles and outliers are indicated by the black circles. Standard deviations bars are shown. The number of SUP05 cells analyzed at station-depths were: U1-30 m (48 cells), U1-60 m (59 cells), L1-50 m (35 cells), L1-200 m (32 cells), and L2-200 m (23 cells).

We conclude that individual SUP05 cells were active and growing in the shelf chemocline and in waters transported offshore from the shelf; whereas, under normal offshore flow conditions SUP05 bacteria may have been present, but were less active.

SUP05 bacteria actively assimilated C in the offshore transported water masses, but the question remains as to whether this activity had any impact on the overall offshore N and S cycling in the ETSP waters. We can estimate the impact of the SUP05 bacteria on sulfur and nitrogen cycling in the offshore "eddy" and "non-eddy" influenced waters, by assuming that the amount of CO_2 fixed per cell SUP05 per mol nitrate reduced or per mol sulfide oxidized is the same for both near-shore and offshore SUP05 cells. Assuming that denitrification rates at the near-shore station U1 were primarily mediated by SUP05 we estimate that SUP05 fixed 0.20-0.29 mol CO_2 per mol nitrate reduced (Table 1). The environmental growth factor for nitrate translates to 0.33-0.49 mol CO_2 fixed per mol H_2S oxidized based on the stoichiometry in Eq. 3. This environmental growth factor for sulfide oxidation is similar to growth factors reported for cultivated sulfide oxidizers growing on sulfide and oxygen (0.35-0.58 mol CO_2 fixed per mol H_2S oxidized (30-32)). Employing the environmental growth factor for nitrate estimated from station U1, we calculate depth-integrated rates of SUP05 mediated denitrification of 2.2 mmol N m^{-2} d^{-1} at the eddy influenced station L1. These estimated rates are similar to the rates of nitrate reduction to N_2 determined from bulk ^{15}N experiments (3.1 mmol N m^{-2} d^{-1}). Accordingly, SUP05 mediated sulfur oxidation rates at the eddy influenced offshore station L1 are 3.6 mmol S m^{-2} d^{-1} (Table 1), assuming that hydrogen sulfide is oxidized to sulfate (as per Eq. 3). More likely, the rate of SUP05 mediated sulfide oxidation was lower (2.7 mmol S m^{-2} d^{-1}) for elemental sulfur oxidation to sulfate (Eq. 2). These estimated sulfide oxidation rates fall within the same range of potential sulfide oxidation rates measured at offshore ETSP stations (up to 2.09 mmol S m^{-2} d^{-1})(13). At the offshore station uninfluenced by shelf waters (L2), calculated rates of SUP05 mediated denitrification (0.12 mmol m^{-2} d^{-1}) and sulfide oxidation 0.07 (mmol m^{-2} d^{-}1) were low. The results demonstrate that SUP05 was capable of supporting rates of denitrification and sulfur oxidation observed in offshore ETSP waters, but principally in water masses that had only recently originated from sulfur rich near-shore regions.

Peru Upwelling SUP05 ecophysiology and survival in offshore waters

Metagenomics, in combination with nanoSIMS analysis, show that SUP05 is well adapted to the sulfide-poor conditions in water masses transported

offshore. We assembled and binned a draft genome at 95% completeness based on Gammaproeobacterial marker genes of the Peru Upwelling SUP05 from the metagenome for station U1. The genome shows that SUP05 encoded for genes involved in the reverse dissimilatory sulfite reduction pathway (*rdsr*) used in the oxidation of intracellular S^0, as well as an incomplete periplasmic thiosulfate oxidation pathway by *sox* (Fig. 4). The incomplete *sox* pathway, specifically the absence of *soxCD* genes has been correlated with intracellular sulfur deposits in other sulfide-oxidizers (33, 34). The absence of *soxCD* genes is consistent with other SUP05 bacterial metagenomes (5, 11, 35, 36). Empirically, sulfur deposits have been shown to accumulate intracellularly in Arctic96BD-19 bacteria, a closely related lineage of SUP05 (37). Moreover, with nanoSIMS, we found that SUP05 cells at stations U1 and L1 had significantly greater (ANOVA, $p = <0.001$) sulfur content compared to cells at station L2 (Fig. 3), which suggested that SUP05 has a capacity to store sulfur. The stored sulfur, deposited in an inorganic or organic form, is putatively oxidized via the *rdsr* pathway (38). The SUP05-ETSP genome further suggests that the energy conserved from the oxidation of sulfur is coupled to nitrate reduction to N_2 or to oxygen respiration (Fig. 4). Such a complete denitrification pathway, with no termination at N_2O, also contrasts with the Saanich Inlet SUP05 metagenome that lacks the nitrous oxidase (*nosZ*) gene (11, 12). In summary, SUP05 organisms active in the ETSP are capable of complete denitrification coupled to sulfide and elemental sulfur oxidation.

The Peru upwelling SUP05 bacteria described here has only a 97.6% 16S rRNA sequence identity with "*Candidatus* Thioglobus autotrophica", and unlike "*Ca.* T. autotrophica", it has the full denitrification pathway. Thus, we are able to distinguish the Peru Upwelling SUP05 at the species level (39), and propose a candidate name for the Peru Upwelling SUP05 bacteria *"Candidatus* Thioglobus perditus*"*. Perditus means lost. The Peru Upwelling SUP05 bacterium, "*Ca.* T. perditus" finds itself lost in the offshore OMZ waters, and fixed nitrogen is lost from the ecosystem as a result of denitrification by "*Ca.* T. perditus".

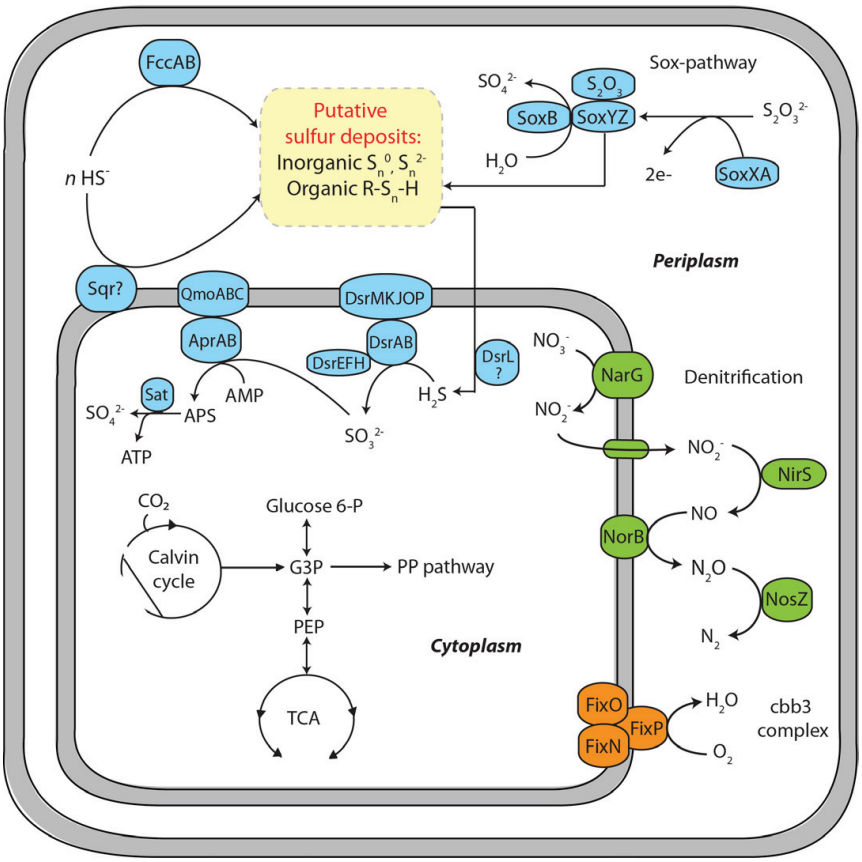

Fig. 4: Key metabolic pathways encoded in a SUP05 "*Candidatus* Thioglobus perditus" population genome bin: Nar, nitrate reductase; Nir, nitrite reductase; Nor, nitric oxide reductase; Nos, nitrous oxide reductase; Dsr, dissmilatory sulfite reductase; Apr, adenylylsulfate reductase; Sat, sulfate adenylyltransferase; Fcc, sulfide binding, flavoprotein; Sqr, sulfide-quinone reductase. The metabolic prediction is based on a 95% complete SUP05 draft genome recovered from station U1. For a complete list of genes please refer to Table S4.

Sulfide produced via microbial sulfate reduction in marine particle aggregates in the offshore stations may support denitrification. We observed aggregates containing delta-proteobacteria (e.g. sulfate-reducing bacteria) in addition to SUP05 in the samples at the shelf water influenced offshore station L1 (Fig. S6). Depth-integrated SUP05 abundances greatly exceeded delta-proteobacteria by nearly 7-fold (Fig. S6), which indicate that local sulfate reduction is only a minor source of reduced sulfur for SUP05. This is also consistent with other metagenomic and functional gene surveys of offshore OMZ waters that find that key sulfur based genes affiliated to sulfide-oxidizing bacteria consistently outnumber genes affiliated to sulfate-reducing bacteria (16, 17). We cannot entirely discount sulfide production from sulfate-reducing bacteria transported with SUP05. Nonetheless, the large inventory of elemental sulfur at the shelf-water influenced "eddy" station L1 (>20 mmol m^{-2} at L1; Fig. S5) can easily support SUP05 driven denitrification for several weeks after transport of SUP05 into offshore ETSP waters.

Implications for ETSP sulfur cycling and nitrogen loss

Sulfide and elemental sulfur in the anoxic inner shelf waters, for instance the 1.6 x 10^9 moles of dissolved sulfide H_2S and 7.0 x 10^8 moles elemental sulfur on the inner shelf that accumulated during course of our research campaign, periodically exchange with offshore waters as a result of mesoscale processes (24). Long-term remote sensing data indicate that mesoscale eddies are omnipresent in the ETSP (40), and may have a substantial impact on offshore waters (41). In March 2013 a number chlorophyll-rich filaments were seen projecting from the ETSP coastline with some of the filaments extending up to a remarkable 1500 km from the coast (Fig. 1 and S7). Similar events occur as well in the Chilean upwelling region where cryptic sulfur cycling has been reported (13) (e.g. Fig. S7). Moreover a number of studies have reported sporadic rates of denitrification in offshore ETSP waters (42-44), with the highest rates often observed within close proximity of the coast (<150 km) and associated with elevated chlorophyll concentrations in surface waters (45). Eddies have recently been shown to impact the distribution of anammox activity in offshore waters (46), and similarly such features will contribute to the dispersal of microbes such as the SUP05-clade bacteria *Ca. T. perditus,* and reduced sulfur to offshore waters. Eddy driven cross-shelf transport combined with *Ca. T. perditus* capacity to denitrify and thrive on elemental sulfur in the absence of dissolved sulfide explains reports of offshore cryptic sulfur cycling and nitrogen loss.

Material and methods

Sampling and hydrography

Waters were sampled in the ETSP region off the coast of Peru (12°S 78.5°W and 13.5°S 77°W) from February 8th to March 4th, 2013 onboard the RV *Meteor*. Either a CTD rosette equipped with twenty-four 10 L Niskin bottles was used to collect water samples or a pump-CTD. Oxygen, temperature and salinity were recorded with depth on both up and downcasts of the CTD. The mesoscale eddy and shelf currents were tracked by horizontal velocities surveyed by glider deployments and vessel mounted acoustic doppler current profilers from January to March, 2013 (24).

Nutrient and sulfur chemistry

Sulfide concentrations were determined by the methylene blue method (47) immediately from Niskin bottles using 4 mL of sample and 320 µL of diamine reagent. The diamine solution and samples were incubated in the dark at ambient temperatures (18-22°C) prior to measuring with a spectrophotometry at 670 nm. The detection limit of this method is 1 µM. Separate nutrient samples were taken for the analysis of nitrate, nitrite and ammonium, and were measured onboard with a QuAAtro autoanalyzer (Seal Analytical). The detection limits are 0.1, 0.1 and 0.3 µM, respectively.

For the analysis of elemental sulfur chemistry sulfidic waters were fixed in zinc chloride (100

µl of 20% (weight/weight) in 50 ml sample), and stored at -20°C. Elemental sulfur was extracted by a chloroform-methanol procedure using 5-15 ml of sample volume(48). Internal standard (31,2mg of 4,4'-Dibromodiphenyl (DBDP; Sigma Aldrich)) dissolved in 100 ml methanol) was added to back calculate the extraction efficiency. Three rounds of chloroform extraction (500 µl each) were performed. After each step the chloroform sample mixture was sonicated for 15 minutes at 4°C and then the chloroform was pipetted off into a glass vial where it was concentrated under an N_2 stream. In the last stage the extracted product was dissolved in methanol and filtered to remove larger particles (0.45 µm filter). The methanol dissolved sample was measured by ultrahigh pressure liquid chromatography (UPLC) using a Waters Acquity H-class instrument with a Waters column (Aquity UPLC BEH C18, 1.7-µm, 2.1 x 50 mm column; Waters, Japan) and methanol eluent flowing at 0.4 ml min^{-1} equipped with a Waters PDA detector (absorbance wavelength set to 265 nm). The detection limit of elemental sulfur using this method was 50 nM.

^{15}N- and ^{13}C-labelled incubation experiments

Seawater was collected from the Niskin into 250 mL glass serum bottles and incubation ^{15}N-labelled incubation experiments were performed according to Holtappels et al.(49). Bottles were allowed to gently overflow 2-3 times and then were capped avoiding oxygen contamination. All bottles, unless sampled from a sulfidic depth, were bubbled with helium gas for 15 min. ^{15}N- and ^{13}C-labelled substrates were added after 5 min of purging in the following experiments: exp1: $^{15}N\text{-}NO_3^-$ + $^{13}C\text{-}HCO_3^-$, exp2: $^{15}N\text{-}NO_2^-$ + $^{14}N\text{-}NH_4^+$ + $^{13}C\text{-}HCO_3^-$, and exp3: $^{15}N\text{-}NH_4^+$ + $^{14}N\text{-}NO_2^-$ + $^{13}C\text{-}HCO_3^-$. Concentrations of labelled substrates were 25 µm, 5 µm, and 5 µm for NO_3^-, NO_2^-, and NH_4^+, respectively. At sulfidic depths serum bottles were not bubbled with gas in order to maintain ambient sulfide concentrations, instead, labelled substrates were mixed by stirring. Serum bottles were overflown 2 times into small glass vials (Exetainers, Labco Limited; 6 or 12 ml) and capped. The caps 2-3 days prior to use were stored in a pre-degassed Duran bottle filled with a helium atmosphere, to reduce oxygen contamination in the incubation experiments (50). Exetainer incubation experiments were incubated at 12°C in the dark. After adding a 2 ml helium headspace, Exetainer samples were terminated at 0, 6, 12, 24, and 48 hours by the addition of 100 µl of saturated mercury chloride solution. Terminated incubation samples were stored cap down at room temperature. For nanoSIMS analysis a separate 24 hour incubation vial was terminated by the addition of a 20% paraformaldehyde solution to a final concentration of 1-2%.

Isotopic ratios of $^{15}N^{15}N$ and $^{15}N^{14}N$ dinitrogen gas were measured from the headspace of the incubation experiments using a gas-chromatography isotope-ratio mass spectrometer (GC-IRMS; VG Optima, Manchester, UK). The nitrite production was determined from amended $^{15}NO_3^-$ experiments performed by converting labeled nitrite to $^{14}N^{15}N$ gas (51). The converted N_2 gas was measured by a GC-IRMS (customized TraceGas coupled to a multicollector IsoPrime100, Manchester, UK). Denitrification and anammox N_2 production rates were calculated from the linear regression slope as a function of time according to Thamdrup et al. (52). A t-test was used to determine whether rates were significantly different from zero ($p < 0.05$). Detection limits were estimated from the median of the standard error of the slope, multiplied by the t-value for $p = 0.05$, the detection limits for anammox, denitrification to N_2 and denitrification to NO_2^- from ^{15}N-labelled experiments were 1.03, 0.13 and 0.80 nM N d^{-1}, respectively.

Bulk CO_2 fixation rates were determined separately from ^{13}C-incubation experiments performed in gas tight 4.5 L bottles (5). To each bottle 4.5 mL of labelled bicarbonate solution (1 g $13C\text{-}HCO_3^-$ in 50 mL water) was added. Depending on sample depth bottles were incubated at *in situ* temperatures on-deck in blue shaded incubation boxes (25% surface irradiance) or in the dark. After 24 hours 1-2 L was filtered onto pre-combusted Whatman GFF filters. GFF filters were dried and then treated to remove inorganic carbon by fuming 37% HCl treatment overnight. The

isotopic ^{13}C enrichment was quantified by an element analyzer EA-IRMS (FlashEA 1112 series coupled with an IRMS, Finnigan Delta plus XP, Thermo Scientific). Carbon fixation rates were calculated according to Schunck et al. (5).

Molecular sampling

Samples collected for microbial enumeration by catalyzed reporter deposition fluorescent in situ hybridization (CARD-FISH) were immediately fixed in 20% paraformaldehyde solution to a final concentration of 1-2%. Fixed samples were filtered onboard after 8-12 hours at 4°C onto a 0.2 µm pore-size polycarbonate (PC) filter. Filtration volumes varied according to depth and location from the coast (i.e. 70-120 ml at offshore stations and 50-70 ml at coastal stations) in order to get adequate cell densities on the filter. Filters for nanoSIMS analysis were collected from ^{13}C-HCO_3^- labelled incubation experiments (exp1) onto pre-coated gold-palladium 0.2 µm PC filters. For biomass collection and subsequent DNA analysis, larger volumes of seawater (1-2 L) were filtered onto a 0.2 µm PC filters. All filters were stored and transported between -20 to -80°C.

DNA extraction, metagenomics and genome binning

DNA was extracted from filtered biomass using a DNA/RNA-Allprep kit (Qiagen). Extracted genomic DNA was sequenced with Illumina MiSeq technology and chemistry (Max Planck Institute for Evolutionary Biology, Plön, Germany). Full length 16S rRNA gene sequences were reconstructed from raw reads using phyloFlash (https://github.com/HRGV/phyloFlash). Adapters and low-quality reads were removed with bbduk (https://sourceforge.net/projects/bbmap/) with a minimum quality value of two and a minimum length of 36, yielding 1,464,909 and 2,143,435 paired end reads for library preparations from station U1 at depths 30 and 40 m, respectively. Single reads were excluded from the analysis. Single library assemblies were performed using SPAdes 3.90 (53) with standard parameters and kmers 21, 33, 55, 77, 99, and 127. Genome binning was performed in Bandage (54) by collecting all contigs linked to the contig that contained the full-length 16S rRNA gene of the SUP05 organism as reconstructed by phyloFlash. The genome completeness for all SUP05 bins was calculated using checkM version 1.07 (55) and the gammaproteobacterial marker gene set using the taxonomy workflow. Annotation was performed using prokka(56). Genes related to nitrate respiration (*nirS*, *narG*, *norB* and *nosZ*) and carbon fixation (*cbbM*) were visualized on the assembly graph of the SUP05 bin using the Bandage BLAST module with 98% query coverage and 98% identity settings.

Clone library and phylogeny

Universal bacterial primers GM3f (5'-AGA GTT TGA TCM TGG C-3') and GM4r (5'- TAC CTT GTT ACG ACT T-3') were used to generate full length 16S rRNA PCR amplicons from DNA samples taken at the redoxcline of sulfidic station U1 (Table S2; (57)). Five PCR replicates were done per sample. The PCR conditions were initial denaturation at 95°C for 5 min, followed by 25 cycles of 95°C for 1 min, 50°C for 1 min, 72°C for 2 min, and a final extension of 72°C for 10 min. The reactions were run on an Eppendorf Mastercycler gradient PCR machine with a ramp rate of 3°C s^{-1}. The five replicate PCR products were pooled. DNA was visualized by gel electrophoresis and quantified by Nanodrop (Thermo Scientific). The 16S rRNA gene product was purified and ligated into a TOPO TA vector using a ligation kit (Invitrogen). Resulting *E. coli* clones were picked and screened for the vector insert by PCR. Colonies with inserts were regrown in fresh media followed by a plasmid extraction using a plasmid extraction kit (MoBio). The plasmid was amplified in two separate final sequencing reactions using forward and reverse M13 primers (M13f 5'-CCC AGT CAC GAC GTT GTA AAA CG-3' and M13r 5'- AGC GGA TAA CAA TTT CAC ACA GG-3'; (58)). The PCR product was purified using Sephadex (G-50 Superfine, Amersham Bioscience) and then sequenced with Sanger sequencing chemistry in Bremen (BigDye sequencing kit, Applied Biosystems).

Raw sequence data was quality controlled and vector ends were trimmed, then forward and reverse amplicons were assembled into near-full length 16S rRNA contigs using Sequencher 4.6 software (Gene Codes Corporation, Ann Arbor, MI). The 16S rRNA contigs were aligned with the SINA aligner (59), and then imported into SILVAref115 curated 16S rRNA reference database (60) using ARB software (61). A 16S rRNA tree was calculated using the parsimony and neighbour joining methods using various filters. A CARD-FISH probe (GSO131) was designed in silico using ARB software to target the 16S rRNA gene of SUP05 bacteria recovered from the ETSP region (Table S2; S3).

Fluorescence in situ hybridization

The CARD-FISH procedure was performed on samples collected on PC filters according to Pernthaler et al., (62). Briefly, filter pieces were treated with lysozyme (10 g L^{-1}) for 45 min at 37°C to permeabilize the cells for hybridization. The filters were washed in PBS buffer and then Milli-Q water before proceeding to the deactivation of endogenous peroxidases with methanol/hydrogen peroxide (0.15%) treatment for 10 min at room temperature. Samples were washed with Milli-Q before performing the hybridization. Filter pieces were incubated for 3 hours at 46°C in the hybridization buffer containing a 35% formamide concentration. Filters were washed in pre-warmed washing buffer containing NaCl (0.08 M final concentration), 5 mM EDTA (pH8.0), 20 mM Tris-HCl (pH7.5), and 0.01% SDS for 15 min at 48°C then washed again for 10 min in 1x PBS buffer at room temperature. Filter pieces were incubated for 45 min at 46°C in amplification buffer containing 0.15% H_2O_2 and 20 µg Oregon Green-labelled tyramide. Filters were washed in 1x PBS and Milli-Q then dried before staining with DAPI (1 ng mL^{-1}) for 10 min at room temperature. Filter pieces were embedded in a mixture of Citifluor/Vectorshield and DAPI and probe hybridized signals were counted on an epifluorescence microscope (Zeiss AxioPlan). Up to 1000 DAPI-stained cells from 10 different fields of view were counted. Separate CARD-FISH probes EUB338 and NON338 were used as positive and negative controls, respectively (62).

nanoSIMS analysis

Select field of views containing hybridized SUP05 cells were marked using a Laser Microdissection microscope (DM 6000 B, Leica). Isotopic composition of single-cells of SUP05 bacteria were analyzed using a NanoSIMS 50L instrument (Cameca). Secondary ions of ^{12}C, ^{13}C, ^{19}F, $^{12}C^{14}N$, $^{12}C^{15}N$, ^{31}P, and ^{32}S were measured simultaneously on 7 electron multiplier detectors. All samples were pre-sputtered with a Cs+ primary ion beam of ~300pA. After pre-sputtering the instrument was tuned on the target area on a 50 x 50 raster size for a mass resolution over 8000. Final analysis and image acquisition was done at 10 x 10 raster size (256 x 256 pixel) and a dwell time of 1 ms per pixel for 40 planes.

The data was processed using Look@NanoSIMS software (63). The field of interest were drift corrected and accumulated using the software. Cells of interest were interactively defined by hand and classified. For each cell $^{13}C/^{12}C$, $^{12}C^{15}N/^{12}C^{14}N$ and $^{32}S/^{12}C+^{13}C$ ratios were calculated. Only cells with Poisson statistics less than 5% were considered reliable measurements.

NanoSIMS was also performed on an untreated (i.e. no CARD-FISH) filter at station U1 (30 m depth) to determine if the isotopic fraction of ^{13}C in SUP05 cells was potentially diluted by the CARD-FISH protocol (64). Based on CARD-FISH enumeration, we assumed that at least half the cells measured by nanoSIMS on the non-CARD-FISH filter were SUP05 bacteria. In this case, no difference in the average isotopic composition was found between the treated (0.24 ± 0.03 fmol C $cell^{-1}$ d^{-1}) and untreated (0.24 ± 0.07 fmol C $cell^{-1}$ d^{-1}; n = 46 cells) samples.

Single-cell calculations

The cell size, determined from Look@NanoSIMS software, was used to estimate the cell biovolume (V). SUP05 cells were coccoid in shape and thus the biovolume was calculated as per a sphere ($V=4/3\pi r^3$). The amount of carbon per cell was calculated according

to a generalized formula (fg C cell^{-1}= 133.754 x V$^{0.438}$) used for bacterial cells larger than 0.025 um^3 (65). From this a single-cell assimilation rate was calculated based on the ^{13}C enrichment, the measured labelling percent, and divided by the incubation period. The contribution of SUP05 bacteria to CO_2 fixation was calculated using the single-cell CO_2 fixation rate (fmol C cell^{-1}d^{-1}) and the SUP05 cell densities (cells mL^{-1}). The percent contribution of SUP05 to bulk carbon fixation was calculated from the SUP05 CO_2 fixation rate divided by the bulk CO_2 fixation rate.

The sulfide, sulfur and nitrate fluxes shown in Table 1 were determined at the chemocline at station U1 from 30-40 m, 20-30 m, and 12-30 m depth, respectively. The eddy diffusivity (1.4 x 10^{-4} m^2 s^{-1}) was determined for the mid to upper shelf of the Peruvian upwelling region from microstructure profiles (Schlosser et al., in prep). A negative value indicates an upward water column flux.

The environmental growth factor was calculated from the chemocline using the measured SUP05 CO_2 fixation rate divided by the measured denitrification rate at 30 m, assuming that SUP05 was primarily responsible for measured denitrification rate (lower value) or 68% of measured denitrification (denitrification based on total sulfide flux; upper value). We convert this growth factor using Eq. 3 to arrive a sulfide oxidation growth factor.

Remote sensing imagery

Remote sensing imagery was acquired by Moderate Resolution Imaging Spectroradiometer (MODIS) downloaded from the NASA Ocean Colour Database (www.oceancolor.gsfc.nasa.gov/cms/). Level 2 and 3 data were processed using SeaDAS software version 7.3.1 (www.seadas.gsfc.nasa.gov/). Sea surface satellite altimetry images were downloaded from the Colorado Center for Astrodynamics Research (www.eddy.colorado.edu/ccar/ssh/nrt_global_grid_viewer).

Data Availability

Metagenomic and 16S rRNA contigs were submitted to the NCBI database under the accession number (XXXXXXX-XXXXXXX application pending). Water column nutrients and physical data are available at Pangaea: https://doi.pangaea.de/10.1594/PANGAEA.860727; while station sulfur chemistry, SUP05 cell densities and rate process measurements have been submitted to Pangea: https://doi.pangaea.de/10.1594/PANGAEA.876062.

Author Contributions

C.M.C., G.L., T.G.F., B.F., H.G-V., S.T., and M.M.M.K. designed the study; C.M.C., H.G-V., P.F.H., S.L., N.J.S., T.K., S.T., and H.S. performed experiments; C.M.C., G.L., T.G.F., H.G-V., P.F.H., S.L., N.J.S., T.K., S.T., H.S., C.L and R.A.S. analysed data; C.M.C., G.L., T.G.F., and M.M.M.K. wrote the manuscript with input from all co-authors.

Acknowledgements

We are grateful to the Peruvian authorities, the captain and crew of the RV Meteor, chief scientist T. Kanzow, C. Schelten for administrative support, and P. Lam, and G. Klockgether for extensive onboard experimental and analytical support. M. Dengler graciously provided pre-publication eddy diffusion coefficients, and the MPI Plön assisted with sequencing. This work was supported by the Max Planck Society for the Advancement of Science and the German National Science Foundation (DFG) Sonderforschungsbereich (SFB754) GEOMAR, Kiel. CMC was supported by a Natural Sciences and Engineering Research Council of Canada (NSERC) scholarship.

References

1. *Codispoti LA, et al. (2001) The oceanic fixed nitrogen and nitrous oxide budgets: Moving targets as we enter the anthropocene? Scientia Marina 65(2):85-105.*
2. *Lam P & Kuypers MMM (2011) Microbial nitrogen cycling processes in oxygen minimum zones. Ann Rev Mar Sci 3:317-345.*
3. *Gruber N & Sarmiento JL (1997) Global patterns of marine nitrogen fixation and denitrification. Global Biogeochemical Cycles 11(2):235-266.*

4. *Naqvi SWA, et al. (2000) Increased marine production of N2O due to intensifying anoxia on the Indian continental shelf. Nature 408(6810):346-349.*

5. *Schunck H, et al. (2013) Giant hydrogen sulfide plume in the oxygen minimum zone off Peru supports chemolithoautotrophy. PLoS One 8(8):e68661.*

6. *Lavik G, et al. (2009) Detoxification of sulphidic African shelf waters by blooming chemolithotrophs. Nature 457(7229):581-584.*

7. *Galán A, Faúndez J, Thamdrup B, Santibáñez JF, & Farías L (2014) Temporal dynamics of nitrogen loss in the coastal upwelling ecosystem off central Chile: Evidence of autotrophic denitrification through sulfide oxidation. Limnology and Oceanography 59(6):1865-1878.*

8. *Weeks SJ, Currie B, & Bakun A (2002) Satellite imaging: Massive emissions of toxic gas in the Atlantic. Nature 415(6871):493-494.*

9. *Weeks SJ, Currie B, Bakun A, & Peard KR (2004) Hydrogen sulphide eruptions in the Atlantic Ocean off southern Africa: implications of a new view based on SeaWiFS satellite imagery. Deep Sea Research Part I: Oceanographic Research Papers 51(2):153-172.*

10. *Ohde T, Siegel H, Reißmann J, & Gerth M (2007) Identification and investigation of sulphur plumes along the Namibian coast using the MERIS sensor. Continental Shelf Research 27(6):744-756.*

11. *Walsh DA, et al. (2009) Metagenome of a versatile chemolithoautotroph from expanding oceanic dead zones. Science 326(5952):578-582.*

12. *Hawley AK, Brewer HM, Norbeck AD, Pasa-Tolic L, & Hallam SJ (2014) Metaproteomics reveals differential modes of metabolic coupling among ubiquitous oxygen minimum zone microbes. Proceedings of the National Academy of Sciences of the United States of America 111(31):11395-11400.*

13. *Canfield DE, et al. (2010) A cryptic sulfur cycle in oxygen-minimum-zone waters off the Chilean coast. Science 330(6009):1375-1378.*

14. *Fuchs BM, Woebken D, Zubkov MV, Burkill P, & Amann R (2005) Molecular identification of picoplankton populationsin contrasting waters of the Arabian Sea. Aquatic Microbial Ecology 39(2):145-157.*

15. *Stevens H & Ulloa O (2008) Bacterial diversity in the oxygen minimum zone of the eastern tropical South Pacific. Environmental microbiology 10(5):1244-1259.*

16. *Stewart FJ, Ulloa O, & DeLong EF (2012) Microbial metatranscriptomics in a permanent marine oxygen minimum zone. Environmental microbiology 14(1):23-40.*

17. *Carolan M & Beman JM (2015) Transcriptomic evidence for microbial sulfur cycling in the eastern tropical North Pacific oxygen minimum zone. Frontiers in microbiology 6.*

18. *Bristow LA, et al. (2017) N2 production rates limited by nitrite availability in the Bay of Bengal oxygen minimum zone. Nature Geosci 10(1):24-29.*

19. *Shah V, Chang BX, & Morris RM (2016) Cultivation of a chemoautotroph from the SUP05 clade of marine bacteria that produces nitrite and consumes ammonium. The ISME Journal.*

20. *Louca S, et al. (2016) Integrating biogeochemistry with multiomic sequence information in a model oxygen minimum zone. Proceedings of the National Academy of Sciences 113:E5925-E5933.*

21. *Johnston DT, et al. (2014) Placing an upper limit on cryptic marine sulphur cycling. Nature advance online publication.*

22. *Nagai T, et al. (2015) Dominant role of eddies and filaments in the offshore transport of carbon and nutrients in the California Current System. Journal of Geophysical Research: Oceans 120(8):5318-5341.*

23. *Gruber N, et al. (2011) Eddy-induced reduction of biological production in eastern boundary upwelling systems. Nature Geosci 4(11):787-792.*

24. *Thomsen S, et al. (2016) The formation of a subsurface anticyclonic eddy in the Peru-Chile Undercurrent and its impact on the near-coastal salinity, oxygen, and nutrient distributions. Journal of Geophysical Research: Oceans: 476–501.*

25. *Brink KH, Halpern D, Huyer A, & Smith RL (1983) The physical environment of the Peruvian upwelling system. Progress in Oceanography 12:285-305.*

26. *Chaigneau A, Le Texier M, Eldin G, Grados C, & Pizarro O (2011) Vertical structure of mesoscale eddies in the eastern South Pacific Ocean: A composite analysis from altimetry and Argo profiling floats. Journal of Geophysical Research: Oceans 116(C11):n/a-n/a.*

27. *Colas F, McWilliams JC, Capet X, & Kurian J (2012) Heat balance and eddies in the Peru-Chile current*

system. Climate Dynamics 39(1):509-529.

28. Johnson GC & McTaggart KE (2010) Equatorial Pacific 13°C Water Eddies in the Eastern Subtropical South Pacific Ocean. Journal of Physical Oceanography 40(1):226-236.

29. Cardoso RB, et al. (2006) Sulfide oxidation under chemolithoautotrophic denitrifying conditions. Biotechnology and Bioengineering 95:1148-1157.

30. Kelly DP (1982) Biochemistry of the chemolithotrophic oxidation of inorganic sulphur. Philosophical transactions of the Royal Society of London. Series B: Biological sciences 298(1093):499-528.

31. Kelly PD (1999) Thermodynamic aspects of energy conservation by chemolithotrophic sulfur bacteria in relation to the sulfur oxidation pathways. Archives of Microbiology 171(4):219-229.

32. Nelson DC, Jørgensen BB, & Revsbech NP (1986) Growth pattern and yield of a chemoautotrophic Beggiatoa sp. in oxygen-sulfide microgradients. Applied and environmental microbiology 52(2):225-233.

33. Dahl C, et al. (2005) Novel genes of the dsr gene cluster and evidence for close interaction of Dsr proteins during sulfur oxidation in the phototrophic sulfur bacterium Allochromatium vinosum. Journal of bacteriology 187(4):1392-1404.

34. Gregersen LH, Bryant DA, & Frigaard N-U (2011) Mechanisms and Evolution of Oxidative Sulfur Metabolism in Green Sulfur Bacteria. Frontiers in Microbiology 2.

35. Kuwahara H, et al. (2007) Reduced genome of the thioautotrophic intracellular symbiont in a deep-sea clam, Calyptogena okutanii. Current Biology 17(10):881-886.

36. Newton IL, et al. (2007) The Calyptogena magnifica chemoautotrophic symbiont genome. Science 315(5814):998-1000.

37. Marshall KT & Morris RM (2013) Isolation of an aerobic sulfur oxidizer from the SUP05/Arctic96BD-19 clade. ISME J 7(2):452-455.

38. Loy A, et al. (2009) Reverse dissimilatory sulfite reductase as phylogenetic marker for a subgroup of sulfur-oxidizing prokaryotes. Environmental Microbiology 11:289-299.

39. Yarza P, et al. (2014) Uniting the classification of cultured and uncultured bacteria and archaea using 16S rRNA gene sequences. Nat Rev Micro 12(9):635-645.

40. Chaigneau A, Gizolme A, & Grados C (2008) Mesoscale eddies off Peru in altimeter records: Identification algorithms and eddy spatio-temporal patterns. Progress in Oceanography 79(2–4):106-119.

41. Chaigneau A, Eldin G, & Dewitte B (2009) Eddy activity in the four major upwelling systems from satellite altimetry (1992–2007). Progress in Oceanography 83(1–4):117-123.

42. Thamdrup B, et al. (2006) Anaerobic ammonium oxidation in the oxygen-deficient waters off northern Chile. Limnology and Oceanography 51(5):2145-2156.

43. Kalvelage T, et al. (2013) Nitrogen cycling driven by organic matter export in the South Pacific oxygen minimum zone. Nature Geosci 6(3):228-234.

44. Hamersley MR, et al. (2007) Anaerobic ammonium oxidation in the Peruvian oxygen minimum zone. Limnology and Oceanography 52(3):923-933.

45. Dalsgaard T, Thamdrup B, Farías L, & Revsbech NP (2012) Anammox and denitrification in the oxygen minimum zone of the eastern South Pacific. Limnology and Oceanography 57(5):1331-1346.

46. Callbeck CM, Lavik G, Stramma L, Kuypers MMM, & Bristow LA (2017) Enhanced nitrogen loss by eddy-induced vertical transport in the offshore peruvian oxygen minimum zone. PloS one 12(1):e0170059.

47. Cline JD (1969) Spectrophotometric Determination of Hydrogen Sulfide in Natural Waters. Limnology and Oceanography 14:454-458.

48. Kamyshny A, Jr., Borkenstein CG, & Ferdelman TG (2009) Protocol for Quantitative Detection of Elemental Sulfur and Polysulfide Zero-Valent Sulfur Distribution in Natural Aquatic Samples. Geostandards and Geoanalytical Research 33(3):415-435.

49. Holtappels M, Lavik G, Jensen MM, & Kuypers MMM (2011) Chapter ten - 15N-Labeling Experiments to Dissect the Contributions of Heterotrophic Denitrification and Anammox to Nitrogen Removal in the OMZ Waters of the Ocean. Methods in Enzymology, Research on Nitrification and Related Processes, Part A, ed Klotz MG (Academic Press), Vol 486, pp 223-251.

50. De Brabandere L, Thamdrup B, Revsbech NP, & Foadi R (2012) A critical assessment of the occurrence and extend of oxygen contamination during anaerobic incubations utilizing commercially available vials.

Journal of microbiological methods 88(1):147-154.

51. *Füssel J, et al. (2012) Nitrite oxidation in the Namibian oxygen minimum zone. The ISME Journal 6:1200-1209.*

52. *Thamdrup B & Dalsgaard T (2002) Production of N2 through Anaerobic Ammonium Oxidation Coupled to Nitrate Reduction in Marine Sediments. Appl Environ Microbiol 68(3):1312-1318.*

53. *Nurk S, et al. (2013) Assembling genomes and mini-metagenomes from highly chimeric reads. Research in Computational Molecular Biology: 17th Annual International Conference, RECOMB 2013, Beijing, China, April 7-10, 2013. Proceedings, eds Deng M, Jiang R, Sun F, & Zhang X (Springer Berlin Heidelberg, Berlin, Heidelberg), pp 158-170.*

54. *Wick RR, Schultz MB, Zobel J, & Holt KE (2015) Bandage: interactive visualization of de novo genome assemblies. Bioinformatics 31(20):3350-3352.*

55. *Parks DH, Imelfort M, Skennerton CT, Hugenholtz P, & Tyson GW (2015) CheckM: assessing the quality of microbial genomes recovered from isolates, single cells, and metagenomes. Genome Research 25(7):1043-1055.*

56. *Seemann T (2014) Prokka: rapid prokaryotic genome annotation. Bioinformatics 30(14):2068-2069.*

57. *Muyzer G, Teske A, Wirsen CO, & Jannasch HW (1995) Phylogenetic relationships of Thiomicrospira species and their identification in deep-sea hydrothermal vent samples by denaturing gradient gel electrophoresis of 16S rDNA fragments. Arch Microbiol 164(3):165-172.*

58. *Messing J (1983) New M13 vectors for cloning. Methods in Enzymology 101:20-78.*

59. *Pruesse E, Peplies J, & Glöckner FO (2012) SINA: Accurate high-throughput multiple sequence alignment of ribosomal RNA genes. Bioinformatics 28(14):1823-1829.*

60. *Quast C, et al. (2013) The SILVA ribosomal RNA gene database project: improved data processing and web-based tools. Nucleic Acids Research 41(D1):D590-D596.*

61. *Ludwig W, et al. (2004) ARB: a software environment for sequence data. Nucleic Acids Research 32(4):1363-1371.*

62. *Pernthaler A, Pernthaler J, & Amann R (2002) Fluorescence in situ hybridization and catalyzed reporter deposition for the identification of marine bacteria. Applied and environmental microbiology 68(6):3094-3101.*

63. *Polerecky L, et al. (2012) Look@NanoSIMS – a tool for the analysis of nanoSIMS data in environmental microbiology. Environmental Microbiology 14:1009-1023.*

64. *Musat N, et al. (2014) The effect of FISH and CARD-FISH on the isotopic composition of 13C- and 15N-labeled Pseudomonas putida cells measured by nanoSIMS. Systematic and Applied Microbiology 37(4):267-276.*

65. *Romanova ND & Sazhin AF (2010) Relationships between the cell volume and the carbon content of bacteria. Oceanology 50(4):522-530.*

Supporting information

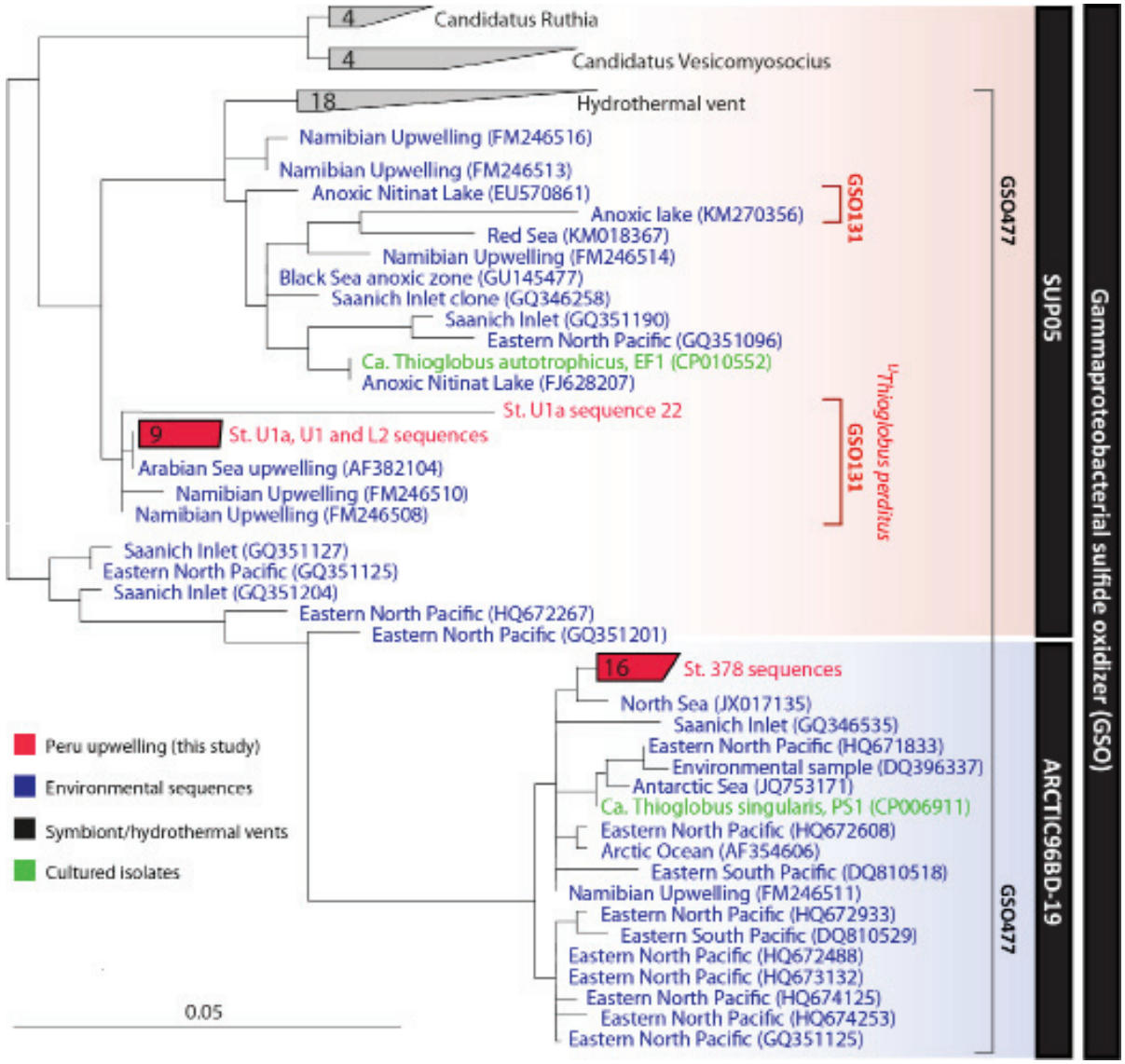

Fig. S1: Phylogenetic diversity of GSO 16S rRNA genes recovered from sulfidic and non-sulfidic stations from the Peruvian upwelling region. The phylogenetic tree was calculated using the neighbor joining and RAxML methods including various filters, an unrooted consensus tree is shown. The typeface in blue, black and green represent sequences recovered from other studies. The sequences indicated in red typeface were recovered from two sulfidic stations U1 and U1a, and from one non-sulfidic, station 378 (Table S1). The coverage and specificity of the newly designed FISH GSO131 probe, is indicated by the red line; for overall probe coverage details see Table S3. The broad coverage, GSO477 probe used elsewhere (1), is indicated by the black line. Note the SUP05 sequences recovered from the sulfidic stations are at 97.6% similarity to "*Candidatus* Thioglobus autotrophica", making it by definition a new species (2), proposed here as "*Candidatus* Thioglobus perditus".

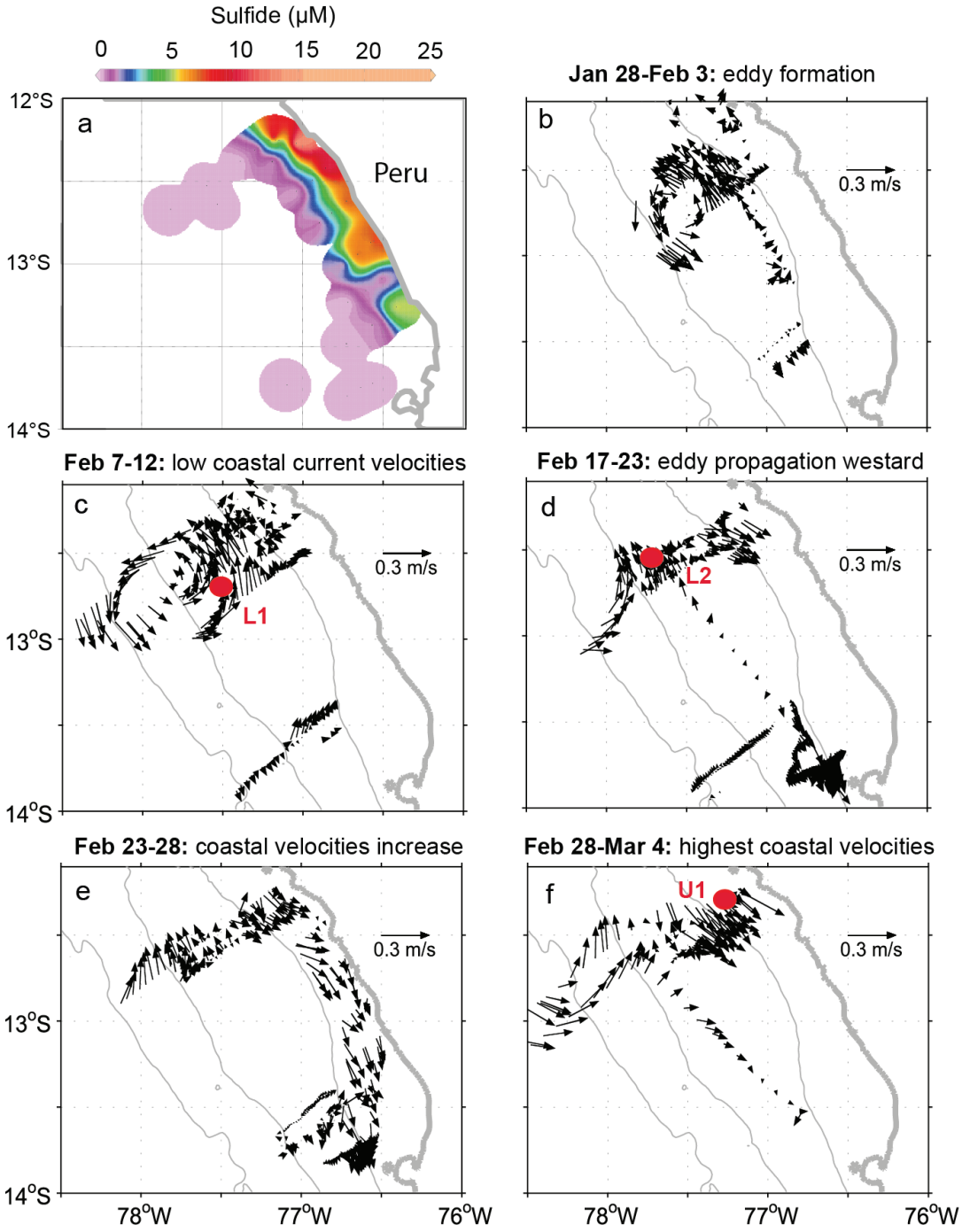

Fig. S2. Development and propagation of a subsurface mesoscale eddy: (a) Highest bottom water sulfide concentration in the 26.1 and 26.2 kg m^{-3} range from February-March, 2013. (b-f) Snapshots of the subsurface current velocities during the formation and propagation of a lower shelf forming mesoscale eddy. The red circles indicate the main stations sampled within the given time period. Full details related to the eddy hydrodynamics are presented in Thomsen et al., (3).

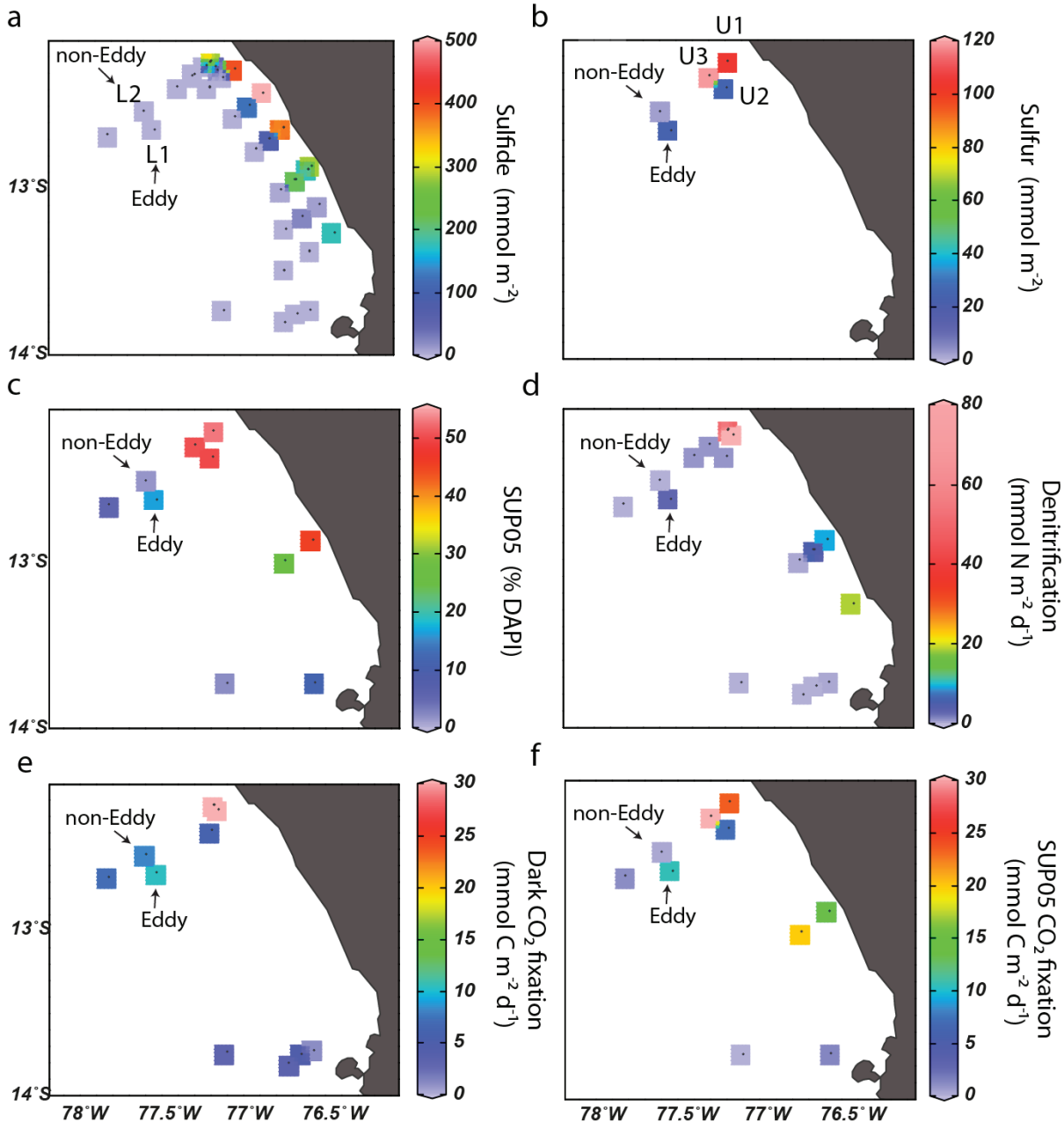

Fig. S3. Distribution of inventories and rates of (a) dissolved sulfide, (b) elemental sulfur, (c) % DAPI as SUP05, (d) denitrification, (e) dark CO_2 fixation, and (f) SUP05 CO_2 fixation. Depths of integration are from 10 m down to the sediments for coastal stations from 10 m down to 300 m depth for offshore stations, with the exception of the dark CO_2 fixation rates that are integrated from 30-70 m for coastal stations and from 100-300 m for offshore stations. In panel c the highest SUP05 abundance is reported for the respective stations.

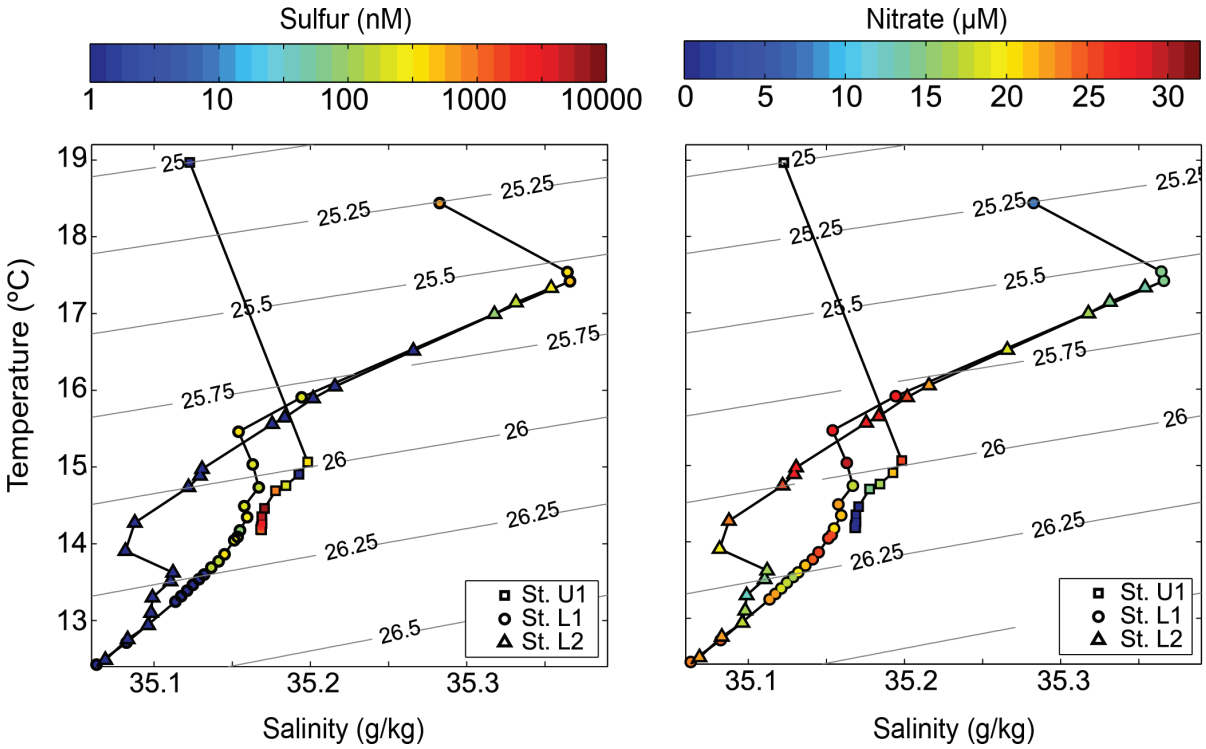

Fig. S4: Elemental sulfur and nitrate concentrations as a function of temperature-salinity for stations U1, L1 and L2. Densities (kg m^{-3}) are indicated by the light gray isopycnals.

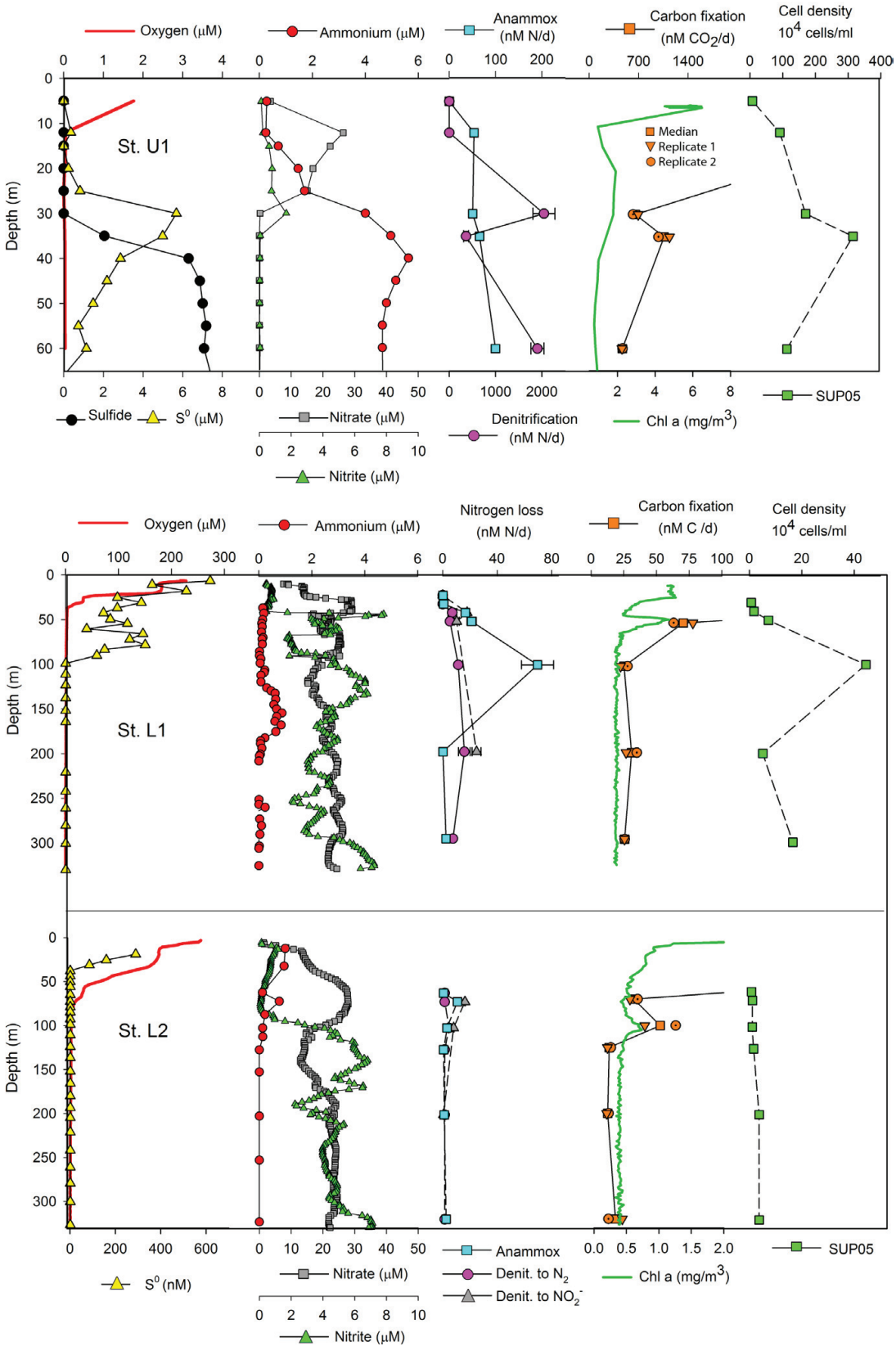

Fig. S5. Depth distributions of dissolved oxygen, key sulfur and nitrogen species, chlorophyll a, SUP05 cell densities (GSO131 probe), and rates of dark carbon fixation and dissimilatory nitrogen transformations at the three main stations U1, L1, and L2. Error bars for nitrogen transformation rates represent the standard error and were estimated according to the slope of the N_2 production rate (see Material and Methods).

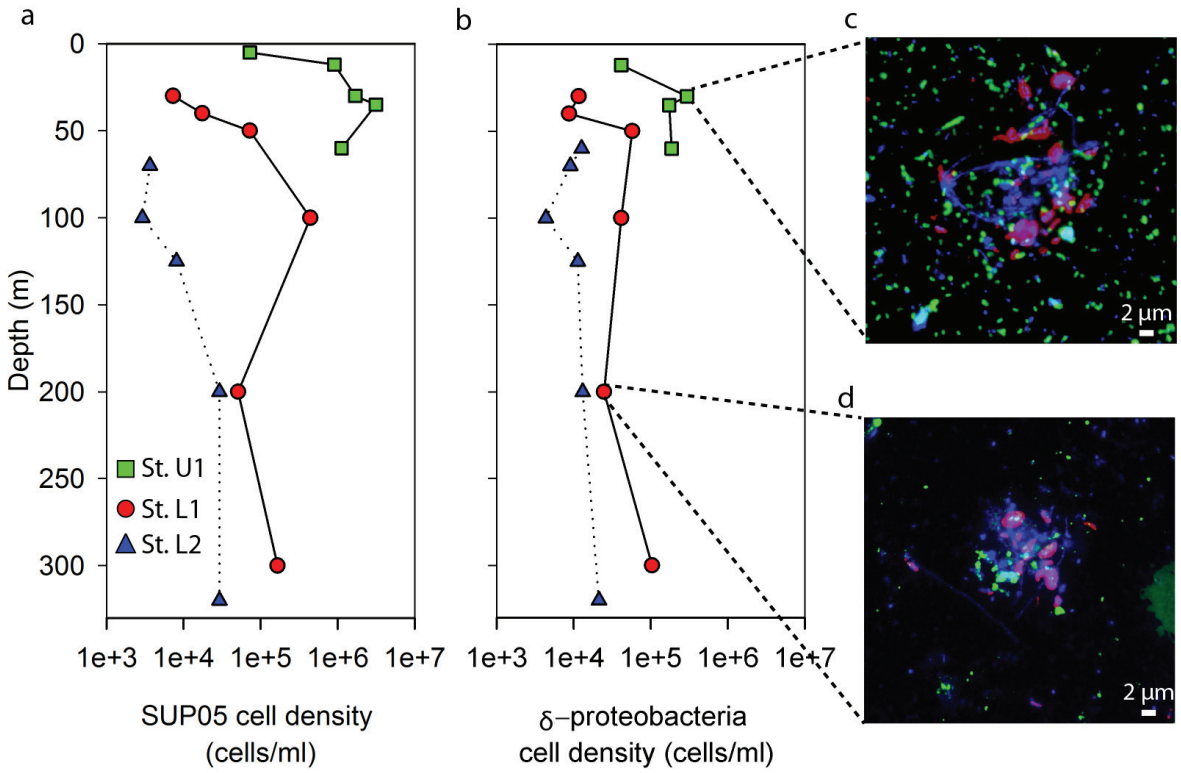

Fig. S6. CARD-FISH quantification of the distribution of SUP05 (GSO131) and deltaproteobacteria (Delta495): depth profiles of (a) SUP05 and (b) deltaprotebacteria cell densities. (c, d) CARD-FISH image of planktonic and aggregate-associated SUP05 and deltaproteobacteria from two samples. Blue-green stained cells (also marked with green arrows) represent SUP05 bacteria hybridized with the GSO131 probe. Blue shows all cells marked with the DNA stain 4′,6-diamidino-2-phenylindole (DAPI). Red stained cells represent deltaproteobacteria hybridized with the Delta495 probe (4).

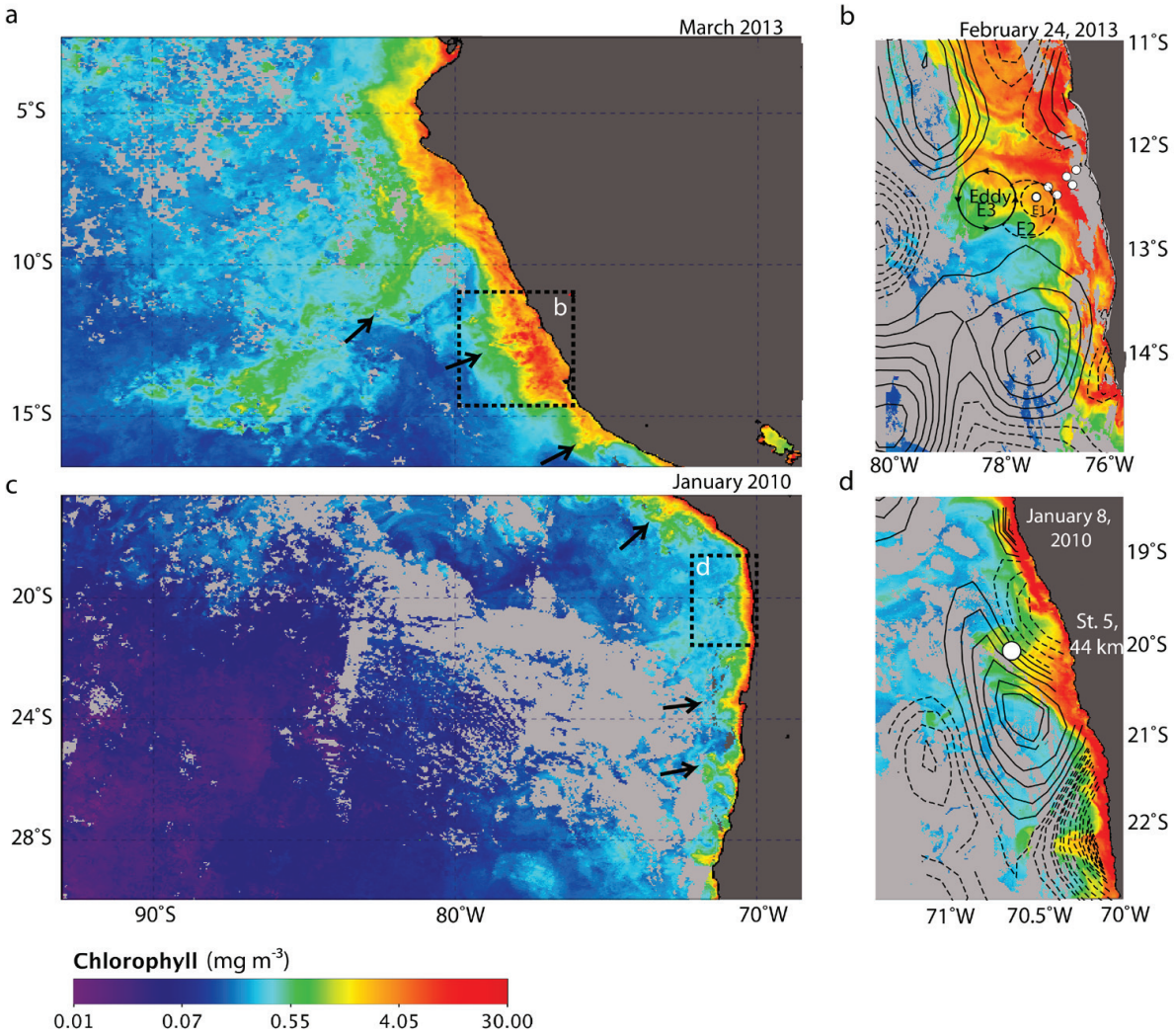

Fig. S7. Distribution of filaments in the Eastern Tropical South Pacific. (a) March, 2013 composite image of near-surface chlorophyll concentrations, where black arrows indicate filaments. (b) February 24, 2013 near-surface chlorophyll concentrations with satellite-sea surface height altimetry (SSHA) overlay. The contours of the subsurface eddy (not detectable by SSHA but detectable based on horizontal velocities is illustrated. (c) January, 2010 composite of near-surface chlorophyll concentrations (d) January 8, 2010 near-surface chlorophyll concentrations with SSHA overlay. Station 5 (white circle) located 44 km from the coast was sampled January 9th, 2010 (5).

Table S1: List of stations sampled during the M93 research cruise February-March, 2013.

Abbreviated station name (used in text)	M90 station name	Date and time sampled	Latitude (°S)	Longitude (°E)
U2	295	Feb 9, 02:02	-12.38	-77.19
L1	318	Feb 11, 11:40	-12.64	-77.53
378	378	Feb 18, 17:04	-13.75	-76.64
L3	391	Feb 20, 21:04	-12.67	-77.82
L2	399	Feb 22, 12:23	-12.52	-77.60
U3	412	Feb 24, 10:00	-12.31	-77.30
U1a	413	Feb 25, 01:00	-12.23	-77.18
U1	471	Mar 4, 09:50	-12.23	-77.18

Table S2: Summary of PCR primers and fluorescence *in situ* hybridization probes used in this study.

Target group	Primer/ probe	Sequence (5' to 3')	Size(bp)	Annealing temp/ formamide conc.	Ref.
Catalysed reported deposition–fluorescence in situ hybridization probes [1]					
SUP05	GSO131[2]	CTA TCC CCC ACT ATC TGG TAG A	22	46°C / 35% [3]	This study
Delta-proteobacteria	Del495a[4]	AGT TAG CCG GTG CTT CCT	18	46°C / 30%	(4)
	Del495b[4]	AGT TAG CCG GCG CTT CCT	18	46°C / 30%	(4)
	Del495c[4]	AAT TAG CCG GTG CTT CCT	18	46°C / 30%	(4)
Polymerse chain reaction primers					
Universal	GM3f	AGA GTT TGA TCM TGG C	16	50°C	(6)
Universal	GM4r	TAC CTT GTT ACG ACT T	16	50°C	(6)

[1] Primer and probe specificity were evaluated *in silico* using the SILVA SSU refnr 128 database. The probe coverage is evaluated in Table S3.

[2] Unlabeled competitor probes (C) are as follows: GSO131-c1: CTA TCC CCC ACT ATC AGG TAG A; GSO131-c2: CTA TCC CCC ACT ATC AGG CAG A. Competitor probe sequences were designed to exclude mismatch sequences indicated in Table S3.

[3] The different probes were tested under various formamide concentrations, the optimal is shown.

[4] Unlabeled competitors probes: cDel495a (AGT TAG CCG GTG CTT CTT), cDel495b (AGT TAG CCG GCG CTT C(T/G) T), and cDel495c (AAT TAG CCG GTG CTT CTT) were used according to (7, 8).

Table S3: FISH probe specificity and coverage. Probes were evaluated *in silico* using the SILVA SSU refnr 128 database. Eligible sequences are the total number of sequences within a given taxonomic group. The number of probe sequence matches is indicated; note that values indicated in parentheses represent the number of matches with a one nucleotide mismatch. Competitor probes were designed towards the mismatch sequences (see Table S2). Coverage represents the number of probe sequence matches divided by the number of eligible sequences expressed as a percentage.

Taxonomy	Coverage (%)	Eligible sequences	Number of probe sequence matches
GSO131 probe: 0 mismatches, total matches = 11 (1 mismatch, total matches = 95)			
Bacteria	0.002 (0.02)	526819	11 (95)
Proteobacteria	0.005 (0.04)	209486	10 (90)
Gammaproteobacteria	0.01 (0.09)	97852	10 (87)
Oceanospirillales	0.2 (1.14)	6164	10 (70)
SUP05 cluster	4.1 (12.24)	245	10 (30)
Outgroup hits: Arctic96BD-19 cluster	0 (15.82)	177	0 (28)
Outgroup hits: Other gammaproteobacteria	0 (0.03)	97852	0 (29)
Outgroup hits: Bacteroidetes	0.002 (0.006)	50630	1 (3)
Outgroup hits: Other			0 (8)
Del495a probe: 0 mismatches, total matches = 11609 (1 mismatch, total matches = 116906)			
Bacteria	2.2 (21.8)	537344	11609 (116906)
Proteobacteria	4.3 (36.5)	214092	9279 (78225)
Deltaproteobacteria	62.5 (88.9)	14649	9149 (13161)
Outgroup hits: SUP05 cluster	0.82 (90.2)	245	2 (221)
Outgroup hits: Non deltaproteobacteria			103745
Del495b probe: 0 mismatches, total matches = 1018 (1 mismatch, total matches = 51283)			
Bacteria	0.2 (9.5)	537344	1018 (51283)
Proteobacteria	0.2 (4.7)	214092	489 (10108)
Deltaproteobacteria	3.3 (66.7)	14649	484 (9765)
Outgroup hits: SUP05 cluster	0 (1.6)	245	0 (4)
Outgroup hits: Non deltaproteobacteria			534 (41518)
Del495c probe: 0 mismatches, total matches = 121 (1 mismatch, total matches = 13111)			
Bacteria	0.02 (2.4)	537344	121 (13111)
Proteobacteria	0.04 (4.8)	214092	86 (10246)
Deltaproteobacteria	0.6 (63.9)	14649	84 (9361)
Outgroup hits: SUP05 cluster	0 (1.6)	245	0 (4)
Outgroup hits: Non deltaproteobacteria			37 (3750)

Table S4: Key enzymes identified in the SUP05-ETSP metagenome.

Gene name	Function/protein	Locus tag
Sulfur metabolism		
soxXYZAB	Oxidation of reduced sulfur compounds	XXXXX
soxX	Sulfur oxidation protein	XXXXX
soxY	Sulfur oxidation protein	XXXXX
soxZ	Sulfur oxidation protein	XXXXX
soxA	Diheme cytochrome	XXXXX
soxB	Sulfate thiol esterase	XXXXX
soxZ	Sulfur oxidation protein	
dsrA	Dissimilatory sulfite reductase	XXXXX
dsrB	Dissimilatory sulfite reductase	XXXXX
dsrEFH	Dissimilatory sulfite reductase	XXXXX
dsrMKJOP	Dissimilatory sulfite reductase	XXXXX
aprA	Adenylylsulfate reductase	XXXXX
aprB	Adenylylsulfate reductase	XXXXX
sat	Sulfate adenylyltransferase	XXXXX
fccA	Sulfide-binding, flavoprotein	XXXXX
fccB	Sulfide-binding, flavoprotein	XXXXX
Nitrogen metabolism		
narG	Nitrate reductase	XXXXX
nirS	Nitrite reductase	XXXXX
norB	Nitric oxide reductase	XXXXX
nosZ	Nitrous oxide reductase	XXXXX

Supporting information references

1. *Lavik G, et al. (2009) Detoxification of sulphidic African shelf waters by blooming chemolithotrophs. Nature 457(7229):581-584.*
2. *Yarza P, et al. (2014) Uniting the classification of cultured and uncultured bacteria and archaea using 16S rRNA gene sequences. Nat Rev Micro 12(9):635-645.*
3. *Thomsen S, et al. (2016) The formation of a subsurface anticyclonic eddy in the Peru-Chile Undercurrent and its impact on the near-coastal salinity, oxygen, and nutrient distributions. Journal of Geophysical Research: Oceans:n/a-n/a.*
4. *Loy A, et al. (2002) Oligonucleotide Microarray for 16S rRNA Gene-Based Detection of All Recognized Lineages of Sulfate-Reducing Prokaryotes in the Environment. Applied and environmental microbiology 68(10):5064-5081.*
5. *Canfield DE, et al. (2010) A cryptic sulfur cycle in oxygen-minimum-zone waters off the Chilean coast. Science 330(6009):1375-1378.*
6. *Muyzer G, Teske A, Wirsen CO, & Jannasch HW (1995) Phylogenetic relationships of Thiomicrospira species and their identification in deep-sea hydrothermal vent samples by denaturing gradient gel electrophoresis of 16S rDNA fragments. Arch Microbiol 164(3):165-172.*
7. *Macalady JL, et al. (2006) Dominant Microbial Populations in Limestone-Corroding Stream Biofilms, Frasassi Cave System, Italy. Applied and environmental microbiology 72(8):5596-5609.*
8. *Lücker S, et al. (2007) Improved 16S rRNA-targeted probe set for analysis of sulfate-reducing bacteria by fluorescence in situ hybridization. Journal of microbiological methods 69(3):523-528.*

CHAPTER 6

Chemolithoheterotrophic bacteria play a key role in sulfide oxidation and denitrification in sulfidic shelf waters

Cameron M. Callbeck, Chris Pelzer, Gaute Lavik, Timothy G. Ferdelmen, Harald Schunck, Jon S. Graf, Sten Littmann, Berhnard Fuchs, Philipp F. Hach, Tim Kalvelage, Ruth A. Schmitz, and Marcel M. M. Kuypers.(2017)Chemolithoheterotrophic bacteria play a key role in sulfide oxidation and denitrification in sulfidic shelf waters. Manuscript in preparation

Abstract

Dissolved sulfide in bottom waters of upwelling regions and stratified basins is assumed to be oxidized by a diverse consortium of chemolithoautotrophic bacteria that couple sulfide oxidation to denitrification. Here, we report the oxidation of sulfide in shelf waters off Peru by an uncultivated *Arcobacter* species capable of oxidizing sulfide and reducing nitrate as an obligate heterotroph. In Peruvian waters we find that *Arcobacter* dominated the microbial community under sulfidic conditions at the nitrate-sulfide redoxcline where enhanced dark carbon fixation rates were measured. However, single-cell nanoSIMS analysis revealed that *Arcobacter* did not substantially contribute to total CO_2 fixation in situ. A novel *Arcobacter* species, enriched from these sulfidic waters and characterized by physiology and genome analysis, indeed, lacked the capacity to fix CO_2 via autotrophic carbon fixation pathways. The genome, in contrast, contained pathways for organic carbon uptake and heterotrophic respiration, and included the capacity to oxidize sulfide and reduce nitrate. Culture experiments showed that the strain grew best on a mix of sulfide, nitrate and labile organic carbon, thus coupling acetate assimilation to sulfide oxidation and denitrification. The energetics of such a chemolithoheterotrophic physiology may provide *Arcobacter* with a competitive advantage over other chemolithoautotrophic bacteria for available sulfide and nitrate, enabling it to form rapid and large blooms in situ. Our findings reveal that chemolithoheterotrophy may play an important role in near-shore eutrophic, sulfide-rich upwelling environments, contributing to the removal of sulfide and to fixed nitrogen loss.

Coastal upwelling systems, such as those found off the coasts of Peru and Namibia, sustain high levels of primary productivity, and 17% of the global fish catch (1). In such eutrophic marine ecosystems, high fluxes of organic carbon export drive enhanced rates of microbial sulfate reduction and sulfide production within the sediments. Enhanced organic matter export rates, combined with the sluggish water column circulation, allow dissolved hydrogen sulfide to accumulate in bottom waters of such ecosystems (2, 3). Hydrogen sulfide is toxic for most eukaryotic organisms. The presence of hydrogen sulfide severely exacerbates the already compressed availability of faunal habitat in hypoxic zones, and leads eventually to a loss of fauna diversity and mass fish die-offs (4-6). As such, "sulfidic events" represent an extreme manifestation of coastal hypoxic and anoxic "dead zones" (6, 7).

A broad variety of bacteria have evolved to catalyze the oxidation of sulfide with dissolved oxygen or nitrate as the electron acceptor, and are able to conserve energy with these reactions. Thus, sulfide-oxidizing bacteria are responsible for mediating the rapid oxidation of sulfide at redoxclines (2, 3, 8, 9). In addition, to oxidizing sulfide to a much less toxic form, many sulfide-oxidizing bacteria couple sulfide oxidation to dissimilatory nitrate reduction to dinitrogen (referred hereafter as denitrification), contributing significantly to nitrogen loss (2, 3, 10-12).

Taxa involved in sulfide oxidation in marine upwelling or stratified water bodies include the gammaproteobacterial sulfide-oxidizing clades SUP05 and Arctic96BD-19, as well as epsilonproteobacteria *Sulfurovum*, *Sulfurimonas* and *Arcobacter* species (2, 3, 13-16). SUP05, a chemolithoautotrophic sulfide-oxidizing denitrifying bacteria, has been shown to be broadly distributed across a wide range of sulfidic and non-sulfidic water masses within oxygen minimum zones (OMZs) (Callbeck et al., ***Chapter 5***). Far less is known of the genus *Arcobacter* in OMZs, which encompasses a diverse assemblage of species that include obligate and facultative chemolithoautotrophs as well as heterotrophs ((17-19) and references therein). *Arcobacter* has been identified as a potentially important sulfide oxidizer in eutrophic coastal marine environments (2, 20, 21), and sulfidic basins (18, 22-25). It is also characteristically enriched in engineered systems containing high sulfide and high organic matter (26-29). In OMZ water columns, the detection of abundant putative CO_2 fixing microbes, in

concert with elevated rates of dark CO_2 fixation at sulfide-nitrate redoxclines, has led to the conclusion that chemolithoautotrophic bacteria are primarily responsible for the oxidation of sulfide in OMZs and closed basins (2, 3, 8, 12, 30, 31).

To understand the role of *Arcobacter* species associated with sulfidic events, we explored the distribution, in situ activity, and metabolic capacity of *Arcobacter* in the coastal sulfidic waters of the Peruvian upwelling region. We investigated the distribution of *Arcobacter*, with respect to key reactants (nitrate, sulfide, oxygen), as well as to the rates of denitrification and dark carbon fixation. At a highly sulfidic station, where *Arcobacter* comprised a substantial fraction of the sulfide-oxidizing bacterial community, we also directly assessed the potential activity of the in situ *Arcobacter* population through stable isotope incubation experiments linked with targeted single-cell FISH-SIMS (fluorescent in situ hybridization coupled to secondary ion mass spectrometry) analysis. We furthermore enriched and isolated a marine *Arcobacter* from a sulfidic Peru shelf station, analyzed its genome, and tested its growth using environment mimicking amendment experiments.

The Peruvian OMZ

The Peru-Chile OMZ is maintained by regional trade winds that drive enhanced upwelling of nutrient-rich waters along the continental margin, resulting in some of the highest rates of primary production in the ocean and making it one of the largest OMZs (1, 32). The Peru-Chile OMZ might be responsible for some 25% of global water column nitrogen loss (33, 34). Callbeck et al., (***Chapter 5***) observed that Peruvian shelf waters early in 2013 were characterized by extreme depletion of dissolved oxygen (< 5 µM below 10 m) and nitrate (below 30 m), and the presence of

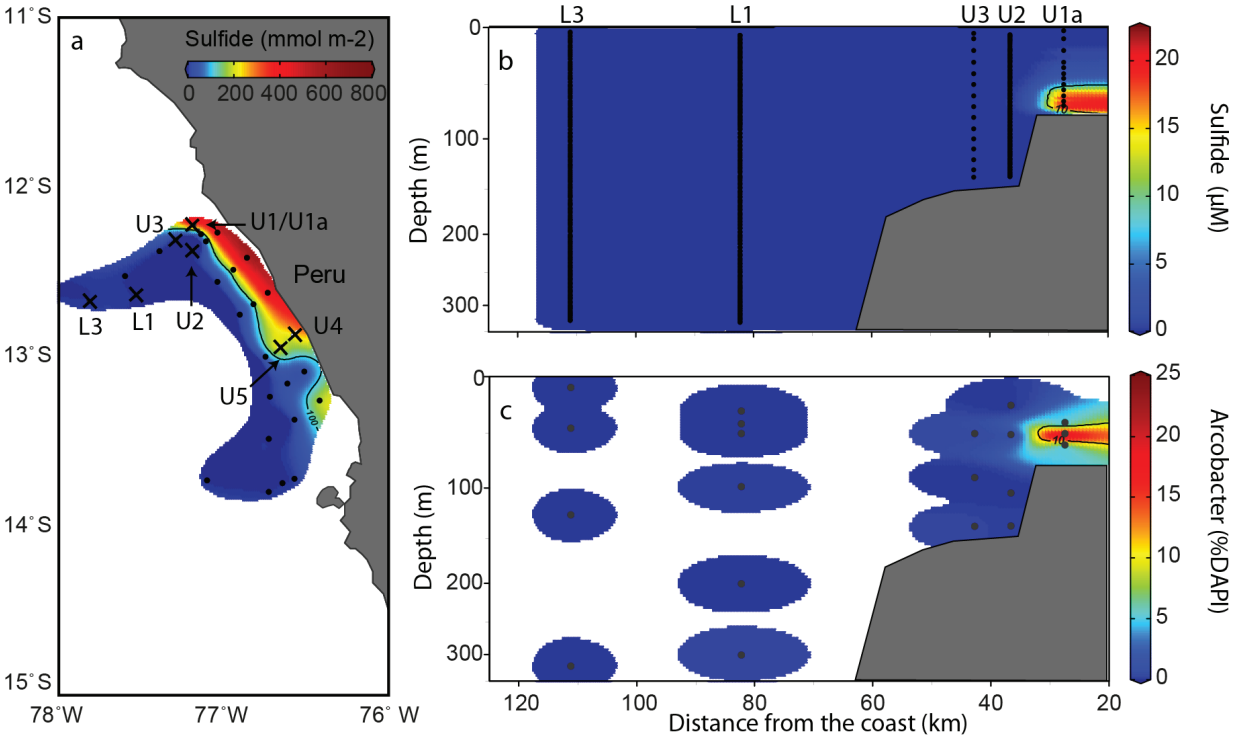

Fig. 1. Distribution of dissolved sulfide and *Arcobacter* abundances in Peruvian upwelling waters. (a) Depth-integrated inventory of dissolved sulfide. Black crosses indicate main sampling stations. (b) Composite cross-shelf depth distribution of dissolved sulfide. (c) Composite cross-shelf depth distribution of *Arcobacter* cell abundances represented as the percent of the total microbial community. Black dots indicate sample depths at each station included in the composite plots. The location and time that stations were sampled are provided in Table S1.

free dissolved hydrogen sulfide in bottom waters. Nitrate-depleted, sulfide- and elemental sulfur-rich bottom waters covered the entire near-shore Peruvian shelf between 12°S 78.3°W and 13.3°S 77°W (Fig. 1a). Bottom water sulfide concentrations in shelf waters exceeded 20 µM at some stations (Fig. 1b). The dissolved sulfide fluxes from the shelf sediment (ranged from 1 to 14 mmol m^{-2} d^{-1}; (35)), reflecting the high rates of microbial sulfate reduction that occur on the Peru shelf (10.1-11.9 mmol m^{-2} d^{-1} (36) and 20 ± 11 mmol m^{-2} d^{-1}, (37)). Overall, the sulfidic event in February-March, 2013 (1.6 x 10^9 moles H_2S and 7.0 x 10^8 moles elemental sulfur) was more than twice as intense as the sulfidic event reported for the same area in 2009 (3).

Material and Methods

Sampling and water chemistry

Peru upwelling waters (12°S 78.5°W and 13.5°S 77°W) were sampled from February 8th to March 4th, 2013 onboard the *RV Meteor* (Expedition M93). Conductivity-temperature-density (CTD) were monitored with depth and seawater was collected using either a CTD-rosette equipped with 10 L Niskin bottles or by a pump-CTD (pCTD), in which case, water was pumped directly onboard. From collected seawater nitrate and nitrite concentrations were determined with a QuAAtro autoanalyzer (Seal Analytical) with precisions of ± 0.1 µM. Sulfide concentrations were determined onboard according to Cline (38) using 4 mL of seawater and 320 µL of diamine reagent (1 µM detection limit). For the determination of water column elemental sulfur, 50 ml samples of seawater were sampled using anaerobic techniques and fixed with 100 µL $ZnCl_2$ (20% wt/wt), and then were stored at -20°C. In Bremen, elemental sulfur was extracted from the Zn-fixed samples using a chloroform-methanol procedure (39). Elemental sulfur in the methanol extracts was determined on a Waters Acquity H-class (Waters, Japan) ultrahigh pressure liquid chromatography system (Aquity UPLC BEH C18, 1.7-µm, 2.1 x 50 mm column with a methanol eluent flow at 0.4 ml min^{-1}) equipped with a Waters PDA detector (absorbance wavelength set to 265 nm; with a limit of detection of 50 nM)(Callbeck et al., ***Chapter 5***).

Microbial diversity analysis

Larger volumes of seawater 1-2L were also collected on polycarbonate filters (0.2 µm pore-size) for genomic DNA extraction. Genomic DNA was extracted using a DNA/RNA Qiagen kit and quantified by nanoDrop technology (Thermo Scientific). Universal Bacterial barcoded PCR primers were used to generate amplicons for 454 pyrosequencing (Max Planck-Genome-Center, Cologne, Germany). Partial 16S rRNA gene sequences from station U1a were uploaded to the SILVAngs pipeline, which provides automated ribosomal data analysis, alignments and taxonomic classification (40). Microbial diversity at station U1a was also analyzed by clone library preparations, which recovered near-full length 16S rRNA gene sequences. The clone library preparation procedure, including raw read quality controls and taxonomic classification using ARB software were performed according to Callbeck et al., ***Chapter 5***.

Cell Identification and Enumeration

Seawater samples collected from Niskin bottles were filtered over polycarbonate filters (0.2 µm pore-size) for analysis of cell densities using catalyzed deposition reporter (CARD)- FISH. The seawater was fixed in paraformaldehyde solution to a final concentration of 1-2% volume and was incubated for 12 hours at 4°C prior to filtration. CARD-FISH was performed on Peruvian upwelling collected seawater samples using *Arcobacter* and general epsilonproteobacteria probes: Arc94 (5'-TTAGCATCCCCGCTTCGA-3'; (41), and Epsi682 (5'-CGGATTTTACCCCTACACM-3'; (42)). The Arc94 and Epsi682 probes were incubated in 20% formamide containing hybridization buffer at 46°C for 3 hours. For the CARD-FISH procedures please refer to Callbeck et al., ***Chapter 5***. The total microbial community was stained by 4',6-Diamidino-2-phenylindole (DAPI) and together DAPI, Arc94 and Epsi682 hybridized cells were visualized and

quantified using an epifluorescence microscope (Zeiss Axioplan 2). Hybridized cells were counted in 10 fields of view and up to 1000 DAPI-stained cells. Negative and positive controls were performed using NON338 and EUB3381-III probes according to (43).

Labelled incubation experiments

Isotope labeling experiments to determine rates of nitrate reduction (^{15}N-labeling) and CO_2 fixation (^{13}C-labeling) were performed according to Callbeck et al., (***Chapter 3***). Briefly, denitrification, as well as bulk and single-cell carbon fixation rates, were determined from 12 mL exetainer incubation experiments as follows: exp1: $^{15}N\text{-}NO_3^-$ + $^{13}C\text{-}HCO_3^-$, exp2: $^{15}N\text{-}NO_2^-$ + $^{14}N\text{-}NH_4^+$ + $^{13}C\text{-}HCO_3^-$, and exp3: $^{15}N\text{-}NH_4^+$ + $^{14}N\text{-}NO_2^-$ + $^{13}C\text{-}HCO_3^-$. Concentrations of labelled substrates were 25 µm, 5 µm, and 5 µm for NO_3^-, NO_2^-, and NH_4^+, respectively. Isotopic ratios of $^{15}N^{15}N$, $^{15}N^{14}N$ and $^{14}N^{14}N$ nitrogen gas were measured on a gas-chromatography isotope-ratio mass spectrometer (GC-IRMS; VG Optima, Manchester, UK). While bulk carbon fixation rates were measured separately in ^{13}C-incubation experiments performed in gas tight 4.5 L bottles (3). The $^{13}C/^{12}C$ Isotope ratio was measured on an element analyzer EA-IRMS (FlashEA 1112 series coupled with an IRMS, Finnigan Delta plus XP, Thermo Scientific).

Single-cell analysis

In addition to the sample for IRMS measurements, extra samples from the last time point of the stable isotope incubation experiments were filtered onto pre-coated gold-palladium polycarbonate filters (0.2 µm pore-size) for FISH-SIMS analysis. NanoSIMS (NanoSIMS 50L, Cameca) was used to simultaneously identify and measure the single-cell activity of Arc94 hybridized cells. NanoSIMS analysis was done according to Callbeck et al., ***Chapter 5***. Secondary ions ^{12}C, ^{13}C, ^{19}F, $^{12}C^{14}N$, $^{12}C^{15}N$, ^{31}P, and ^{32}S were measured on 7 mass detectors. The ^{19}F signal was used to specifically identify Arc94 hybridized cells (Fig. 4a). The $^{13}C/^{12}C$ and $^{32}S/(^{12}C+^{13}C)$ ratios were calculated using look@nanoSIMS software as outlined elsewhere (45). Single-cell carbon fixation rates were determined using the $^{13}C/^{12}C$ enrichment, the labeling percent, the cell carbon content (estimated from the cell biovolume according to (46)), and divided over the incubation period.

Physiology and genome analysis

The *Arcobacte*r culture used in this study was pre-enriched from the sulfidic station U1a (Table S1) at 50 m depth onboard the research vessel. We used sterile-filtered Peru seawater with additions of sodium nitrate and either sodium sulfite, sodium thiosulfate, or elemental sulfur as electron donors to a final concentration of 100 µM. A total of three transfers were made (with a 1% v/v inoculum) into new media over the course of the research campaign. In the Bremen laboratory cultures were maintained using autoclaved anaerobic (N_2:CO_2 atmosphere) Peruvian seawater amended with sulfide and nitrate, and incubated at close to ambient water temperatures (14° C). After five transfers (1% v/v inoculum) on nitrate and dissolved sulfide, genomic DNA was extracted from a cultured isolate using the QIAamp genomic DNA kit (QIAGEN, the Netherlands). *De novo* whole genome sequencing was performed using *Pacific Biosciences RS II* technology (P4-C2 chemistry) (Max Planck Genome Center Cologne, Germany). Collected data were processed and filtered using the SMRT analysis software (v.2.1). For genome assembly SMRT analysis routine HGAP3 was applied, after which annotation was performed using RAST (47). This annotation is based on a manually curated library of subsystems (48) and on protein families, largely derived from the subsystems *FIGfams*. Further analysis of the annotated genome was performed using both RAST and Pathway Tools (49).

The *Arcobacter* strain (hereafter PSE-93) was maintained and progressively enriched on sterile anaerobic North Sea water (saNS media). Seawater was prepared in a Widdel flask. The media was filter sterilized, autoclaved and then allowed to cool under an N_2:CO_2 (90:10) atmosphere. The media was buffered to a final concentration of 2 mM HCO_3^-. Sulfur species sulfide and nitrate were amended to the media, which

was eventually dispensed into smaller serum bottles under an N_2:CO_2 atmosphere and inoculated with a 1% v/v culture from Peruvian seawater medium. The enrichment was eventually plated on DSMZ 1071 PY-BROTH medium (DSMZ, Germany) to enhance purity of PSE-93, and incubated at 14° C under oxic conditions. Colonies were picked for inoculation of fresh sterile saNS medium with 50 – 100 µM nitrate and sulfide. PSE-93 was also grown on synthetic seawater medium (Sas medium). Sas medium was prepared in a Widdel flask and contained per liter of Milli-Q 27.5 g NaCl, 5 g $MgCl_2 \cdot 6H_2O$, 4.1 g $MgSO_4 \cdot 7H_2O$, 0.66 g $CaCl_2 \cdot 2H_2O$ and 1.02 g KCl (50). The media was autoclaved and allowed to cool under a N_2:CO_2 (90:10) atmosphere. After cooling sterile trace element, vitamin and mineral solutions were added according to Kamp et al., (50). The medium was buffered by the addition HCO_3^- (to a final concentration of 2 mM) and the pH adjusted to 7.5.

For time-course experiments, media was dispensed anaerobically under N_2:CO_2 using Hundgate techniques into sterile Duran bottles that were mounted and sealed at the top with a 50-mL glass syringe (SGE Analytical Science, Australia). Duran bottles including the connected syringe were filled without a headspace. Organic matter compounds glucose, yeast extract, and ^{13}C-acetate, as well as inorganic substrates sulfide, ^{15}N-nitrate, and ^{13}C-bicarbonate, in addition to the PSE-93 inoculum (2% v/v) were added via a sidearm port in different combinations (discussed below). Experiments were run at 14 °C mimicking *in situ* conditions. Regular subsamples were taken via the sidearm port over the course of the experiment for the analysis of sulfide, nitrate and nitrite (1 mL subsample fixed in 500 µL 5% $ZnCl_2$) as well as for the analysis of labeled N_2 production (1 mL subsample in 12-mL exetainers with helium atmosphere and 50 µL saturated $HgCl_2$ solution). Additionally, 1 mL subsampled was fixed in 100 µL 20% PFA for cell count analysis. Finally, at the end of the experiment the incubation was filtered onto a pre-combusted Whatman™ glass microfiber GFF filter (GE Healthcare Life Sciences, UK). Samples for N_2 measurements were stored cap down in the dark at room temperature (RT). While all other samples were stored at -20 °C until further analysis.

Sulfide concentrations in $ZnCl_2$–fixed samples were determined photometrically (38) as described above. Nitrate and nitrite concentrations were determined by a CLD 60 Chemiluminescence NO/NO_x analyser (Eco Physics AG, Switzerland) after reduction to NO with acidic sodium Iodide (NaI) and acidic vanadium (II) chloride, respectively (51, 52). Isotopic ratios of $^{15}N^{15}N$, $^{15}N^{14}N$ and $^{14}N^{14}N$ nitrogen gas were measured on a gas-chromatography isotope-ratio mass spectrometer (GC-IRMS; VG Optima, Manchester, UK). Cell counts were obtained by flow cytometry on a BD FACSCalibur System (BD Biosciences, CA, USA) after the 2% PFA-fixed cells were stained 20 min with CYBR Green. Calibration of the flow rate was done with saNS medium and samples were measured for 1 min each. Background noise from the seawater, measured in the samples of the not-inoculated control bottles was subtracted from the bacterial counts. To quantify the amount of ^{15}N and ^{13}C incorporated into biomass the GFF filters were decalcified overnight, dried at 60°C for 1 hour, pelletized into tin cups and analyzed by a Thermo Flash EA 1112 elemental analyzer coupled to an isotopic ratio mass spectrometer Finnigan Delta Plus XP (Thermo Fisher Scientific, USA). Gases calibrated against IAEA references, and caffeine was used as standards for isotope correction and for C/N quantification, respectively.

Results and Discussion

Distribution and single-cell activity

The presence and abundance of *Arcobacter* in the Peru Upwelling was closely linked to sulfide containing shelf waters. At station U1a, where the dissolved sulfide concentrations in the bottom waters reached up to 23 µM (Fig. 2a), the nitrate-sulfide redoxcline supported a large *Arcobacter* population that reached $>10^6$ cells ml^{-1}, or 25% of the entire microbial community (Fig. 1c and 2b, c). At stations containing <10 µM dissolved sulfide *Arcobacter* was still present, but cell densities were typically < 3% of the microbial community (Fig. S1). At the sulfidic stations *Arcobacter* cell

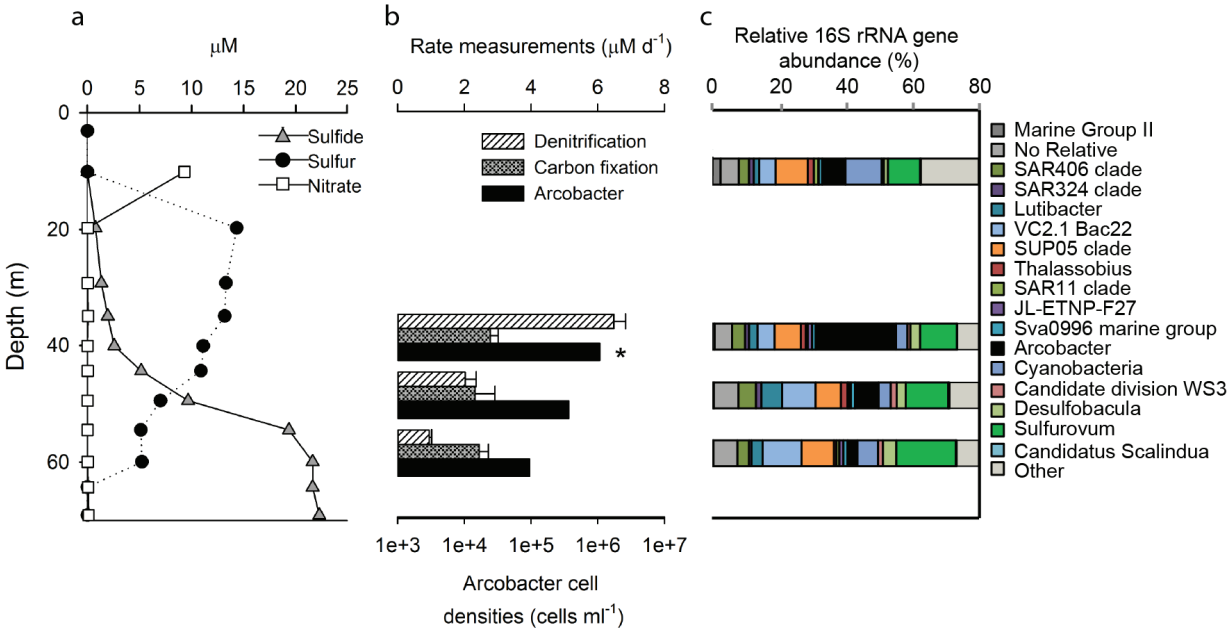

Fig. 2. Depth distribution of concentrations, cell abundances, rates of dark carbon fixation denitrification and community diversity at the main sulfidic station U1a. (a) Depth profiles of sulfide, sulfur and nitrate. Nitrite concentrations were below the limit of detection throughout the water column, except at 10 m depth (up to 0.69 μM). (b) *Arcobacter* cell densities (Arc94 probe), and rates of dark carbon fixation and denitrification are shown. Denitrification rates are in units of μM N d^{-1}. Error bars represent the standard error. The asterisk indicates the depth where samples were analyzed with nanoSIMS. (c) Microbial 16S rRNA gene diversity and relative abundances of key taxa; top eighteen most abundant taxa are shown.

abundances typically peaked in the nitrate-sulfide redoxcline (Fig. 2b, c and S1). Offshore, where dissolved sulfide was absent, *Arcobacter* made up <0.1% of the microbial community (Fig. 1c). Thus, *Arcobacter spp*. were predominately constrained to near-shore, highly productive, sulfidic waters off Peru (particularly where sulfide exceeded >20 μM in the bottom waters). This finding is consistent with reports elsewhere of *Arcobacter* occurring principally at oxic-sulfidic or nitrate-sulfidic redoxclines (42, 53-55).

At station U1a, where *Arcobacter* comprised 25% of the microbial community in the nitrate-sulfide redoxcline, other sulfide-oxidizing bacteria were also present. Microbial 16S rRNA gene diversity analysis of station U1a redoxcline waters, using clone library and pyrosequencing techniques, identified common OMZ-occurring sulfide-oxidizing bacteria such as SUP05 and Arctic96BD-19 clades within the gammaproteobacteria, as well as uncultured *Sulfurovum* and *Arcobacter spp.* within the epsilonproteobacteria (Fig. 2c and 3). Sulfide concentrations at station U1a were highest in bottom waters (55 to 65 m depth) and decreased gradually across the water column to zero, at 20 m depth (Fig. 2a). Both dissolved oxygen and nitrate were depleted within the redoxcline. Nitrate (10 μM) was detected only in the upper 20 m of the water column, where sulfide and elemental sulfur concentrations fell below the detection limit (<1 μM). Elemental sulfur, reaching concentrations over 15 μM, was present throughout the redoxcline (20-50 m), and reached concentrations of 5 μM in the uppermost meters of the sulfidic zone. *Arcobacter* abundances peaked in the middle of the broad redoxcline at 40 m based on both CARD-FISH cell counts and 16S rRNA gene abundances from pyrosequencing analysis (Fig. 2b, c). Potential denitrification rates decreased from the redoxcline (6.5 ± 0.4 μM N d^{-1}) to the deeper sulfidic zone (0.9 ± 0.1 μM N d^{-1}), while dark carbon fixation rates remained constant at 2.8 ± 0.2 μM C d^{-1} within the redoxcline. Nitrogen loss and carbon fixation rates were consistent with other measured rates in the Peru-Chile and Namibia shelf waters, indicating active chemolithoautotrophic activity (2, 3, 12).

Despite the abundance of *Arcobacter* at station

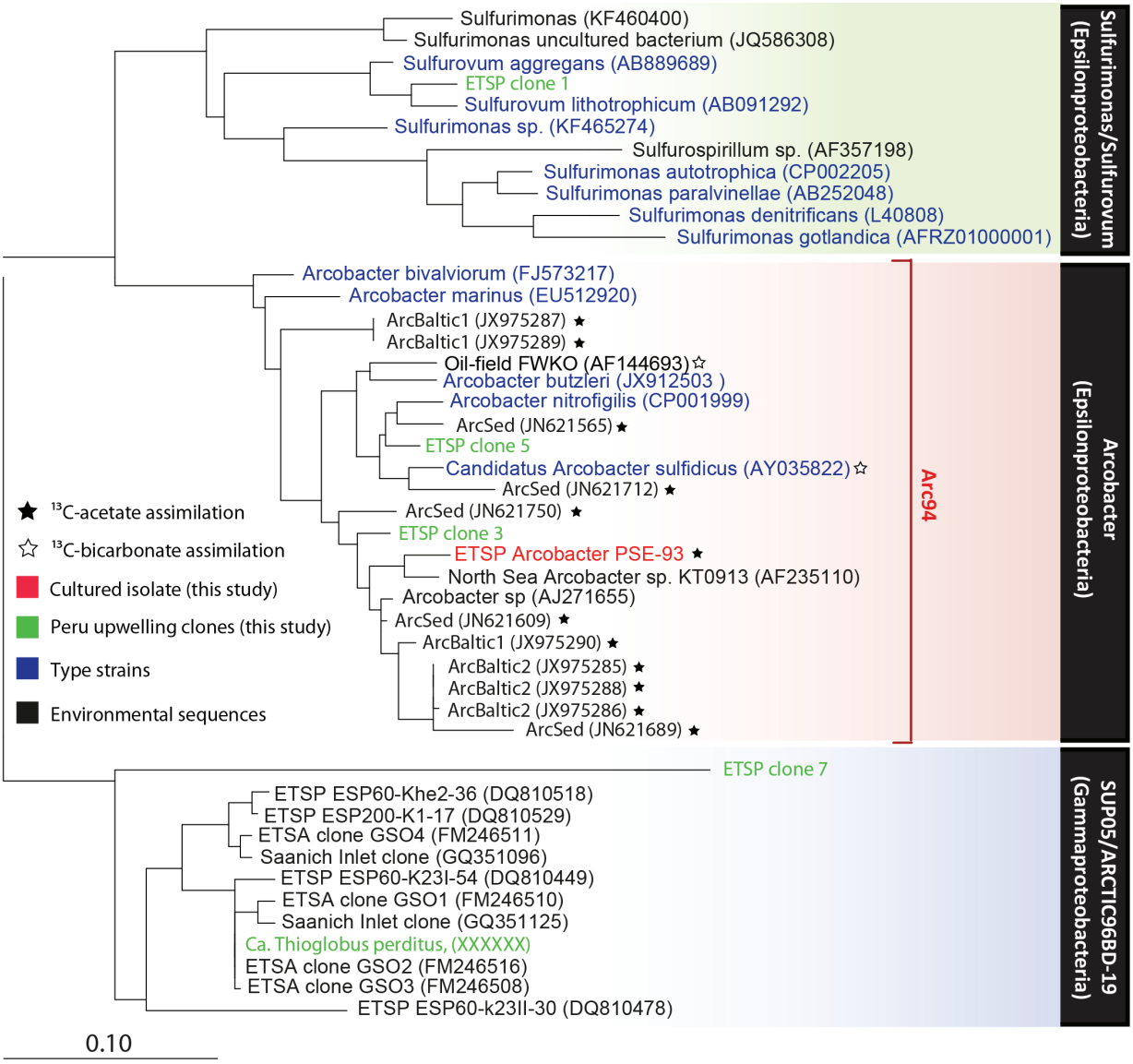

Fig. 3. Phylogeny of 16S rRNA genes of key sulfide-oxidizing bacteria recovered from Peruvian shelf waters. The phylogenetic tree was calculated according to neighboring joining, parsimony and RaXML methods applying various filters; an unrooted consensus tree is shown. Included are partial and near-full length 16S rRNA sequences. Sequences recovered from sulfidic stations U1 and U1a (green typeface; Fig. 1b; S1), and the cultivated Arcobacter PSE-93 enriched from sulfidic station U1a (red typeface) are indicated. Arcobacter species recovered from sulfidic sediments or from the Baltic Sea oxic-sulfidic redoxcline enriched in 13C-acetate, based on RNA-stable isotope incubation experiments, are indicated by black stars (21,25), conversely, strains capable of autotrophic carbon fixation are indicted by the open stars (17). The in silico coverage of the Arc94 CARD-FISH probe is indicated.

U1a, *Arcobacter* contributed only 1% to dark CO_2 fixation in these waters. Based on the single-cell ^{13}C-HCO_3^- assimilation rates and the measured *Arcobacter* cell densities (Table 1), we calculated that *Arcobacter* fixed 0.04 ± 0.01 fmol C cell^{-1} d^{-1} (Fig. 4a, b). The gammaproteobacterial clade SUP05, and other ε-proteobacteria (e.g. *Sulfurovum spp.*), in contrast, exhibited CO_2 assimilation rates of 1.18 ± 0.04 and 0.24 ± 0.02 fmol C cell^{-1} d^{-1} (ANOVA, df= 2, $p<0.001$, significant difference). These two taxa jointly accounted for nearly one-third of dark carbon fixation rates at station U1a (Table 1), with doubling times of 4 (SUP05) and 10 (other ε-proteobacteria) days. *Arcobacter* doubling times based only on single-cell

Table 1: Chemolithoautotrophic contributors to dark carbon fixation rates measured in situ at stations U1 and U1a.

	SUP05	ε-proteobacteria	*Arcobacter*
[a] ***Single-cell carbon fixation rates***			
Number of SUP05 cells analyzed	107	58	37
Growth rate (doublings per day)	0.080 ± 0.005	0.279 ± 0.020	0.011 ± 0.004
Cell size (μm)	0.81 ± 0.02	1.11 ± 0.02	0.89 ± 0.03
Cell carbon content ($pmols\ C\ cell^{-1}$)	6.42×10^{-3}	10.0×10^{-3}	10.0×10^{-3}
Per cell fixation rate ($fmol\ C\ cell^{-1}\ d^{-1}$)	0.24 ± 0.03	1.18 ± 0.04	0.04 ± 0.02
Contribution to CO_2 fixation			
[b] Depth-integrated cell densities (cells m^{-2})	3.14×10^{13}	9.23×10^{12}	1.44×10^{13}
[b] Depth-integrated CO_2 fixation rate			
Dark ($mmol\ C\ m^{-2}\ d^{-1}$)	7.55	10.90	0.59
[b] Bulk depth-integrated CO_2 fixation:			
Dark ($mmol\ C\ m^{-2}\ d^{-1}$)	60.35	60.35	60.35
Contribution to dark CO2 fixation (%)	13	18	1

[a] Single-cell SUP05 values were measured at station U1 at 30 and 60 m (average is shown). While epsilonproteobacteria and *Arcobacter* single-cell values were measured from station U1a (60 m). For details regarding single-cell calculations please see Methods.

[b] Depth-integrated from 40-65 m (Fig. 2).

$^{13}C\text{-}HCO_3^-$ uptake rates would be too low (doubling once per 100 days) to support the in situ cell densities (10^6 cells ml^{-1}). Thus, the Peru Upwelling *Arcobacter* obtains carbon for growth using organic matter.

Physiology and genome analysis

To gain further insights into the Peru upwelling *Arcobacter* physiology we enriched and cultivated a novel *Arcobacter* species from station U1a, designated PSE-93, under anaerobic conditions with natural seawater amended with sulfide and nitrate. Sequences closely related to the PSE-93 were recovered from Peruvian sulfidic bottom waters as well as from North Sea waters (Fig. 3) (56).

A complete circular PSE-93 genome (2.8 Mbp in size with 27.8% GC content and 2773 genes) revealed a great capacity for physiological adaptability (Fig. 5). *Arcobacter* PSE-93 specifically has the genomic potential to reduce nitrate to N_2 via denitrification as well as the gene-coding regions for various terminal oxidases necessary for oxic respiration. Furthermore, the genome indicated the capacity of PSE-93 to oxidize sulfide via a sulfide dehydrogenase (*sudA*) to S^0, and oxidize zerovalent sulfur and thiosulfate via a periplasmic sox-pathway (*soxABCDXYZ*) to sulfate. Autotrophic CO_2 fixation pathways (e.g. CBB, rTCA and 3-HPB) were not found in the PSE-93 genome (Fig. 5). Instead a number of organic matter dependent carboxylases involved in acetate and propionate assimilation was detected, as well as carboxylases involved in fatty acid biosynthesis and anaplerotic reactions.

We tested PSE-93 capacity to oxidize sulfide and reduce nitrate with various carbon substrates. In all experiments, sufficient sulfide was available to oxidize added nitrate to N_2, assuming full sulfide oxidation to sulfate. In synthetic seawater media (Sas

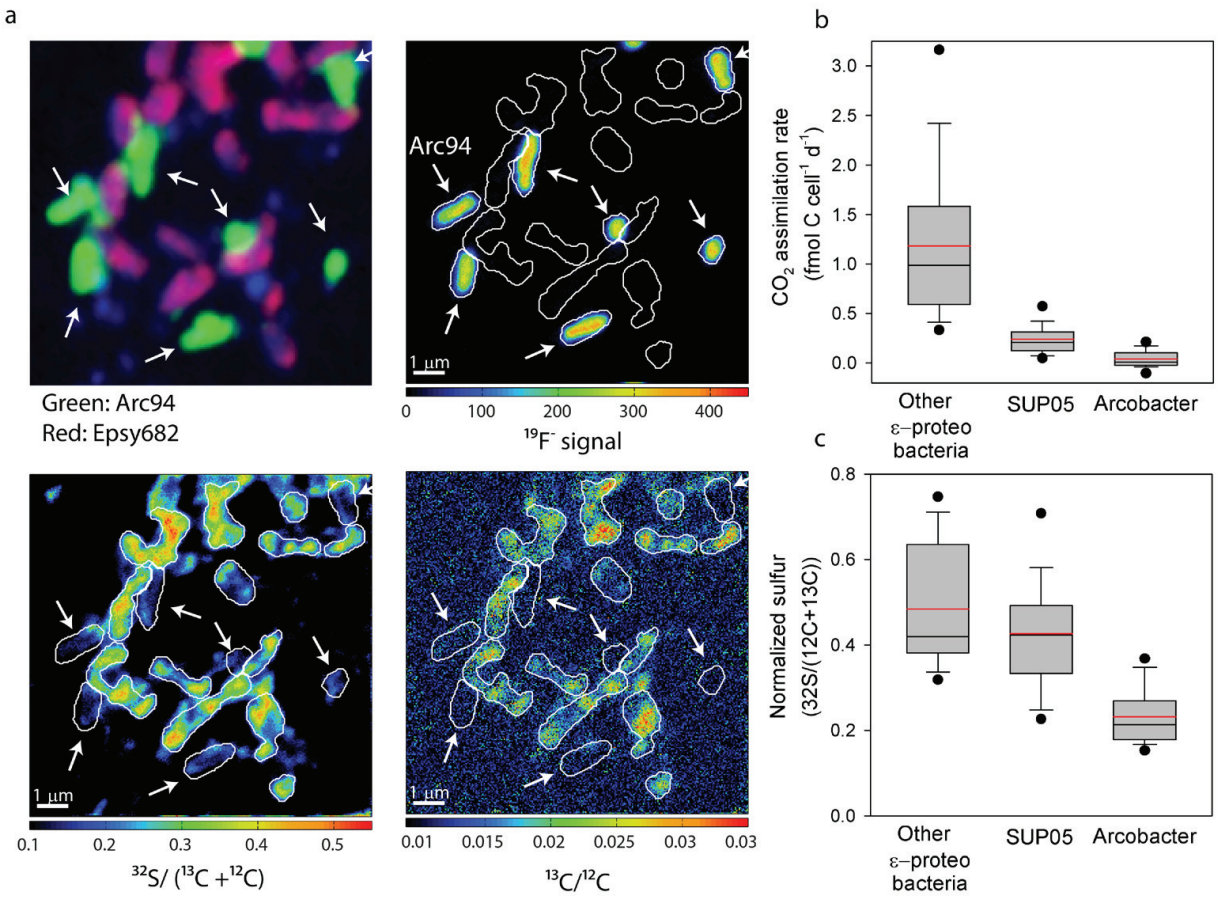

Fig. 4. ***Arcobacter*** **single-cell activity and sulfur content at the Peruvian upwelling station U1a (60 m depth).** The composite images show (a) CARD-FISH hybridization image and the single-cell isotope ratios. The ^{19}F signal indicates cells hybridized with the Arc94 probe (also indicated by the white arrows). (b,c) Single-cell ^{13}C-HCO_3^- assimilation rates and cell sulfur content of *Arcobacter*, SUP05 and other epsilonproteobacteria (excluding *Arcobacter*) are shown. The average and (red line) median (black line) as well as the 5th and 95th percentiles (closed circles) are indicated. Error bars represent the standard deviation. The number of cells analyzed by nanoSIMS is 58, 37, and 107 for epsilonproteobacteria, *Arcobacter* and SUP05, respectively. Note that data related to SUP05 (including the SUP05 single-cell assimilation rates and sulfur content) is presented in Callbeck et al., ***Chapter 5***.

medium), without an organic carbon background, PSE-93 sulfide oxidation (0.70 ± 0.20 µM h^{-1}) and nitrate reduction (0.50 ± 0.20 µM h^{-1}) rates were detectable (Figs. 6a and Table 2). However, cell numbers never reached more than 3 x 10^5 cells mL^{-1} (Fig. 6a), roughly an order of magnitude lower, than cell densities at station U1a (Fig. 2). In natural seawater experiments (saNS media), PSE-93 showed slightly enhanced sulfide oxidation (1.29 ± 0.26 µM h^{-1}) and nitrate reduction (1.00 ± 0.04 µM h^{-1}) rates (Fig. 6b and Table 2). However, cell densities were below the detection limit (< 9 x 10^4 cells mL^{-1}). In both experiments, roughly half the nitrate was reduced to N_2 while the rest was reduced to nitrite (Figs. 6a, b). PSE-93 had only low to non-detectable ^{13}C-bicarbonate assimilation rates (Fig. 6), comparable in magnitude to single-cell rates measured in situ (Table 1). The lack of autotrophic CO_2 fixation and the plethora of organic carbon dependent carboxylases in the genome (Fig. 5), suggest that measured rates of CO_2 assimilation reflect anaplerotic growth or growth associated with a heterotrophic lifestyle. Thus, the carbon limitations in Sas medium, likely restricted the complete reduction of nitrate to N_2 and hindered cell growth, suggestive that PSE-93 was dependent on organic carbon.

Indeed, enhanced sulfide oxidation (2.6 µM

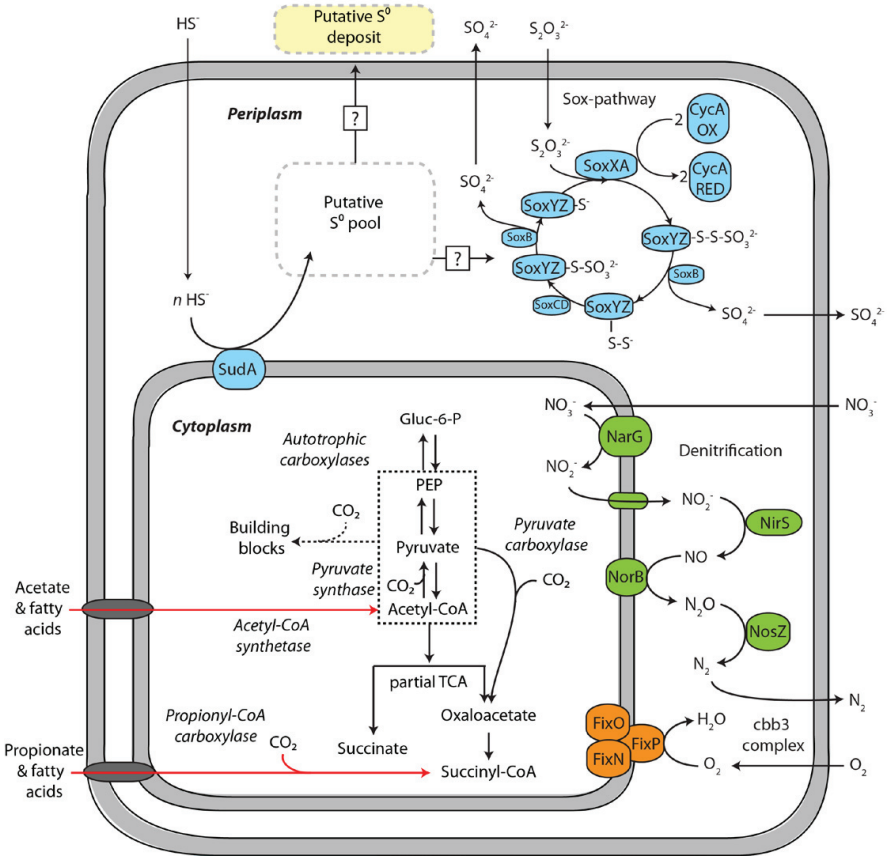

Fig. 5. Metabolic model of *Arcobacter* PSE-93 based on the genome analysis. The PSE-93 genome was 2.8 Mbp and a single complete circular chromosome composed of 2773 genes with 2696 protein genes, 77 RNA genes and 27.8% GC content. Electron donating and accepting as well as organic carbon assimilation pathways are indicated. Pathways for acetate and propionate assimilation are highlighted by the red arrows. No autotrophic pathways for CO_2 fixation were detected, however, a number of carboxylases associated to organic matter assimilation (pyruvate synthase; propionyl-CoA carboxylase), as well as anaplerotic (pyruvate carboxylase) and biosynthetic (acetyl/propionyl-CoA carboxylase) reactions were detected. Key precursor molecules (PEP, pyruvate and acetyl-CoA) involved in biosynthetic reactions are indicated by the dotted rectangle.

h^{-1}) and nitrate reduction (4.6 μM h^{-1}) rates were observed when PSE-93 was grown with glucose and yeast extract (Table 2). Growth on acetate yielded the greatest sulfide oxidation (6.6 ± 0.67 μM h^{-1}) and nitrate reduction (6.2 ± 1.69 μM h^{-1}) rates (Fig. 6c and Table 2) for PSE-93. Moreover, the nitrite that formed as an intermediate was completely reduced to N_2 by the end of the experiment (Fig. 6c). Concomitantly in this experiment, ^{13}C-labeled acetate was assimilated into PSE-93 biomass with a single-cell assimilation rate of 1.55 ± 0.19 fmol C $cell^{-1}$ d^{-1}, derived from the ^{13}C-enrichment, the background label, and the cell carbon content. PSE-93 growth on acetate, sulfide and nitrate was also manifested by high cell densities of 4 x 10^6 cells mL^{-1} (with a doubling rate of 1.8 per day), which were comparable to Arcobacter cell densities at station U1a (Fig. 2b). Similar cell densities were previously reported for sulfidic Namibian shelf waters (2).

In separate incubation experiments, designed to test PSE-93 growth under even lower nitrate concentrations (i.e. 20 μM nitrate to 100 μM sulfide), showed a similar capacity to oxidize sulfide, reduce nitrate and assimilate acetate (Fig. 6d). However, rates of sulfide oxidation (1.10 ± 0.01 μM h^{-1}), nitrate reduction (0.91 ± 0.04 μM h^{-1}) and acetate assimilation (0.17 ± 0.04 fmol C $cell^{-1}$ d^{-1}) were lower than in the experiments with higher nitrate concentrations (Table 2). Nevertheless both sulfide, nitrate and acetate amendment experiments demonstrate that PSE-93 is capable of chemolitho-heterotrophic growth, coupling sulfide oxidation and nitrate reduction to acetate assimilation. PSE-93 could also grow heterotrophically coupling acetate oxidation to nitrate reduction (Fig. 6e). However, nitrate reduction (1.3 ± 0.22 μM h^{-1}) and acetate assimilation (0.38 ± 0.06 fmol C $cell^{-1}$ d^{-1}) rates were over 4-fold lower, and likewise the calculated doublings per day (0.79) were two-fold lower compared to PSE-93 rates reported with sulfide, nitrate and acetate (Fig. 6e and Table 2).

Thus, the genome analysis and the physiological

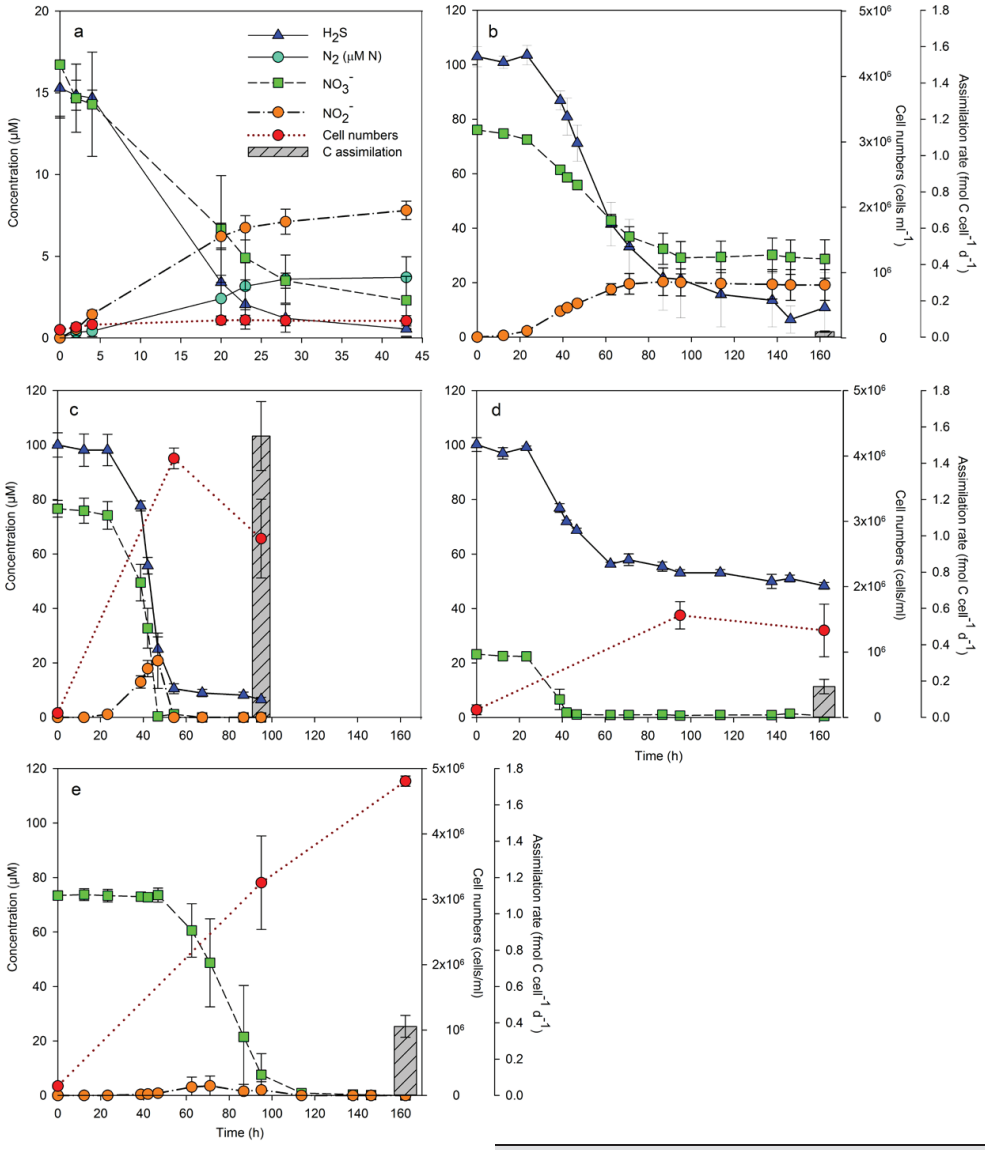

Fig. 6. *Arcobacter* PSE-93 activity and growth. Activity and growth on: (a) nitrate, hydrogen sulfide, and ^{13}C-bicarbonate, performed in Sas medium. Experiments (b-e) were performed in saNS medium as follows: (b) sulfide, nitrate and ^{13}C-bicarbonate, (c) sulfide, nitrate and ^{13}C -acetate, (d) sulfide, low nitrate (20 µM) and ^{13}C-acetate, (e) nitrate and ^{13}C-acetate. Cell densities were below the detection limit in panel b. Error bars represent the standard deviation from triplicate incubation experiments. Note the variability in x-axis scales.

Table 2: Arcobacter PSE-93 sulfide oxidation and nitrate reduction activity in amendment experiments. Experiments were performed in synthetic seawater (Sas) media or North Sea seawater (saNS) media as indicated. Sulfide and nitrate turnover rates shown here were determined from the change in the substrate concentration divided by time (Fig. 6). Carbon assimilation rates are reported in text. BD = below the limit of detection.

Experiment	Sulfide oxidation (µM h^{-1})	Nitrate reduction (µM h^{-1})
Sas: NO_3^- + HS^- + HCO_3^-	0.70 ± 0.20	0.50 ± 0.20
saNS: NO_3^- + HS^- + HCO_3^-	1.29 ± 0.26	1.00 ± 0.04
saNS: NO_3^- + HS^- + Glucose	1.50	4.1
saNS: NO_3^- + HS^- + Yeast extract	2.60	4.7
saNS: NO_3^- + HS^- + Acetate	6.60 ± 0.67	6.20 ± 1.69
saNS: NO_3^- (low) + HS^- + Acetate	1.10 ± 0.01	0.91 ± 0.04
saNS: NO_3^- + Acetate		1.3 ± 0.22

experiments demonstrate that the Arcobacter strain PSE-93 is an obligate heterotroph, capable of chemolithoheterotrophic and chemoorganoheterotrophic growth. Moreover, these experiments show that sulfide, nitrate and acetate could sustain the high Arcobacter cell densities and rates of nitrate reduction observed in situ (Fig. 2 and 6).

Ecophysiology of a chemolithoheterotroph

The chemolithoheterotrophic physiology of *Arcobacter* PSE-93 suggests that it is well-suited to the sulfide and organic matter rich environment in Peru shelf waters. Acetate, a short chain fatty acid produced during the degradation of organic matter via fermenting bacteria could be essential to support *Arcobacter* growth in the Peruvian OMZ waters. Studies of sediments and redoxcline interfaces have highlighted a diverse consortium of *Arcobacter* species capable of assimilating acetate under sulfidic conditions (21, 25) (Fig. 3). In permanently sulfidic marine basins, acetate concentrations are often highest in sulfidic bottom waters and in the redoxcline of sulfidic stations, in some cases reaching upwards of 3 μM (57, 58). These environments not only exhibit elevated rates of dark carbon fixation, but also high rates of both acetate production and acetate assimilation (0.05 to 0.5 μM d^{-1}) (58). Although acetate was not measured in situ, around the time of sampling, shallow Peruvian OMZ shelf waters reported high concentrations of dissolved organic matter (80-100 μmol L^{-1}) in both surface and in benthic-influenced bottom waters (59). In the Peruvian upwelling, *Arcobacter* could assimilate acetate by converting it to acetyl-CoA (by acetyl-CoA synthetase), which then enters gluconeogenesis, the partial TCA cycle and other biosynthesis pathways (Fig. 5).

Such chemolithoheterotrophic growth confers energetic advantages over a chemolithoautotrophic physiology. For pyruvate, a key building block in biosynthesis, autotrophic CO_2 fixation requires between 0.6-2.3 mol ATP mol^{-1} C per mol of pyruvate formed, while acetate assimilation requires only 0.5 mol ATP mol^{-1} C per mol of pyruvate formed (60). Our enrichment culture experiments show that PSE-93 more efficiently assimilates C under heterotrophic as compared to autotrophic conditions. A growth factor for PSE-93 assimilating acetate, while oxidizing sulfide with nitrate was determined of 3.1 mol C assimilated per mol H_2S oxidized, based on the PSE-93 single cell acetate assimilation (1.55 fmol C $cell^{-1}$ d^{-1}) and sulfide oxidation (0.50 fmol C $cell^{-1}$ d^{-1}) rates. This growth factor exceeds factors reported for cultivated chemolithoautotrophic sulfide-oxidizing bacteria, which range from 0.35-0.58 mol C assimilated per mol H_2S oxidized (61-63)(Callbeck et al., ***Chapter 5***). Thus, the lower energy constraints of PSE-93 may enable *Arcobacter* (and presumably other sulfide-oxidizing chemolithoheterotrophic bacteria) to displace/outcompete chemolithoautotrophs (e.g. SUP05 bacteria (Fig. 2c and 3)) for available sulfide and nitrate when labile organic matter is replete. The favorable energetics may therefore enable the Peruvian upwelling *Arcobacter* to rapidly bloom under highly sulfidic and organic matter rich conditions.

The advantage of a chemolithoheterotrophic physiology is, however, not without its drawbacks. The requirement of labile organic matter, along with sulfide and nitrate, places *Arcobacter* at a competitive disadvantage alongside chemolithoautotrophic bacteria that are able to generate biomass (i.e. via CO_2 fixation) independently of organic matter availability. This ultimately constrains *Arcobacter* to sulfidic and organic matter rich shelf waters. In addition, compared to other co-occurring sulfide-oxidizing bacteria (e.g. SUP05), *Arcobacter* showed no capacity to store intracellular sulfur. For instance, the PSE-93 genome contained a complete sulfide oxidation Sox pathway; as opposed to a truncated pathway missing *soxCD* genes that have been shown in other sulfide oxidizers to be correlated with intracellular sulfur storage (64). In further support, the single-cell sulfur content observed in the Peruvian upwelling *Arcobacter* were significantly lower (ANOVA, df= 2, $p<0.001$) than SUP05 and non-*Arcobacter* Epsilonproteobacteria cells (Fig. 4a, c). This might place *Arcobacter* at a disadvantage under dynamic shelf conditions. For example, SUP05 bacteria, which co-occur with *Arcobacter* in the sulfidic shelf waters, continues to

denitrify using stored intracellular elemental sulfur and are more widespread in the Peruvian upwelling OMZ (Callbeck et al., ***Chapter 5***). Nevertheless, in the zone where *Arcobacter* dominates, it likely contributes significantly to measured rates of denitrification and stands as a key barrier to the release of toxic sulfide into overlying waters.

Such a chemolithoheterotrophic metabolism has been remained overlooked in sulfidic environments, where chemolithoautotrophic bacteria are thought to be primarily responsible for the oxidation of dissolved sulfide in OMZs and closed basins (2, 3, 8, 12, 30, 31). A broader review of the marine literature shows that only a few microbes have the been identified with the capacity for chemolithoheterotrophy (19, 65-70). Our combined study using in situ, physiological and genomic techniques demonstrates that litho-heterotrophy may play an important role in eutrophic, sulfide-rich upwelling environments. With expanding OMZs (71), and increased anthropogenic induced eutrophication of coastal regions (6), the areas where sulfide-oxidizing, denitrifying heterotrophs such as *Arcobacter* thrive are likely to increase.

Author Contributions

C.M.C., C.P., and G.L., designed the study; C.M.C., C.P., S.H., and K.L. performed experiments; C.M.C., C.P., G.L., S.H., and K.L. analysed data; C.M.C., wrote the original draft; C.M.C., G.L., T.G.F. and M.M.M.K. edited the manuscript.

Acknowledgements

We are grateful to the Peruvian authorities for access to national waters as well as the crew of the RV Meteor (M93 research expedition) for providing the technical assistance to sample the ocean. We would also like to thank the administrative support by C. Schelten; assistance by A. Schwedt, and G. Klockgether; and the student research assistance by S. Haas and K. Latham. This work was supported by the MPG and by the DFG the Sonderforschungsbereich (SFB754) GEOMAR, Kiel. The stipend of C.M.C was also supported by a Natural Sciences and Engineering Research Council of Canada (NSERC) scholarship.

References

1. *Carr M-E (2001) Estimation of potential productivity in Eastern Boundary Currents using remote sensing. Deep Sea Research Part II: Topical Studies in Oceanography 49(1–3):59-80.*

2. *Lavik G, et al. (2009) Detoxification of sulphidic African shelf waters by blooming chemolithotrophs. Nature 457(7229):581-584.*

3. *Schunck H, et al. (2013) Giant hydrogen sulfide plume in the oxygen minimum zone off Peru supports chemolithoautotrophy. PloS one 8(8):e68661.*

4. *Copenhagen WJ (1954) The periodic mortality of fish in the Walvis region. S Afr Med J 28(18):381.*

5. *Levin LA, et al. (2009) Effects of natural and human-induced hypoxia on coastal benthos. Biogeosciences 6(10):2063-2098.*

6. *Diaz RJ & Rosenberg R (2008) Spreading dead zones and consequences for marine ecosystems. Science 321(5891):926-929.*

7. *Rabalais NN, Turner RE, & Scavia D (2002) Beyond Science into Policy: Gulf of Mexico Hypoxia and the Mississippi RiverNutrient policy development for the Mississippi River watershed reflects the accumulated scientific evidence that the increase in nitrogen loading is the primary factor in the worsening of hypoxia in the northern Gulf of Mexico. BioScience 52(2):129-142.*

8. *Taylor GT, et al. (2001) Chemoautotrophy in the redox transition zone of the Cariaco Basin: A significant midwater source of organic carbon production. Limnology and Oceanography 46(1):148-163.*

9. *Glaubitz S, Labrenz M, Jost G, & Jurgens K (2010) Diversity of active chemolithoautotrophic prokaryotes in the sulfidic zone of a Black Sea pelagic redoxcline as determined by rRNA-based stable isotope probing. FEMS microbiology ecology 74(1):32-41.*

10. *Löscher CR, et al. (2016) Water column biogeochemistry of oxygen minimum zones in the eastern tropical North Atlantic and eastern tropical South Pacific oceans. Biogeosciences 13(12):3585-3606.*

11. *Brüchert V, et al. (2006) Biogeochemical and physical control on shelf anoxia and water column hydrogen sulphide in the Benguela upwelling system of Namibia*

Past and Present Water Column Anoxia, ed Neretin NL (Springer Netherlands, Dordrecht), pp 161-193.

12. *Galán A, Faúndez J, Thamdrup B, Santibáñez JF, & Farías L (2014) Temporal dynamics of nitrogen loss in the coastal upwelling ecosystem off central Chile: Evidence of autotrophic denitrification through sulfide oxidation. Limnology and Oceanography 59(6):1865-1878.*

13. *Grote J, et al. (2012) Genome and physiology of a model Epsilonproteobacterium responsible for sulfide detoxification in marine oxygen depletion zones PNAS 109(2):506-510.*

14. *Grote J, Jost G, Labrenz M, Herndl GJ, & Jurgens K (2008) Epsilonproteobacteria represent the major portion of chemoautotrophic bacteria in sulfidic waters of pelagic redoxclines of the Baltic and Black Seas. Applied and environmental microbiology 74(24):7546-7551.*

15. *Hawley AK, Brewer HM, Norbeck AD, Pasa-Tolic L, & Hallam SJ (2014) Metaproteomics reveals differential modes of metabolic coupling among ubiquitous oxygen minimum zone microbes. Proceedings of the National Academy of Sciences of the United States of America 111(31):11395-11400.*

16. *Wright JJ, Konwar KM, & Hallam SJ (2012) Microbial ecology of expanding oxygen minimum zones. Nature reviews. Microbiology 10(6):381-394.*

17. *Gevertz D, Telang AJ, Voordouw G, & Jenneman GE (2000) Isolation and characterization of ctrains CVO and FWKO B, two novel nitrate-reducing, sulfide-oxidizing bacteria isolated from oil field brine. Applied and environmental microbiology 66(6):2491-2501.*

18. *Wirsen CO, et al. (2002) Characterization of an Autotrophic Sulfide-Oxidizing Marine Arcobacter sp. That Produces Filamentous Sulfur. Applied and Environmental Microbiology 68(1):316-325.*

19. *Roalkvam I, et al. (2015) Physiological and genomic characterization of Arcobacter anaerophilus IR-1 reveals new metabolic features in Epsilonproteobacteria. Frontiers in microbiology 6:987.*

20. *Llobet-Brossa E, Rosselló-Mora R, & Amann R (1998) Microbial Community Composition of Wadden Sea Sediments as Revealed by Fluorescence In Situ Hybridization. Applied and Environmental Microbiology 64(7):2691-2696.*

21. *Vandieken V & Thamdrup B (2013) Identification of acetate-oxidizing bacteria in a coastal marine surface sediment by RNA-stable isotope probing in anoxic slurries and intact cores. FEMS Microbiology Ecology 84(2):373-386.*

22. *Madrid VM, Taylor GT, Scranton MI, & Chistoserdov AY (2001) Phylogenetic Diversity of Bacterial and Archaeal Communities in the Anoxic Zone of the Cariaco Basin. Applied and Environmental Microbiology 67(4):1663-1674.*

23. *Borin S, et al. (2009) Sulfur cycling and methanogenesis primarily drive microbial colonization of the highly sulfidic Urania deep hypersaline basin. Proceedings of the National Academy of Sciences 106(23):9151-9156.*

24. *Fuchsman CA, Murray JW, & Staley JT (2012) Stimulation of Autotrophic Denitrification by Intrusions of the Bosporus Plume into the Anoxic Black Sea. Frontiers in microbiology 3:257.*

25. *Berg C, Beckmann S, Jost G, Labrenz M, & Jürgens K (2013) Acetate-utilizing bacteria at an oxic–anoxic interface in the Baltic Sea. FEMS Microbiology Ecology 85(2):251-261.*

26. *Callbeck C, et al. (2011) Microbial community succession in a bioreactor modeling a souring low-temperature oil reservoir subjected to nitrate injection. Appl Microbiol Biotechnol 91(3):799-810.*

27. *Gieg L, Jack T, & Foght J (2011) Biological souring and mitigation in oil reservoirs. Appl Microbiol Biotechnol 92(2):263-282.*

28. *Gevertz D, Telang AJ, Voordouw G, & Jenneman GE (2000) Isolation and Characterization of Strains CVO and FWKO B, Two Novel Nitrate-Reducing, Sulfide-Oxidizing Bacteria Isolated from Oil Field Brine. Applied and Environmental Microbiology 66(6):2491-2501.*

29. *Hubert CRJ, et al. (2012) Massive dominance of Epsilonproteobacteria in formation waters from a Canadian oil sands reservoir containing severely biodegraded oil. Environmental microbiology 14(2):387-404.*

30. *Zopfi J, Ferdelman TG, Jorgensen BB, Teske A, & Thamdrup B (2001) Influence of water column dynamics on sulfide oxidation and other major biogeochemical processes in the chemocline of (Mariager Fjord Denmark). Marine Chemistry 74:29-51.*

31. *Glaubitz S, et al. (2009) 13C-isotope analyses reveal that chemolithoautotrophic Gamma- and Epsilonproteobacteria feed a microbial food web in a pelagic*

redoxcline of the central Baltic Sea. Environmental microbiology 11(2):326-337.

32. Lam P & Kuypers MMM (2011) Microbial Nitrogen Cycling Processes in Oxygen Minimum Zones. Annual Review of Marine Science 3(1):317-345.

33. Codispoti LA (2007) An oceanic fixed nitrogen sink exceeding 400 Tg N a-1 vs the concept of homeostasis in the fixed-nitrogen inventory. Biogeosciences 4(2):233-253.

34. DeVries T, Deutsch C, Primeau F, Chang B, & Devol A (2012) Global rates of water-column denitrification derived from nitrogen gas measurements. Nature Geosci 5(8):547-550.

35. Sommer S, et al. (2016) Depletion of oxygen, nitrate and nitrite in the Peruvian oxygen minimum zone cause an imbalance of benthic nitrogen fluxes. Deep Sea Research Part I: Oceanographic Research Papers 112:113-122.

36. Böning P, et al. (2004) Geochemistry of Peruvian near-surface sediments. Geochimica et Cosmochimica Acta 68(21):4429-4451.

37. Fossing H & Jørgensen BB (1989) Measurement of bacterial sulfate reduction in sediments: Evaluation of a single-step chromium reduction method. Biogeochemistry 8(3):205-222.

38. Cline JD (1969) Spectrophotometric determination of hydrogen sulfide in natural waters Limnology and Oceanography 14(3):454-458.

39. Kamyshny A, et al. (2008) Speciation of polysulfides and zerovalent sulfur in sulfide-rich water wells in southern and central Israel. Aquatic Geochemistry 14(2):171-192.

40. Quast C, et al. (2013) The SILVA ribosomal RNA gene database project: improved data processing and web-based tools. Nucleic Acids Research 41(D1):D590-D596.

41. Snaidr J, Amann R, Huber I, Ludwig W, & Schleifer KH (1997) Phylogenetic analysis and in situ identification of bacteria in activated sludge. Applied and environmental microbiology 63(7):2884-2896.

42. Moussard H, Corre E, Cambon-Bonavita M-A, Fouquet Y, & Jeanthon C (2006) Novel uncultured Epsilonproteobacteria dominate a filamentous sulphur mat from the 13°N hydrothermal vent field, East Pacific Rise. FEMS microbiology ecology 58(3):449-463.

43. Pernthaler A, Pernthaler J, & Amann R (2002) Fluorescence in situ hybridization and catalyzed reporter deposition for the identification of marine bacteria. Applied and environmental microbiology 68(6):3094-3101.

44. Callbeck CM, Lavik G, Stramma L, Kuypers MMM, & Bristow LA (2017) Enhanced nitrogen loss by eddy-induced vertical transport in the offshore peruvian oxygen minimum zone. PloS one 12(1):e0170059.

45. Polerecky L, et al. (2012) Look@NanoSIMS--a tool for the analysis of nanoSIMS data in environmental microbiology. Environmental microbiology 14(4):1009-1023.

46. Romanova ND & Sazhin AF (2010) Relationships between the cell volume and the carbon content of bacteria. Oceanology 50(4):522-530.

47. Aziz RK, et al. (2008) The RAST Server: Rapid Annotations using Subsystems Technology. BMC Genomics 9(1):75.

48. Overbeek R, et al. (2005) The subsystems approach to genome annotation and its use in the project to annotate 1000 genomes. Nucleic Acids Res 33.

49. Caspi R, et al. (2012) The MetaCyc database of metabolic pathways and enzymes and the BioCyc collection of pathway/genome databases. Nucleic Acids Research 40(D1):D742-D753.

50. Kamp A, Røy H, & Schulz-Vogt HN (2008) Video-supported Analysis of Beggiatoa Filament Growth, Breakage, and Movement. Microbial ecology 56(3):484-491.

51. Braman RS & Hendrix SA (1989) Nanogram nitrite and nitrate determination in environmental and biological materials by vanadium(III) reduction with chemiluminescence detection. Analytical Chemistry 61(24):2715-2718.

52. Cox RD (1980) Determination of nitrate and nitrite at the parts per billion level by chemiluminescence. Analytical Chemistry 52(2):332-335.

53. Fuchsman C, Murray J, & Staley J (2012) Stimulation of Autotrophic Denitrification by Intrusions of the Bosporus Plume into the Anoxic Black Sea. Frontiers in microbiology 3(257).

54. Taylor CD & Wirsen CO (1997) Microbiology and Ecology of Filamentous Sulfur Formation. Science 277(5331):1483-1485.

55. Grünke S, et al. (2011) Niche differentiation among mat-forming, sulfide-oxidizing bacteria at cold seeps

of the Nile Deep Sea Fan (Eastern Mediterranean Sea). Geobiology 9(4):330-348.

***56.** Eilers H, Pernthaler J, Glöckner FO, & Amann R (2000) Culturability and In Situ Abundance of Pelagic Bacteria from the North Sea. Applied and environmental microbiology 66(7):3044-3051.*

***57.** Albert DB & Martens CS (1997) Determination of low-molecular-weight organic acid cocentrations in seawater and pore-water samples via HPLC. Marine Chemistry 56:27-37.*

***58.** Ho T-Y, et al. (2002) Acetate cycling in the water column of the Cariaco Basin: Seasonal and vertical variability and implication for carbon cycling. Limnology and Oceanography 47(4):1119-1128.*

***59.** Loginova AN, Thomsen S, & Engel A (2016) Chromophoric and fluorescent dissolved organic matter in and above the oxygen minimum zone off Peru. Journal of Geophysical Research: Oceans 121(11):7973-7990.*

***60.** Erb TJ (2011) Carboxylases in Natural and Synthetic Microbial Pathways. Applied and environmental microbiology 77(24):8466-8477.*

***61.** Kelly DP (1982) Biochemistry of the chemolithotrophic oxidation of inorganic sulphur. Philosophical transactions of the Royal Society of London. Series B: Biological sciences 298(1093):499-528.*

***62.** Kelly PD (1999) Thermodynamic aspects of energy conservation by chemolithotrophic sulfur bacteria in relation to the sulfur oxidation pathways. Archives of Microbiology 171(4):219-229.*

***63.** Nelson DC, Jørgensen BB, & Revsbech NP (1986) Growth pattern and yield of a chemoautotrophic Beggiatoa sp. in oxygen-sulfide microgradients. Applied and environmental microbiology 52(2):225-233.*

***64.** Dahl C, et al. (2005) Novel genes of the dsr gene cluster and evidence for close interaction of Dsr proteins during sulfur oxidation in the phototrophic sulfur bacterium Allochromatium vinosum. Journal of bacteriology 187(4):1392-1404.*

***65.** Nunoura T, et al. (2014) Physiological and Genomic Features of a Novel Sulfur-Oxidizing Gammaproteobacterium Belonging to a Previously Uncultivated Symbiotic Lineage Isolated from a Hydrothermal Vent. PloS one 9(8):e104959.*

***66.** Meyer B & Kuever J (2007) Molecular Analysis of the Diversity of Sulfate-Reducing and Sulfur-Oxidizing Prokaryotes in the Environment, Using aprA as Functional Marker Gene. Applied and environmental microbiology 73(23):7664-7679.*

***67.** Moran MA, et al. (2004) Genome sequence of Silicibacter pomeroyi reveals adaptations to the marine environment. Nature 432(7019):910-913.*

***68**. Miroshnichenko ML, et al. (2003) Oceanithermus profundus gen. nov., sp. nov., a thermophilic, microaerophilic, facultatively chemolithoheterotrophic bacterium from a deep-sea hydrothermal vent. International Journal of Systematic and Evolutionary Microbiology 53(3):747-752.*

***69.** Larkin JM & Strohl WR (1983) Beggiatoa, Thiothrix, and Thioploca. Annual review of microbiology 37:341-367.*

***70.** Sorokin DY (2003) Oxidation of Inorganic Sulfur Compounds by Obligately Organotrophic Bacteria. Microbiology 72(6):641-653.*

***71.** Stramma L, Johnson GC, Sprintall J, & Mohrholz V (2008) Expanding oxygen-minimum zones in the tropical oceans. Science 320(5876):655-658.*

Supporting information

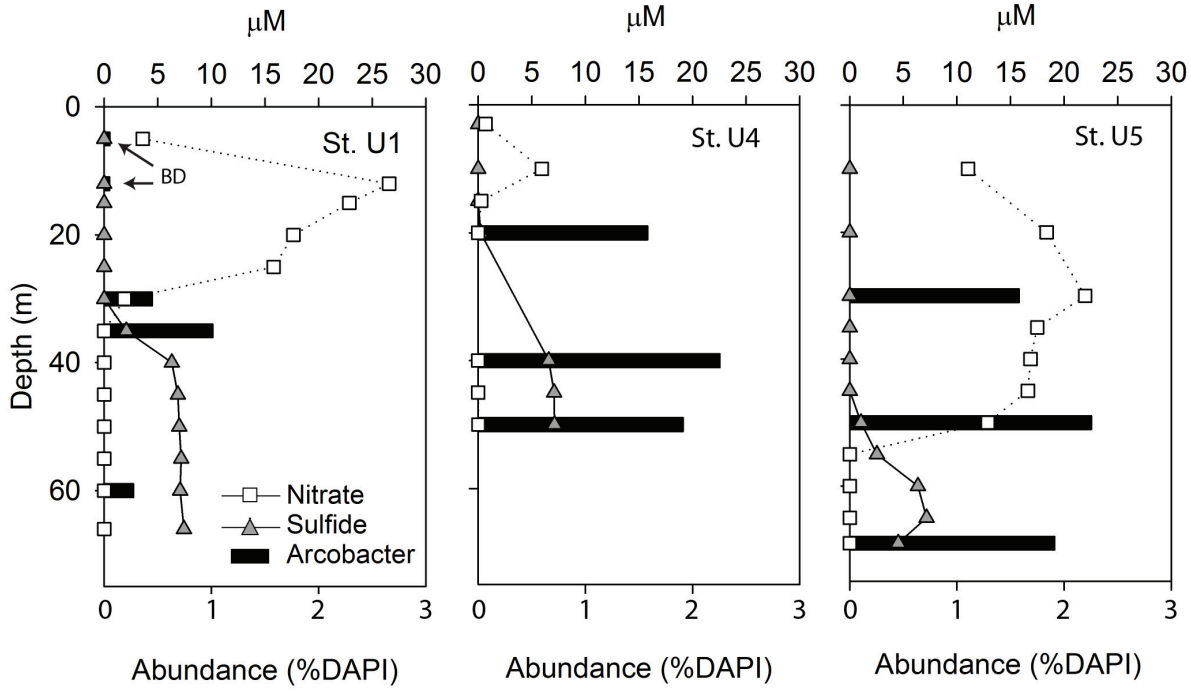

Fig. S1. Vertical profiles of sulfide, nitrate and *Arcobacter* abundances for sulfidic stations containing less than 10 µM of sulfide in bottom waters. *Arcobacter* abundances are represented as the percent of the microbial community (%DAPI); BD = below detection.

Table S1: List of stations sampled during the M93 research cruise February-March, 2013.

Abbreviated station name (used in text)	M90 station name	Date and time sampled	Latitude (°S)	Longitude (°E)
U2	295	Feb 9, 02:02	-12.38	-77.19
L1	318	Feb 11, 11:40	-12.64	-77.53
L3	391	Feb 20, 21:04	-12.67	-77.82
L2	399	Feb 22, 12:23	-12.52	-77.60
U3	412	Feb 24, 10:00	-12.31	-77.30
U1a	413	Feb 25, 01:00	-12.23	-77.18
U4	420	Feb 25, 16:00	-12.87	-76.58
U5	421	Feb 25, 18:00	-12.94	-76.66
U1	471	Mar 13, 09:50	-12.23	-77.18

CHAPTER 7

Conclusions and Outlook

OMZs are central areas in the global marine nitrogen budget, despite representing less than 1% of the ocean volume (1). The highly eutrophic and low-oxygen waters of OMZs sustain an active nitrogen cycle along with substantial nitrogen loss rates driven by anammox and denitrification. While nitrogen cycling dominates OMZs, eutrophic conditions in combination with widespread functional anoxia also drive an active and tightly coupled sulfur cycle in these waters (***Chapter 4***). Together both anammox and sulfide-oxidizing denitrifying bacteria contribute to the removal of fixed nitrogen. The aim of this thesis was to disentangle the processes regulating the distribution and activity of anammox and sulfide-oxidizing bacteria in the framework of OMZ hydrodynamics. This work employed an interdisciplinary approach involving cultivation, metagenomics, ^{15}N-labelled stable isotope incubation experiments, and single-cell techniques in combination with oceanographic tools. The following section places the major findings (highlighted in Fig. 1) from this thesis work in context of our current understanding of OMZ biogeochemistry.

Interaction of N-cycling processes: importance of oxygen in regulating N-loss

Organic matter remineralization, nitrate reduction to nitrite, and DNRA are important sources of nitrite and ammonium supporting anammox activity; while microaerobic ammonium and nitrite oxidization are important sinks (2-5). Previous studies have shown that microaerobic ammonium and nitrite oxidization processes can continue to operate under nanomolar concentrations of oxygen and thereby potentially outcompete anammox for available nitrite and ammonium in OMZs (6). In the broad, functionally anoxic zones of the ETSP and Arabian Sea OMZs, the overlap of anammox and nitrification is most likely to form in oxycline waters (3, 4), and in areas where oxygen is introduced via mixing processes into the OMZ (6-8). Thus, the role that oxygen plays in structuring the microbial community and nitrogen

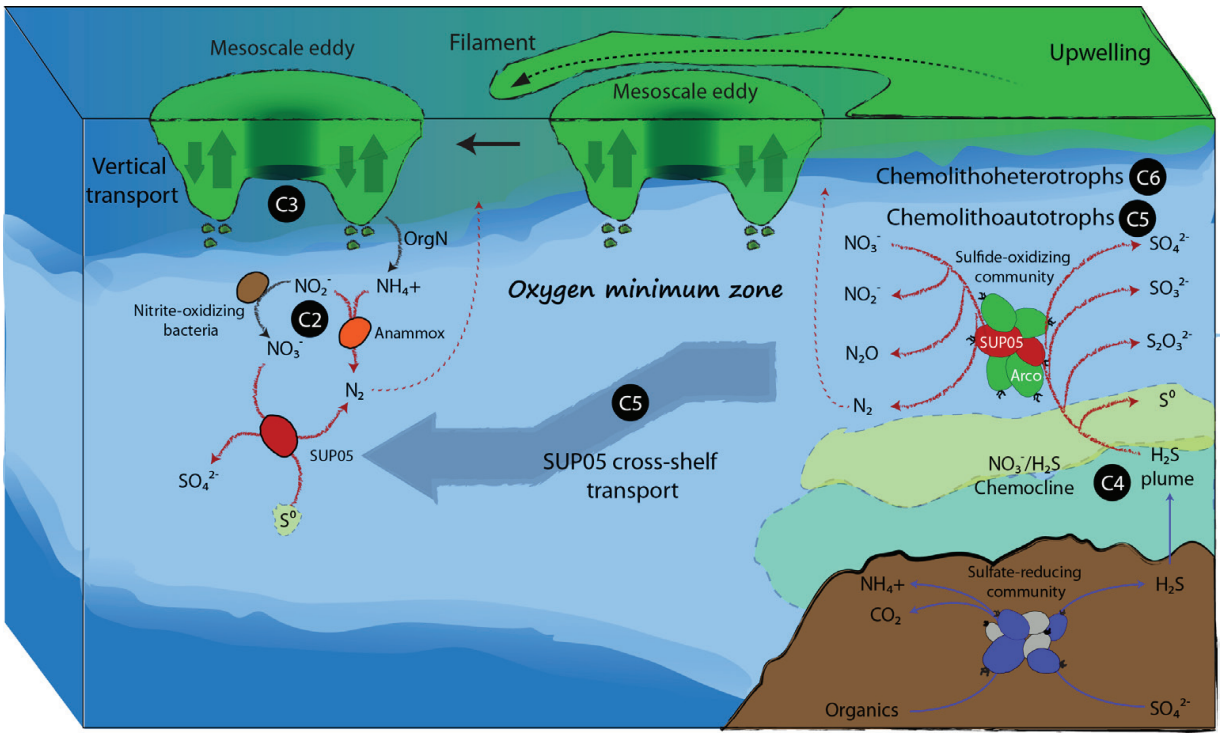

Fig. 1. A cartoon illustration summarizing the main findings of this thesis work. The findings from the respective chapters (C2-C6) are indicated.

loss processes is complex. The BoB proved to be an interesting test case to examine the effects of low oxygen on nitrogen loss. Unlike the ETSP region and Arabian Sea, the BoB contained low, but persistent oxygen concentrations (sub-micromolar) below the subeuphotic zone (***Chapter 2***). Despite the persistent oxygen concentrations, qPCR gene abundance data revealed that these waters support a complete N-cycling community consisting of anammox, denitrification and nitrification processes, with similar zonation as in other OMZs. Using ^{15}N-labelled stable isotope incubations we showed further that the BoB supports low rates of anammox activity. However, anammox rates, based on NH_4^+ incubation experiments, were only measureable when NO_2^- was amended. Process rates in combination with the general lack of a secondary nitrite maximum suggested that nitrite availability limited anammox activity. In situ oxygen manipulation experiments revealed that anaerobic anammox and aerobic nitrite oxidation activities could co-exist at low-levels of oxygen, in line with findings elsewhere (6, 9). Together our results indicate that the low but persistent oxygen concentrations in the BoB support nitrite oxidization indirectly restricting the amount of nitrite available for anammox.

If the nitrite limitations were lowered, by removing the last traces of oxygen in the water column, then the BoB would become a major global sink of fixed nitrogen (***Chapter 2***). Global warming or anthropogenic eutrophication could prompt such a decline in dissolved oxygen. The rise in global temperatures would lower the solubility of oxygen in water, thereby contributing to ocean deoxygenation. A fifty-year survey of dissolved oxygen indicates that OMZs are expanding (10), in accordance with global ocean deoxygenation trends (11). In addition, the fluvial input of fertilizers into coastal systems could enhance primary productivity and organic matter respiration thereby attenuating dissolved water column oxygen concentrations. A number of major rivers (e.g Ganges River) that are in contact with heavily populated drainage areas, discharge into the BoB, making it one of the most impacted areas of anthropogenic riverine input (12). While the high degree of atmospheric fixed nitrogen deposition into the BoB (12), attributed to the immense combustion and agriculture emissions from surrounding lands (13); could induce more widespread regional eutrophication. Even a slight increase in organic matter, which is predicted based on model simulations (12), may push the BoB past its tipping point and closer towards resembling the biogeochemistry of other major OMZs. The BoB, is thus, an important bellwether of global change, but is one of the most understudied of the major OMZ regions. This thesis work articulates that continual long-term monitoring of N-loss in these waters is needed in order to assess how regional biogeochemistry will change in face of anthropogenic induced eutrophication and global warming.

Influence of mesoscale and submesoscale hydrodynamics on anammox and denitrification

Despite the ubiquity of mesoscale eddies in the ocean (14) and their capacity to mediate the vertical transport of nutrients (15, 16), the impact of eddies on primary production and nitrogen loss processes in OMZs remains poorly constrained. Such features are known to drive the vertical transport of nutrients by Ekman and non-linear Ekman forces (otherwise known as submesoscale dynamics). These transport processes do not act uniformly across the eddy; wind-driven Ekman transport operates in the eddy center, while submesoscale dynamics, driven by the eddies horizontal velocities, are greatest along the eddy periphery (15-17). Models predict that submesoscale vertical transport velocities exceed Ekman wind-driven velocities in the eddy center by an order of magnitude (17).

In OMZs, the few studies that have investigated N-loss within eddies have employed only geochemical tools (N*, $\delta^{15}N$, and N_2/Ar) to quantify N-loss (18-21). These studies find that N-loss signatures are highest in the eddy center, coinciding with where the highest chlorophyll concentrations are observed (18-21). This enhanced activity is attributed to Ekman driven vertical transport, in what's known as the 'hotspot' theory (18-21). However, these enhanced geochemical

signatures reported in the eddy center (18-21), may have alternatively reflected the trapping of N-loss signatures from coastal waters caused by the inward swirling velocity of the eddy (17, 22). In contrast with previous OMZ eddy studies, we demonstrate using ^{15}N-labelled incubation experiments that anammox rates are highest on the eddy periphery. Although the center of the eddy reported the highest volumetric chlorophyll concentrations, depth-integrated chlorophyll was greatest along the eddy periphery coinciding with the measured rates of anammox activity (Fig. 1; ***Chapter 3***). The enhanced depth-integrated chlorophyll and subsequent organic matter export, driven by submesoscale dynamics, likely fueled the measured rates of nitrogen loss. Given the ubiquity of eddies, and the heterogeneity of anammox rates (***Chapter 1***; Fig. 4a), we suggest that mesocale eddies and the associated submesoscale dynamics are important drivers of offshore primary production and nitrogen loss in ETSP waters.

Mesoscale eddies, during their development in shelf waters; also mediate extensive cross-shelf transport of coastal chlorophyll and nutrients offshore (22-24). Widespread and persistent cross-shelf advection in OMZs is apparent in satellite remote sensing imagery (***Chapter 1***: Fig. 2). Some studies invoke cross-shelf transport processes as an explanation for the presence of sulfate-reducing and sulfide-oxidizing denitrifying bacteria in sulfide-free offshore OMZs waters, which they posited originated from coastal sulfidic waters (25, 26). Alternatively, Canfield et al., (27), employing metagenomics and rate process incubation experiments, proposed the presence of a cryptic sulfur cycle operating in offshore OMZ waters. Time-integrated geochemical records of sulfate reduction show no discernable signal in ETSP waters, (albeit the method sensitivity is at the detection limit of observed rates by (27); see ***Chapter 4***) (28). Nevertheless, the consistent finding of sulfide-oxidizing denitrifying bacteria in microbial community surveys of sulfide-free offshore waters of all major OMZs is perplexing. We empirically demonstrated, using molecular, stable-isotope and single-cell approaches in combination with oceanography, that eddies mediate the co-transport of sulfidic shelf chemistry and sulfide-oxidizing denitrifying bacteria from the coast into the open ocean (***Chapter 5***).

Our findings affirm that sulfidic shelf waters represent large inventories of elemental sulfur (7.0×10^8 moles) and sulfide-oxidizing nitrate-reducing bacteria (up to 10^6 cells ml^{-1}) that intermittently exchange with offshore waters by eddy-driven transport (***Chapter 5 and 6***). Sulfide-oxidizing denitrifying bacteria within the SUP05 cluster ("*Candidatus* Thioglobus perditus") and *Arcobacter* dominate in sulfidic waters, and are therefore susceptible to offshore transport. However, despite co-occurring in sulfidic waters "*Ca.* T. perditus" and *Arcobacter* exhibited different distributions in offshore ETSP waters; a subject of further investigation in ***Chapters 5 and 6***. Metagenomics and cultivation approaches revealed that both "*Ca.* T. perditus" and *Arcobacter* have a capacity to oxidize sulfide and to reduce nitrate to N_2, contributing to the elevated rates of denitrification measured in sulfidic waters (Fig. 1). For growth, "*Ca.* T. perditus" was reliant on autotrophic CO_2 fixation, while in contrary to previous hypothesizes; *Arcobacter* was incapable of fixing CO_2 autotrophically, but was instead dependent on organic matter for growth. As an obligate heterotroph *Arcobacter* grew best in the presence of sulfide and nitrate. This chemolithoheterotrophic metabolism gave *Arcobacter* a competitive advantage over chemolithoautotrophs for available sulfide and nitrate. This finding thus demonstrates that lithoheterotrophy may play an important role in the highly sulfidic and eutrophic waters of OMZs, where it was assumed that such waters are detoxified by primarily chemolithoautotrophic bacteria.

In contrast to *Arcobacter*, chemolithoautotrophic "*Ca.* T. perditus" bacteria, not restricted by carbon availability and with a capacity to store or to utilize co-transported elemental sulfur were more widespread (***Chapter 5***). Based on ^{13}C-HCO_3^- single-cell uptake rates SUP05 bacteria remained active not only in sulfidic shelf waters, but also continued to thrive, in waters transported from the shelf into the open ocean. This indicated that "*Ca.* T. perditus" bacteria are well-adapted to dynamic low-sulfide conditions. "*Ca.* T. perditus" capacity to utilize elemental sulfur ostensibly fueled the rates of denitrification measured

in offshore ETSP waters. Indeed, in ETSP waters sporadic rates of denitrification are often reported in close proximity to the coast and are associated with elevated chlorophyll concentrations in surface waters (29) (***Chapter 1***; Fig. 4). Cross-shelf filaments, as seen in remote sensing imagery, form frequently off the Peru coast and can extend hundreds of kilometers into the open ocean, with similar phenomena also occurring off the coast of Chile where cryptic sulfur cycling was observed (***Chapter 5***). Eddy-driven lateral advection combined with "*Ca.* T. perditus" ability to denitrify and thrive on elemental sulfur in waters void of sulfide feasibly underlines reports of cryptic sulfur cycling and nitrogen loss by denitrification in OMZs.

Together, using an interdisciplinary approach, this thesis demonstrates that mesoscale eddies and eddy-driven submesoscale dynamics play a pivotal role in regulating the distribution and activity of anammox and denitrification in ETSP waters (Fig. 1). At present, mesoscale and submesoscale dynamics are not yet incorporated into regional models due to the limited spatial resolution. Parameterization of vertical and horizontal transport dynamics associated to mesocale eddies will enable a more accurate estimation of the marine OMZ nitrogen budget.

Directions for future research

This thesis touched on a number of characteristics of OMZ biogeochemistry (N- and S-cycling processes) and oceanography (mesoscale and submesoscale dynamics). In which direction do we proceed next? In ***Chapter 4*** we outline open questions related to OMZ sulfur cycling. In this outlook, I focus on outlining areas of research coupling biogeochemistry and oceanography that I believe are of research interest. As was highlighted in this thesis, mesoscale eddy dynamics have the potential to underpin various facets of OMZ biogeochemistry including primary production, nitrogen loss and the distribution of microbes. However, our understanding of the impact of regional mesoscale and submesoscale hydrodynamics on OMZ sulfur and nitrogen cycling is still in its infancy. A number of caveats and gaps in our knowledge persist that can be attained through multidisciplinary approaches.

To date, the factors controlling sulfidic event formation in ETSP waters are unknown. In other OMZs, sulfidic events are prone to develop during seasonally anoxic periods. For example, in the Namibia upwelling, large sulfidic events form during enhanced water column stratification periods, driven by changes in seasonal wind-stress patterns (30, 31). Whereas in the Arabian Sea, anoxic bottom waters are enhanced following the monsoon rains, which create a freshwater lens isolating shelf bottom waters, and thereby establishing conditions conducive for sulfate reduction and sulfide accumulation (32). In

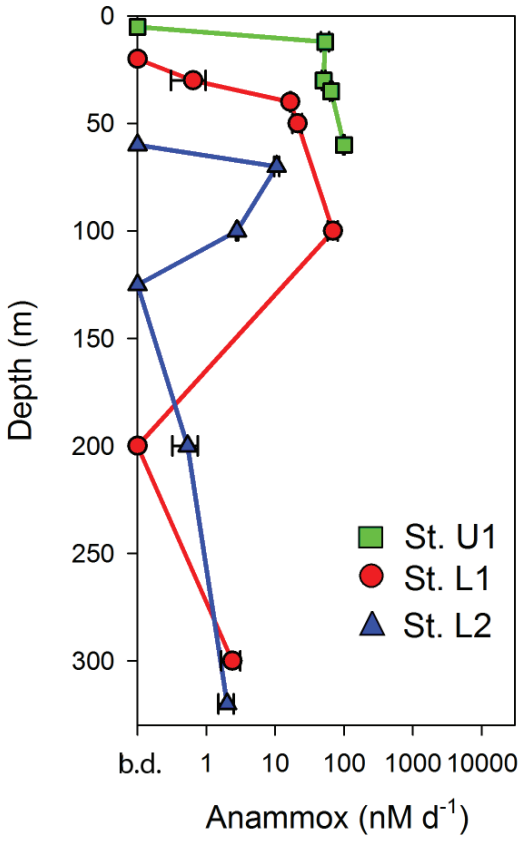

Fig. 2. Enhanced anammox activity in the eddy-driven offshore filament. Stations L1, L2 and U1 are described in Chapter 5. Station U1 is the sulfidic shelf station, station L1 is an eddy inlfuenced offshore station and station L2 was sampled after the eddy had passed under normal flow conditions. The error bar represents the standard error. b.d = below the limit of detection.

the ETSP region, regional remote sensing of sulfur plumes has revealed that sulfidic events form and dissipate at irregular intervals and on much smaller spatial-temporal timescales, suggesting that other physical forces are at play (see ***Chapter 4***).

Mesoscale eddies are potential triggers of sulfidic event formation. The development of a sulfidic event forming adjacent to a mesoscale eddy (22), reported in ***Chapters 5*** **and** ***6***, was perhaps no coincidence. The tracking of the subsurface eddy by bottom water velocity measurements showed that during its formation the Peru-Chile undercurrent, which normally runs poleward along the shelf, was diverted around the eddy, causing stagnant curent velocities in shelf waters adjacent to the eddy (22). During this stagnant period, nitrate depleted conditions intensified over the upper shelf, which may initiated the sulfidic event described in February-March 2013 (***Chapters 5*** **and** ***6***). As the eddy propagated westward, conditions progressively reversed (22): the fast-moving Peru-Chile undercurrent resumed along the upper shelf, and in accordance sulfide declined and nitrate increased at shelf stations (data not shown). The replenishment of nitrate concentrations over the shelf in concert with the flushing of any coastal sulfide/sulfur away may have contributed to the termination of the sulfidic event reported in February-March, 2013. While this offers an exciting glimpse into the mechanisms potentially regulating sulfidic event foramtion in ETSP waters, I caution that further work is needed to fully assess the impact of eddies on sulfidic event regulation.

2 Eddy-driven cross-shelf transport has potentially important implications for OMZ biogeochemistry. Gruber et al., (23) highlight that the lateral advection of chlorophyll from the coast into offshore waters followed by its subduction by submesocale processes contributes to lowering the overall productivity of upwelling regions. In addition, our findings show that mesoscale eddy activity underlines the distribution of sulfide-oxidizing denitrifying bacteria and the transport of elemental sulfur in offshore waters. Presumably, eddy-driven horizontal transport also effects other coastal OMZ processes. For instance, rates of anammox activity in the offshore eddy influenced station L1 (see ***Chapter 5***), exceeded rates measured at the non-eddy influenced station L2 (Fig. 2), suggesting that eddy-driven cross-shelf transport may also redistribute coastal anammox activity into the offshore ETSP region. Whether eddy-driven processes also co-transport ammonium is unknown, but would be worthy of further investigation as this may represent a supply of ammonium fueling offshore ETSP anammox activity. Employing biogeochemical methods in concert with oceanography may help to further resolve the impact of eddy-driven cross-shelf transport mechanisms on OMZ N-cycling processes.

3 How do we improve upon current sampling strategies for OMZs? Our findings articulate that high-resolution sampling is needed to constrain the mesoscale (~10-100 km) and submesoscale (<10 km) dynamics that dominate OMZ nitrogen loss. Improving sampling resolution, is as simple as taking more stations across a defined transect, but could be improved using the side-by-side deployment of autonomous gliders. The advantage of gliders is that they provide near-real time information regarding current velocities and nutrients ahead of the research vessel, permitting more informed decisions on where to perform ship-based experiments (e.g. ^{15}N-labelled

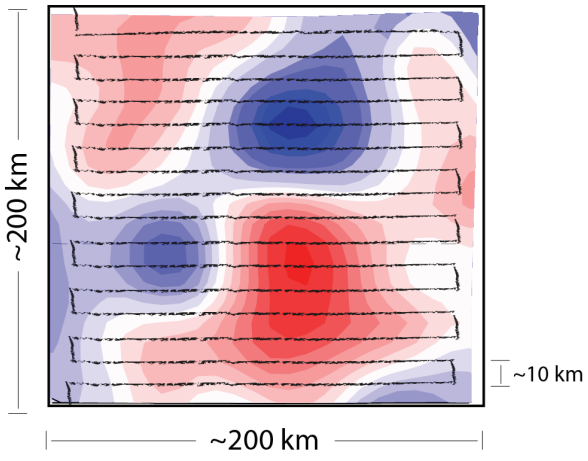

Fig. 3. Example of a high-resolution sampling strategy for an offshore OMZ (200 x 200 km grid size.) A hypothetical research vessel and glider track (black line) is overlaid over sea surface height altimetry. Anticyclonic and cyclonic mesoscale eddies are indicated in red and blue, respectively.

stable isotope incubation) (e.g.Fig. 3). This is particularly important as mesoscale eddies and associated submesocale dynamics can change rapidly. Using this approach, mesoscale and submesoscale features could be sampled more accurately, providing a synoptic view of the various spatial temporal dynamics that govern OMZ biogeochemistry and N-cycling processes. I hope that work presented in this thesis will help guide the design of future sampling strategies in OMZs.

References

1. *Lam P & Kuypers MMM (2011) Microbial nitrogen cycling processes in oxygen minimum zones. Ann Rev Mar Sci 3:317-345.*
2. *Jensen MM, et al. (2011) Intensive nitrogen loss over the Omani Shelf due to anammox coupled with dissimilatory nitrite reduction to ammonium. The ISME journal 5(10):1660-1670.*
3. *Fussel J, et al. (2012) Nitrite oxidation in the Namibian oxygen minimum zone. The ISME journal 6(6):1200-1209.*
4. *Kalvelage T, et al. (2013) Nitrogen cycling driven by organic matter export in the South Pacific oxygen minimum zone. Nature Geosci 6(3):228-234.*
5. *Lam P, et al. (2009) Revising the nitrogen cycle in the Peruvian oxygen minimum zone. Proceedings of the National Academy of Sciences of the United States of America 106(12):4752-4757.*
6. *Bristow LA, et al. (2016) Ammonium and nitrite oxidation at nanomolar oxygen concentrations in oxygen minimum zone waters. Proceedings of the National Academy of Sciences 113(38):10601-10606.*
7. *Tiano L, et al. (2014) Oxygen distribution and aerobic respiration in the north and south eastern tropical Pacific oxygen minimum zones. Deep Sea Research Part I: Oceanographic Research Papers 94:173-183.*
8. *Thamdrup B, Dalsgaard T, & Revsbech NP (2012) Widespread functional anoxia in the oxygen minimum zone of the Eastern South Pacific. Deep Sea Research Part I: Oceanographic Research Papers 65:36-45.*
9. *Kalvelage T, et al. (2011) Oxygen Sensitivity of Anammox and Coupled N-Cycle Processes in Oxygen Minimum Zones. PloS one 6(12):e29299.*
10. *Stramma L, Johnson GC, Sprintall J, & Mohrholz V (2008) Expanding oxygen-minimum zones in the tropical oceans. Science 320(5876):655-658.*
11. *Schmidtko S, Stramma L, & Visbeck M (2017) Decline in global oceanic oxygen content during the past five decades. Nature 542(7641):335-339.*
12. *Jickells TD, et al. (2017) A reevaluation of the magnitude and impacts of anthropogenic atmospheric nitrogen inputs on the ocean. Global Biogeochemical Cycles 31(2):2016GB005586.*
13. *Vetter SH, et al. (2017) Greenhouse gas emissions from agricultural food production to supply Indian diets: Implications for climate change mitigation. Agriculture, Ecosystems & Environment 237:234-241.*
14. *Chelton DB, Schlax MG, Samelson RM, & de Szoeke RA (2007) Global observations of large oceanic eddies. Geophysical Research Letters 34(15).*
15. *Mahadevan A (2016) The Impact of Submesoscale Physics on Primary Productivity of Plankton. Annual Review of Marine Science 8(1):161-184.*
16. *McGuillicuddy DJM (2016) Mechanisms of Physical-Biological-Biogeochemical Interaction at the Oceanic Mesoscale. Annual Review of Marine Science 8(1):125-159.*
17. *Mahadevan A, Thomas LN, & Tandon A (2008) Comment on "Eddy/Wind Interactions Stimulate Extraordinary Mid-Ocean Plankton Blooms". Science 320(5875):448-448.*
18. *Altabet MA, et al. (2012) An eddy-stimulated hotspot for fixed nitrogen-loss from the Peru oxygen minimum zone. Biogeosciences 9(12):4897-4908.*
19. *Stramma L, Bange HW, Czeschel R, Lorenzo A, & Frank M (2013) On the role of mesoscale eddies for the biological productivity and biogeochemistry in the eastern tropical Pacific Ocean off Peru. Biogeosciences 10(11):7293-7306.*
20. *Bourbonnais A, et al. (2015) N-loss isotope effects in the Peru oxygen minimum zone studied using a mesoscale eddy as a natural tracer experiment. Global Biogeochemical Cycles 29(6):793-811.*
21. *Löscher CR, et al. (2015) N2 fixation in eddies of the eastern tropical South Pacific Ocean. Biogeosciences Discuss. 12(22):18945-18972.*
22. *Thomsen S, et al. (2016) The formation of a subsurface anticyclonic eddy in the Peru-Chile Undercurrent and its impact on the near-coastal salinity, oxygen, and*

nutrient distributions. Journal of Geophysical Research: Oceans:n/a-n/a.

23. *Gruber N, et al. (2011) Eddy-induced reduction of biological production in eastern boundary upwelling systems. Nature Geosci 4(11):787-792.*

24. *Nagai T, et al. (2015) Dominant role of eddies and filaments in the offshore transport of carbon and nutrients in the California Current System. Journal of Geophysical Research: Oceans 120(8):5318-5341.*

25. *Stevens H & Ulloa O (2008) Bacterial diversity in the oxygen minimum zone of the eastern tropical South Pacific. Environmental microbiology 10(5):1244-1259.*

26. *Finster KW & Kjeldsen KU (2010) Desulfovibrio oceani subsp. oceani sp. nov., subsp. nov. and Desulfovibrio oceani subsp. galateae subsp. nov., novel sulfate-reducing bacteria isolated from the oxygen minimum zone off the coast of Peru. Antonie van Leeuwenhoek 97(3):221-229.*

27. *Canfield DE, et al. (2010) A cryptic sulfur cycle in oxygen-minimum-zone waters off the Chilean coast. Science 330(6009):1375-1378.*

28. *Johnston DT, et al. (2014) Placing an upper limit on cryptic marine sulphur cycling. Nature 513(7519):530-533.*

29. *Dalsgaard T, Thamdrup B, Farías L, & Revsbech NP (2012) Anammox and denitrification in the oxygen minimum zone of the eastern South Pacific. Limnology and Oceanography 57(5):1331-1346.*

30. *Monteiro PMS, van der Plas AK, Mélice JL, & Florenchie P (2008) Interannual hypoxia variability in a coastal upwelling system: Ocean–shelf exchange, climate and ecosystem-state implications. Deep Sea Research Part I: Oceanographic Research Papers 55(4):435-450.*

31. *Weeks SJ, Currie B, Bakun A, & Peard KR (2004) Hydrogen sulphide eruptions in the Atlantic Ocean off southern Africa: implications of a new view based on SeaWiFS satellite imagery. Deep Sea Research Part I: Oceanographic Research Papers 51(2):153-172.*

32. *Levin LA, et al. (2009) Effects of natural and human-induced hypoxia on coastal benthos. Biogeosciences 6(10):2063-2098.*

APPENDIX

Coauthorships and publications in preparation

Water column biogeochemistry of oxygen minimum zones in the eastern tropical North Atlantic and eastern tropical South Pacific Oceans

Carolin R. Löscher[1,4], Hermann W. Bange[1], Ruth A. Schmitz[2], **Cameron M. Callbeck**[3], Anja Engel[1], Helena Hauss[1], Torsten Kanzow[1], Rainer Kiko[1], Gaute Lavik[3], Alexandra Loginova[1], Frank Melzner[1], Judith Meyer[1], Sven C. Neulinger[2], Markus Pahlow[1], Ulf Riebesell[1], Harald Schunck[2], Sören Thomsen[1], and Hannes Wagner[1]

Abstract

Recent modeling results suggest that oceanic oxygen levels will decrease significantly over the next decades to centuries in response to climate change and altered ocean circulation. Hence, the future ocean may experience major shifts in nutrient cycling triggered by the expansion and intensification of tropical oxygen minimum zones (OMZs), which are connected to the most productive upwelling systems in the ocean. There are numerous feedbacks among oxygen concentrations, nutrient cycling and biological productivity; however, existing knowledge is insufficient to understand physical, chemical and biological interactions in order to adequately assess past and potential future changes. In the following, we summarize one decade of research performed in the framework of the Collaborative Research Center 754 (SFB754) focusing on climate–biogeochemistry interactions in tropical OMZs. We investigated the influence of low environmental oxygen conditions on biogeochemical cycles, organic matter formation and remineralization, greenhouse gas production and the ecology in OMZ regions of the eastern tropical South Pacific compared to the weaker OMZ of the eastern tropical North Atlantic. Based on our findings, a coupling of primary production and organic matter export via the nitrogen cycle is proposed, which may, however, be impacted by several additional factors, e.g., micronutrients, particles acting as microniches, vertical and horizontal transport of organic material and the role of zooplankton and viruses therein.

Manuscript published in *Biogeosciences*

[1]GEOMAR Helmholtz Centre for Ocean Research Kiel, Düsternbrooker Weg 20, 24105 Kiel, Germany. [2]Institute of General Microbiology, Christian-Albrechts-Universität zu Kiel, Am Botanischen Garten 1–9, 24118 Kiel, Germany. [3]Max Planck Institute for Marine Microbiology, Celsiusstraße 1, 28359 Bremen, Germany

[4]Corresponding author: cloescher@geomar.de

Selective organic matter mineralization leads to overestimation of oceanic nitrogen loss

Philipp F. Hach[1], Gaute Lavik[1], Judith Meyer[2], **Cameron M. Callbeck**[1], Tim Kalvelage[1,3], Helena Osterholz[2], Ulf Riebesell[2], Thorsten Dittmar[4], Marcel M. M. Kuypers[1,5]

Abstract

Phytoplankton growth in the Ocean is nitrogen limited because the fixation of N_2 cannot make up for the removal of fixed inorganic nitrogen (nitrate, nitrite and ammonium) by anaerobic microbial processes. Biogeochemical and ocean circulation models are used to quantify oceanic gain and loss of fixed nitrogen (N). These models generally assume that biological uptake and release of inorganic N and phosphorus (P) occurs with a nearly constant N:P ratio of 16:1 (Redfield 1958) and that negative deviation of this so-called Redfield ratio is due to the loss of fixed inorganic N as N_2 gas (Gruber & Sarmiento 1997). Here we show that preferential organic P remineralization strongly biases N-loss estimates for one of the main regions of oceanic N-loss, the Peruvian Oxygen Minimum Zone (OMZ). The analysis of the elemental and molecular composition of organic matter from the Peruvian OMZ revealed a strong preference in organic P mineralization relative to N upon organic matter breakdown. The resulting preferential release of inorganic P accounts for nearly half of the inorganic N:P ratio based N-deficit for Peruvian OMZ waters, which was so far solely attributed to N-loss processes. This substantially lower N-deficit agrees well with low N-loss rates determined from ^{15}N-incubations. Our combined results indicate that N-loss estimates based on inorganic nutrient stoichiometry might be overestimated by as much as 50% for marine OMZ waters.

Manuscript in preparation

[1]Max Planck Institute for Marine Microbiology, Celsiusstrasse 1, 28359 Bremen, Germany. [2]GEOMAR Helmholtz Centre for Ocean Research Kiel, Düsternbrooker Weg 20, 24105 Kiel, Germany. [3]Institute of Biogeochemistry and Pollutant Dynamics, ETH Zürich, Switzerland. [4]University of Oldenburg, Postfach 2503, 26111 Oldenburg, Germany.

[5]Corresponding author; mkuypers@mpi-bremen.de

Corrosive metabolism of the oil-field sulfide-oxidizing nitrate-reducing epsilonproteobacterium *Sulfurimonas* sp. strain CVO

Sven Lahme[1,4], **Cameron M. Callbeck**[2], Ian Head[1], Casey Hubert[3]

Abstract

Nitrate injection for souring and corrosion control is widely applied in the oil industry. However, in vitro and in situ trials have shown that nitrate injection has the potential to accelerate iron corrosion under certain conditions. In this regard, sulfide-oxidizing nitrate-reducing bacteria (soNRB) are frequently associated with oil exploitations and have been linked to MIC during souring control via nitrate injection. To gain a better mechanistic understanding of nitrate- and soNRB-mediated corrosion, we conducted a detailed metabolic analysis of the oil field soNRB Sulfurimonas sp. strain CVO during MIC at varying nitrate to sulfide (N/S) ratios. Strain CVO accelerated corrosion to 0.20–0.27 mm/y at high N/S ratios (>1.4) and corrosion decreased by nearly 50% during nitrate limitation (N/S ≤1.3). Detailed S and N compound speciation revealed formation of a variety of potentially corrosive metabolic intermediates (e.g. biogenic S^0, $S_2O_3^{2-}$, SO_3^{2-}, NO_2^-) and sterile incubations with individual S and N compounds revealed biogenic S^0 and NO_2^- as the main corrosion agents. In addition, the presence of FeS on iron coupons had a stimulating effect on both S^0 and NO_2^- corrosion and reaction rates. Additional RNA sequencing was conducted to identify genes involved in the formation of these corrosive intermediates. Gene expression analysis suggests involvement of a putative polysulfide reductase (psrABC) in oxidation of H_2S to S^0. On the other hand, genes coding for sulfide quinone reductases (sqr) as well as a truncated thiosulfate-oxidizing multi-enzyme complex (soxCDYZ) showed high expression during S^0 oxidation phase. In addition, various genes coding for hypothetical cytochrome c proteins showed increased expression in the presence of metallic iron and might be involved in iron storage or additional redox processes. The combination of corrosion and gene expression analysis allowed identification of metabolic key-processes involved in corrosive events and refines our understanding of oil-field MIC processes to improve existing souring and corrosion mitigation strategies.

Manuscript in preparation

[1]School of Civil Engineering and Geosciences, Newcastle University, Newcastle upon Tyne, NE1 7RU UK. [2]Max Planck Institute for Marine Microbiology, Celsiusstrasse 1, 28359 Bremen, Germany. [3]Department of Geosciences, University of Calgary, Calgary, Canada, T2N 1N4, Canada.

[4]Corresponding author; sven.lahme@newcastle.ac.uk

A new player in the Marine N cycle? Genome and physiology of a new diazotroph isolate from the Peruvian oxygen minimum zone

Clara Martínez-Pérez[1], Wiebke Mohr[1], Anne Schwedt[1], **Cameron M. Callbeck**[1], Harald Schunck[2], Gaute Lavik[1], Jimena Barrero-Canosa[1], Laura Zeugner[1], Bernhard Fuchs[1], Marcel M. M. Kuypers[1]

Abstract

Phytoplankton growth in the Ocean is nitrogen limited because the fixation of N_2 cannot make up for the removal of fixed inorganic nitrogen (nitrate, nitrite and ammonium) by anaerobic microbial processes. Biogeochemical and ocean circulation models are used to quantify oceanic gain and loss of fixed nitrogen (N). These models generally assume that biological uptake and release of inorganic N and phosphorus (P) occurs with a nearly constant N:P ratio of 16:1 (Redfield 1958) and that negative deviation of this so-called Redfield ratio is due to the loss of fixed inorganic N as N_2 gas (Gruber & Sarmiento 1997). Here we show that preferential organic P remineralization strongly biases N-loss estimates for one of the main regions of oceanic N-loss, the Peruvian Oxygen Minimum Zone (OMZ). The analysis of the elemental and molecular composition of organic matter from the Peruvian OMZ revealed a strong preference in organic P mineralization relative to N upon organic matter breakdown. The resulting preferential release of inorganic P accounts for nearly half of the inorganic N:P ratio based N-deficit for Peruvian OMZ waters, which was so far solely attributed to N-loss processes. This substantially lower N-deficit agrees well with low N-loss rates determined from ^{15}N-incubations. Our combined results indicate that N-loss estimates based on inorganic nutrient stoichiometry might be overestimated by as much as 50% for marine OMZ waters.

Manuscript in review

[1]Max Planck Institute for Marine Microbiology, Celsiusstrasse 1, 28359 Bremen, Germany. [2]GEOMAR Helmholtz Centre for Ocean Research Kiel, Düsternbrooker Weg 20, 24105 Kiel, Germany.